

**POLITECNICO DI MILANO**

School of Civil, Environmental and Land Management Engineering  
Master of science in Civil Engineering for Risk Mitigation



**FLOOD RISK ASSESSMENT AND MITIGATION FOR RIO  
MAGUIDE IN CABO DELGADO, MOZAMBIQUE**

Supervisor: Dr. Alessio Radice

Co-supervisor: Dr. Davide Biotto

Thesis of:

Benedetta Corti Matr. 899732

Sara Rrokaj Matr. 897489

Academic Year 2018/2019



# ACKNOWLEDGEMENT

We would like to express the deepest appreciation to our thesis advisor Dr. Alessio Radice of the school of Civil, Environmental and Land Management Engineering at Politecnico di Milano. It was only thanks to his valuable guidance, constant encouragement and precise teachings that we were able to complete our work. He made the conclusion of our academic journey the most formative, exciting and unexpected experience, providing constant support to our uncertainties and fears.

Our very profound gratitude goes to *Istituto Oikos* and, in particular, to Davide Biotto, not only for being the promoter and co-advisor of this thesis, but also for being the friendly guide of our African trip: living this experience driven by his tales and teachings deeply changed our perspective on life. We are gratefully indebted with him for making this dream come true.

We would also like to acknowledge Dr. Daniela Carrion and Dr. Giovanna Venuti of the school of Civil, Environmental and Land Management Engineering of the department of Cartography and Topography at Politecnico di Milano for providing us support in searching DEM data and satellite images at the beginning of our thesis project.

Thank you.

Sara e Benedetta

December 2019





## ENGLISH ABSTRACT

Floods are among the most frequent natural disasters, in the last century have been increasing in terms of both intensity and frequency as a result of population growth and climate change. In the sub-Saharan context an increasing number of floods and drought are hitting the population and human activities. The scope of this thesis is to conduct a flood hazard study and provide proper mitigation measure for the downstream course of Rio Maguide, that flows within the province of Cabo Delgado, in the Northern Mozambique, where frequent flood events occur during the rainy season.

The area under study can be defined as a flatland where the river flows without a well-defined path, buried from the large amount of sediment afforded during the flood event increasing the inundated area.

The flood modelling and risk has been performed considering a 10 years return period rainfall event and the mitigation measure, which consists in excavation of the river bed and use of the material dug to build levees, are designed also for larger discharge coming from a 300 years return period event.

To conduct the analysis several freely available Digital Elevation Models, soil coverage maps and open rainfall data source were analysed in order to produce Depth-Duration-Frequency curves and consequently runoff in order to determine the corresponding flooded area.

## ITALIAN ABSTRACT

Le alluvioni sono tra le calamità naturali più frequenti e, nell'ultimo secolo, sono cresciute in termini di frequenza e intensità come conseguenza dell'aumento della popolazione mondiale e del cambiamento climatico in atto. Nel contesto sub-Sahariano, fenomeni alluvionali e di siccità, provocano danni a popolazione e attività umane sempre con maggior frequenza. Lo scopo della tesi è volto allo studio della pericolosità alluvionale, e a fornire contromisure adeguate, del tratto a valle del fiume Rio Maguide, il quale scorre lungo la provincia di Cabo Delgado, situata a nord del Mozambico, dove le alluvioni sono solite avvenire durante la stagione di pioggia. L'area in esame è caratterizzata da basse pendenze e il letto del fiume è interrato a causa della grande quantità di sedimenti trasportati dal flusso intenso caratterizzante gli eventi alluvionali, con conseguente aumento delle aree inondate.

Il modello alluvionale e l'analisi di rischio vengono condotti considerando un evento di pioggia con tempo di ritorno decennale mentre le opere di mitigazione, che consistono nello scavo del letto e costruzione di argini col materiale dissotterrato lungo lo stesso, vengono progettate inoltre considerando un evento caratterizzato da un tempo di ritorno di 300 anni.

L'analisi è stata condotta considerando numerosi modelli di elevazione digitale del terreno (DEM), mappe di copertura del suolo e diverse piattaforme meteorologiche per poter produrre Curve di Possibilità Pluviometrica e conseguentemente un idrogramma di deflusso superficiale atto a determinare l'alluvione dell'area in esame.

# INDEX

ACKNOWLEDGEMENT .....	III
ENGLISH ABSTRACT .....	V
LIST OF FIGURES .....	IX
LIST OF TABLES .....	XIII
1. INTRODUCTION .....	16
1.1. SCOPE AND OBJECTIVES OF THE THESIS.....	16
1.2. CONTEXT.....	18
1.2.1 THE MISSION.....	22
1.3. PAST EVENTS.....	29
1.3.1. MAIN PAST EVENTS HITTING THE AREA OF INTEREST .....	29
1.3.2. CYCLONE KENNETH.....	31
2. COLLECTED DATA.....	35
2.1. DIGITAL ELEVATION MODEL.....	35
2.1.1. DEMs FOUND.....	35
2.1.2. COMPARISON BETWEEN THE DIFFERENT DEMs .....	38
2.1.3. DEM CHOICE .....	46
2.2 SOIL COVER.....	46
2.3 HYDROLOGICAL DATA.....	48
2.3.1 RAIN DATA SOURCES .....	48
2.3.2 COMPARISON BETWEEN THE DATA FROM DIFFERENT SOURCES.....	51
2.3.3 RAINFALL DATA CHOICE.....	53
2.4 MAPS FOR EXPOSURE AND FACILITIES .....	53
3. FLOOD IN THE RURAL AREA.....	56
3.1 HYDROLOGY.....	56
3.1.1 DEPTH-DURATION-FREQUENCY CURVES (DDF).....	56
3.1.2 HYDROLOGICAL LOSSES.....	60
3.1.3 TIME OF CONCENTRATION .....	63
3.1.4 CHOICE OF A BASIN TO SUPPORT THE ANALYSIS .....	66
3.1.5 RAINFALL-TO-RUNOFF MODELLING .....	67
3.2 FLOOD MODELING.....	71
3.2.1 COMPUTATIONAL DOMAIN.....	71
3.2.2 MATHEMATICAL MODEL AND BOUNDARY CONDITIONS.....	73
3.2.3 COMPUTATIONAL TOOLS USED.....	74
4. MITIGATION MEASURES.....	86
4.1. CONCEPT.....	86

4.2.	MODELLING APPROACH .....	93
4.3.	MODELLING APPROACH .....	95
4.3.1.	SCENARIO 1: DEEP EXCAVATION ONLY .....	95
4.3.2.	SCENARIO 2: DEEP EXCAVATION WITH LEVEE.....	100
4.3.3.	SCENARIO 3: SHALLOW EXCAVATION WITH LEVEE.....	105
4.3.4.	SCENARIO 4: INTERMEDIATE EXCAVATION WITH LEVEE .....	112
4.4.	SYNTHESIS AND RECOMMENDATIONS.....	121
5.	CONCLUSIONS .....	123
	BIBLIOGRAPHY .....	126
	APPENDIX 1: SATELLITE IMAGES PROCESSING.....	1
	APPENDIX 2: TWO-DIMENSIONAL MODELLING OF DESIGN CONDITION.....	5

## LIST OF FIGURES

Figure 1 World map of the climate change vulnerability index .....	16
Figure 2 Area of interest of Cabo Delgado on the left, logo of Istituto Oikos on the right.....	17
Figure 3 Geolocation of Mozambique on the left, Detail of Cabo Delgado province on the right .....	18
Figure 4 Tomato fields on the left. Cornfields, Banana and coconut trees on the background on the right .	20
Figure 5 Sugarcane .....	20
Figure 6 Rio Maguide catchment and detail of its path .....	20
Figure 7 Rio Maguide during the dry season.....	21
Figure 8 Field survey map.....	22
Figure 9 Field survey map and Flood extent by SNAP elaboration of satellite images .....	23
Figure 10 Evidences of the passage of Cyclone Kenneth in the village of Nanjua (left) and Namuapala (right) .....	23
Figure 11 Map and photos of Nanjua and Nanjua 2 .....	24
Figure 12 Photos from field survey depicting a branch in poor condition.....	24
Figure 13 Photos from field survey depicting a branch in fair condition .....	25
Figure 14 Photos from field survey depicting a branch in good condition .....	25
Figure 15 Photos from field survey depicting a branch in very good condition .....	25
Figure 16 Map of the sub-reach classification.....	26
Figure 17 Map with outflows location.....	26
Figure 18 Outflow 1 detailed with photos.....	27
Figure 19 Outflow 2 detailed with photos.....	28
Figure 20 Provinces of Mozambique .....	30
Figure 21 Precipitation forecast on the left, satellite image of cyclone Kenneth on the right .....	31
Figure 22 Resulting image of the flooded area .....	32
Figure 23 Effect of the Cyclone Kenneth on a village in Cabo Delgado up, damaged bridge down .....	33
Figure 24 Flood map and zoom of the inundated area .....	34
Figure 25 SRTM with cells of 90m size DEM.....	35
Figure 26 SRTM with 30m cell resolution DEM .....	36
Figure 27 ASTER DEM .....	37
Figure 28 AP DEM .....	37
Figure 29 Difference in elevation between AP DEM and SRTM 90 DEM .....	38
Figure 30 AP DEM corrected .....	38
Figure 31 Map of the elevation difference between ASTER DEM and SRTM 90 DEM.....	39
Figure 32 Map of the elevation difference between SRTM 30 DEM and SRTM 90 DEM.....	39
Figure 33 Map of the elevation difference between AP corrected DEM and SRTM 90 DEM .....	40
Figure 34 Area of interest within the entire basin .....	40
Figure 35 Zoom of the elevation difference between ASTER DEM and SRTM 90 DEM in the area of interest .....	41
Figure 36 Statistical distribution of the elevation difference between ASTER DEM and SRTM 90 DEM.....	41
Figure 37 Zoom of the elevation difference between AP DEM and SRTM 90 DEM.....	42
Figure 38 Zoom of the elevation difference between SRTM 30 DEM and SRTM 90 DEM.....	42
Figure 39 Statistical distribution of the elevation difference between SRTM 30 DEM and SRTM 90 DEM....	42
Figure 40 Zoom of the elevation difference between AP DEM and SRTM 30 DEM.....	43
Figure 41 Statistical distribution of the elevation difference between Alos Palsar DEM And SRTM 90 DEM	43
Figure 42 Statistical distribution of the elevation differences between the AP DEM and SRTM 30 DEM.....	44
Figure 43 Basin perimeters and mainstream paths for the four DEMs.....	44

Figure 44 Detail of the different river paths in the area of interest.....	45
Figure 45 SRTM 30 flow network and Mainstream of SRTM 30 and SRTM 90 .....	45
Figure 46 Copernicus soil coverage map .....	46
Figure 47 ESA soil coverage map .....	47
Figure 48 Fao Geonetwork soil coverage .....	47
Figure 49 Logo of TuTiempo .....	48
Figure 50 Logo of CRU Data .....	49
Figure 51 CRU Data world grid on the left and specific cell info on the right .....	49
Figure 52 Meteonorm web interface .....	50
Figure 53 Logo of Meteoblue .....	50
Figure 54 Averaged rainfall data distribution.....	50
Figure 55 Comparison 1961-1990 .....	51
Figure 56 Comparison 2000-2009 .....	51
Figure 57 Comparison 2014-2017 .....	52
Figure 58 Comparison and statistic distribution .....	53
Figure 59 Emergency map, external accessibility.....	54
Figure 60 Emergency map internal accessibility .....	55
Figure 61 DDF and linear regression .....	57
Figure 62 Comparison between frequency and probability for $\Theta=1$ day.....	58
Figure 63 Comparison between frequency and probability for $\Theta=50$ days .....	58
Figure 64 $P(x)$ Gumbel for all the $\theta$ times of measure.....	59
Figure 65 Depth Duration Frequency curves from Meteoblue rainfall data.....	60
Figure 66 Sub-basins referred to Table 16 .....	65
Figure 67 Graphs representing the relationship between increasing basin area and $T_0$ on the left and increasing river length and $T_0$ on the right .....	66
Figure 68 Network of the tributaries of Rio Maguide on the left and detail of the chosen basin on the right .....	66
Figure 69 Hyetograph corresponding to the chosen event.....	67
Figure 70 HEC-HMS icon.....	68
Figure 71 Sub-basin representation in HEC-HMS.....	68
Figure 72 Precipitation and hydrological losses graph.....	69
Figure 73 Screen of HEC-HMS results.....	69
Figure 74 Runoff Hydrograph .....	70
Figure 75 Rainfall-Runoff graph.....	70
Figure 76 Extension of the area of flood modelling .....	71
Figure 77 DEM elevation map of the domain.....	72
Figure 78 Slope map of the domain .....	72
Figure 79 Position of the boundary conditions .....	73
Figure 80 Detail of the section .....	74
Figure 81 Different spatial resolution zones .....	75
Figure 82 iRIC interface and elevation representation of the area of interest .....	77
Figure 83 Flooded area with R2D compared with the flooded area extracted by SNAP .....	79
Figure 84 Flooded area with iRIC compared with the flooded area extracted by SNAP.....	79
Figure 85 iRIC flood extension.....	81
Figure 86 R2D flood extension .....	81
Figure 87 iRIC water depth.....	82
Figure 88 R2D water depth.....	82
Figure 89 Risk map of the studied area .....	84

Figure 90 Risk map.....	85
Figure 91 Sub-reaches of the Rio Maguide after the field survey.....	86
Figure 92 The lake near 25 de Junho (September 2019).....	87
Figure 93 Solution A .....	87
Figure 94 Solution B.....	88
Figure 95 Solution C.....	88
Figure 96 Plan for the one-dimensional models of design conditions.....	89
Figure 97 Section of sub-reach c with excavation depth for each scenario.....	90
Figure 98 Section of sub-reach b with excavation depth for each scenario .....	90
Figure 99 Section of sub-reach a with excavation depth for each scenario .....	90
Figure 100 Sketch of the section of a levee.....	92
Figure 101 River bed condition (same of Figure 8) .....	93
Figure 102 Percentage distribution of discharges in reach b.....	94
Figure 103 Hydrograph, case of peak discharge $Q=47,5 \text{ m}^3/\text{s}$ .....	94
Figure 104 Hydrograph, case of peak discharge $Q=100 \text{ m}^3/\text{s}$ .....	95
Figure 105 Profile of steady case of reach c, Scenario 1, $Q=47,5 \text{ m}^3/\text{s}$ .....	96
Figure 106 Profile of steady case of reach b, Scenario 1, $Q=47,5 \text{ m}^3/\text{s}$ .....	96
Figure 107 Profile of steady case of reach a, Scenario 1, $Q=47,5 \text{ m}^3/\text{s}$ .....	96
Figure 108 Profile of steady case of reach c, Scenario 1, $Q=100 \text{ m}^3/\text{s}$ .....	97
Figure 109 Profile of steady case of reach b, Scenario 1, $Q=100 \text{ m}^3/\text{s}$ .....	97
Figure 110 Profile of steady case of reach a, Scenario 1, $Q=100 \text{ m}^3/\text{s}$ .....	97
Figure 111 Comparison between steady and unsteady case of reach c, Scenario 1, $Q=47,5 \text{ m}^3/\text{s}$ .....	98
Figure 112 Comparison between steady and unsteady case of reach b, Scenario 1, $Q=47,5 \text{ m}^3/\text{s}$ .....	98
Figure 113 Comparison between steady and unsteady case of reach b, Scenario 1, $Q=100 \text{ m}^3/\text{s}$ .....	98
Figure 114 Comparison between steady and unsteady case of reach c, Scenario 1, $Q=100 \text{ m}^3/\text{s}$ .....	99
Figure 115 Hydrographs of the upstream and downstream section of the lateral weir, Scenario1, $Q = 47,5 \text{ m}^3/\text{s}$ .....	99
Figure 116 Hydrographs of the upstream and downstream section of the lateral weir, Scenario1, $Q = 100 \text{ m}^3/\text{s}$ .....	100
Figure 117 Profile of water depth and uniform levees in reach a for the Scenario 2 of table 20, $Q=47,5 \text{ m}^3/\text{s}$ .....	101
Figure 118 Profile of water depth and uniform levees in reach c for the Scenario 2 of table 20, $Q=47,5 \text{ m}^3/\text{s}$ .....	102
Figure 119 Profile of water depth and uniform levees in reach b for the scenario 2 of table 20, $Q=47,5 \text{ m}^3/\text{s}$ .....	102
Figure 120 Profile of water depth and levees in reach a for the Scenario 2 of table 21, $Q=47,5 \text{ m}^3/\text{s}$ .....	103
Figure 121 Profile of water depth and levees in reach c for the Scenario 2 of table 21, $Q=47,5 \text{ m}^3/\text{s}$ .....	103
Figure 122 Profile of water depth and levees in reach c for the Scenario 2 of table 21, $Q=47,5 \text{ m}^3/\text{s}$ .....	103
Figure 123 profile of water depth for $Q = 47,5 \text{ m}^3/\text{s}$ in reach a, Scenario 3 .....	105
Figure 124 profile of water depth for $Q = 47,5 \text{ m}^3/\text{s}$ in reach c, Scenario 3.....	105
Figure 125 profile of water depth for $Q = 47,5 \text{ m}^3/\text{s}$ in reach b, Scenario 3 .....	105
Figure 126 profile of water depth for $Q = 100 \text{ m}^3/\text{s}$ in reach c, Scenario 3.....	106
Figure 127 profile of water depth for $Q = 100 \text{ m}^3/\text{s}$ in reach b, Scenario 3 .....	106
Figure 128 profile of water depth for $Q = 100 \text{ m}^3/\text{s}$ in reach a, Scenario 3 .....	106
Figure 129 hydrographs in the upstream and downstream sections of the weir for $Q = 47,5 \text{ m}^3/\text{s}$ , Scenario 3 .....	107
Figure 130 hydrographs in the upstream and downstream sections of the weir for $Q = 100 \text{ m}^3/\text{s}$ , Scenario 3 .....	107

Figure 131 Profile of water depth and uniform levees in reach b for the Scenario 3 of table 22, $Q=47,5 \text{ m}^3/\text{s}$	108
Figure 132 Profile of water depth and uniform levees in reach a for the Scenario 3 of table 22, $Q=47,5 \text{ m}^3/\text{s}$	108
Figure 133 Profile of water depth and uniform levees in reach c for the Scenario 3 of table 22, $Q=47,5 \text{ m}^3/\text{s}$	108
Figure 134 Profile of water depth and levees in reach b for the Scenario 3 of table 23, $Q=47,5 \text{ m}^3/\text{s}$	109
Figure 135 Profile of water depth and levees in reach a for the Scenario 3 of table 23, $Q=47,5 \text{ m}^3/\text{s}$	109
Figure 136 Profile of water depth and levees in reach c for the Scenario 3 of table 23, $Q=47,5 \text{ m}^3/\text{s}$	109
Figure 137 profile of water depth for $Q = 47,5 \text{ m}^3/\text{s}$ in reach a, Scenario 4	112
Figure 138 profile of water depth for $Q = 47,5 \text{ m}^3/\text{s}$ in reach b,, Scenario 4	112
Figure 139 profile of water depth for $Q = 47,5 \text{ m}^3/\text{s}$ in reach c, Scenario 4	112
Figure 140 profile of water depth for $Q =100 \text{ m}^3/\text{s}$ in reach c, Scenario 4	113
Figure 141 profile of water depth for $Q =100 \text{ m}^3/\text{s}$ in reach a, Scenario 4	113
Figure 142 profile of water depth for $Q =100 \text{ m}^3/\text{s}$ in reach b, Scenario 4	113
Figure 144 Hydrographs in the upstream and downstream sections of the weir for $Q = 100 \text{ m}^3/\text{s}$ , Scenario 4	114
Figure 143 Hydrographs in the upstream and downstream sections of the weir for $Q = 47,5 \text{ m}^3/\text{s}$ , Scenario 4	114
Figure 145 Profile of water depth and levees in reach c for the Scenario 4 of table 26, $Q=47,5 \text{ m}^3/\text{s}$	115
Figure 146 Profile of water depth and levees in reach b for the Scenario 4 of table 26, $Q=47,5 \text{ m}^3/\text{s}$	115
Figure 148 Profile of water depth and levees in reach c for the Scenario 4 of table 27, $Q=47,5 \text{ m}^3/\text{s}$	116
Figure 147 Profile of water depth and levees in reach b for the Scenario 4 of table 27, $Q=47,5 \text{ m}^3/\text{s}$	116
Figure 149 Profile of water depth and levees in reach a for the Scenario 4 of table 27, $Q=47,5 \text{ m}^3/\text{s}$	116
Figure 150 Profile of water depth and levees in reach c for the Scenario 4 of table 28, $Q=100 \text{ m}^3/\text{s}$	118
Figure 151 Profile of water depth and levees in reach b for the Scenario 4 of table 28, $Q=100 \text{ m}^3/\text{s}$	118
Figure 152 Profile of water depth and levees in reach a for the Scenario 4 of table 28, $Q=100 \text{ m}^3/\text{s}$	118
Figure 153 Profile of water depth and levees in reach a for the Scenario 4 of table 29, $Q=100 \text{ m}^3/\text{s}$	119
Figure 154 Profile of water depth and levees in reach b for the Scenario 4 of table 29, $Q=100 \text{ m}^3/\text{s}$	119
Figure 155 Profile of water depth and levees in reach c for the Scenario 4 of table 29, $Q=100 \text{ m}^3/\text{s}$	119



## LIST OF TABLES

Table 1 Climate data for Pemba, Cabo Delgado, Mozambique .....	19
Table 2 Name, dimension and characteristics of the bridges/culverts .....	28
Table 3 Recent history of flooding in Mozambique .....	29
Table 4 Geometrical characteristics of the extrapolated basins .....	44
Table 5 Statistical parameter distribution .....	52
Table 6 Moments for different durations and logarithmic transformation .....	56
Table 7 DDF parameters .....	57
Table 8 KT and a(T) values for different return period .....	59
Table 9 Rainfall depth for different return period .....	59
Table 10 CN values (Handbook of Hydrology, David R. Maidment, 1993) .....	61
Table 11 CN values (WSDOT) .....	62
Table 12 CN estimation from FAO Geonetwork map .....	62
Table 13 CN estimation from Copernicus map .....	63
Table 14 CN estimation from ESA map .....	63
Table 15 CN value of the entire basin .....	63
Table 16 Time of concentration varying the area and the length .....	65
Table 17 CN values for the chosen basin .....	66
Table 18 Descriptions of 13 public domain flow and morphodynamics models available in the iRIC interface .....	76
<i>Table 19 Section width of each section for the different scenarios .....</i>	<i>91</i>
Table 20 Table of uniform levee design .....	101
Table 21 Table of design levee with freeboard of 1m, Scenario 2, Q=47,5 m <sup>3</sup> /s .....	104
Table 22 Table of uniform levee design for Q=47,5 m <sup>3</sup> /s, Scenario 3 .....	109
<i>Table 23 Table of levee design with freeboard of 1m, Q=47,5 m<sup>3</sup>/s, Scenario 3 .....</i>	<i>110</i>
<i>Table 24 Table of uniform levee design for Q=100 m<sup>3</sup>/s, Scenario 3 .....</i>	<i>111</i>
Table 25 Table of levee design with freeboard of 1m for Q=100 m <sup>3</sup> /s, Scenario 3 .....	111
<i>Table 26 Table of uniform levee design for Q=47,5 m<sup>3</sup>/s, Scenario 4 .....</i>	<i>115</i>
<i>Table 27 Table of the levee design with freeboard of 1m, Q=47,5 m<sup>3</sup>/s, Scenario 4 .....</i>	<i>117</i>
<i>Table 28 Table of uniform levee design for Q=100 m<sup>3</sup>/s, Scenario 4 .....</i>	<i>119</i>
Table 29 Table of levee design with a freeboard of 1m, Q=100 m <sup>3</sup> /s, Scenario 4 .....	120
<i>Table 30 Summary of the design scenario. In bold, the cases with excavated volumes largely insufficient to build the levees. ....</i>	<i>121</i>





# 1. INTRODUCTION

## 1.1. SCOPE AND OBJECTIVES OF THE THESIS

During the last century flood events have been increasing in terms of both intensity and frequency, mainly as a result of population growth and climate change. The Cop 21 (Conference of the Parties) meeting in Paris (2015) has strongly highlighted the situation of Africa, the least responsible for the climate changing and the most vulnerable to its effects, in terms of both droughts and floods. According to the Climate Change Vulnerability Index (CCVI), released by Global Risks Advisory firm Maplecroft<sup>1</sup> in 2016, seven of the ten most vulnerable countries in the world, in terms of vulnerability of human populations to extreme climate events and changes in

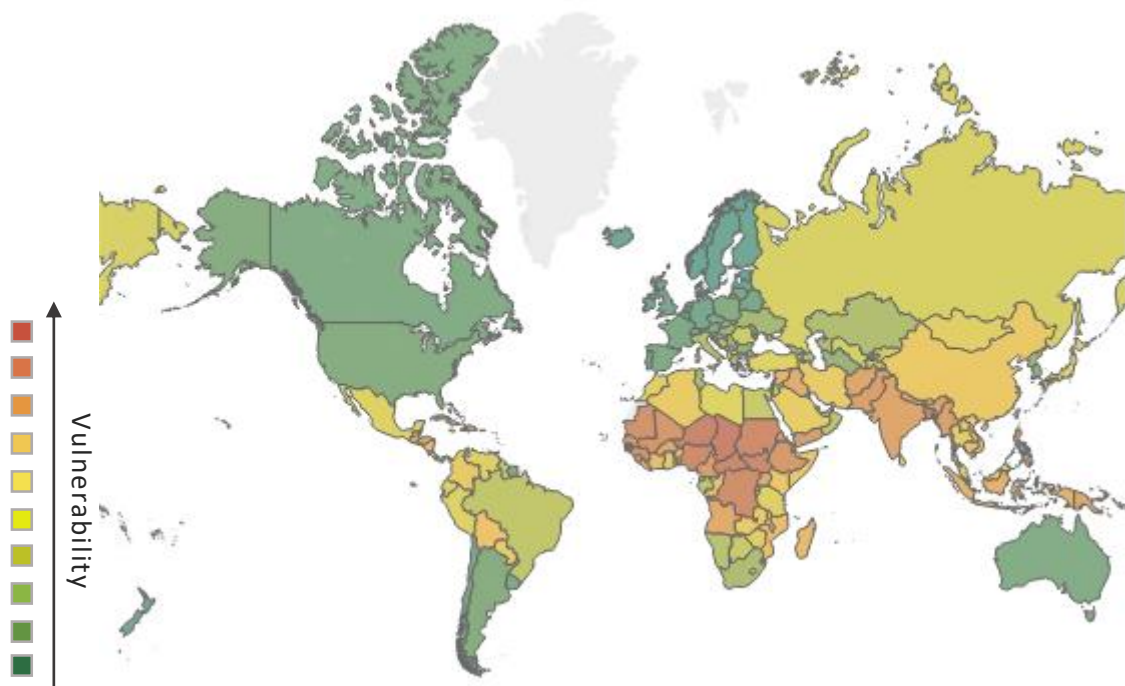


Figure 1 World map of the climate change vulnerability index

During the last 25 years the number of catastrophes linked to climatic events has doubled producing the highest ever recorded death rate in Africa. The main problem is the impossibility of the African countries to face this change; a new study coordinated by the Overseas Development Institute (ODI) and the Climate and Development Knowledge Network (CDKN)<sup>2</sup> has analysed the reasons behind this figure. According to the study<sup>3</sup> the companies and the institutions operating in these areas do not manage to take into account the long-term consequences of climate change due to many factors: first of all, the institutions are focused on many other challenges, such as the elimination of poverty and the promotion of the access to the primary and secondary education, that force the decision makers to take limited time horizons; secondly, the long-term climate issues badly fit the economic Sub-Saharan context that always tries to reach an immediate profit; moreover, the lack of skills and financial resources leads to stagnation (in this sense, a great influence is given by the lack of communication between the producers and the users of the climate information).

<sup>1</sup> [www.maplecroft.com](http://www.maplecroft.com)

<sup>2</sup> [www.odi.org/projects/2202-climate-and-development-knowledge-network-cdkn](http://www.odi.org/projects/2202-climate-and-development-knowledge-network-cdkn)

<sup>3</sup> <https://cdkn.org/future-climate-africa/#intro>

A key role in facing the climate change is played by humanitarian groups and environmentalists that stress the UN to cooperate in order to concretely find solutions. The main message that the NGOs want to send to the mighty is to inaugurate a new course of the green economy trying to match environmental and social sustainability, and to defend nature in order to protect the right to life of everyone.

This is also the aim of *Istituto Oikos*, a non-profit organization that wants to preserve the biodiversity of some countries in Europe and in the southern hemisphere: “We work for a responsible management of the natural resources and for the diffusion of more sustainable models to be used as instruments for a social and economic development and to fight poverty.”<sup>4</sup>

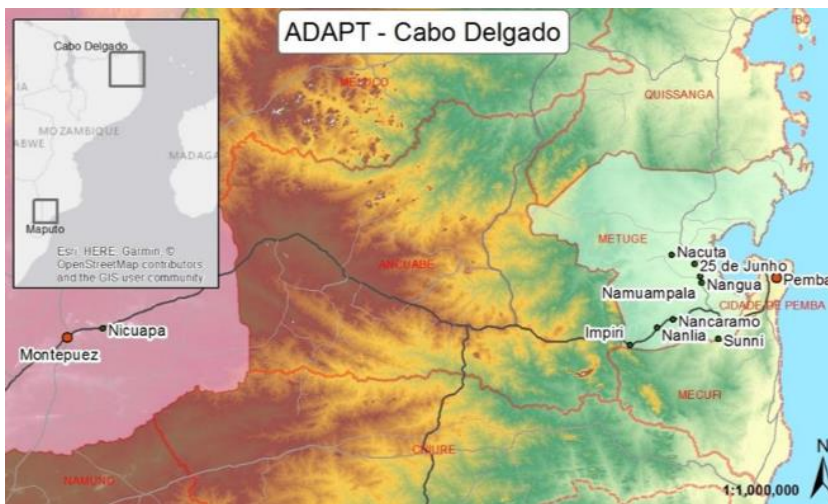


Figure 2 Area of interest of Cabo Delgado on the left, logo of *Istituto Oikos* on the right

Following this principle *Istituto Oikos* is working on a variety of projects concerning different fields. One of this projects is called *ADAPT*, financed by the Italian Cooperation (AICS) in Mozambique. This project is developed over three years (2017-2020) in two provinces of Mozambique: Cabo Delgado and Maputo (Figure 2). It has 4 areas of intervention that develop themselves in parallel and that are integrated with each other:

- water sector: use and management of the water resources with agricultural purpose in the area;
- rural sector: definition and implementation of training activities for the local farmers in order to spread more sustainable and profitable techniques;
- economic sector: spread the idea that associations of farmers working together can lead to more profitable and efficient results;
- social sector: spread, through communities and schools, the positive result that the project has achieved.

With reference to the above, during the project it has become evident that the farmers’ activity is particularly prone to the negative effects of climate change. During the rainy season, vast agricultural areas are flooded by the neighbouring rivers, whose conveyance has progressively reduced in time, also as a consequence of the lack of river maintenance or restoration works. Therefore, *Istituto OIKOS* has sought the cooperation of the Politecnico di Milano to strengthen the *ADAPT* activities related to flood impacts on agriculture. The first objective of this thesis is thus to perform flood hazard assessment for the area of the Rio Maguide, in the province of Cabo Delgado in northern Mozambique. Furthermore, a second objective is related to proposing appropriate interventions to mitigate the flood risk.

<sup>4</sup> <https://www.istituto-oikos.org/>



Mozambique is divided into ten provinces and one capital city with provincial status; the provinces are subdivided into 129 districts that are further divided into 405 “Postos Administrativos” (administrative posts). As mentioned, this thesis is related to the province of Cabo Delgado that is the northernmost province in Mozambique, located within the coastal plain. It has an area of 82.625 km<sup>2</sup> and a population of 2.333.278 (2017)<sup>7</sup>; the capital is Pemba and other important cities include Montepuez and Mocimboa da Praia (*Figure 3*).

The majority of inhabitants in the province relies on subsistence (mainly rainfed) agriculture, which, given the geographical location, is hindered by poor market access and limited infrastructure, including roads. Recent research has ranked Cabo Delgado as one of the poorest provinces in Mozambique (Fox et al., 2005) with the highest prevalence of stunting in the country (FAO, 2010).

The climate of Cabo Delgado is sub-humid and characterized by a long dry season (May–November) and a rainy season (December–April). Nevertheless, in the northern area the temperatures are fairly stable throughout the year and decrease a bit from May to August, when a cool air can arrive from the south, especially in inland areas. Annual rainfall height in the province is 800–1000 mm, though the intensity of rainfall sometimes results in heavy flooding throughout the province. The following table (*Table 1*) shows the average trend of rainfall and temperature during the year for the city of Pemba.

*Table 1 Climate data for Pemba, Cabo Delgado, Mozambique* <sup>8</sup>

Month	Average Daily Min Temperature (°C)	Average Daily Max Temperature (°C)	Average Total Rainfall (mm)	Average Number of Rain Days
Jan	23.2	30.8	146.4	11.0
Feb	23.1	30.9	156.0	10.4
Mar	22.8	30.8	202.2	12.6
Apr	22.0	30.4	122.0	9.4
May	20.3	29.5	32.4	3.2
Jun	18.6	28.3	15.0	2.4
Jul	18.2	27.7	11.3	1.6
Aug	19.6	27.8	7.9	1.2
Sep	19.8	28.7	2.2	0.6
Oct	21.6	29.5	11.3	1.5
Nov	23.0	30.4	41.6	3.6
Dec	23.5	30.8	124.5	8.4

The river under study is called Rio Maguide and flows through the districts of Ancuabe and Metuge-Pemba. The main crops incorporated into the cropping system used in these districts are maize, cowpea, sesame and pigeon pea. Lablab and mucuna are also grown; these are perennial legumes of the Fabaceae family native to Africa, which are widely grown in the tropics for their edible seeds and pods. Strictly focusing on the area of interest, through fields surveys following the path of Rio Maguide, the wide presence of tomatoes, cucumber, sugarcane and cassava manioc crops has also been noticed. Moreover, the whole area is surrounded by coconut, banana and mango trees (*Figure 4-5*).

<sup>7</sup> <https://web.archive.org/web/20140924062250/http://www.geohive.com/cntry/mozambique.aspx#>

<sup>8</sup> <http://worldweather.wmo.int/en/city.html?cityId=120>





Figure 4 Tomato fields on the left. Cornfields, Banana and coconut trees on the background on the right



Figure 5 Sugarcane

The region covered by these two districts is characterized by the presence of streams and rivers that spring from the inner region of the highlands and becomes flatter as they approach the ocean. The Rio Maguide rises in the inner region of the highlands and flows into the Indian Ocean after crossing the districts of Ancuabe and Metuge-Pemba (Figure 6).



Figure 6 Rio Maguide catchment and detail of its path



The river length is 130 km, with a difference in altitude of 600 m between the springs and the outlet into the sea. The path of the river is quite well defined and confined for most of its course but, in the last 15 km, it braids creating multiple sub-reaches; some of the latter are completely filled with sediment (*Figure 7*), due to the fact that during the wet season the river carries a large amount of sand from upstream to downstream; this sediment deposits due to the lower slope of the final reaches. Moreover, during high flows, the bank erosion is very high and sediment transport is further increased; consequently, during the dry season, this large quantity of sediments and sand deposits causing the burying of the river in this region.



*Figure 7 Rio Maguide during the dry season*

It is also worth noting that, during a long part of the wet season, the area is flooded and is nearly impossible to distinguish the river path from the flooded surfaces. The documentation and the maps available on the web and in the literature regarding the area of study has not been sufficient to perform a complete analysis of the network of sub-reaches considering their path, dimensions, type of soil, bank vegetation and interaction with the neighbouring villages. To fill those gaps, a mission to Mozambique has been undertaken. The mission lasted two weeks, during which daily field surveys have been performed and new data have been collected. The details of the mission are shown in the following of this chapter.

### 1.2.1 THE MISSION

The field trip has lasted two weeks. Observations have been collected walking along several sub-reaches of the Rio Maguide carrying a GPS receiver that enabled to track our route on the map and to geolocate crucial spots (presence of bridges, change of the soil type, etc). *Figure 8* shows all the paths along which we have been walking during the different days of mission.

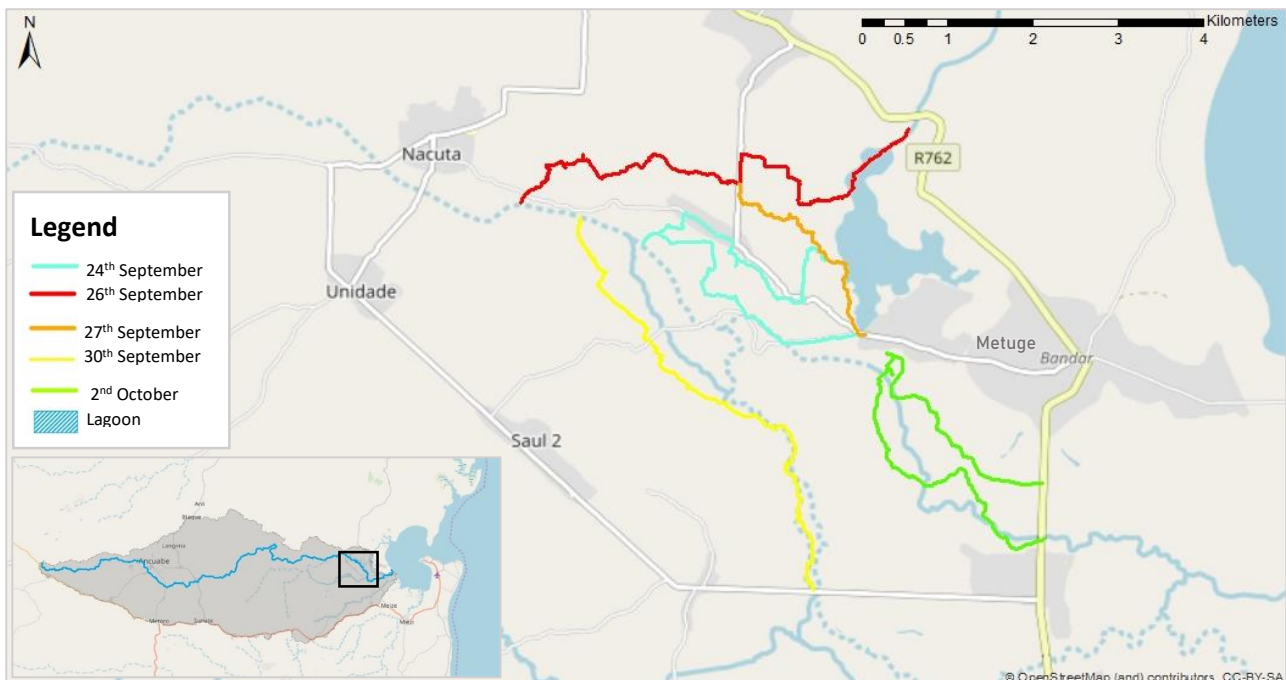


Figure 8 Field survey map

The paths highlighted in the previous figure are just a part of all the possible sub-reaches that are created during the wet season; the decision of exploring these specific routes was based on different considerations:

- an initial sketch of the preferential way of flooding water had been extrapolated after a preliminary study of the area through a procedure that extracts the river network from a GIS calculation based on a DEM (the details on the DEM creation will be given in chapter 2). Consequently, the field survey has been organized in order to cover those flooded branches.
- Evidences of the preferential ways of running water had also been obtained processing satellite images taken during/after the flood caused by cyclone Kenneth using a software called SNAP; these are also depicted in *Figure 10*. The SNAP processing procedure is detailed in *Appendix 1*. Consequently, the field survey has been organized in order to cover those flooded branches.
- Finally, have been evidenced, from satellite images, some sub-reach paths that disappear and reappear downstream. In this case the field survey was necessary in order to collect soil properties of the buried zones and to identify a possible way in need of future digging.

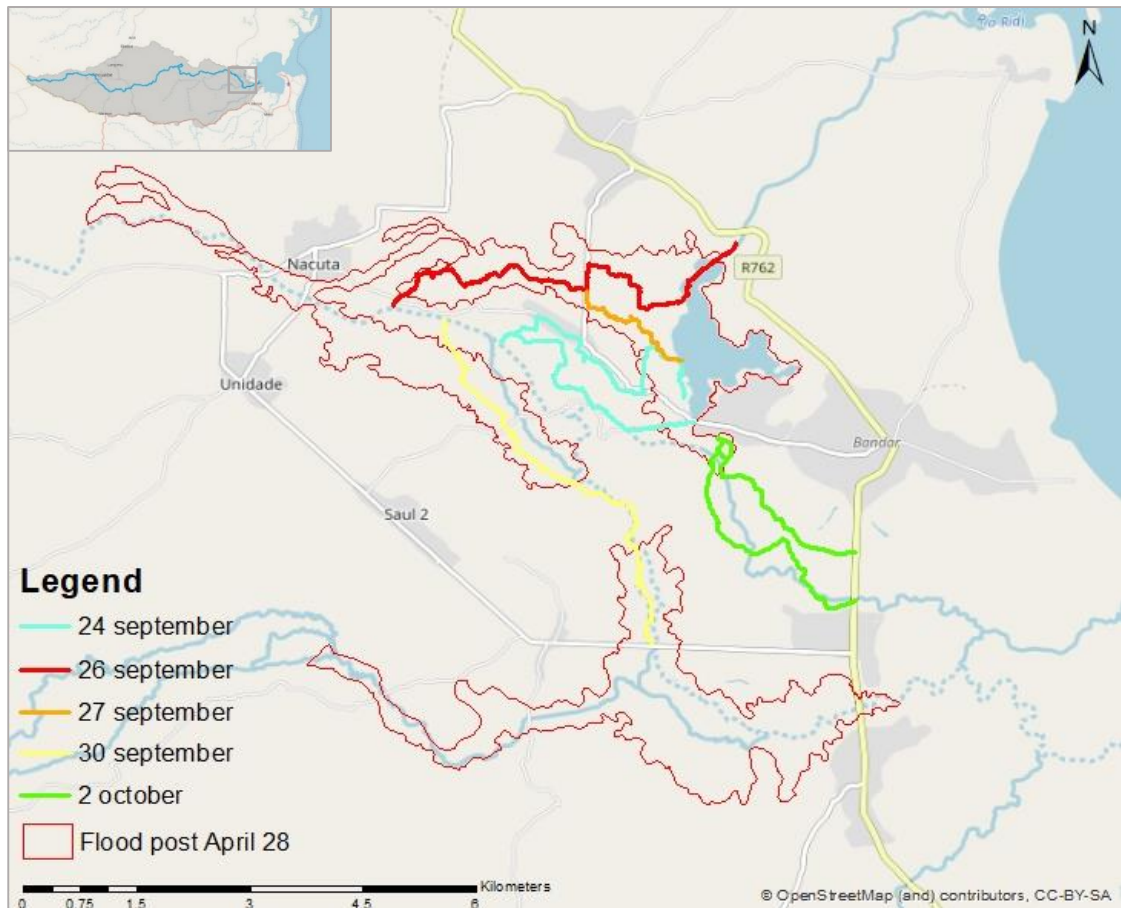


Figure 9 Field survey map and Flood extent by SNAP elaboration of satellite images

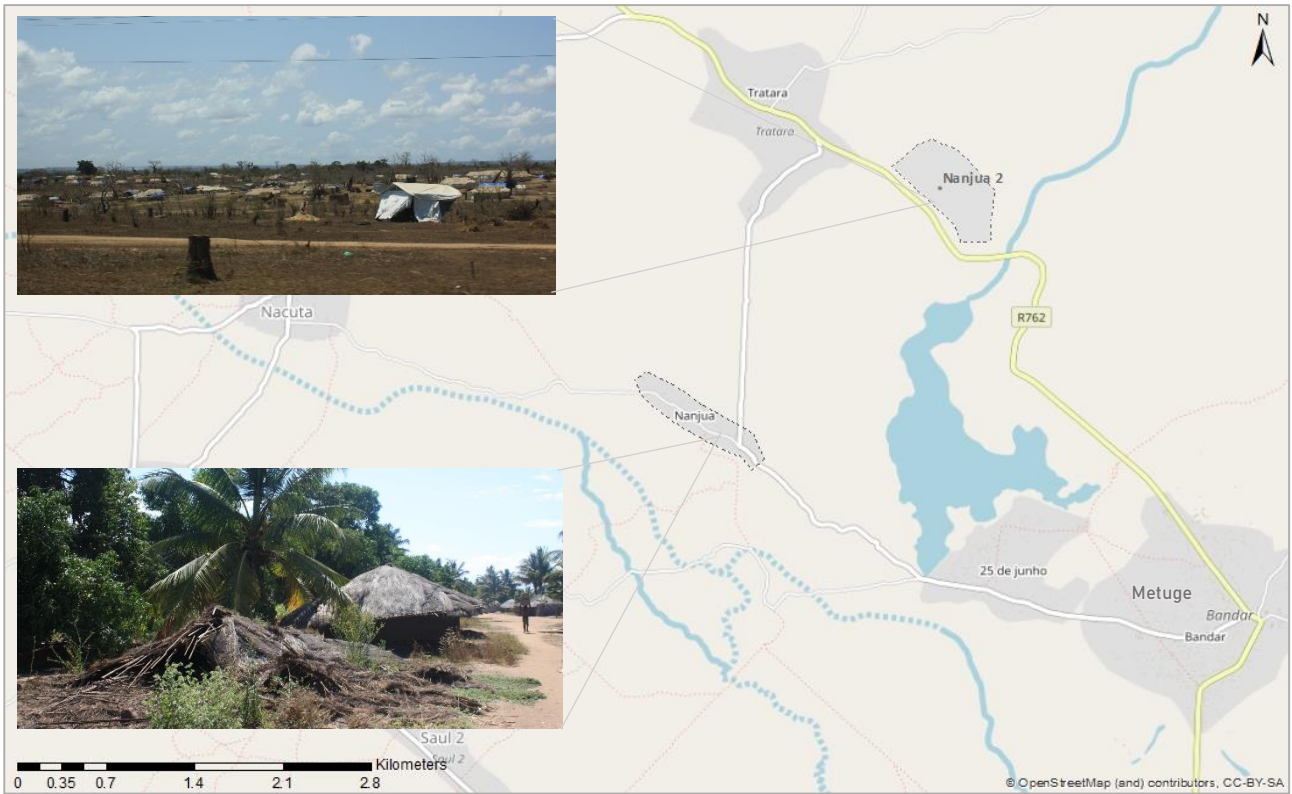
A second purpose of the mission was that of collecting available data regarding the past events, their intensity and GPS localization; to do that, local people of the villages neighbouring the river have been interviewed. Finally, a large photographic documentation has been collected, with the aim of validating the model of the flooded area and the water depth elevation extrapolated from it, by comparing them with the traces left by past events and with the memory of the inhabitants



Figure 10 Evidences of the passage of Cyclone Kenneth in the village of Nanjua (left) and Namuapala (right)



Besides all the quantitative data collected about past events and their intensity, the interview to the population brought out that the village of Nanjua has been completely destroyed by Cyclone Kenneth and the reconstruction of Nanjua 2 has started on the road connecting Metuge and the village of Tratara (*Figure 11*)



*Figure 11 Map and photos of Nanjua and Nanjua 2*

Finally, photographic documentation has been also taken of the vegetation and of the soil covering the investigated area. Besides the general evaluation of the type of crops surrounding the area done above to contextualize the problem, an evaluation of the different river bed soils, jointly with the presence or absence of banks and the presence or absence of water in it has been done. The results brought out four classes outlined as follows:

- Poor condition: bed is densely vegetated, water is present in few spots, banks are absent (*Figure 12*).



*Figure 12 Photos from field survey depicting a branch in poor condition*

- Fair condition: narrow bed made of ground, water is present in few spots, banks are present in interval but with limited height (*Figure 13*).



*Figure 13 Photos from field survey depicting a branch in fair condition*

- Good condition: large bed made of sand, no water, banks are almost absent but digging is easy (*Figure 14*).



*Figure 14 Photos from field survey depicting a branch in good condition*

- Very good condition: bed in good state, running water is present, well dug with evident banks (*Figure 15*).



*Figure 15 Photos from field survey depicting a branch in very good condition*



Each sub-reach is identified by different classes, this means that the type and the importance of future interventions could be different even on the same reach. This classification represents the first step to be taken into consideration in the decision-making process of possible flood mitigation measures. The result is shown in the following map (Figure 16).

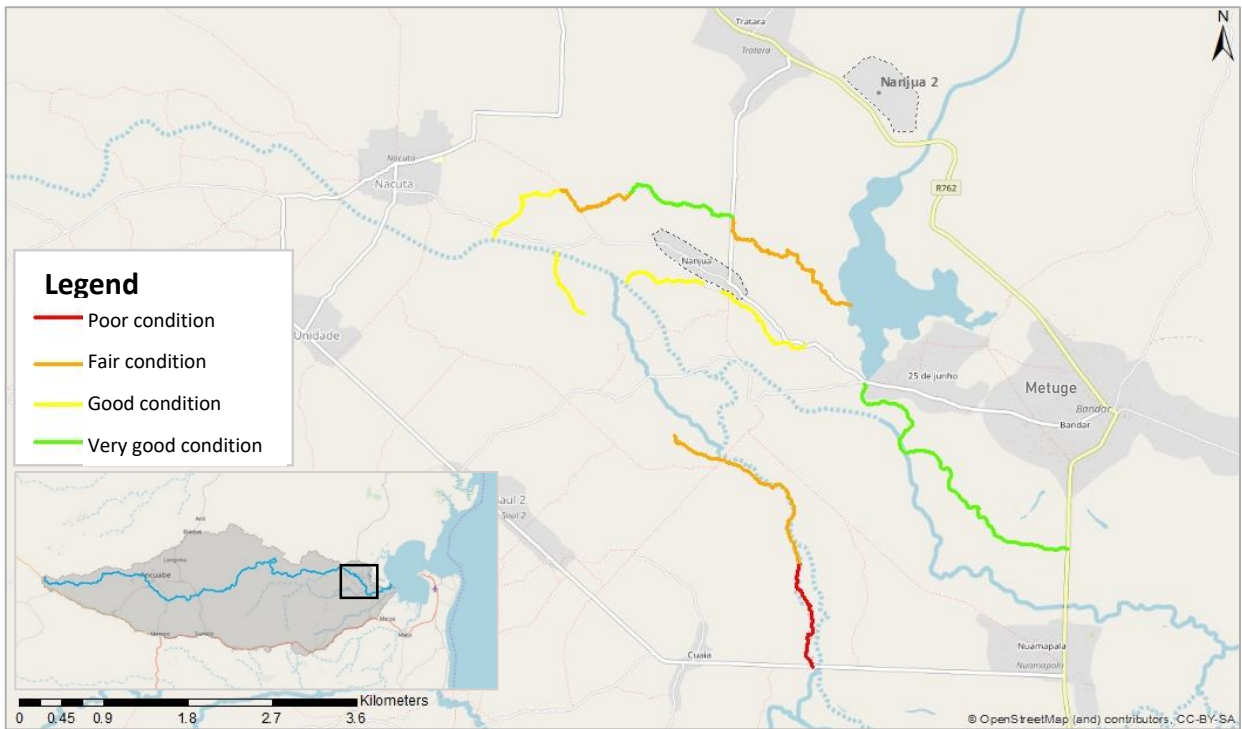


Figure 16 Map of the sub-reach classification

The last day of the mission was spent collecting data about bridges and culverts that are present along two roads visible in Figure 17. These roads will delimit the hydraulic models described in chapters 3 and 4,

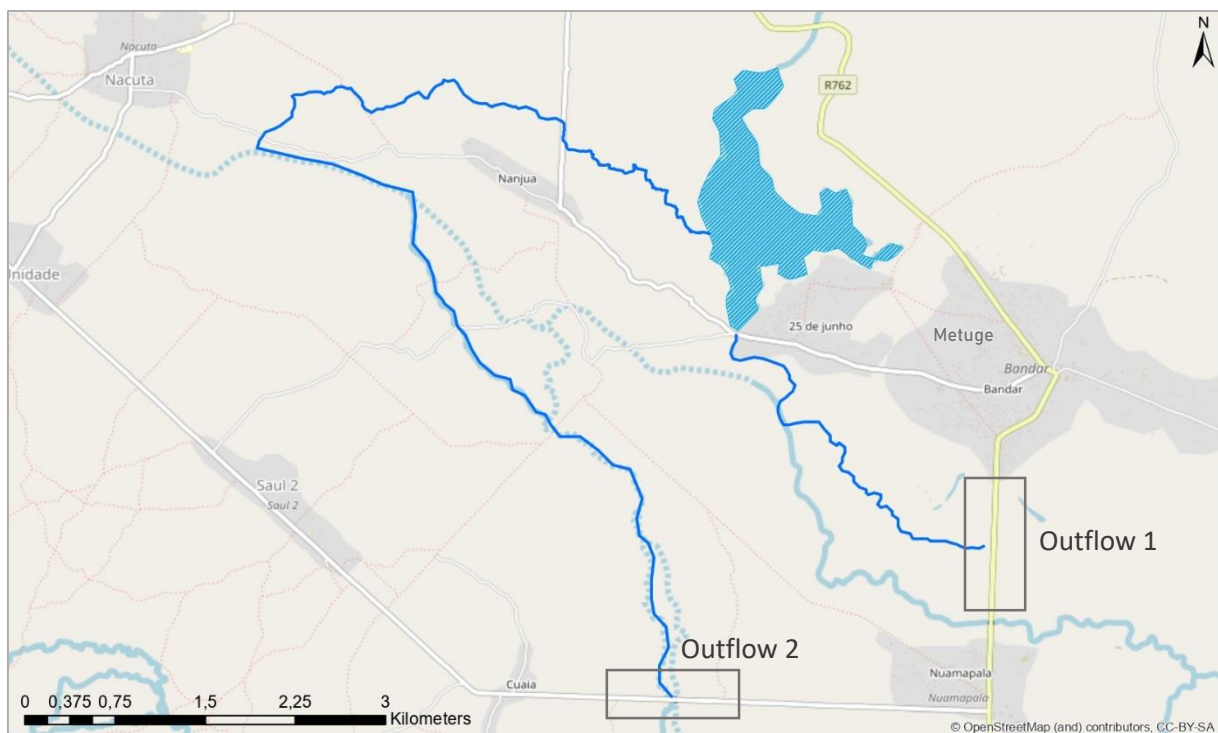


Figure 17 Map with outflows location

therefore information on the crossing structures will support the creation of the downstream boundary conditions of the models.

Multiple openings are present due to the fact that the river spread in different sub-reaches, as detailed above; so, in order to define the dimensions of the output sections, it was necessary to measure all the bridges and culverts pertinent to the position of the two boundary conditions.

All the outflows of the various sub-reaches have been named, measured and geolocated along the boundary condition line. A photographic documentation was crucial to identify the differences among the various bridges and culvert. All the data are organized in *Table 2* while the location on the map and the relative photos are shown in *Figures 18* and *19*.



Figure 18 Outflow 1 detailed with photos



Figure 19 Outflow 2 detailed with photos

Table 2 Name, dimension and characteristics of the bridges/culverts

Name	type	H [m]	B [m]	d [m]	n° of tubes	state
p1	bridge	1,40	6,40	-	-	no obstructions
p2	bridge	1,40	3,00	-	-	no obstructions
p3	bridge	1,33	2,83	-	-	no obstructions
p4	culvert	-	-	2,00	4	no obstructions
p5	bridge	3,95	29,70	-	-	no obstructions
u1	culvert	-	-	0,80	3	partially blocked
u2	culvert	-	-	0,80	3	blocked
u3	culvert	-	-	0,80	1	blocked
u4	culvert	-	-	0,80	1	blocked
u5	bridge	1,20	1,50	-	-	partially blocked
u6	bridge	1,20	2,30	-	-	partially blocked
u7	bridge	2,50	5,50	-	-	no obstructions
u8	bridge	1,90	2,30	-	-	no obstructions
u9	culvert	-	-	0,50	6	partially blocked
u10	culvert	-	-	1,20	3	no obstructions
u11	culvert	-	-	1,20	6	partially blocked
u12	culvert	-	-	1,00	3	no obstructions



## 1.3.PAST EVENTS

### 1.3.1. MAIN PAST EVENTS HITTING THE AREA OF INTEREST

Mozambique is a coastal country, located in a region that is cyclically threatened by extreme events like floods, droughts, tropical cyclones, earthquakes, and disease epidemics. Over the past decades Mozambique has been subject to a conspicuous number of large flood events. *Table 3* provides details of the major flood events hitting the country in the past 40 years. The floods that occurred in 2000 were the worst in the last 150 years causing almost 800 deaths and serious damage to crops, livestock, rural housing, communication infrastructure and business assets<sup>9</sup>. The more recent cyclone Idai (2019) caused damages to crops, people and infrastructures that had approximately the same dimension of those for the event of 2000.

*Table 3 Recent history of flooding in Mozambique*

<b>Year</b>	<b>Location</b>	<b>Consequence</b>
1975	Southern Mozambique (Limpopo and Incomati Rivers)	75 000 people affected
1977	Southern Mozambique (Limpopo River)	300 casualties, 40 000 people displaced, 400 000 people affected
1978	Central Mozambique (Zambeze River)	50 casualties, 220 000 people affected
1981	No region given	500 000 people affected
1985	Southern Mozambique (Maputo Province)	500 000 people affected
1988	Central and southern Mozambique (Sofala, Zambezia and Maputo Provinces)	12 000 people displaced
1996	Central and southern Mozambique (Zambeze, Incomati, Umbeluzi, Limpopo, Pungue and Buzi Rivers)	11 casualties and 200 000 people affected
1997	Central and northern Mozambique (Sofala, Tete, Zambezia and Manica)	87 casualties and 300 000 to 400 000 people affected
1998/1999	Central and southern Mozambique (Sofala, Igambane, Gaza, Nampula, Zambezia Provinces)	15 casualties and 400 000 people affected
2000	Central and southern Mozambique	800 casualties and, 650 000 people displaced, 4.5 million people affected
2001	Central Mozambique (Sofala, Manica and Zambezia Provinces)	200 casualties and, 220 000 people displaced, 550 000 people affected
2003	Central and Northern Mozambique (Nampula and Zambezia Provinces)	15 casualties and, 200 000 people displaced
2004	Central Mozambique (Sofala)	1000 displaced
2005/2006	Central and southern Mozambique (Nampula, Sofala, Zambezia and Gaza Provinces)	22 casualties and 9000 people left homeless
2007	Central and northern Mozambique (Tete, Zambezia, Manica and Nampula Provinces)	46 casualties and, 165 000 people displaced
2008	Central Mozambique (Zambezia and Nampula Provinces)	100 000 people affected
2012/2013	Central and southern Mozambique (cholera spreads through the whole country)	135 casualties and 170 000 people displaced
2019 March <b>Idai</b>	Central and northern Mozambique (Tete, Zambezia and Niassa Provinces)	600 casualties and 70 000 people displaced
2019 April <b>Kenneth</b>	Northern Mozambique (Cabo Delgado Provinces)	45 casualties and 30 000 people displaced

For the region under study, Cabo Delgado, the most important events were those registered in 1997 and 2012/2013 (due to the diffusion of the cholera), even if the most catastrophic is the more recent one caused by cyclone Kenneth in April 2019 (a specific sub-section 1.3.2 will be devoted to this event).

<sup>9</sup> Christie and Hanlon, 2001

## Flood in 1997<sup>10</sup>

As a consequence of an active Intertropical Convergence Zone (ITCZ) tropical cyclogenesis was quite common over the southern Indian Ocean throughout the month of February 1997, especially over the Mozambique channel. Earlier, during the same year, the country had been affected by cyclone Josie, but it was the tropical storm Lisette that caused major damages bringing additional flooding to the nation. The Nampula province was severely flooded and many infrastructures were damaged. Mozambique rainfall records ranged from 60 mm to 200 mm in few days. The Sofala and Inhambane Provinces were also badly affected, then the storm moved towards the northern Mozambique affecting also the province of Cabo Delgado at the extreme north-east.

## Flood in 2013

The heavy rains in January 2013 lasted more than one week and hence increased significantly the hydrometric levels of the main rivers. The situation was already critical due to the intense rainfalls that had struck the country starting from October 2012 and with these further worsening of the precipitation intensity the impact of the floods in communities rapidly increased and the Government of Mozambique (GoM) declared an institutional Orange emergency Alert on 12 January 2013, which was upgraded to Red Alert on 22 January 2013. As can be read in the description of the event drawn up for “Mozambique Floods 2013 – Consolidated Early Recovery Strategy” written by the Humanitarian Country team, “[...] *the Maputo City, Gaza, Zambezia and Inhambane Provinces were the most affected by the floods, but also other areas such as Nampula, Niassa and Cabo Delgado were also affected. Additionally, in Cabo Delgado a cholera outbreak kept Government and partners actively working to monitor and respond to any new cases and mitigating the potential for additional cases*”. The alert was lifted by the Disaster Management Technical Council (CTGC) only on 19 April 2013; this long period of alert (three months) gives an idea of the dimension of the devastating effects that the heavy rains and the consequent floods had on the population in terms of damages to house, livelihoods like agriculture, cattle and trade, to basic social services such as schools, healthcare centres and to community infrastructures like roads, bridges, electricity and drainage systems. The balance saw 119 people losing their lives, with 17 additional deaths due to the cholera outbreak in Northern provinces.



Figure 20 Provinces of Mozambique

<sup>10</sup> "October 1996-April 1997: Southern Africa rainy season". *United States National Oceanic and Atmospheric Administration*. United States Climate Prediction Center. 1997. Retrieved August 16, 2013.

### 1.3.2. CYCLONE KENNETH

A timeline of this event, occurred in April 2019, is provided below.

**17<sup>th</sup> of April:** the Météo-France office on La Réunion (MFR) begins monitoring a vortex to the north of Madagascar. During the following day of monitoring MFR noticed a significant increase in the deep convection that, as we can read on the article *Deep thought on deep convection*<sup>11</sup> “[...] it refers to the thermally driven turbulent mixing that moves air parcels from the lower to the upper atmosphere.” In the meanwhile, the MFR began issuing advisories designating it as Tropical Disturbance.

**22<sup>nd</sup> of April:** the Joint Typhoon Warning Centre (JTWC) issued a tropical cyclone formation alert, noting that the disturbance was located in a favourable environment with low vertical wind shear and warm sea surface temperatures of 29-30 °C.

**23<sup>rd</sup> of April:** the JTWC began issuing warnings on the system, classifying it as Tropical Cyclone. After few hours the MFR upgraded the system to a tropical depression assigning the name *Kenneth* to the storm. At that point Kenneth started increasing its intensity and the JTWC noticed the formation of an eye, typical of very intense storms.

**24<sup>th</sup> of April:** the MFR upgraded the system from moderate to severe tropical storm and in few hours Kenneth strengthened into the equivalent of a Category 3 hurricane on the Saffir–Simpson hurricane wind scale. The *Hahaya International Airport* on the Comoros island of Grand Comore registered winds of 36 knots.

**25<sup>th</sup> of April:** at 06:00 UTC, Kenneth reached peak intensity, with 10-minute sustained winds of 215 km/h. After few hours the JTWC estimated that Kenneth peaked as a Category 4-equivalent tropical cyclone, with 1-minute sustained winds of 230 km/h and started approaching the Mozambique coastline. With this movement the system started decrease its velocity due to the eyewall replacement cycle and the frictional effects of land interaction. Later that same day at 13:15 UTC, Kenneth made landfall in Mozambique, just north of Pemba, with 1-minute sustained winds of 220 km/h.

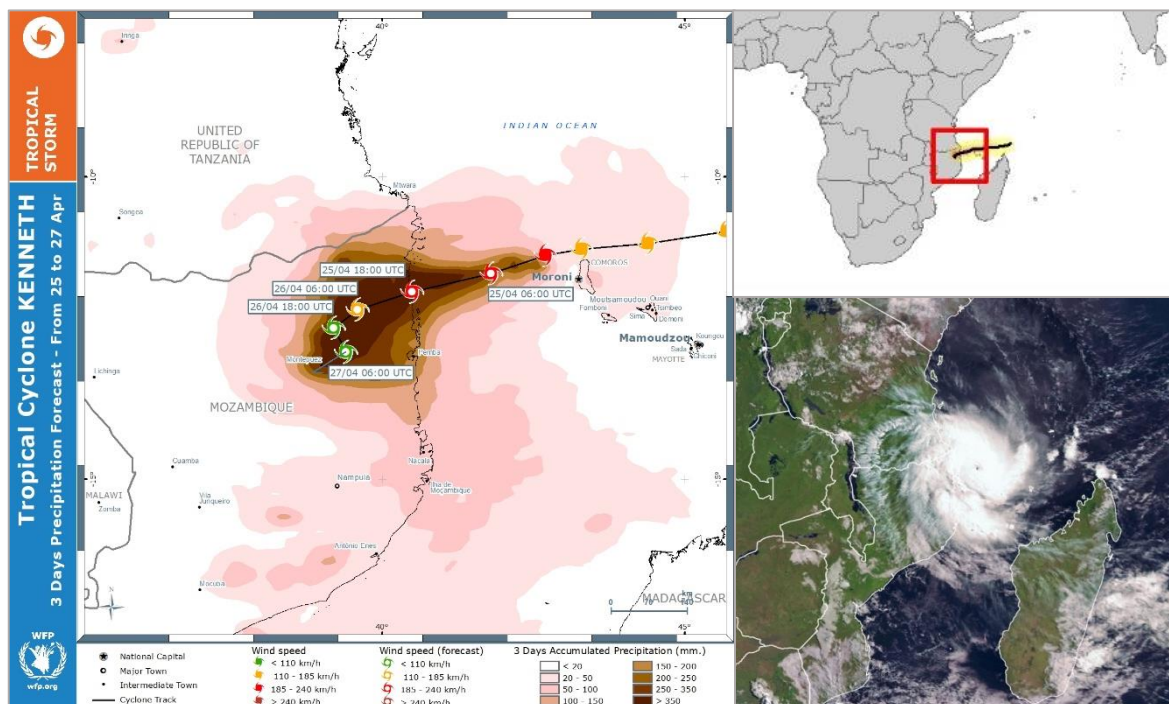


Figure 21 Precipitation forecast on the left, satellite image of cyclone Kenneth on the right

<sup>11</sup> <https://blogs.ei.columbia.edu/2009/03/01/deep-thoughts-on-deep-convection/>

**26<sup>th</sup> of April:** at midnight the MFR issued its last warning on Kenneth, reporting 10-minute sustained winds of 65 km/h (40 mph), while the system was located about 110 km inland in Mozambique. From that moment the cyclone Kenneth gradually decreased its intensity.

**29<sup>th</sup> of April:** Kenneth dissipated by 12:00 UTC.

As can be read on the Flash Update No. 5<sup>12</sup> on Cyclone Kenneth released by UNOCHA (United Nations Office for the Coordination of Humanitarian Affairs):

*“More than 570 mm of rain has been recorded since 25 April in Pemba, the highest in Cabo Delgado. The area between Pemba (Mozambique) and Dar er Salaam (Tanzania) is expected to receive significant rainfall over the next four days meaning that people already impacted by the cyclone face the prospect of being caught in torrential rains. [...] The flood peak for rivers in the region has not yet occurred and is generally expected to take place between 30 April and 2 May”.*

This was a correct forecast: the following intense rainfall provoked the cut-off of the city of Pemba due to the flooding of different bridges, cropping fields washed away in few hours and the cutting of almost every kind of communications.

As already mentioned above, SNAP 6.0 software was used to figure out the extent of the flooded area. Some simple passages, explained in *Appendix 1*, were implemented in the processing of satellite images comparing pre to the immediate post event. The image chosen dates back to 28<sup>th</sup> of April 2019; on this date the flood had not reached its maximum extent yet but, from the processing of the following freely available image (dated 4<sup>th</sup> of May 2019), no traces of flood were visible. The product is shown in *Figure 22*.

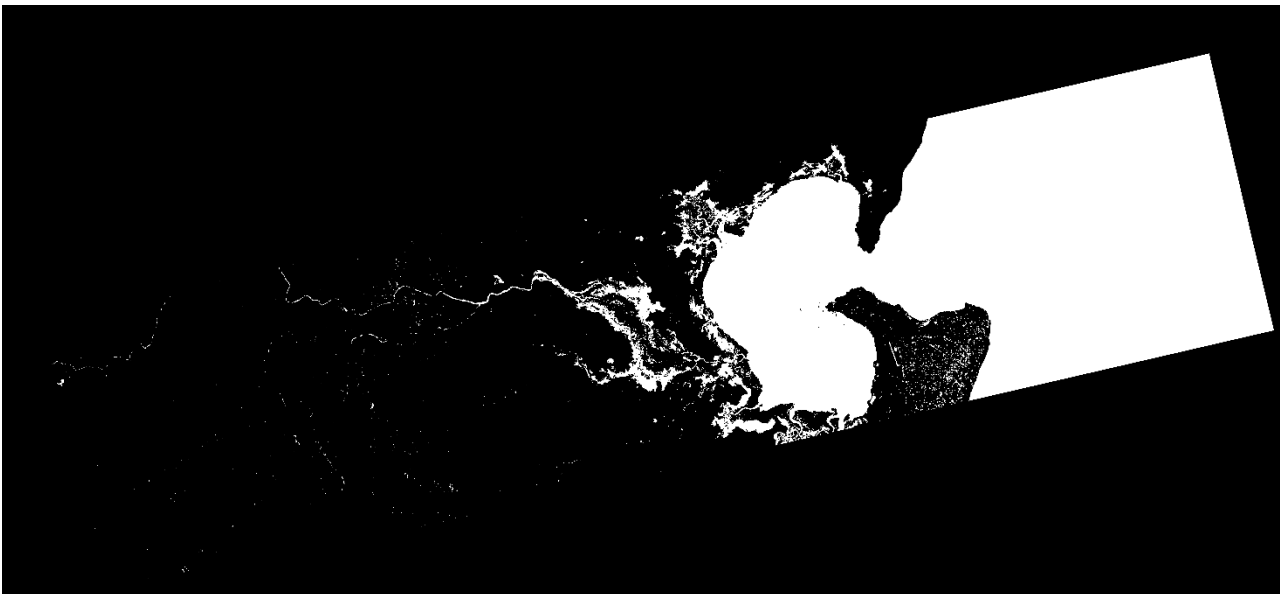


*Figure 22 Resulting image of the flooded area*

On 28<sup>th</sup> of April, the Emergency Relief Coordinator, Mark Lowcock, released 13 million \$ from the UN Central Emergency Response Fund to provide life-saving food, shelter, health, water and sanitation assistance to people affected by Tropical Cyclone Kenneth in Comoros (3 million \$) and Mozambique (10 million \$). World Food Programme (WFP), UNICEF, Save the Children, Oxfam and CARE cooperated in order to deliver basic necessities.

<sup>12</sup>[https://reliefweb.int/sites/reliefweb.int/files/resources/ROSEA\\_20190429\\_SouthernAfrica\\_TCKenneth\\_FlashUpdate5\\_for%20upload.pdf](https://reliefweb.int/sites/reliefweb.int/files/resources/ROSEA_20190429_SouthernAfrica_TCKenneth_FlashUpdate5_for%20upload.pdf)

In order to size the impact of the Cyclone Kenneth and to summarize its effects in term of numbers, Unicef Mozambique drafted a list<sup>13</sup> of the consequences, dated on July, as follows:

- 373 thousand people in need of humanitarian services
- 200 thousand children in need of humanitarian services
- Death toll: 45
- Injured: 94
- Affected provinces: Cabo Delgado (9 districts) and Nampula (5 districts)
- Number of people in need of assistance: 286,282 (half of which were children)
- Confirmed cholera cases: 282
- Houses destroyed: 45,000
- People displaced: 3,000
- Crop damage: 55,488 ha
- Classrooms affected: 473
- Students affected: 41,046
- Health facilities affected: 19



*Figure 23 Effect of the Cyclone Kenneth on a village in Cabo Delgado up, damaged bridge down*

These numbers give just an approximate idea of the impact and the devastation that followed Kenneth, especially considering that, just six weeks before, the country had been struck by cyclone Idai, another important storm whose dimensions were even bigger and whose trails had to be added to those listed above. Idai did not hit directly the Province of Cabo Delgado, as a matter of fact the most damaged city was Beira in the Province of Sofala in central Mozambique, but, to give an idea of the size of the impact, is worth knowing that the total death toll was approximately of 600 people and the injured were about 1600.

Finally *Figure 24* presents a map obtained overlapping the flood extent extracted from SNAP and the critical facilities. Open Street map has been used to download the road network, while other information about the facilities and the dislocation of the emergency point and services has been taken from already processed map from the Copernicus Emergency service. The location of the bridges was taken from field investigation or by Google Earth.

---

<sup>13</sup> <https://www.unicef.org/mozambique/en/cyclone-idai-and-kenneth>



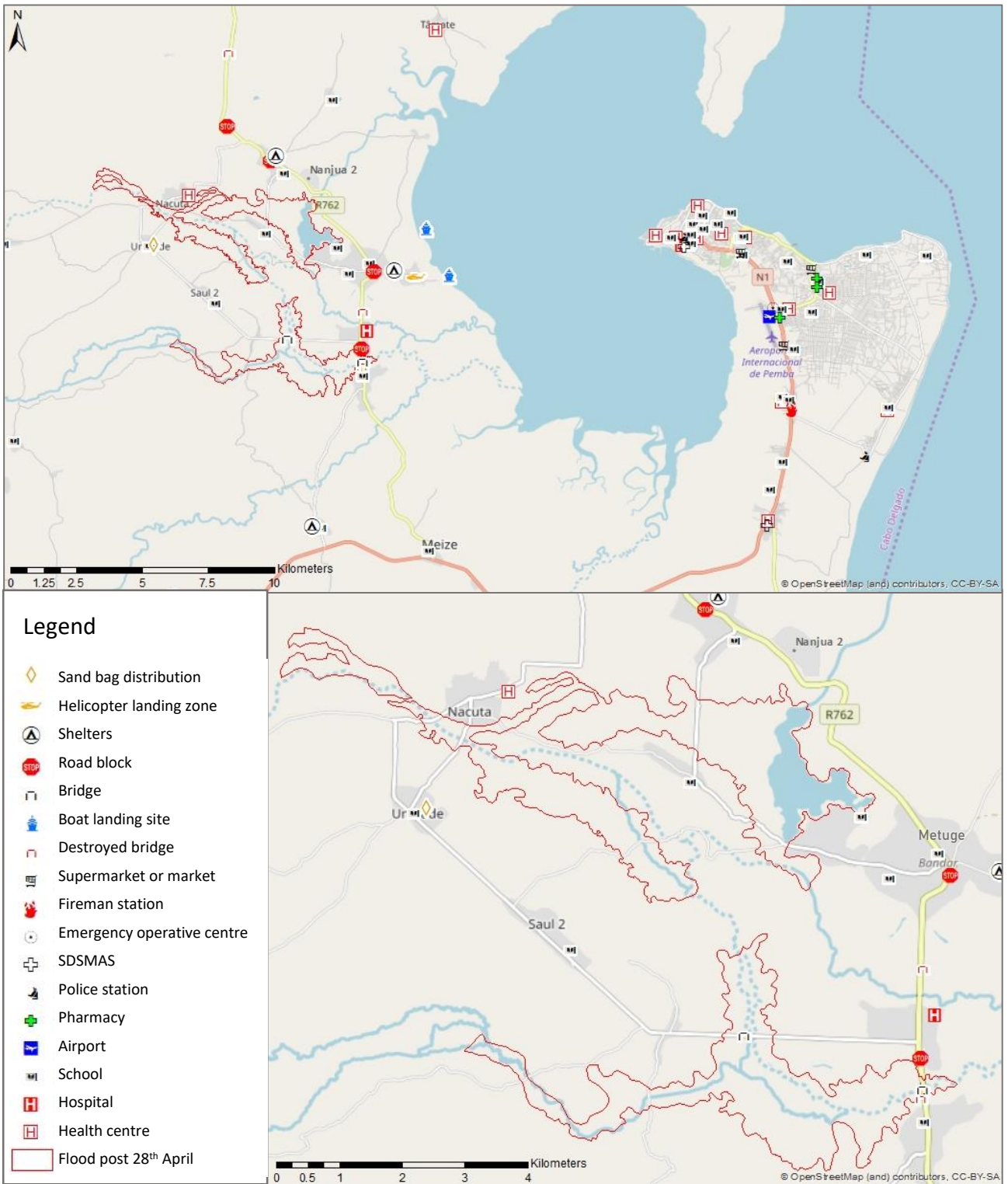


Figure 24 Flood map and zoom of the inundated area

## 2. COLLECTED DATA

This chapter describes the data collected and used to get inundation hazard maps for the present condition. The area in consideration is located in a developing country, and it is well known that these regions typically suffer from data scarcity. On the other hand, the extent of the study area made detailed field survey unfeasible. All the data presented in this chapter have been thus acquired by extensive web search for open databases and critical comparison between the information obtained from different sources. First, different Digital Elevation Models with different spatial resolution, ranging from 90 m to 12,5 m, have been acquired and compared. Second, different maps for the soil cover have been retrieved to complete the geomorphologic description and as a basis for rainfall-to-runoff transformation. Third, several sources of rainfall data, differing for spatial and temporal resolution, have been considered. Finally, information about exposed items has been retrieved.

### 2.1. DIGITAL ELEVATION MODEL

Digital Elevation Models (DEMs) are digital representations of the land surface elevation and are frequently used in hydrologic and hydraulic studies field. In fact, a DEM is of primary importance to obtain fundamental parameters, such as the time of concentration, necessary to compute hydrological transformation and also represents a key piece of information to create a terrain geometry for computation of a flood propagation. Moreover, DEMs are used to determine the boundaries of a watershed and the hydrographic network.

#### 2.1.1. DEMs FOUND

At the beginning of this thesis project, a considerable time was dedicated to searching free Digital Elevation Models. Four global DEMs with different spatial and vertical resolution were found.

The first one<sup>14</sup> is the SRTM DEM with 90 meters of resolution. The Shuttle Radar Topography Mission (SRTM) data were collected during an 11-day mission in February 2000 by a radar system mounted on the Space Shuttle Endeavor. The SRTM project was led by the National Geospatial-Intelligence Agency (NGA) and NASA, in order to provide accessibility of high quality elevation data for large portions of the tropics and other areas

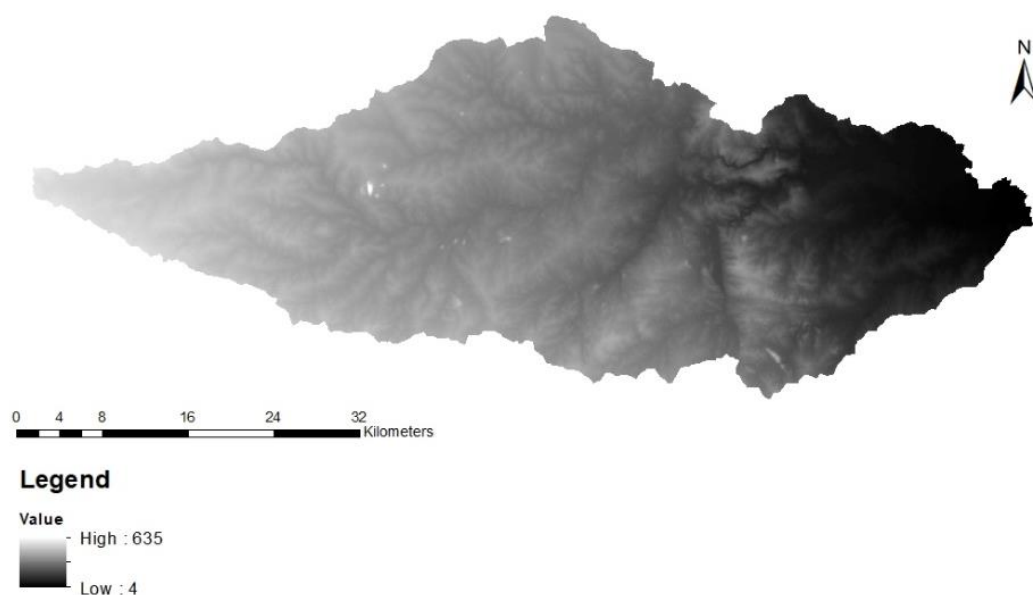
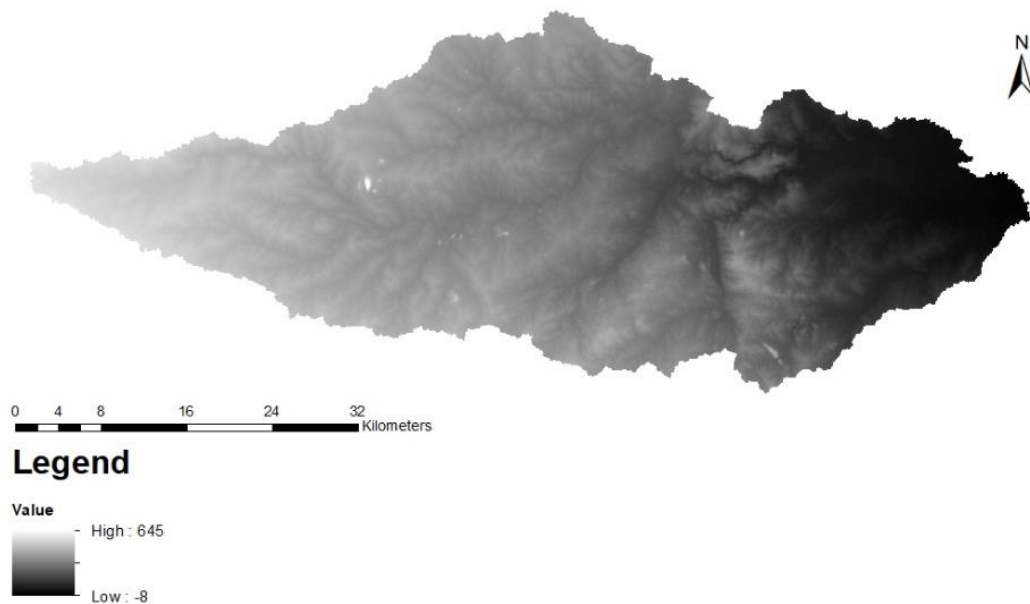


Figure 25 SRTM with cells of 90m size DEM

<sup>14</sup><http://srtm.csi.cgiar.org>

of the developing world. A search for watershed boundaries starting from a downstream section was run to obtain the perimeter of the catchments of the Rio Maguide, using the town of Pemba as the downstream section for the computation. *Figure 25* presents the hydrographic basin obtained and a color map of elevations, ranging from near-sea levels up to 635 m a.s.l. The study area considered in this thesis is at the right of the map, in the zone with lowest elevations.

The second one<sup>15</sup> is the SRTM DEM with 30 meters of resolution (shown in *Figure 26*, again for the portion corresponding to the catchments as determined by a search of the watershed). This finer global digital information is available freely since 2014.



*Figure 26 SRTM with 30m cell resolution DEM*

The third one<sup>16</sup> is the ASTER GDEM with 30-meter resolution (*Figure 27*). The Advanced Spaceborne Thermal Emission and Reflection Radiometer (ASTER) Global Digital Elevation Model (GDEM) was led by the Ministry of Economy, Trade, and Industry (METI) of Japan and the United States National Aeronautics and Space Administration (NASA) and its first version was released in June 2009. Moreover, the Advanced Spaceborne Thermal Emission and Reflection Radiometer is a Japanese sensor which is a remote sensory device on the Terra satellite launched into Earth orbit by NASA in 1999.

---

<sup>15</sup> <https://dwtkns.com/srtm30m/>

<sup>16</sup> <https://search.earthdata.nasa.gov/search/>



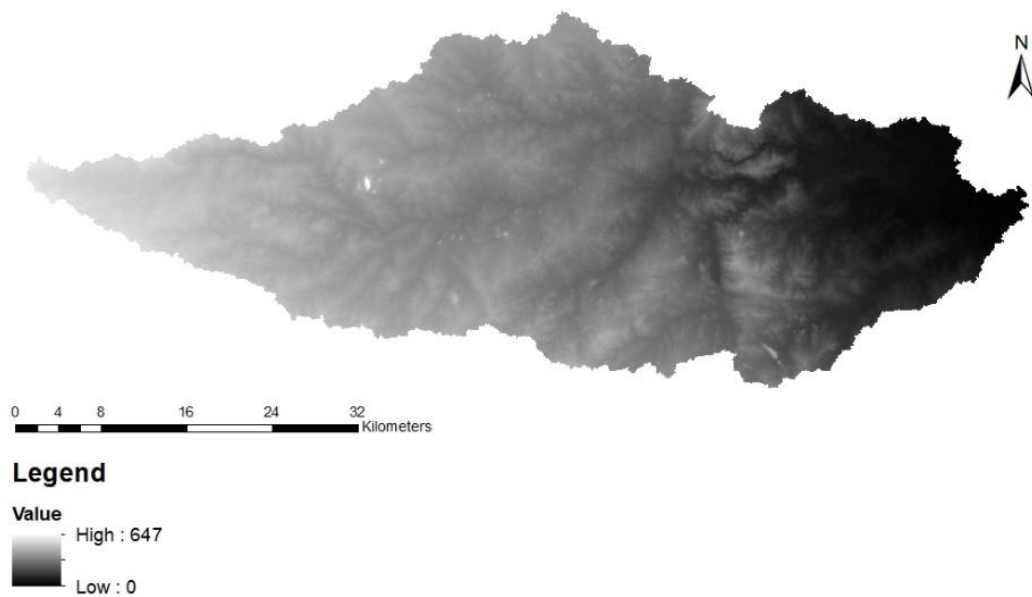


Figure 27 ASTER DEM

The fourth<sup>17</sup> DEM is the finest one. It is the ALOS PALSAR DEM with a spatial resolution of 12,5 m (Figure 28). PALSAR was one of three instruments on the Advanced Land Observing Satellite-1 (ALOS) “[...] developed to contribute to the fields of mapping, precise regional land-coverage observation, disaster monitoring, and resource surveying. ALOS was a mission of the Japan Aerospace Exploration Agency (JAXA).”<sup>18</sup>

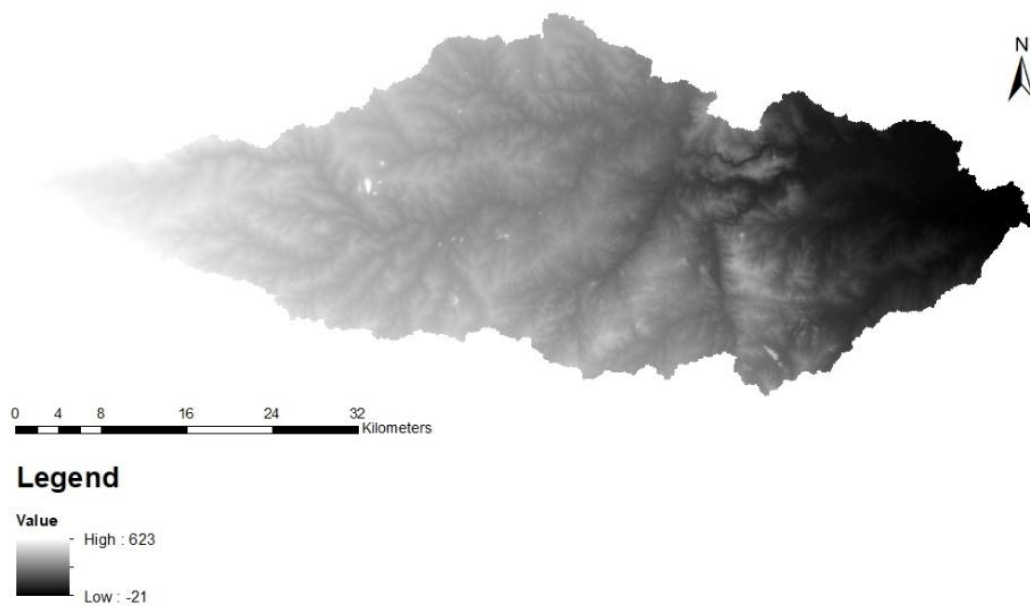


Figure 28 AP DEM

<sup>17</sup> <https://search.asf.alaska.edu/>

<sup>18</sup> <https://portal.asf.alaska.edu/sar-data/palsar/about-palsar/>

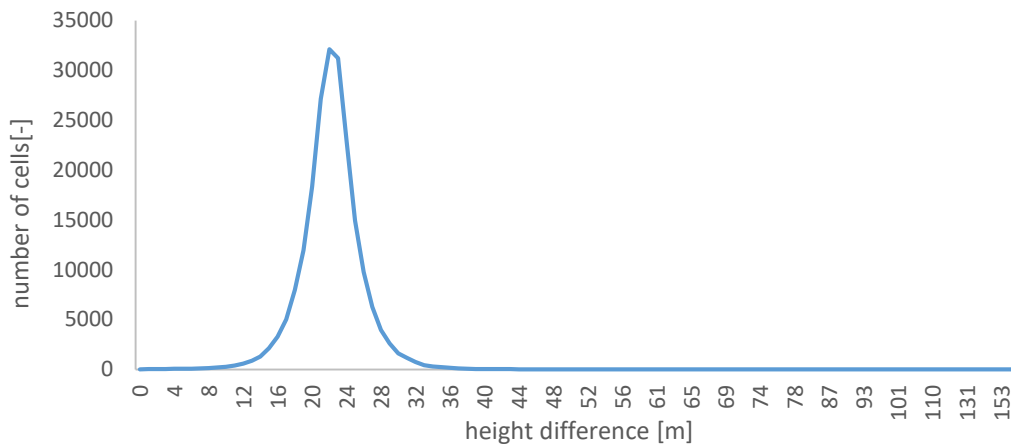


Figure 29 Difference in elevation between AP DEM and SRTM 90 DEM

As it can be noticed by the maps presented in *Figures 25 to 28*, the four Digital Elevation Models have different elevation ranges, this being possibly due to the different vertical and spatial resolution or to errors in image registration. In particular, the fourth one presents a range of elevation values very different from the others: it presents points with topographic depressions, and the smallest elevation is under the sea level and equal to -21 m a.s.l. However, no large depressions are present in that area, as people in field confirmed and, as can be also deduced, comparing this last DEM with the others. The graph of *Figure 29* presents a distribution of the difference between the elevation values of the ALOS PALSAR DEM and those of the SRTM, in absolute value; the modal value of the curve is around 21 m, which is indeed the minimum value of elevation for the ALOS PALSAR DEM. Therefore, in the following, elevation values for this DEM were modified adding 21 m to the elevation of each cell. The resultant correction is presented in the following map (*Figure 30*).

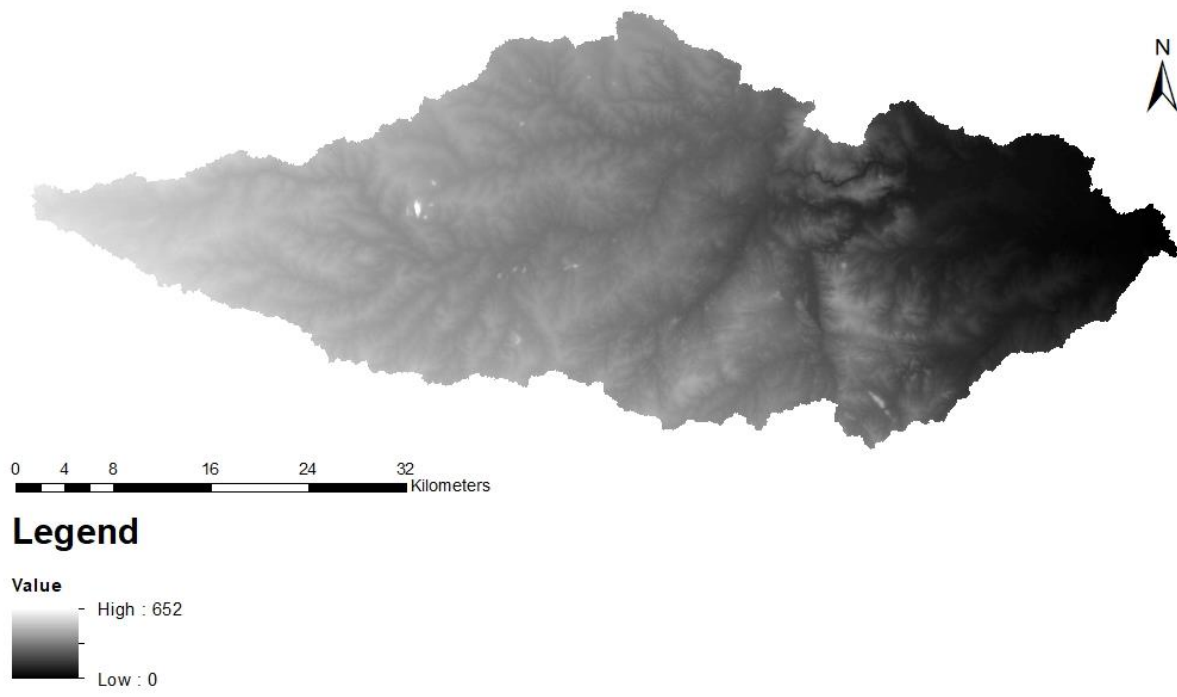


Figure 30 AP DEM corrected

### 2.1.2. COMPARISON BETWEEN THE DIFFERENT DEMs

The maps depicted in *Figures 25, 26, 27* and *30* look all similar, but differences exist as one notes comparing the maximum values in the color scales. Since elevation values of ground control points were not available,

the DEMs were compared in detail, to choose a 'best' one to perform the following analyses. This comparison was performed analysing the mathematical difference between the four raster data and overlapping the various watershed boundaries and mainstream paths of the river as determined for all the DEMs.

Three elevations subtractions have been computed maintaining, as common subtrahend, the SRTM DEM with the lowest spatial resolution of 3 arc-seconds (corresponding to 90 m). To compute this operation, we used the raster calculator of ArcGIS, which permits to subtract the values in each cell from one raster file to another. However, the cells present different dimension and, therefore, a preliminary operation of resampling has been done in order to get all the DEMs with a cell size of 90 m.

The first image (*Figure 31*) represents the difference between the ASTER and the SRTM.

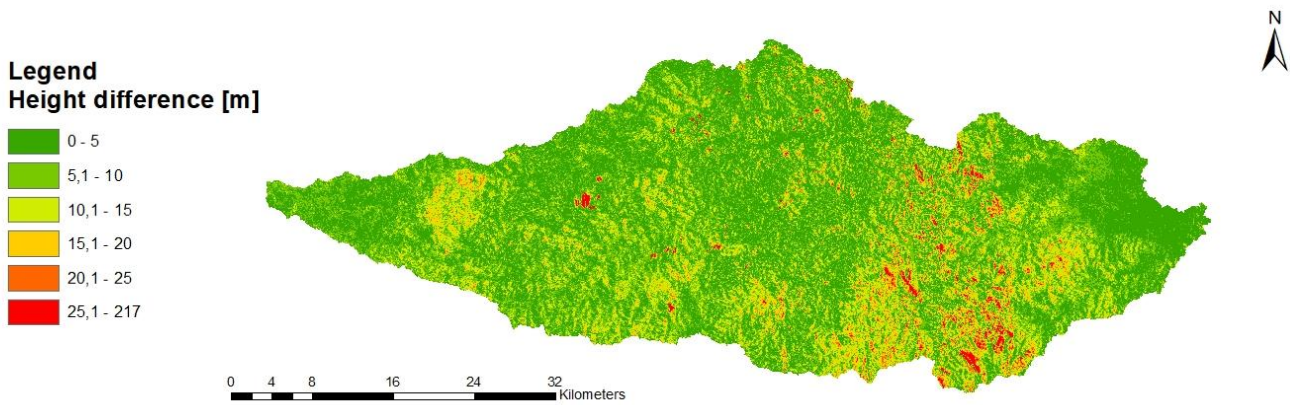


*Figure 31 Map of the elevation difference between ASTER DEM and SRTM 90 DEM*

*Figure 32* represents the difference between the two SRTM DEMs.

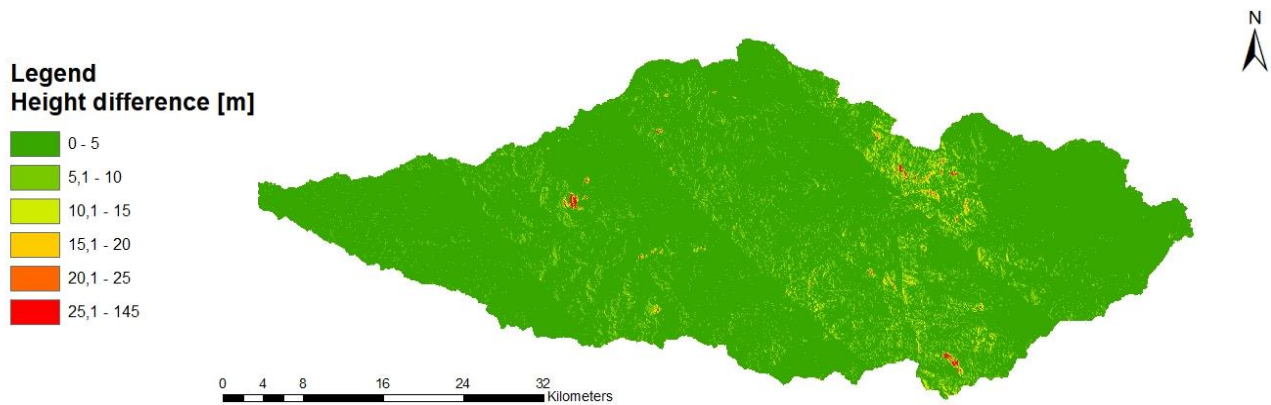


*Figure 32 Map of the elevation difference between SRTM 30 DEM and SRTM 90 DEM*

*Figure 33* represents the difference between the ALOS PALSAR DEM corrected and the SRTM 90 DEM.

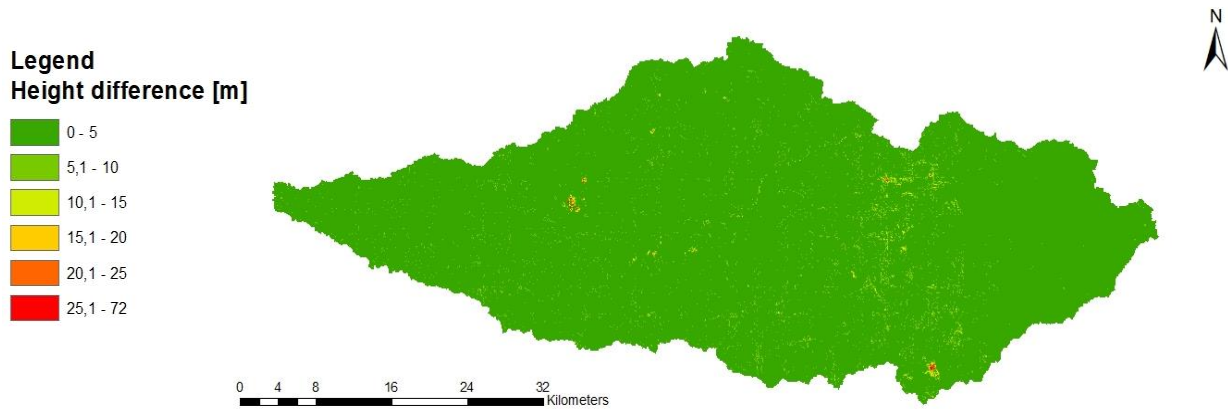


Figure 33 Map of the elevation difference between AP corrected DEM and SRTM 90 DEM

The difference between the two SRTM DEMs with different spatial resolution (Figure 32) is in general quite small, as might have been expected considering that the two DEMs come from the same source. Instead, it can be noticed that the ASTER and the SRTM (Figure 31) may locally differ by more than 25 m. This discrepancy cannot be solved with a simple translation of elevations. Finally, the difference between ALOS PALSAR and SRTM (Figure 33) is in general small, indicating that the translation of 21 m applied to the former was able to provide a good match over the entire catchments. One can also note that in the last map the maximum value of the elevation difference is the least among all the computed ones.

The present area of interest is much smaller than the entire basin, thus a further analysis has been made on the area contoured in Figure 34. Within this area, we will present contour maps and frequency distributions (for classes and cumulative) of the elevation difference between two DEMs

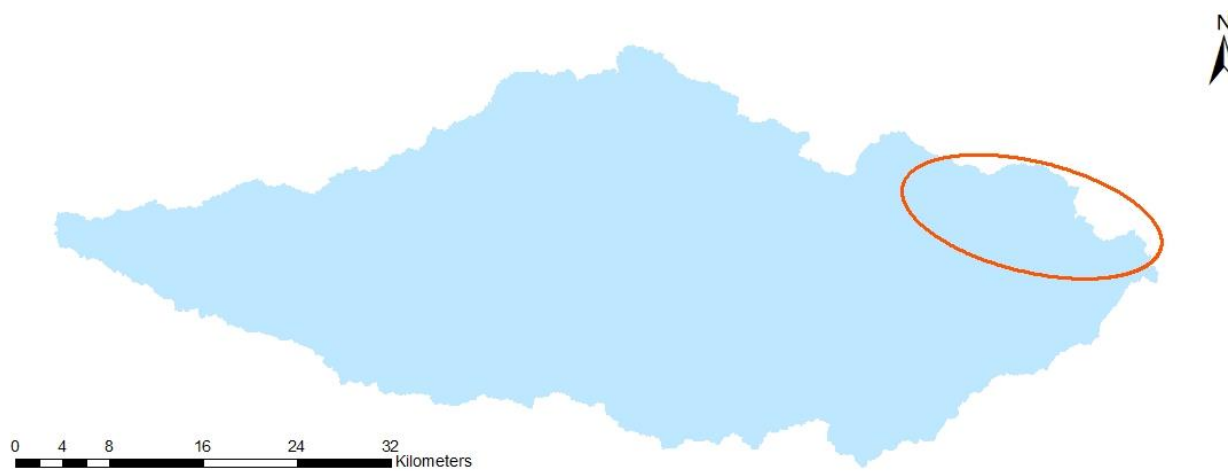


Figure 34 Area of interest within the entire basin

**Legend**  
**Height difference [m]**

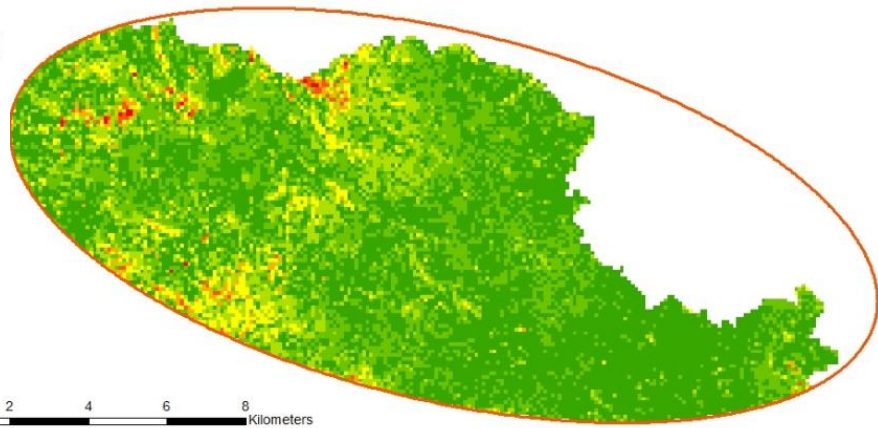
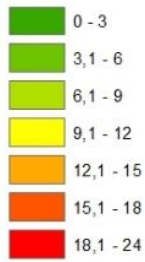


Figure 35 Zoom of the elevation difference between ASTER DEM and SRTM 90 DEM in the area of interest

As can be noticed observing the graph of Figure 36, in the area of interest, the most frequent differences between the ASTER and the SRTM90 DEMs are within a limited range of 0 to 10 m. In fact, after this value the cumulative frequency curve presents a plateau which indicates that there are few cells with higher difference in elevation.

Comparing the SRTM90 and SRTM30 DEMs (Figure 38), the range of discrepancy is between 0 and 6 m. As expected the two Shuttle Radar Topography Mission Digital Elevation Model present smaller differences than the previous comparison.

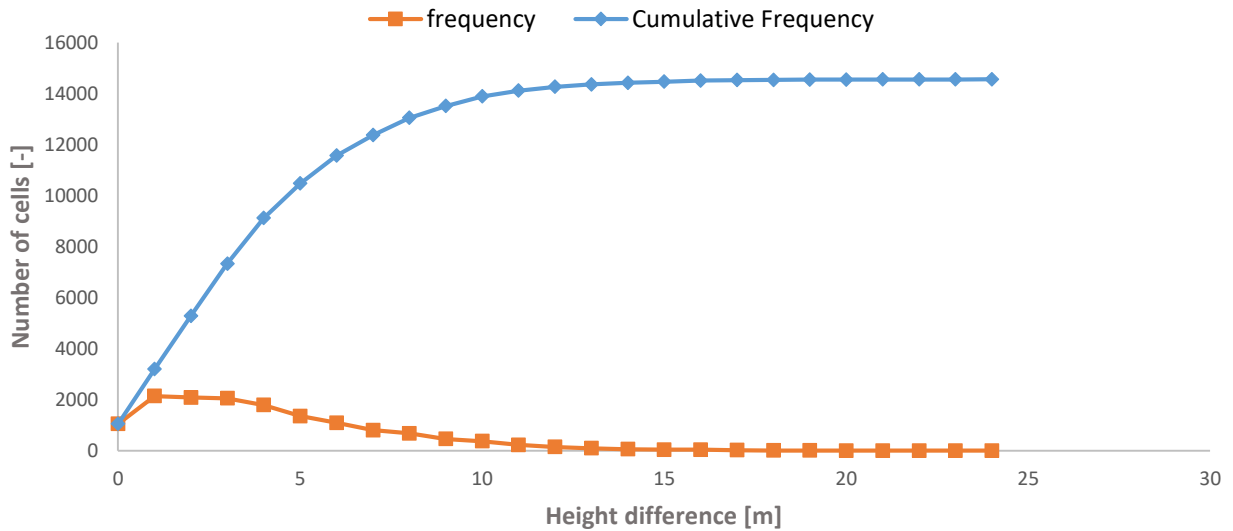


Figure 36 Statistical distribution of the elevation difference between ASTER DEM and SRTM 90 DEM



**Legend**  
**Height difference [m]**

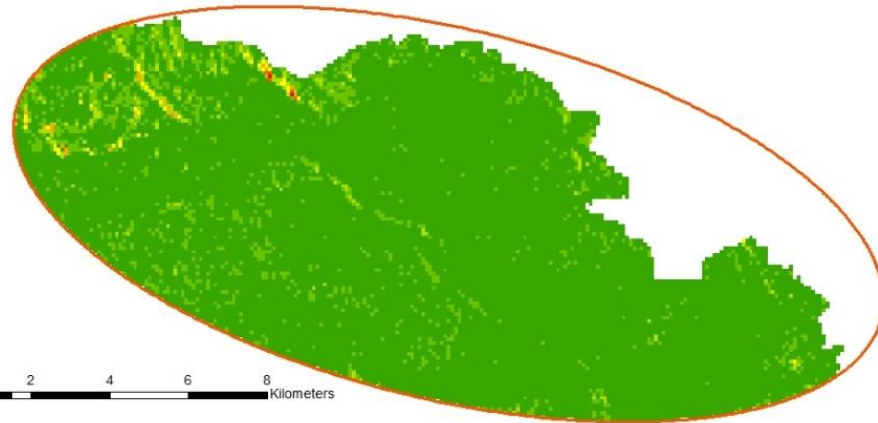
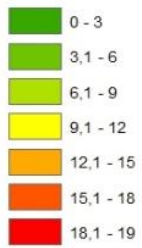


Figure 38 Zoom of the elevation difference between SRTM 30 DEM and SRTM 90 DEM

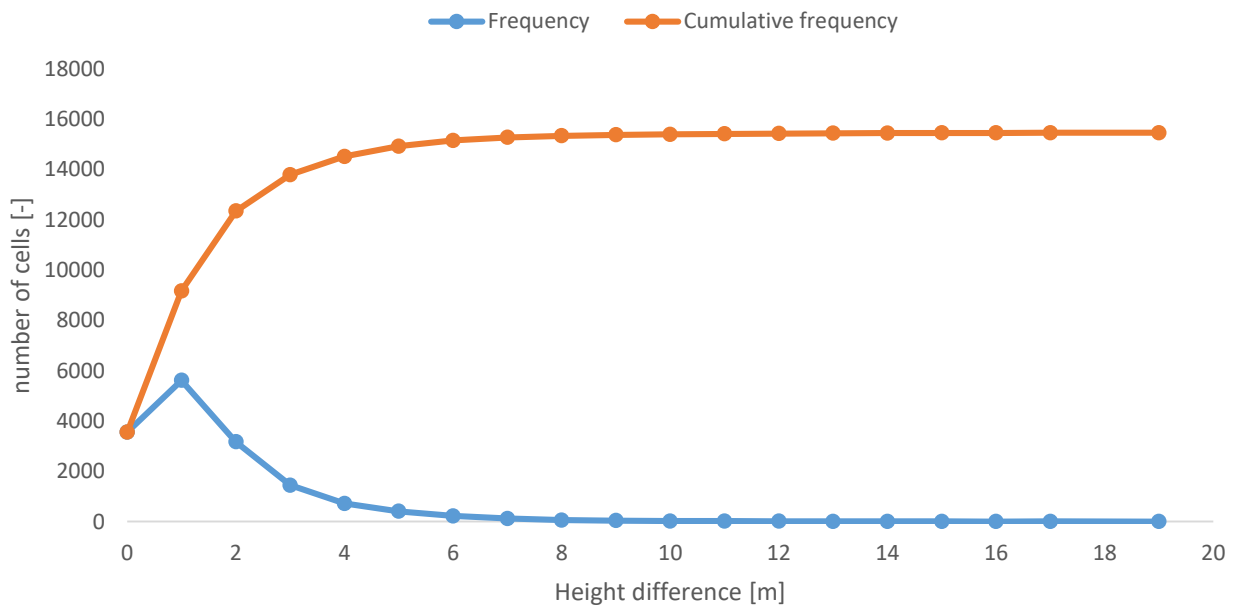


Figure 39 Statistical distribution of the elevation difference between SRTM 30 DEM and SRTM 90 DEM



**Legend**  
**Height difference [m]**

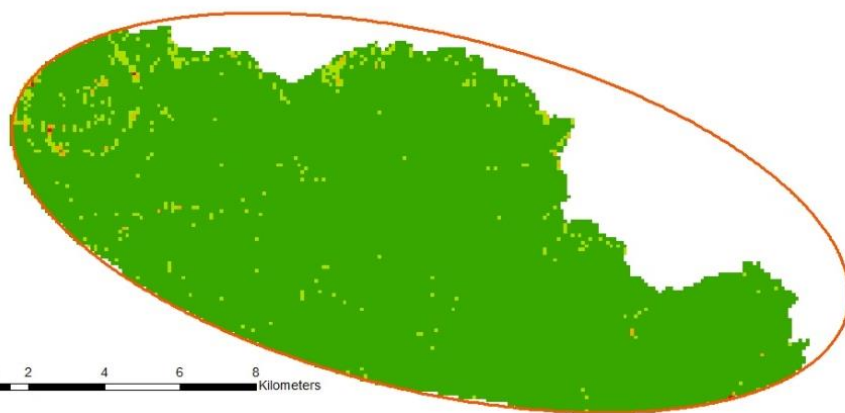
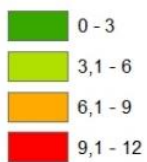


Figure 37 Zoom of the elevation difference between AP DEM and SRTM 90 DEM



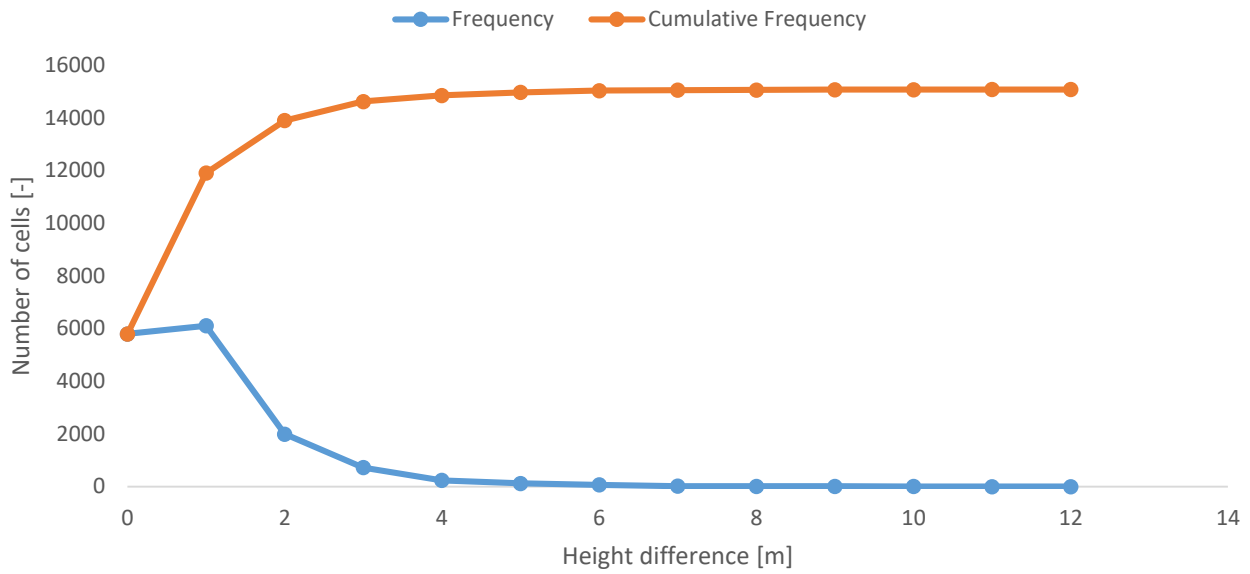


Figure 40 Zoom of the elevation difference between AP DEM and SRTM 30 DEM

The ALOS PALSAR DEM is compared to the SRTM-90 and SRTM-30 in Figures 39 to 42. In this cases, the plateau of the cumulative distribution of elevation difference is reached at 5 m. Moreover, the number of cells with zero value, so with the same elevation in two DEMs, is about twice the previous one.

**Legend**  
**Height difference [m]**

- 0 - 3
- 3,1 - 6
- 6,1 - 9
- 9,1 - 12
- 12,1 - 13

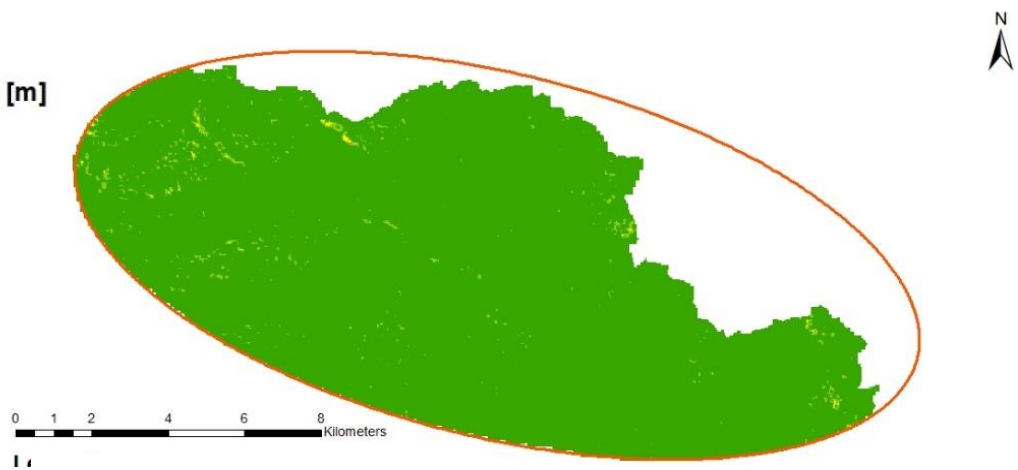


Figure 41 Statistical distribution of the elevation difference between Alos Palsar DEM And SRTM 90 DEM

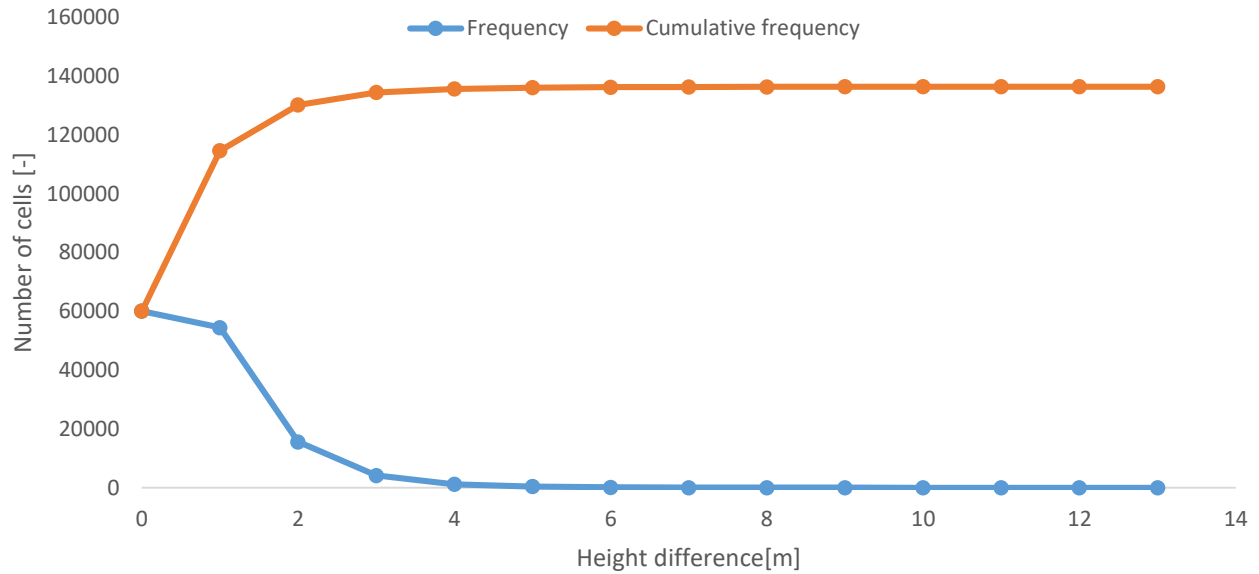


Figure 42 Statistical distribution of the elevation differences between the AP DEM and SRTM 30 DEM

As mentioned above, the boundaries of the catchments and the paths of the main stream were determined by GIS operations for each source of topographic information. *Table 4* presents a comparison of geometric parameters (basin area and perimeter, length of the main stream). In addition, *Figures 43-44* present the overlap between watersheds and main streams obtained starting from the four DEMs.

Table 4 Geometrical characteristics of the extrapolated basins

DEM	CELL SIZE [m]	BASIN AREA [km <sup>2</sup> ]	BASIN PERIMETER [km]	RIVER LENGTH [km]
SRTM 90	90	1742.14	248.73	129.49
SRTM 30	30	1744.11	283.03	134.09
ASTER	30	1728.62	299.95	132.54
ALOS PALSAR (AP)	12.5	1740.69	295.59	132.84

The perimeter and the area of the four catchments are similar. Also the path of the mainstream is the same for most of its length. However, the major discrepancy is detected in the area of interest. In fact, in that zone the result, in term of mainstream course, is very different between one DEM and another.

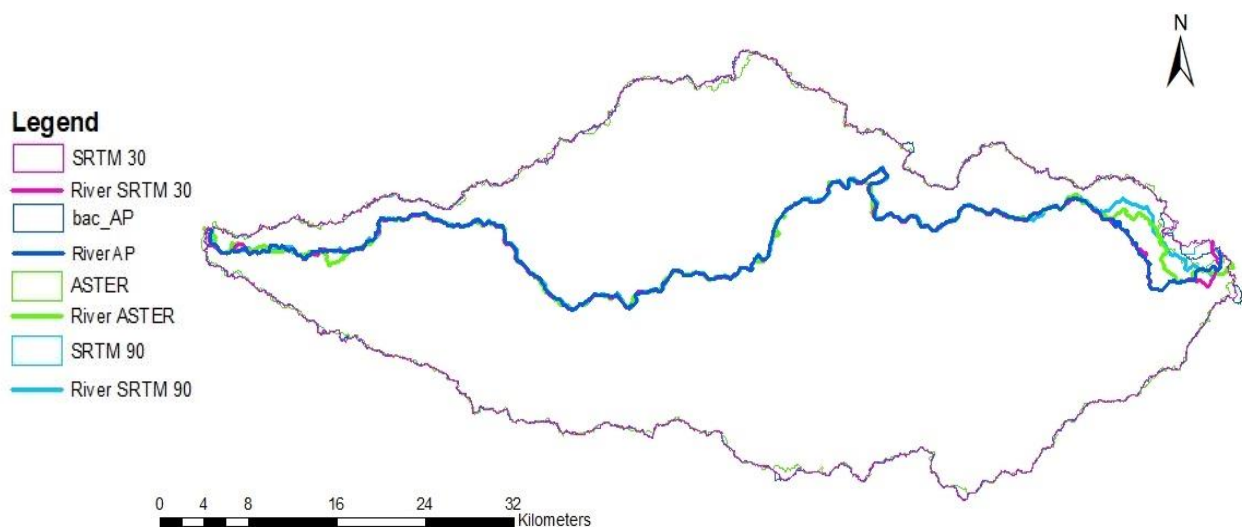


Figure 43 Basin perimeters and mainstream paths for the four DEMs



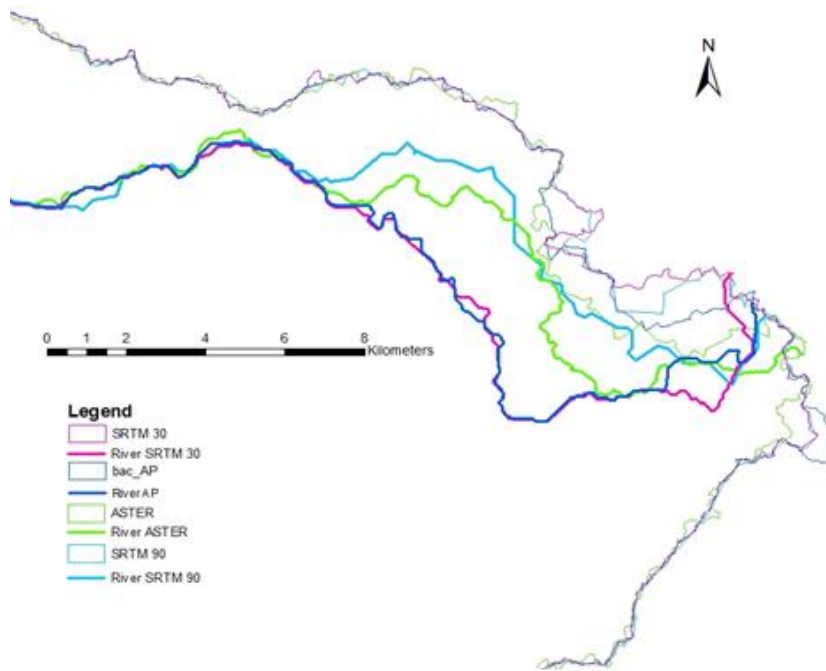


Figure 44 Detail of the different river paths in the area of interest

This happens because the mainstream is identified, in ArcGIS, by the cells in which the maximum number of cells flow; but lowering the flow accumulation order, the flow network of the entire basin can be appreciated and the four different paths are almost represented in each flow network of the different DEM sources. In the *Figure 45* is depicted the flow network of the SRTM 30 DEM, on which are overlapped the paths of the SRTM 90 and SRTM 30 river. It can be noticed that a part of the stream of SRTM 90 is crossed by the reaches of the network of the SRTM 30; no perfect correspondence is present maybe due to the difference in cell size. Moreover, the paths obtained in *Figures 43-44* are those on which the field surveys described in chapter 1 were based.

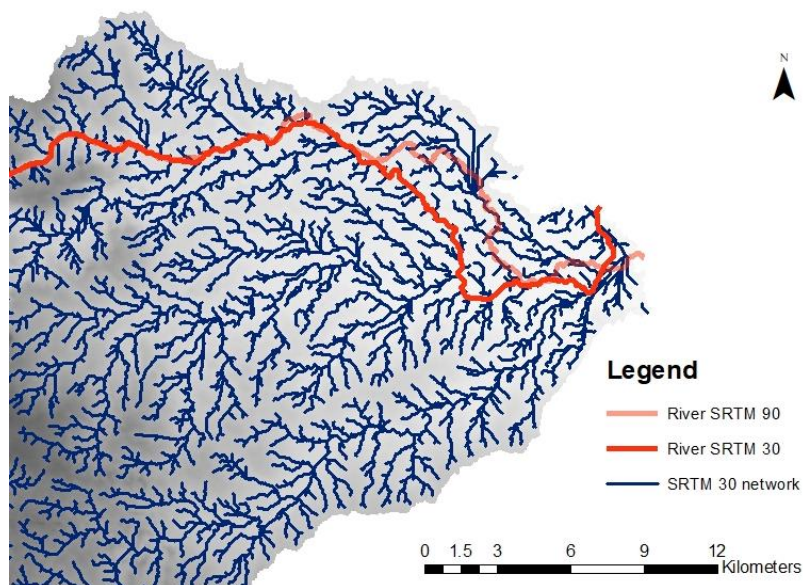


Figure 45 SRTM 30 flow network and Mainstream of SRTM 30 and SRTM 90

### 2.1.3. DEM CHOICE

After the comparison of the different Digital Elevation Models available freely, the ALOS PALSAR DEM has been chosen in order to proceed with the analysis, based on the following criterion. From the comparison of the difference between the cells of each DEM with the SRTM 90 DEM, it results that the lower discrepancy is present between the SRTM DEMs and the AP one, while the ASTER DEM is the more discordant. From the data in accordance, it has been chosen the DEM with the higher spatial resolution which is a fundamental characteristic to take into account in order to perform a more accurate flood modelling.

## 2.2 SOIL COVER

A few sources of information about the soil cover were found, and maps were produced as a part of the geomorphologic description of the hydrographic basin. The maps are depicted in *Figures 46-48* for the European Space Agency<sup>19</sup> (ESA), Copernicus<sup>20</sup> and Fao Geonetwork<sup>21</sup>, and present similarities and differences. For example, the central part of the catchments mostly falls in the category “open broadleaved deciduous forest” in *Figures 46* and *47*, while it falls in “closed broadleaved deciduous forest” in *Figure 48*. The final reach of the Rio Maguide is within “mosaic vegetation croplands” or “grassland / open broadleaved deciduous forest” depending on the map. From field survey it was observed that this area is actually characterized mainly by croplands, and some sparse forests of coconut, banana and mango trees.

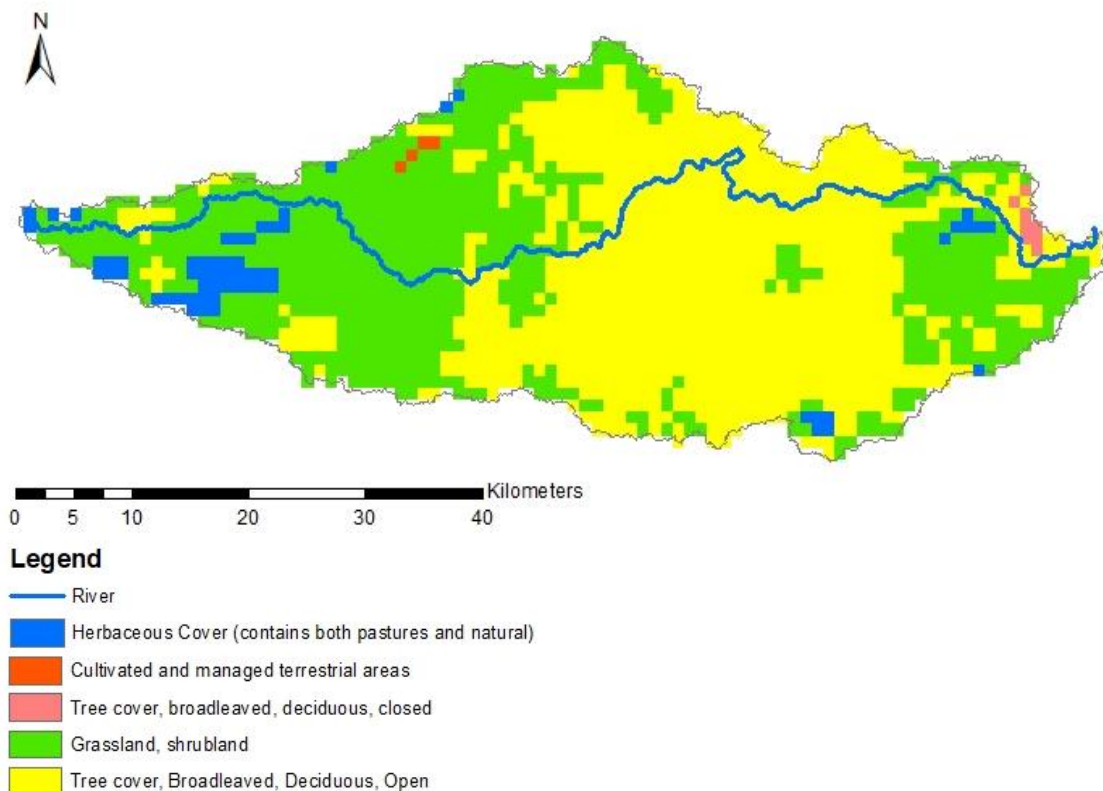


Figure 46 Copernicus soil coverage map

<sup>19</sup> <http://maps.elie.ucl.ac.be/CCI/viewer/download.php>

<sup>20</sup> <https://emergency.copernicus.eu/>

<sup>21</sup> <http://www.fao.org/geonetwork/srv/en/main.home>

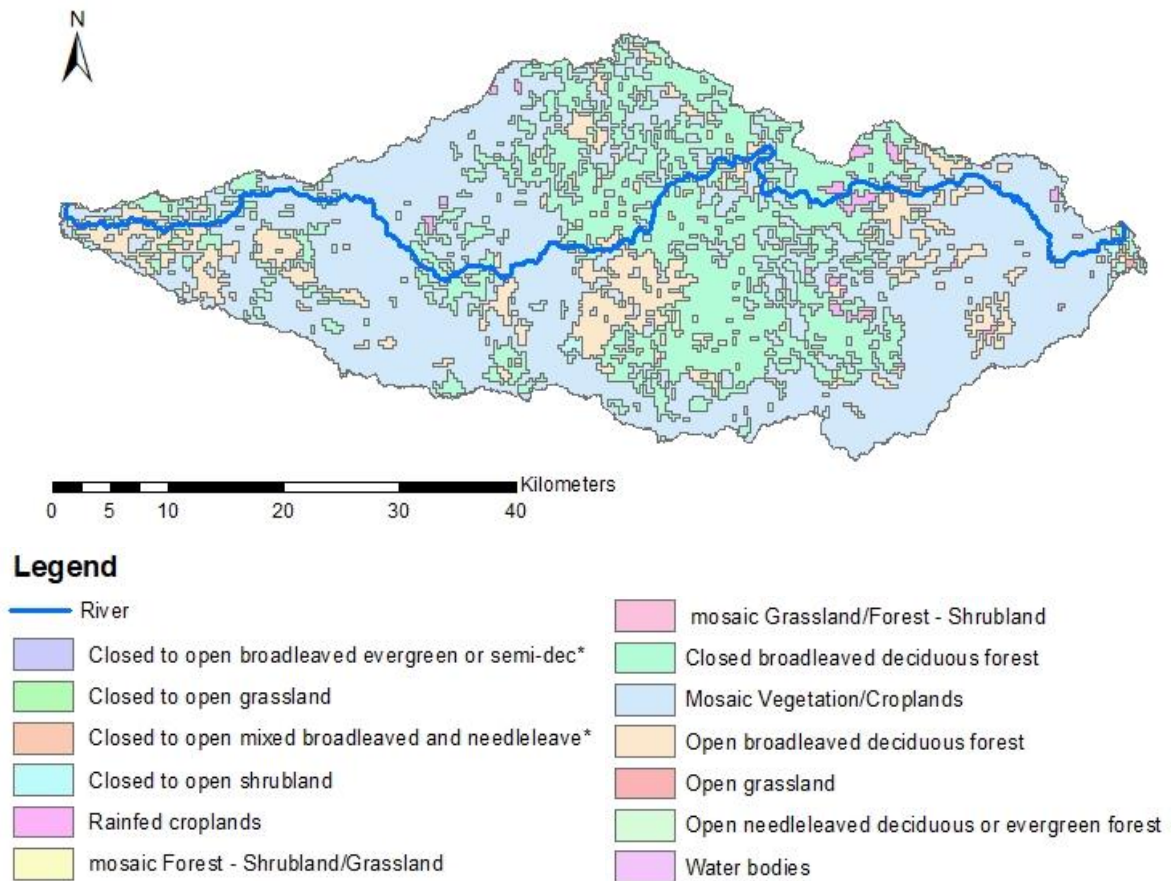


Figure 48 Fao Geonetwork soil coverage

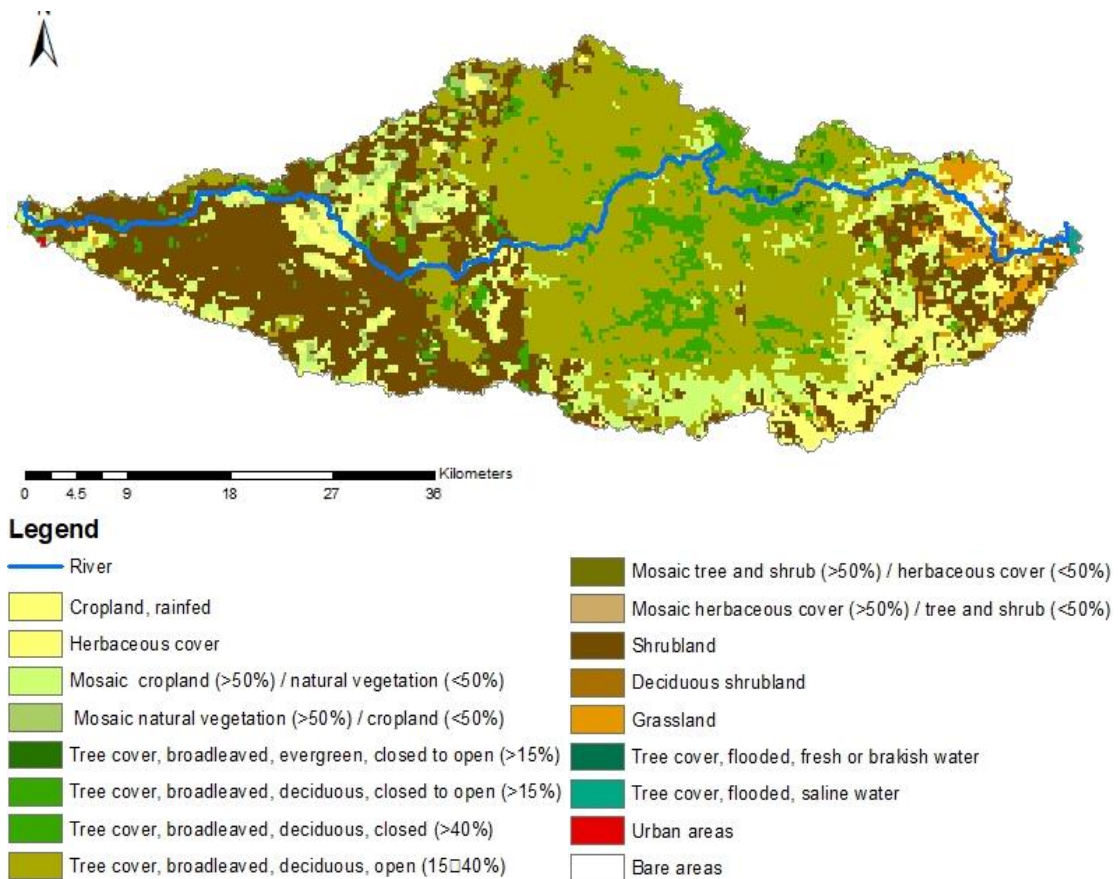


Figure 47 ESA soil coverage map

## 2.3 HYDROLOGICAL DATA

Besides the morphologic data, a crucial point for the computation of any flood model is the construction of a synthetic hydrograph. The latter results from a rainfall-to-runoff model that simulates the complete hydrologic processes of dendritic watershed systems. The modelling procedure will be detailed in the following chapter while here we refer to the data gathering. The main steps performed are listed below:

- web search of several rainfall data, coming both from punctual weather stations (pluviometers) and from models based on satellite images jointly with historical documents; some other pluviometric data were provided by *Istituto Oikos* that recently installed a weather station in Metuge;
- analysis and comparison of rainfall data collected on the different scales (some data cover a period of almost 30 years while some other span the last decade or one year only);
- statistic distribution of the dispersion and critical choice of the best data, also considering the temporal resolution.

### 2.3.1 RAIN DATA SOURCES

A wide number of weather forecast portals has been analysed in order to find historical rainfall data of the area covering the district of Metuge. As already mentioned above, the area under study is affected by data scarcity: for rainfall, available data are not well distributed in space and time and not always for free. A list of the portals with the type of rainfall data provided is reported below.

#### **TuTiempo<sup>22</sup>**

This service provides daily rainfall data taken from weather stations. These data are available since 1980 and the only weather station pertinent to our study area is located in Pemba. Gaps are sometimes present in the temporal series, due to maintenance periods, temporary dysfunctions, etc. of the weather station.



Figure 49 Logo of TuTiempo

#### **Chirps<sup>23</sup>**

Climate Hazards Group InfraRed Precipitation with Station data (CHIRPS) is a 35+ year quasi-global rainfall data set. As can be read on the Climate Hazard Service website<sup>24</sup> “*Spanning 50°S-50°N (and all longitudes) and ranging from 1981 to near-present, CHIRPS incorporates our in-house climatology, 0.05° resolution satellite imagery, and in-situ station data to create gridded rainfall time series for trend analysis [...]*”. Also in this case the rainfall data extracted are daily. To better explain how the numbers are extrapolated, an extract from the paper titled *The climate hazards infrared precipitation with stations—a new environmental record for monitoring extremes* (Funk et al.)<sup>25</sup> is reported: “*CHIRPS incorporates station data in a two phase process, producing two unique products. In the first phase, which yields a preliminary rainfall product with 2-day latency, sparse World Meteorological Organization’s Global Telecommunication System (GTS) gauge data are blended with CCD-derived rainfall estimates at every pentad. There are six pentads in a calendar month, five 5-day pentads and one pentad with the remaining 3 to 6 days of the month. Stations from Mexico are also included, because these data can be obtained in near real-time as well. In the second phase, which yields a final product with a ~3 week latency, the best available monthly (and pentadal) station data are combined*

<sup>22</sup> <https://it.tutiempo.net/>

<sup>23</sup> <https://www.chc.ucsb.edu/data/chirps>

<sup>24</sup> <https://www.chc.ucsb.edu/data/chirps>

<sup>25</sup> <https://www.nature.com/articles/sdata201566>



with monthly (and pentadal) high resolution CCD-based rainfall estimates to produce fields that are similar to gridded monthly station products like those produced by the Global Precipitation Climatology Centre (GPCC) or University of East Anglia’s Climate Research Unit (CRU). Thus, the CHIRPS falls somewhere between heavily curated interpolated gauge datasets like the GPCC and sparse gauge plus satellite products.”

### Chirps GEFS

GEFS is the acronym of Global Ensemble Forecast System. This service is similar to the previous one but with the difference that in this case the weather forecast model is based on 21 different forecasts. It tries to quantify the uncertainty of any forecast generating a collection of different forecasts varying the initial observations. The rainfall data extracted are daily and span from 1981 until 2019.

### CRU Data<sup>26</sup>

The Climate Research Unit provides weather forecast data acquired from different weather stations in the world jointly with satellite images. The temporal resolution of CRU Data is one month and the data set covers the last century. These data are related to different cells covering the globe, as shown in *Figure 51* and, as one cell is selected, all the required data are available.

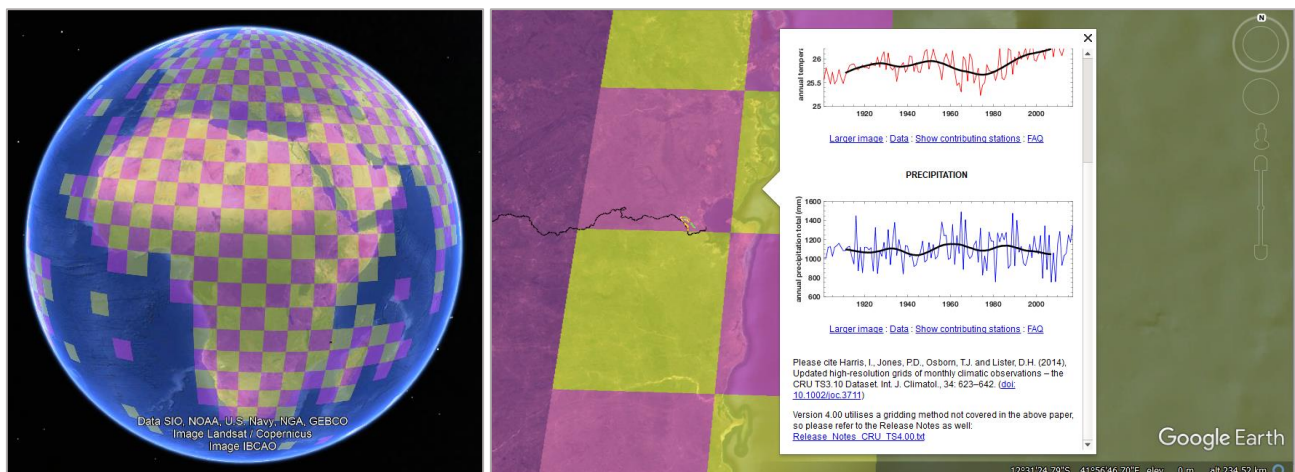


Figure 51 CRU Data world grid on the left and specific cell info on the right



Figure 50 Logo of CRU Data

### Meteonorm<sup>27</sup>

Data are furnished from more than 8000 weather stations worldwide and five geostationary satellites. The database of ground stations, taken from the National Climatic Data Centre, is extended with data from five geostationary satellites to fill gaps in areas where no weather stations are available. The satellite data is available on a global grid. Meteonorm provided two sets of rainfall data of Pemba, one from 1961 until 1990 and the second from 2000 to 2009, both on monthly scale.

<sup>26</sup> <http://www.cru.uea.ac.uk/data>

<sup>27</sup> <https://meteonorm.com/en/>

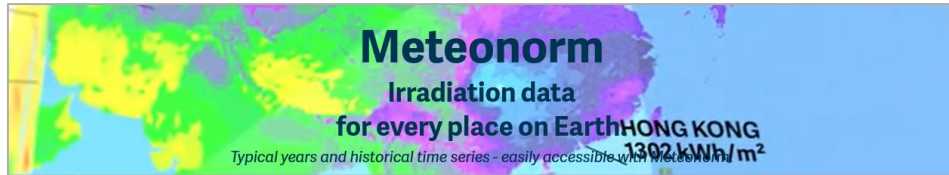


Figure 52 Meteornorm web interface

### Meteoblu<sup>28</sup>

This is an online-paid archive that offers consistent weather simulation data with hourly resolution since 1985. These simulations are assembled in continuous time series. All weather variables are available for any place on the Earth and on different altitude levels.



Figure 53 Logo of Meteoblu

As mentioned, finally, some other pluviometric data were provided by *Istituto Oikos* that recently installed a weather station in Metuge; those data are taken since 2014 and are on monthly scale.

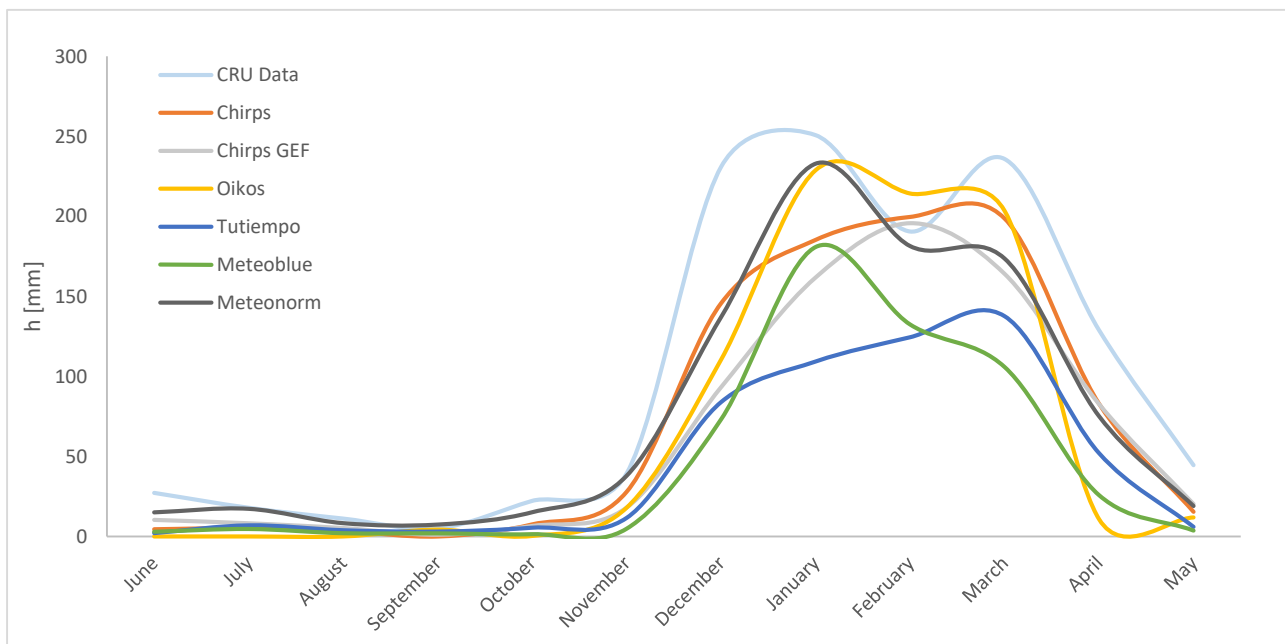


Figure 54 Averaged rainfall data distribution

The rainfall data collected have been plotted on a graph (Figure 54) that spans over one year and presents the depth of the rainfall on the vertical axis. Obviously, if any source of data uses a temporal resolution finer than one month, a monthly measure has been summing all the values for a month. Secondly, if the rainfall data are available for more than one year, an average value has been computed for each month. The plot of Figure 54 starts from June to separate the dry (May - November) and wet seasons (December - April) that present at first sight a strong difference in terms of rainfall height. The differences between the curves are obviously related to the origin of the datum; further considerations are reported below analysing separately each group of values and comparing sources that provide historical data for any time interval.

<sup>28</sup> [https://www.meteoblu.com/en/weather/historyclimate/weatherarchive/pemba\\_mozambique\\_1028918](https://www.meteoblu.com/en/weather/historyclimate/weatherarchive/pemba_mozambique_1028918)



### 2.3.2 COMPARISON BETWEEN THE DATA FROM DIFFERENT SOURCES

Firstly, data have been divided based on the time interval for which they were available, in order to make a more reliable comparison. With this aim three ranges have been chosen:

- 1961-1990 comparing CRU Data and Meteonorm (*Figure 55*)

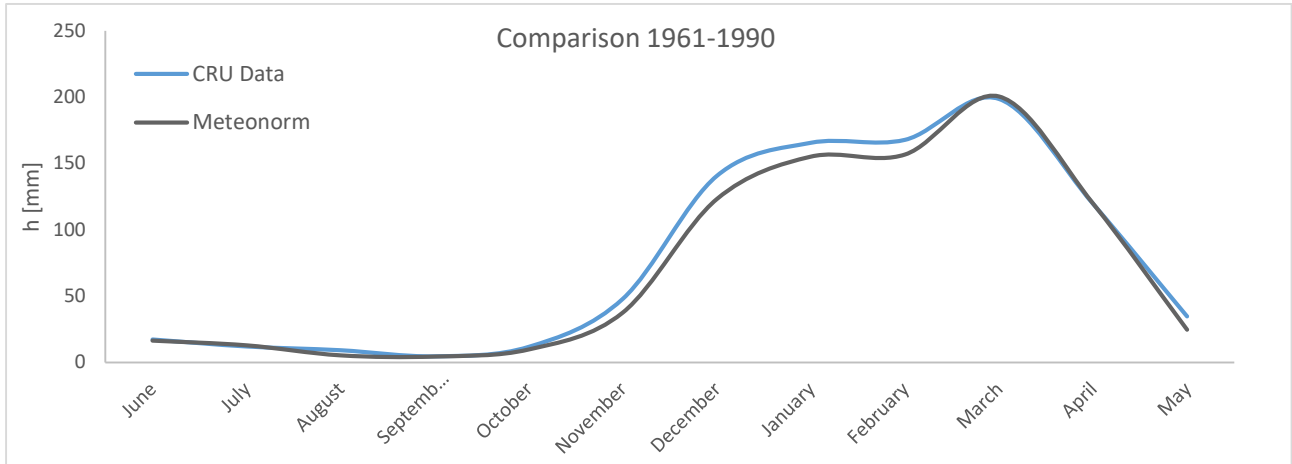


Figure 55 Comparison 1961-1990

- 2000-2009 comparing CRU Data, Meteonorm, TuTiempo, Meteoblue, Chirps and Chirps GEF (*Figure 56*)

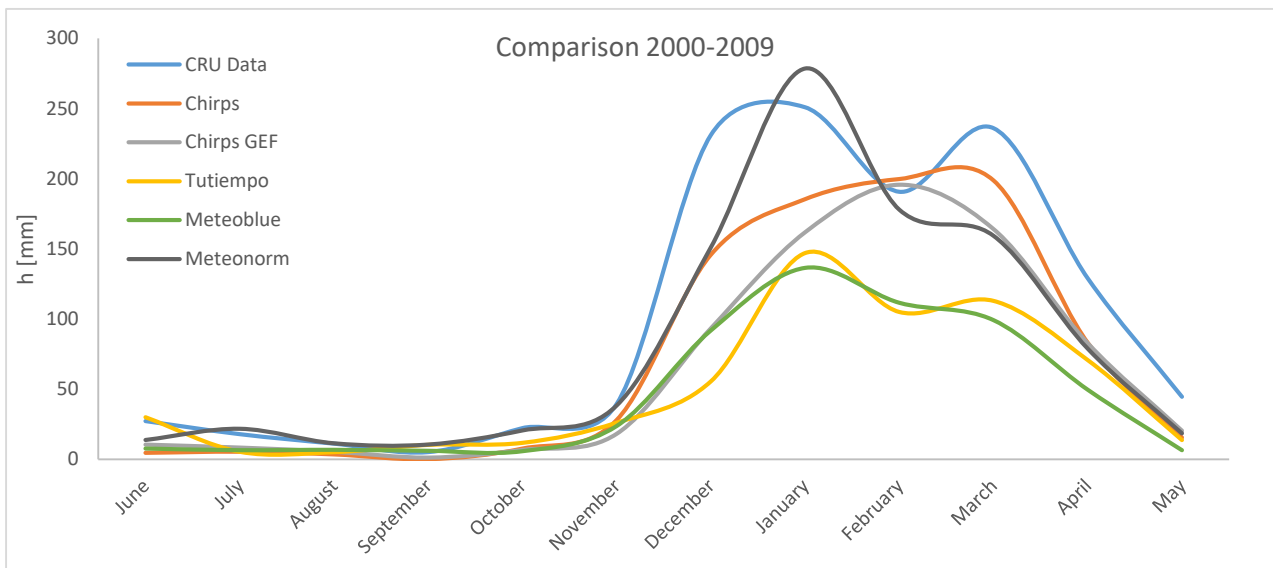


Figure 56 Comparison 2000-2009

- 2014-2017 comparing CRU Data, Meteonorm, TuTiempo, Meteoblue Chirps and Chirps GEF (Figure 57)

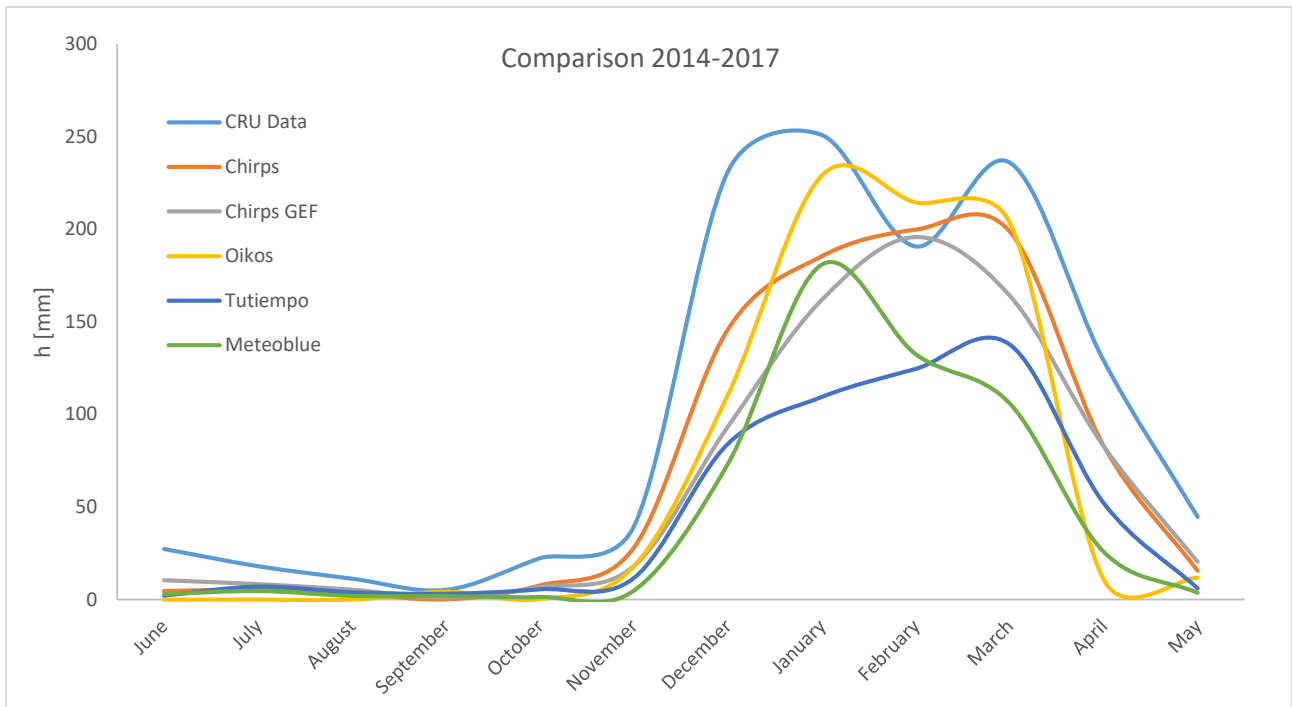


Figure 57 Comparison 2014-2017

There is a good agreement between CRU Data and Meteonorm for the period 1961-1990, while for the other periods the plots are similar to the comprehensive one of Figure 54. The mean of all the sources has been computed in order to visualize how much each data differs from it; also the standard deviation (measure used to quantify the amount of variation or dispersion of a set of data), calculated as the square root of the variance, and the variation coefficient (standardized measure of dispersion of the distribution of the random variable) calculated as the ratio of the mean to the standard deviation, have been computed and the relative table (Table 5) and graph are shown below (Figure 58).

Table 5 Statistical parameter distribution

Month	Standard deviation	Coeff. of variation
June	9,6262	1,1
July	6,6506	0,7708
August	3,8056	0,7809
September	2,5394	0,7740
October	7,7808	0,9275
November	13,0525	0,5796
December	53,8608	0,4310
January	49,0055	0,2541
February	34,6538	0,1958
March	43,5522	0,2500
April	39,7269	0,6065
May	13,5529	0,7849

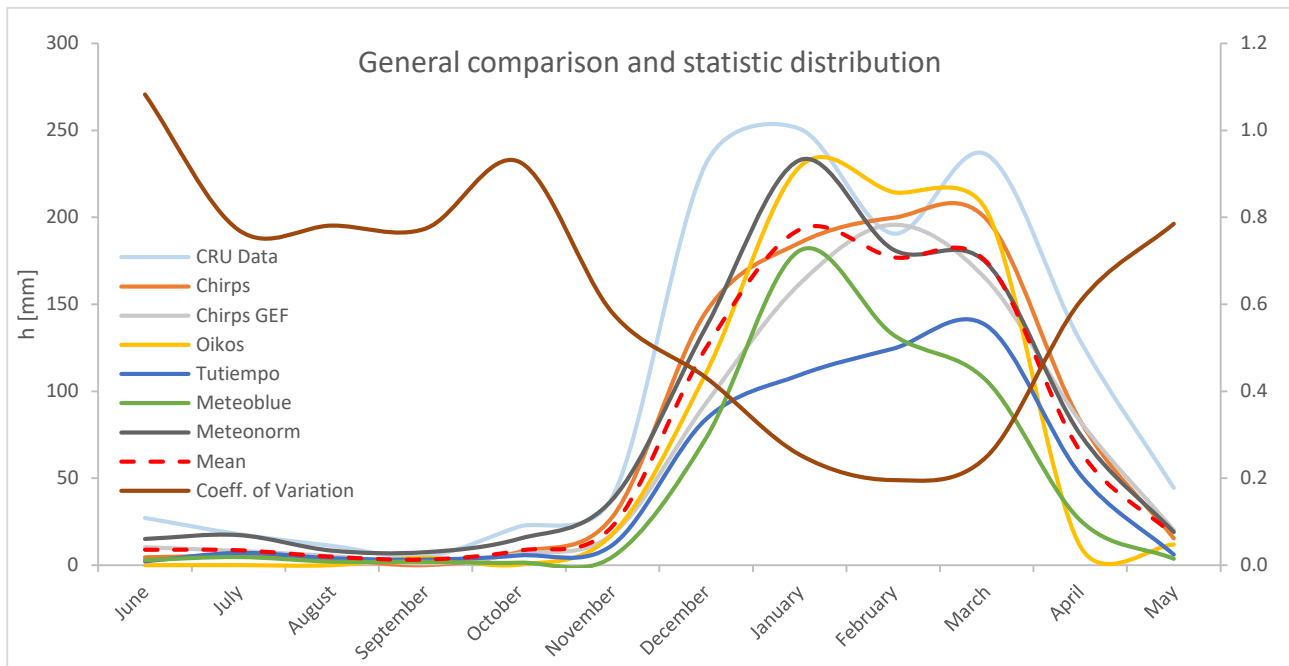


Figure 58 Comparison and statistic distribution

From this analysis one notes that TuTiempo is the trend that mostly differs from the others; the reason for this behaviour has to be attributed to the fact that this source is based only on pluviometer measurements that are, in general, the most accurate but, in the case of Pemba, suffers from the problem of several missing data. Also CRU Data differs from the general trend: is an overestimation of the mean value. In this case the reason could be the fact that the size of the cell on which the satellite works is too large, especially if compared with the other sources that works on a spatial scale that is, at most, sized on district dimension. However, the coefficient of variation for the months in the wet season is around 20%, that is reasonable in light of the differences among all the data sources and encouraging for the reliability of the following evaluations.

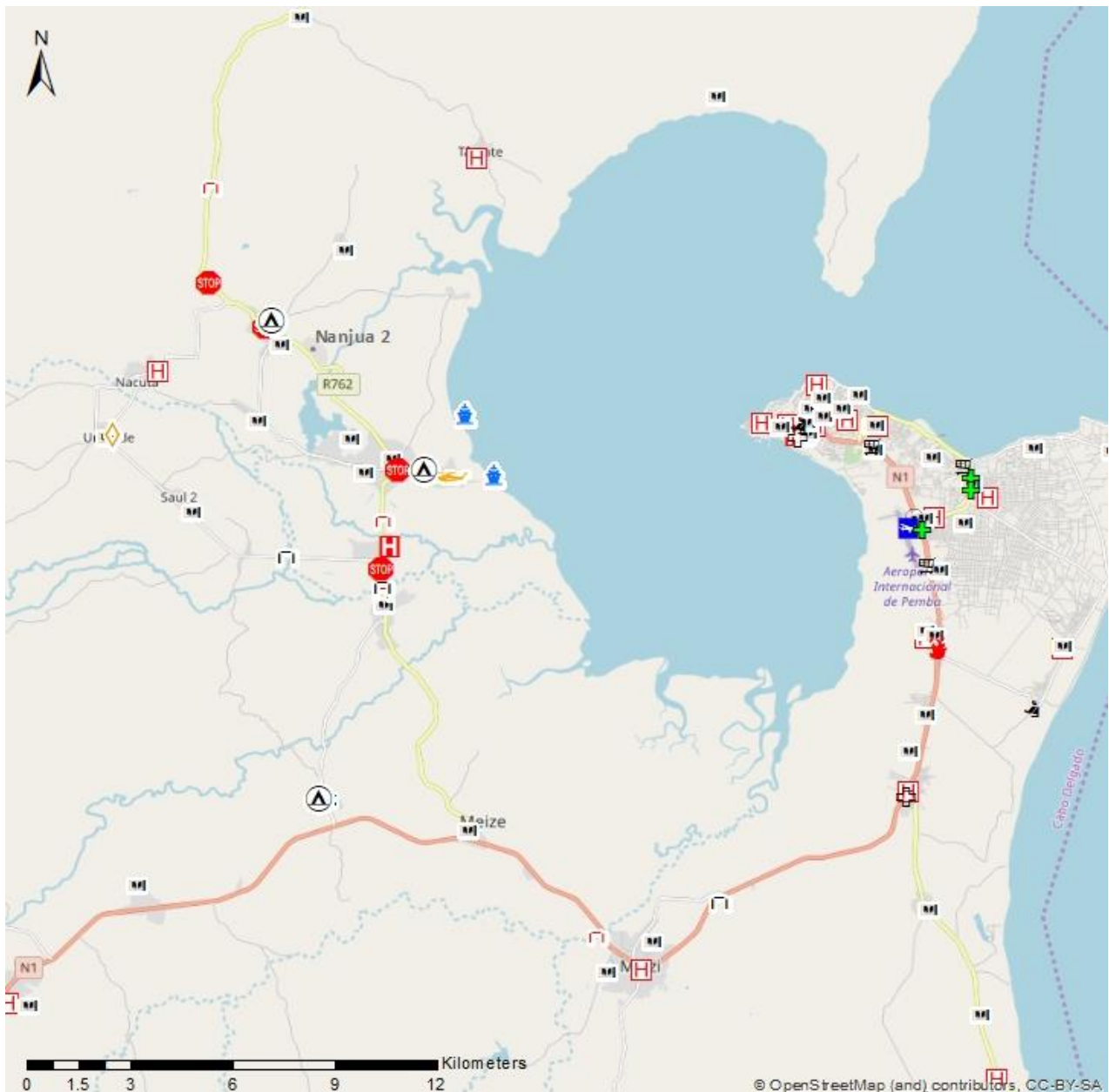
### 2.3.3 RAINFALL DATA CHOICE

The previous analyses have shown that some scatter exist between the different data and no reasons to consider one source more reliable than another. Therefore, a choice for a preferred data set has been based on the time resolution. It has been decided to use the data taken from Meteoblue that, contrary to all the other sources, have a temporal resolution of one hour; these data will be used in the following chapter to build DDF curves with a minimum duration  $\theta=1$  hour.

## 2.4 MAPS FOR EXPOSURE AND FACILITIES

Figure 59 shows the principal facilities on the area (most of them are located at Pemba) and the road network linking them: the operative emergency centre, police and firemen stations but also health centres, pharmacies and hospitals; moreover, the map also shows the position of sand bag distribution point, helicopter landing zone, boat landing site and eventual sheltering area, that are useful in case of an emergency. The map has been produced taking as a reference the cyclone Kenneth; with this scope the updates and the maps released by UNOCHA (United Nations Office for the Coordination of Humanitarian Affairs) have been used. Those maps have been georeferenced and different layers have been produced for

the above listed facilities, offices, crucial points, etc. The layer with the roads has been instead provided by *Istituto Oikos*, jointly with other maps concerning bridges, schools and libraries on the area. Also the field survey helped in adding information about villages and real estimate of roads, that remotely were misread.



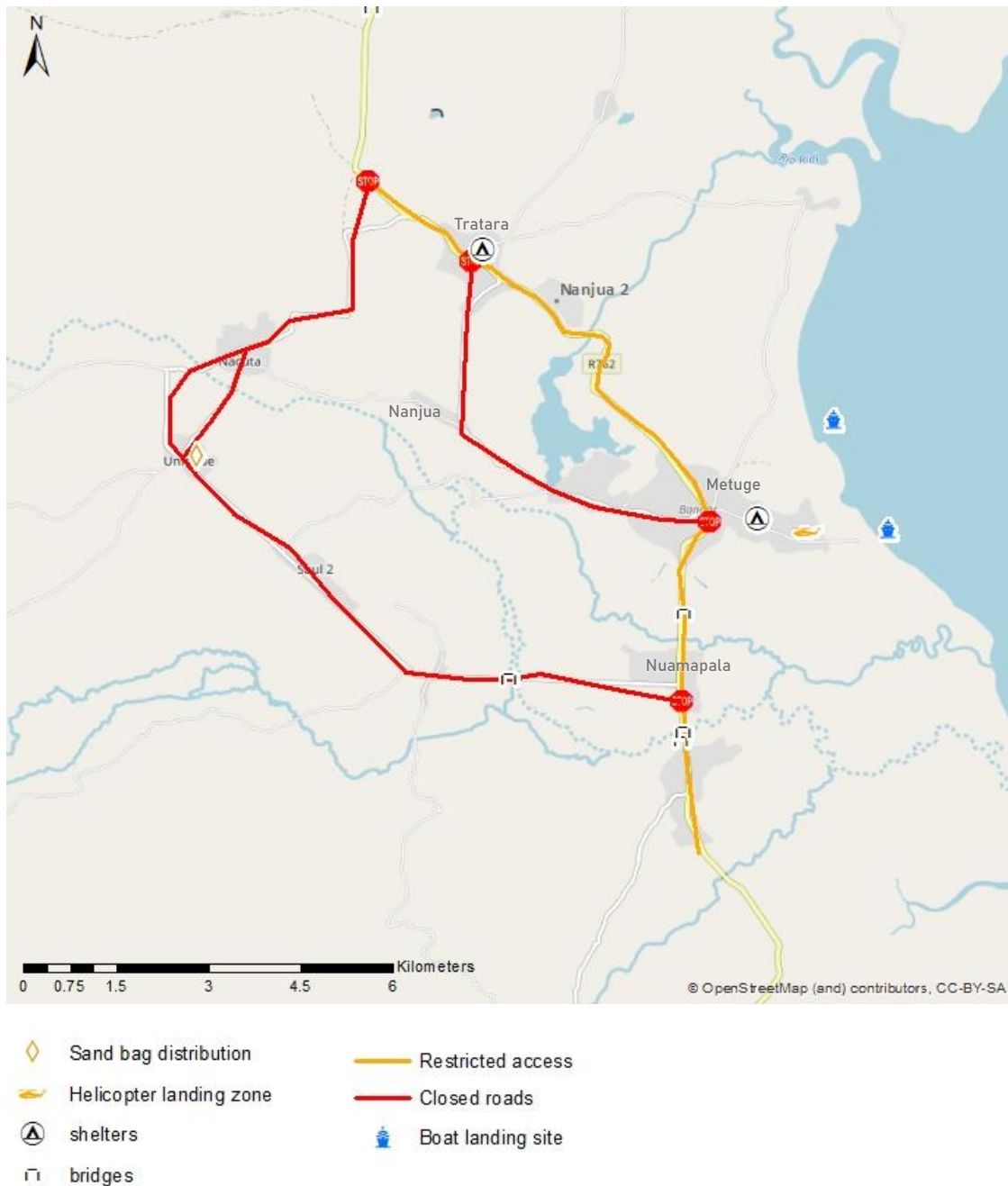
- |  |                         |  |                            |  |               |
|--|-------------------------|--|----------------------------|--|---------------|
|  | Sand bag distribution   |  | Destroyed bridge           |  | Pharmacy      |
|  | Helicopter landing zone |  | Supermarket or market      |  | Airport       |
|  | Shelters                |  | Fireman station            |  | School        |
|  | Road block              |  | Emergency operative centre |  | Hospital      |
|  | Bridge                  |  | SDSMAS                     |  | Health centre |
|  | Boat landing site       |  | Police station             |  | Primary road  |
|  | Secondary road          |  | Pathway                    |  |               |

Figure 59 Emergency map, external accessibility

It is worth noting that the only paved road is the primary road, while the secondary road is a dirt road and driving on it takes a lot of time. Schools and library are shown because, in case of emergency, can be used as

meeting points or first aid places. This is due to the fact that, in this area, the concrete buildings are rare and, most of the times, are used as schools or provincial offices.

A more detailed Emergency map is shown in *Figure 60* where sand bag distribution point, helicopter landing zone, boat landing site and eventual sheltering area are better visualized. The location of a sheltering zone has been chosen after the field survey and after interviewing the population about the preferential ways of water during Kenneth and typical events of the wet season, with the purpose of locating shelters in a safe zone. Helicopter landing zone and boat landing site were taken from maps provided by UNOCHA in the post Kenneth. The road blocks have been located taking as reference cyclone Kenneth, and the same for the



*Figure 60 Emergency map internal accessibility*

restricted access and the closed roads. It is also important to remember that the interview to the population brought out that the village of Nanjua has been completely destroyed by Cyclone Kenneth and the reconstruction of Nanjua 2 has started on the road connecting Metuge and the village of Tratara. In this same place was, in the first emergency phase, located a sheltering camp.

## 3. FLOOD IN THE RURAL AREA

The data collected and selected in the second chapter are now used to perform the hydrologic transformation and then run a synthetic flood modelling for the present condition of the study area.

### 3.1 HYDROLOGY

#### 3.1.1 DEPTH-DURATION-FREQUENCY CURVES (DDF)

The DDF curves estimate the maximum rainfall depth  $h$  for given return periods  $T$  and rainfall duration  $\theta$ . This method uses the following monomial equation:

$$h = a * \theta^n$$

*Equation 1 DDF curve equation*

where  $a$  is a coefficient depending on the return period and  $n$  is a constant exponent. For extreme events it is possible to use the following two properties:

- $n$  does not depend on  $T$  (actually sometimes  $n$  is indicated as dependent on a range of durations, but this is discarded in the following analyses since data for durations lower than 1 hour are not available);
- statistical self-similarity (what is valid for the variable  $h$  is still valid for one of its sample moments).

Using the second property:

$$\mu(\theta) = a_\mu * \theta^n,$$

*Equation 2 Eq. 1 rewritten following self-similarity property*

Where  $a_\mu$  is the value of the parameter  $a$  for the DDF curve referred to the means  $\mu(\theta)$  that in logarithm scale is:

$$\ln \mu = \ln a_\mu + n * \ln \theta$$

*Equation 3 Eq. 2 in logarithmic form*

The following table (*Table 6*) contains the values of the mean rainfall depth for each duration and the respective logarithm values, together with the other parameters needed for the calculation of the DDF curves. Rainfall hourly datum has been summarized for durations of 1, 3, 6, 12 and 24 hours and the maximum value over all years has been taken. After that the logarithm of the mean value and the logarithm of the frequencies are calculated, one obtains the DDF curve shown in *Figure 61* where the linear regression is highlighted.

*Table 6 Moments for different durations and logarithmic transformation*

Duration $\theta$ [hours]	1	3	6	12	24
Mean $\mu$	6,2	16,7	28,6	41,9	56,7
Standard deviation $\sigma$	3,236	9,508	17,527	29,107	46,671
Coeff. of variation $V$	0,520	0,569	0,612	0,695	0,823
$V^2$	0,271	0,323	0,374	0,483	0,678
$\ln(\theta)$ [hours]	0,000	1,099	1,792	2,485	3,178
$\ln(\mu)$ [mm]	1,828	2,817	3,355	3,735	4,038



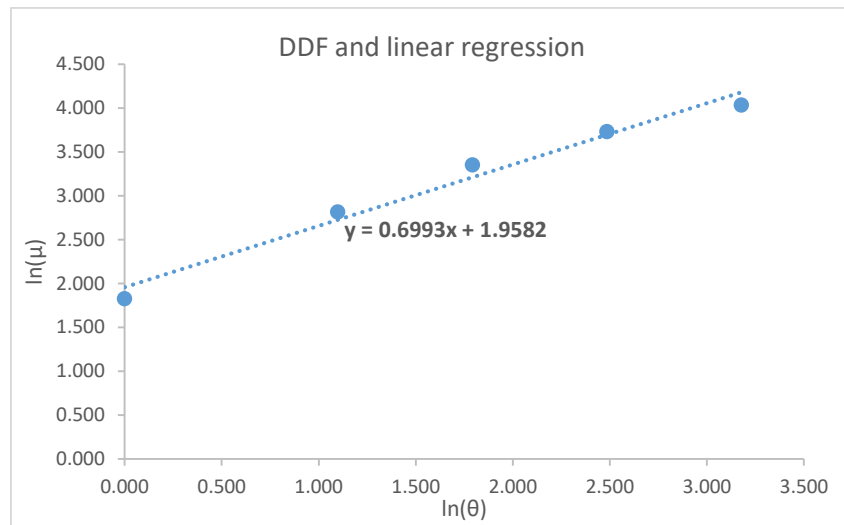


Figure 61 DDF and linear regression

Consequently, parameters  $b$  and  $m$  are extracted with the linear interpolator ( $y=mx+b$ ) and considering  $a_\mu = e^b$ ;  $n = m$  the values are reported in the following table

Table 7 DDF parameters

<b>b</b>	1,9582
<b>m</b>	0,6993
<b><math>\ln(a_\mu)</math> [mm/h]</b>	1,9582
<b><math>a_\mu</math> [mm/h]</b>	7,08655977
<b>n</b>	0,6993

Now the value of  $a$  is needed, it can be obtained from the expression

$$h = \mu * (1 + V * K_T)$$

Equation 4 Rainfall depth

where the latter can be achieved from the Gumbel probability distribution function (Figure 64)

$$P(h) = e^{-e^{-\frac{(h-u)}{\alpha}}}$$

Equation 5 Gumbel probability distribution function

using twice the logarithm

$$h(\theta) = u(\theta) - \alpha(\theta) * \ln(-\ln(P(h))).$$

Equation 6 Eq. 4 rewritten using Eq. 5

Through some arithmetical calculations it is possible to obtain the aforementioned expression where:

the Coefficient of variation is given by

$$V=\sigma/\mu;$$

Equation 7 Coefficient of variation

the frequency factor is given by

$$KT = -[0,45+0,779*\ln(-\ln(1-(1/T)))];$$

Equation 8 Frequency factor

the return period is given by

$$T=1/(1-P(h)).$$

Equation 9 Return period

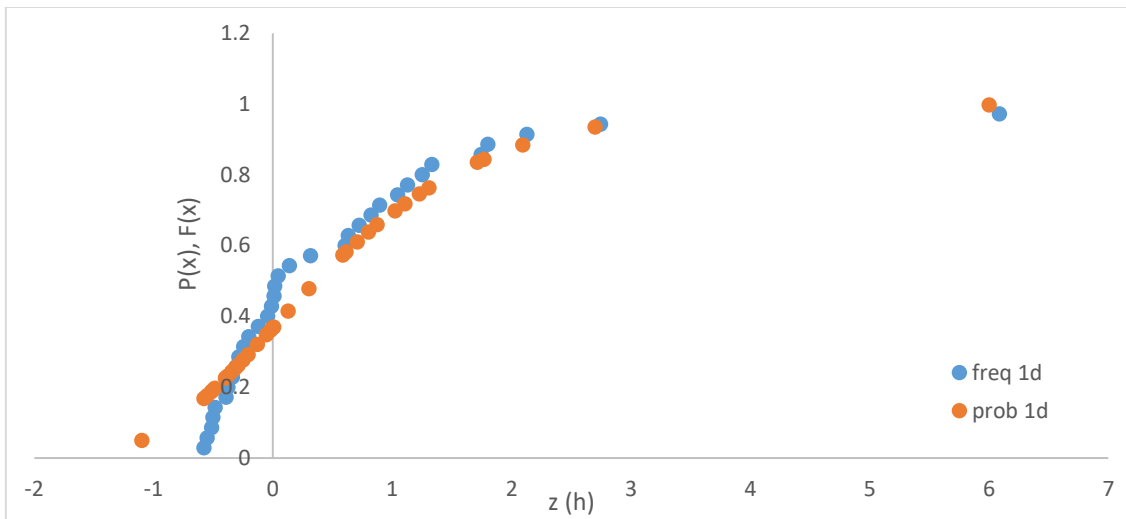


Figure 62 Comparison between frequency and probability for  $\Theta=1$  day

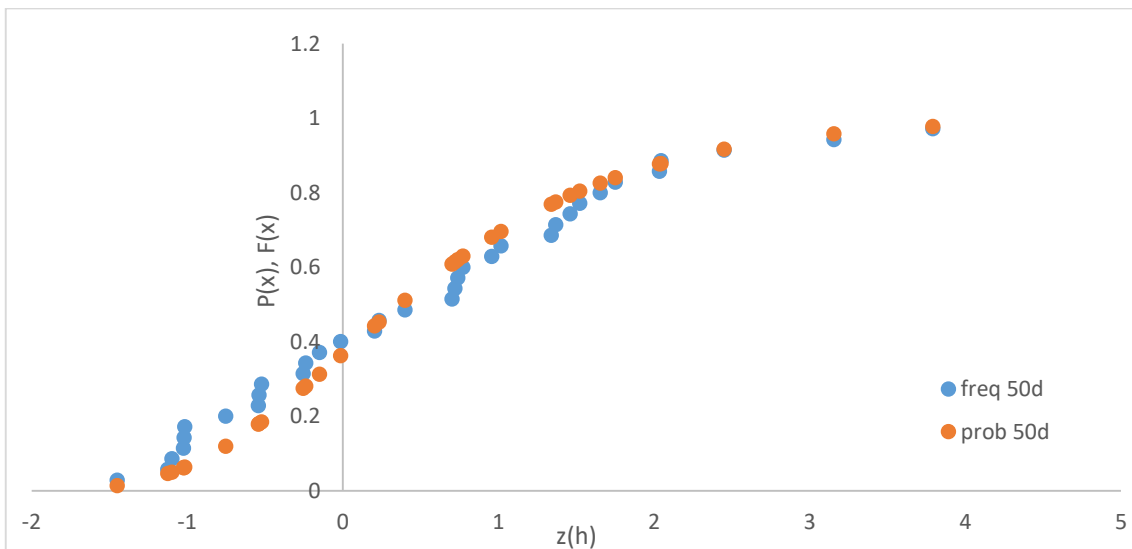


Figure 63 Comparison between frequency and probability for  $\Theta=50$  days

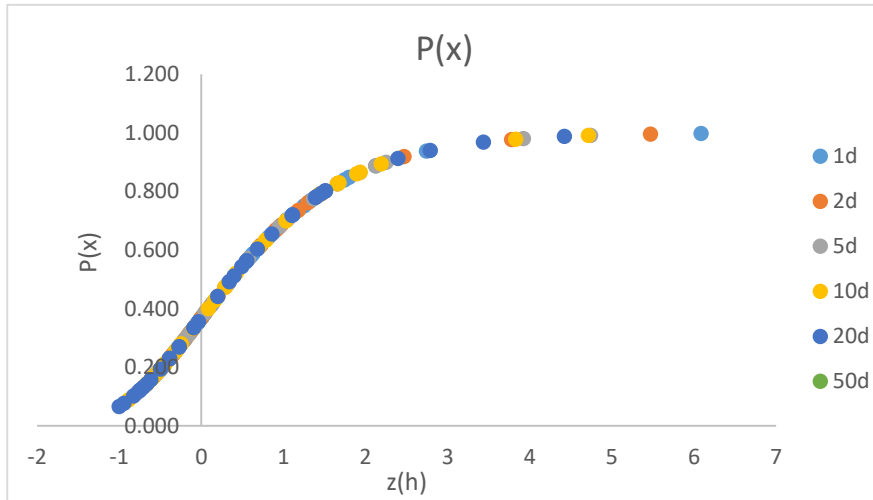


Figure 64  $P(x)$  Gumbel for all the  $\vartheta$  times of measure

At this point, to find coefficient  $a$ , the first formula is used and for the second property of an extreme event (statistical self-similarity):

$$h = \mu * (1 + V * K_T) = a_\mu * (1 + V_m * K_T) * \theta^n$$

Equation 10 Eq. 4 rewritten following statistical self-similarity

so

$$a = a_\mu * (1 + V_m * K_T) ,$$

Equation 11 Eq. 10 rewritten for  $a$

where  $V_m$  is computed as

$$V_m = \sqrt{\sum_{i=1}^k \frac{1}{k} * V_i^2}.$$

Equation 12 Eq. 11 rewritten for  $V_m$

In the following table (Table 8) are shown the values of  $K_T$  and  $a(T)$  considering these different periods  $T$ .

Table 8  $K_T$  and  $a(T)$  values for different return period

T [years]	2	5	10	20	50
<b>K<sub>T</sub></b>	-0,164	0,718	1,303	1,864	2,590
<b>a(T)</b>	6,326	10,409	13,112	15,705	19,061

After determining these two parameters, rainfall depth is calculated and Depth Duration Frequency curves are plotted in the following graph (Figure 65) that is referred to Table 9.

Table 9 Rainfall depth for different return period

$\theta$ [h]	h(T=2)	h(T=5)	h(T=10)	h(T=20)	h(T=50)
<b>1</b>	6,326	10,409	13,112	15,705	19,061
<b>3</b>	13,639	22,441	28,269	33,860	41,096
<b>6</b>	22,146	36,438	45,901	54,979	66,728
<b>12</b>	35,958	59,166	74,531	89,270	108,347
<b>24</b>	58,386	96,068	121,017	144,948	175,925

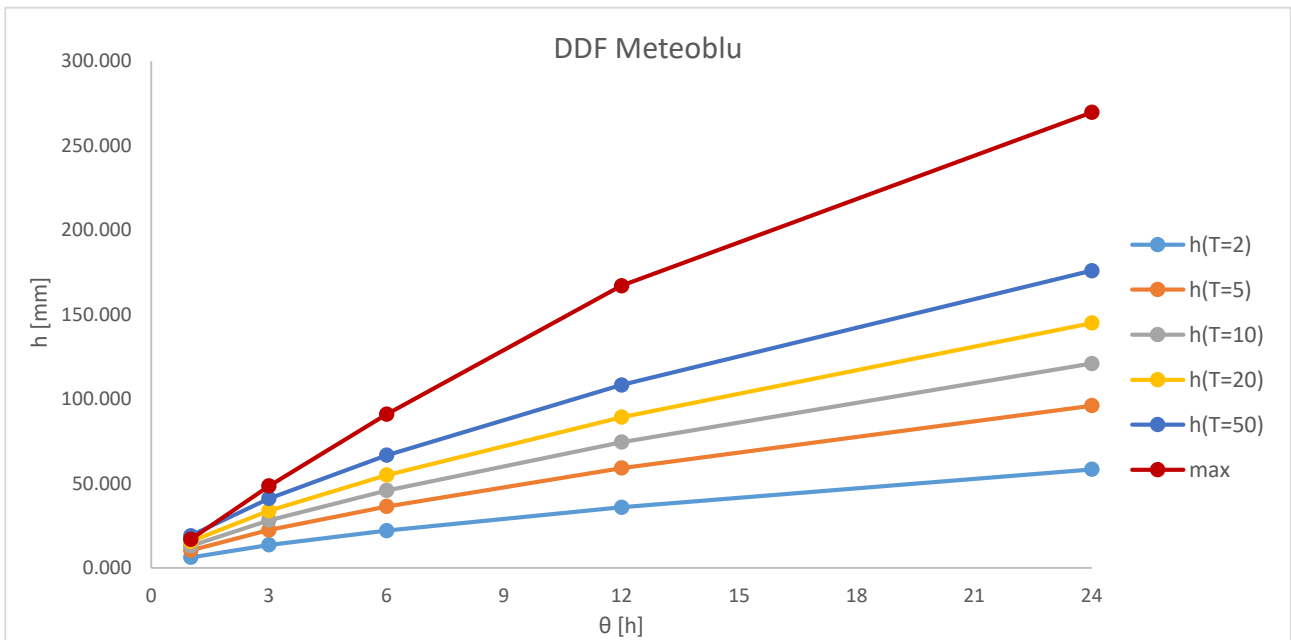


Figure 65 Depth Duration Frequency curves from Meteoblu rainfall data

### 3.1.2 HYDROLOGICAL LOSSES

The hydrological losses are important inputs in design flood estimation; they can be defined as the part of rainfall which is not transformed directly in runoff. These losses are due to evapotranspiration, interception, depression storage or infiltration that is the most important part in a rainfall event. Infiltration is the process by which part of the precipitation is captured and absorbed by the soil. To estimate this phenomenon there are several methods; the most diffuse are the Horton method and the CN-SCS method, which is the one used in this study. The CN-SCS model is based on:

- Mass balance equation

$$Q(t) = P(t) - F(t)$$

Equation 13 Mass balance equation

- Hypothesis of proportionality

$$S'(t)/S = Q(t)/P(t)$$

Equation 14 Hypothesis of proportionality

where

$Q(t)$  is the cumulated runoff volume per unit area [mm];

$P(t)$  is the cumulated rainfall volume per unit area [mm];

$S'(t)$  is the cumulated infiltrated volume per unit area [mm];

$S$  is the maximum volume that can be stored per unit area [mm]:

$$S = \frac{25400}{CN} - 254$$

Equation 15 Max volume stored per unit area

where

CN, the Curve Number, is an empirical parameter and depends on the type of soil and ranges from 0 to 100; it depends on the lithology and on the soil coverage/land use of the basin taken in consideration. For the lithology, the basin is usually classified as belonging to one of the 4 classes (A, B, C and D) listed below and related to the permeability of the soil:

- A. High permeability
- B. Moderate permeability
- C. Low permeability
- D. Very low permeability.

Unfortunately, no maps of the lithology covering this area of Mozambique were found but, after reading a paper related to this topic (Macey et al., 2013)<sup>29</sup> it is possible to assume our basin as characterized by medium-low permeability. For the soil coverage, three different maps were found as reported in chapter 2. The estimation of the Curve Number has been done considering two different tables (*Table 10-11*); the first was found in literature<sup>30</sup> and the second is taken from the Washington State Department of transportation (WSDOT) Highway Runoff Manual, Appendix 4B<sup>31</sup>.

Table 10 CN values (*Handbook of Hydrology, David R. Maidment, 1993*)

Runoff Curve Numbers for Selected Agricultural, Suburban, and Urban Land Uses (Antecedent Moisture Condition II, Ia-0.2S)		Hydrologic Soil Group			
Land-use Description		A	B	C	D
Cultivated Land	Without conservation treatment	72	81	88	91
	With conservation treatment	62	71	78	81
Pasture or range land	Poor condition	68	79	86	89
	Good condition	39	61	74	80
Meadow	Good condition	30	58	71	78
Wood or forest land	Thin stand, poor cover, no mulch	45	66	77	83
	Good cover	25	55	70	77
Open spaces, lawns, parks, golf courses, cemeteries, etc.	Good condition: grass cover on 75% or more of the area	39	61	74	80
	Fair condition: grass cover on 50 to 75% of the area	49	69	79	84
	Commercial and business areas (65% impervious)	89	92	94	95
Residential by lot size	Industrial districts (72% impervious)	81	88	91	93
	1/8 acre or less (65% impervious)	77	85	90	92
	1/4 acre (38% impervious)	61	75	83	87
	1/3 acre (30% impervious)	57	72	81	86
	1/2 acre (25% impervious)	54	70	80	85
	1 acre (20% impervious)	51	68	79	84
Streets and roads	Paved parking lots, roofs, driveways, etc.	98	98	98	98
	Paved with curbs and storm sewers	98	98	98	98
	Gravel	76	85	89	91
	Dirt	72	82	87	89

<sup>29</sup> Geology of the Monapo Klippe, NE Mozambique and its significance for assembly of central Gondwana, Macey et al., 2013

<sup>30</sup> Handbook of Hydrology, David R. Maidment, 1993

<sup>31</sup> [https://www.wsdot.wa.gov/publications/fulltext/Hydraulics/HRM/App4B\\_2014.pdf](https://www.wsdot.wa.gov/publications/fulltext/Hydraulics/HRM/App4B_2014.pdf)



Table 11 CN values (WSDOT)

Cover Type <sup>a</sup> (Hydrologic Condition)	National Land Cover Dataset Types	ID #	Curve Numbers for HSG			
			A	B	C	D
Water	Open Water	11	100	100	100	100
Open Space (Good)	Developed, Open Space	21	39	61	74	80
Residential - 1/2 acre	Developed, Low Intensity	22	54	70	80	85
Residential - 1/8 acre	Developed, Medium Intensity	23	77	85	90	92
Commercial & Business	Developed, High Intensity	24	89	92	94	95
Grassland-Bare Soil	Barren Land	31	77	86	91	94
Park-Aspen (Good)	Deciduous Forest	41	30	30	41	48
Woods (Good)	Evergreen Forest	42	30	55	70	77
Woods (Fair)	Mixed Forest	43	36	60	73	79
Brush (Fair)	Shrub/ Scrub	52	35	56	70	77
Pasture, Grassland (Fair)	Grassland/ Herbaceous	71	49	69	79	84
Meadow	Pasture, Hay	81	30	58	71	78
Row Crops - SR (Good)	Cultivated Crops	82	67	78	85	89
Wetlands	Woody Wetlands	90	100	100	100	100
Wetlands	Emergent Herbaceous Wetlands	95	100	100	100	100

Through GIS tools, the area (or number of cells) with each soil coverage listed in the legend is measured, the percentage for each class is then computed and multiplied by the corresponding value of CN read on the table. Averaging the values, the numbers in the Tables 12,13 and 14 are computed for the three sources of soil cover data.

Table 12 CN estimation from FAO Geonetwork map

Fao Geonetwork soil coverage map	Bacino		Table 11		Table 10	
	n°	%	CN (B)	CN (C)	CN (B)	CN (C)
Closed to open broadleaved evergreen or semi-dec.	2	0,34	55	70	66	77
Close to open grassland	3	0,51	69	79	79	86
closed to open mixed broadleaved and and needleleave	1	0,17	60	73	79	86
closed to open shrubland	35	5,94	56	70	79	86
rainfed croplands	29	4,92	78	85	81	88
mosaic Forest - Shrubland/Grassland	2	0,34	60	73	79	86
mosaic Grassland/Forest-Shrublan	1	0,17	60	73	79	86
Closed broadleaved deciduous forest	164	27,84	30	41	66	77
Mosaic Vegetation/Croplands	178	30,22	78	85	81	88
Open broadleaved deciduous forest	154	26,15	30	41	66	77
Open grassland	3	0,51	69	79	79	86
Open needleleaved deciduous or evergreen forest	16	2,72	60	73	66	77
Water bodies	1	0,17	100	100	100	100
Tot	589	100,00	50,03	59,86	72,32	81,59

Table 13 CN estimation from Copernicus map

Copernicus soil coverage map	Bacino		Table 11		Table 10	
	n°	%	CN (B)	CN (C)	CN (B)	CN (C)
Herbaceous cover (both pastures and natural)	61	3,28	69	79	79	86
Cultivated and managed terrastrial areas	4	0,22	78	85	81	88
Grassland, Shrubland	829	44,59	69	79	79	86
Tree cover, broadleaved, deciduous, closed	8	0,43	30	41	66	77
Tree cover, broadleaved, deciduous, open	957	51,48	30	41	66	77
Tot	1859		48,77	59,29	72,26	81,33

Table 14 CN estimation from ESA map

ESA soil coverage map	Bacino		Table 11		Table 10	
	n°	%	CN (B)	CN (C)	CN (B)	CN (C)
Cropland, rainfed	1028	5,47	78	85	81	88
Mosaic cropland, natural vegetation	2212	11,77	78	85	81	88
Tree cover, broadleaved, deciduous, closed	126	0,67	30	41	66	77
Tree cover, broadleaved, deciduous, open	6965	37,05	30	41	66	77
Shrubland	5502	29,26	56	70	79	86
Grassland	441	2,35	69	79	79	86
Herbaceous cover	526	2,80	69	79	79	86
Mosaic natural vegetation (>50%) cropland (<50%)	347	1,85	78	85	81	88
Tree cover, broadleaved, evergreen, closed to open (>15%)	28	0,15	60	73	66	77
Tree cover, broadleaved, deciduous, closed (>40%)	1362	7,24	30	41	66	77
Mosaic tree and shrub (>50%) herbaceous cover (<50%)	11	0,06	69	79	79	86
Mosaic herbaceous cover (>50%) tree and shrub (<50%)	7	0,04	69	79	79	86
Shrubland, deciduous	5	0,03	56	70	79	86
Tree cover, flooded, fresh or brakish water	1	0,01	100	100	100	100
Tree cover, flooded, saline water	20	0,11	100	100	100	100
Urban areas	140	0,74	61	74	61	74
Bare areas	80	0,43	86	91	86	91
Tot	18801	100	49,41	60,45	73,44	82,27

The choice done was that of using *Table 10* and lithology type C, to stay in favour of safety. The value of CN is the average of the 3 values coming from the different soil coverage maps as shown in *Table 15*.

Table 15 CN value of the entire basin

FAO Geonetwork	81,59
Copernicus	81,33
ESA	82,27
<b>CN chosen</b>	<b>81,73</b>

### 3.1.3 TIME OF CONCENTRATION

The time of concentration (or corrivation)  $T_0$  can be defined as the maximum temporal distance from a point where the raindrop reaches the soil to the downstream section of the catchment. There are several formulae to compute this parameter, as reviewed in the following.

## Giandotti

$$T_0 = \frac{4 * \sqrt{A} + 1.5 * L}{0.8\sqrt{H_m - h_0}}$$

*Equation 16 Giandotti formula*

Where

T<sub>0</sub> [h]: concentration time

A [Km<sup>2</sup>]: basin area

L [Km]: length of the longest hydraulic path

H<sub>m</sub> [m a.s.l.]: average altitude of the basin

h<sub>0</sub> [m a.s.l.]: altitude of the downstream section

## Kirpich

$$T_0 = 0.0078 * \frac{L^{0.77}}{S^{0.385}}$$

*Equation 17 Kirpich formula*

Where

T<sub>0</sub> [min]: concentration time

L [feet]: length of the longest hydraulic path

S [-]: average channel slope

## Pezzoli

$$T_0 = 0.055 * \frac{L}{\sqrt{i}}$$

*Equation 18 Pezzoli formula*

Where

T<sub>0</sub> [h]: concentration time

L [Km]: length of the longest hydraulic path

i [-]: average channel slope

## Ventura

$$T_0 = 0.127 * \frac{\sqrt{A}}{\sqrt{i}}$$

*Equation 19 Ventura formula*

Where

T<sub>0</sub> [h]: concentration time

A [Km<sup>2</sup>]: basin area

i [-]: average channel slope

**Viparelli**

$$T_0 = \frac{L}{A}$$

Equation 20 Viparelli formula

Where

T0 [h]: concentration time

A [Km<sup>2</sup>]: basin area

L [Km]: length of the longest hydraulic path

We performed a sensitivity analysis of the time of concentration to a sub-basin used for its computation. For the estimation the Kirpich equation has been excluded because it is more suitable for little basins. Furthermore, also the Viparelli formula has been neglected because its returned values are three orders of magnitude less than the others. Therefore, we considered the average of Pezzoli's, Giandotti's and Ventura's formulae. The chosen sub-basin and their properties are furnished in *Figure 66* and *Table 16*, while the variability of T<sub>0</sub> is shown in *Figure 67*.

Table 16 Time of concentration varying the area and the length

	T0 [h]	T0 [h]	T0 [h]	T0 [h]	T0 [h]
Giandotti	25,735	24,881	21,289	22,262	19,628
Kirpich	8,261	7,368	4,968	4,114	3,070
Pezzoli	28,982	24,982	14,975	11,720	8,015
Ventura	20,990	21,049	12,960	11,789	8,336
Viparelli	0,077	0,088	0,163	0,165	0,230
T0 medio	25,236	23,637	13,548	12,471	6,473

Area [km <sup>2</sup> ]	1728,14	978,4842	267,2166	192,5358	93,24527
River length [km]	132,54	85,72566	43,61531	31,85153	21,43882

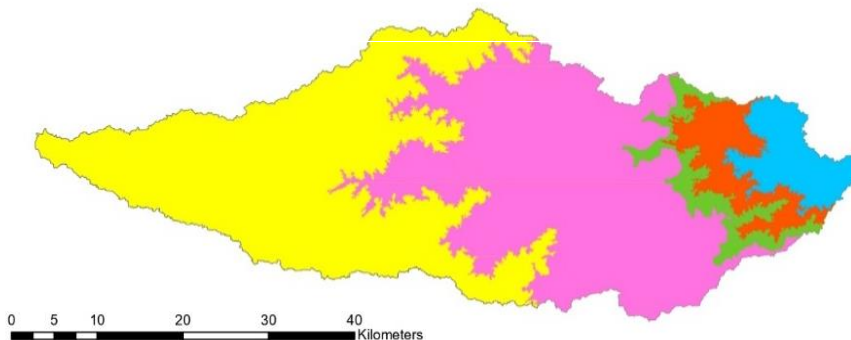


Figure 66 Sub-basins referred to Table 16

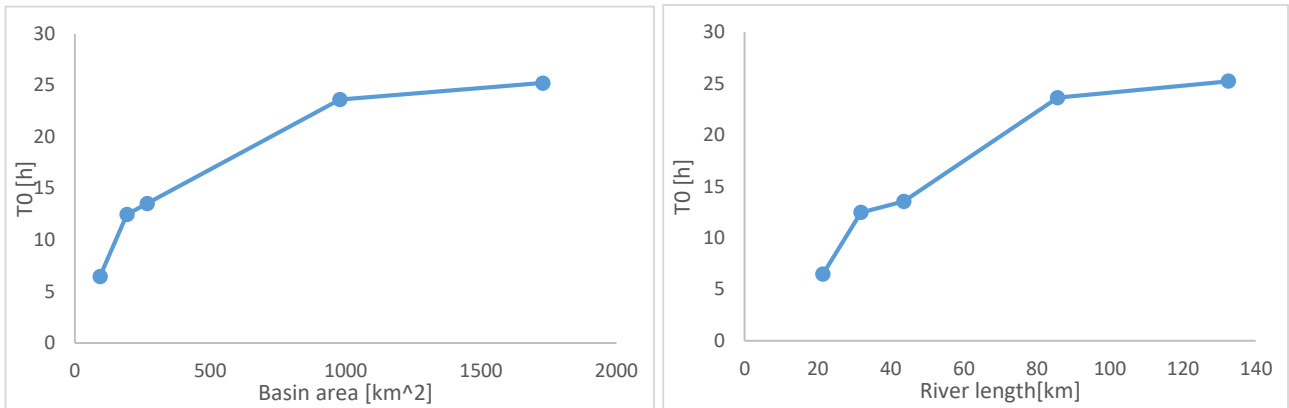


Figure 67 Graphs representing the relationship between increasing basin area and TO on the left and increasing river length and TO on the right

### 3.1.4 CHOICE OF A BASIN TO SUPPORT THE ANALYSIS

The computation of a synthetic hydrograph requires choosing a sub-basin for the analysis. Almost the entire, 1700 km<sup>2</sup> basin, contributes to the flow rates in the study area (see the hydrographic network depicted in Figure 68). However, an assumption of uniform rainfall over the entire basin, that is necessary considering the available data, would be hardly true for the entire basin. Therefore, it was preferred to run models for a smaller basin, located close to the study area. This increases the rainfall intensity and reduce the water volumes compared to a computation with reference to the entire basin. The sub-basin highlighted in Figure

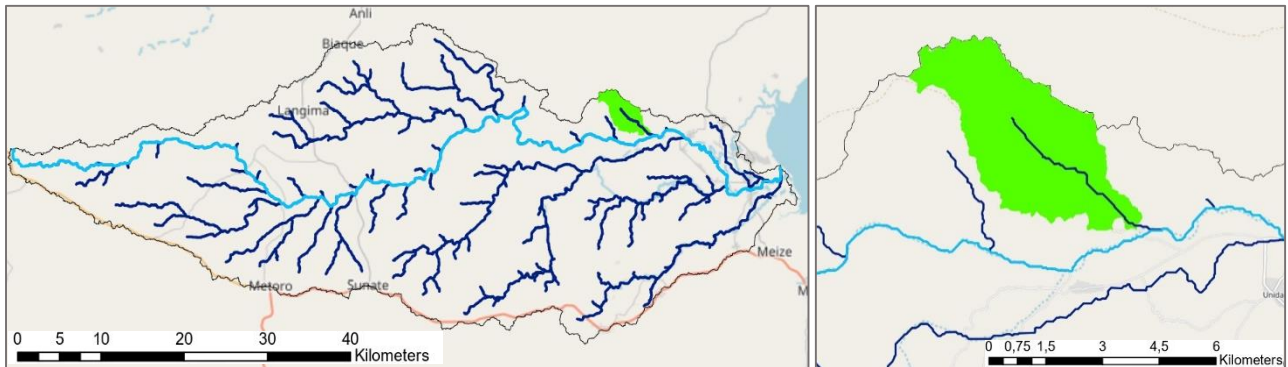


Figure 68 Network of the tributaries of Rio Maguide on the left and detail of the chosen basin on the right

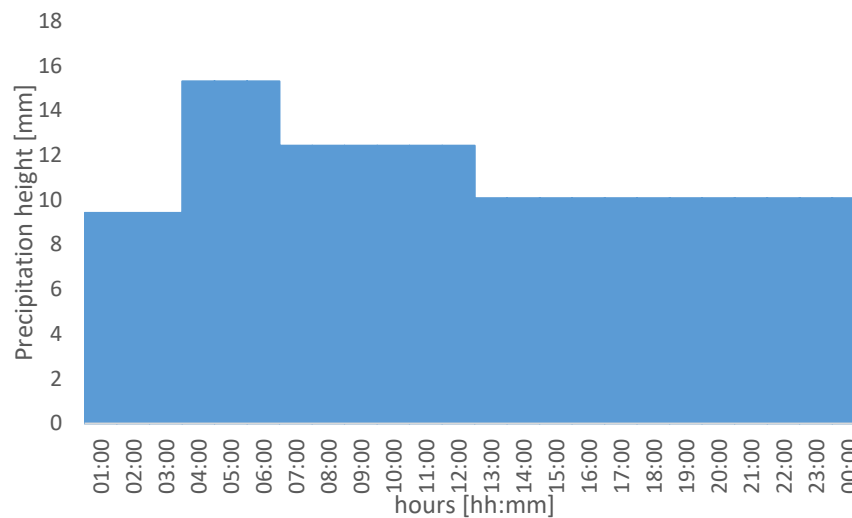
68 was chosen to run the models. In this way all the computations were referred to a rainfall event localized in a small area immediately upstream of the region that is usually flooded. This basin that has an area of 15,1 km<sup>2</sup>, a mean slope of 0,015 and a time of concentration of 4 hours. The computation of the Curve Number has been performed also for this little basin, clipping the land use map following its boundaries; the same calculation done above on the entire basin have been repeated on this second one and the CN has been computed as shown in the following summarizing table (Table 17).

Table 17 CN values for the chosen basin

FAO Geonetwork	77
Copernicus	84,60
ESA	96,34
<b>CN chosen</b>	<b>85,98</b>

### 3.1.5 RAINFALL-TO-RUNOFF MODELLING

The area of interest is affected by flood events that frequently occur during the rainy season, and are capable to flood the surroundings despite their high frequency. Therefore, the analysis has been performed for a moderate return period of 10 years. The corresponding DDF curve is depicted in *Figure 65* together with those for other return periods. For a duration of 4 hours, equal to the time of concentration of the computational sub-basin, one obtains a rainfall depth of 35 mm which turns a small runoff discharge of  $6\text{m}^3/\text{s}$ . Therefore, a duration of one day has been chosen and the synthetic hyetograph is represented in *Figure 69*. It has been obtained using the DDF precipitation values, which are representative of the duration: 1h, 3h, 6h, 12h and 24h. However, the software, used to compute the analysis, divides in equal time interval, corresponding to the one chosen for the results, the rainfall values of the above mentioned durations.



*Figure 69 Hyetograph corresponding to the chosen event*

The Hydrologic Modeling System (HEC-HMS) is a software developed in 1992, by the Hydrologic Engineering Center within the U.S. Army Corps of Engineers (<https://www.hec.usace.army.mil/software/hechms/downloads.aspx>). The software permits to simulate a complete hydrologic process taking as input data the rainfall event and the geometric characteristics of the watershed. In particular, it has been designed to simulate the precipitation and outflow processes of river basins and it is applicable in a wide range of geographical areas. HEC-HMS, in fact, provides the hydrological modeling of a basin, which can be represented by conceptual elements connected with one another. Furthermore, to support the distribution of this elements in a spatial context, a background map can be used.



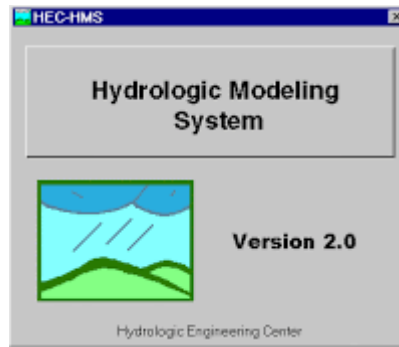


Figure 70 HEC-HMS icon

In particular, to perform a hydrological simulation, the software requires the specification of four components: Basin Models, Meteorologic Models, Control specifications and Time-series data.

The "Basin Model" component allows to specify hydrological elements (such as Sub-basin, Reach, Reservoir, Junction, Diversion, Source, Sink, all of which is identified by a convenient symbol), basin infiltration methods

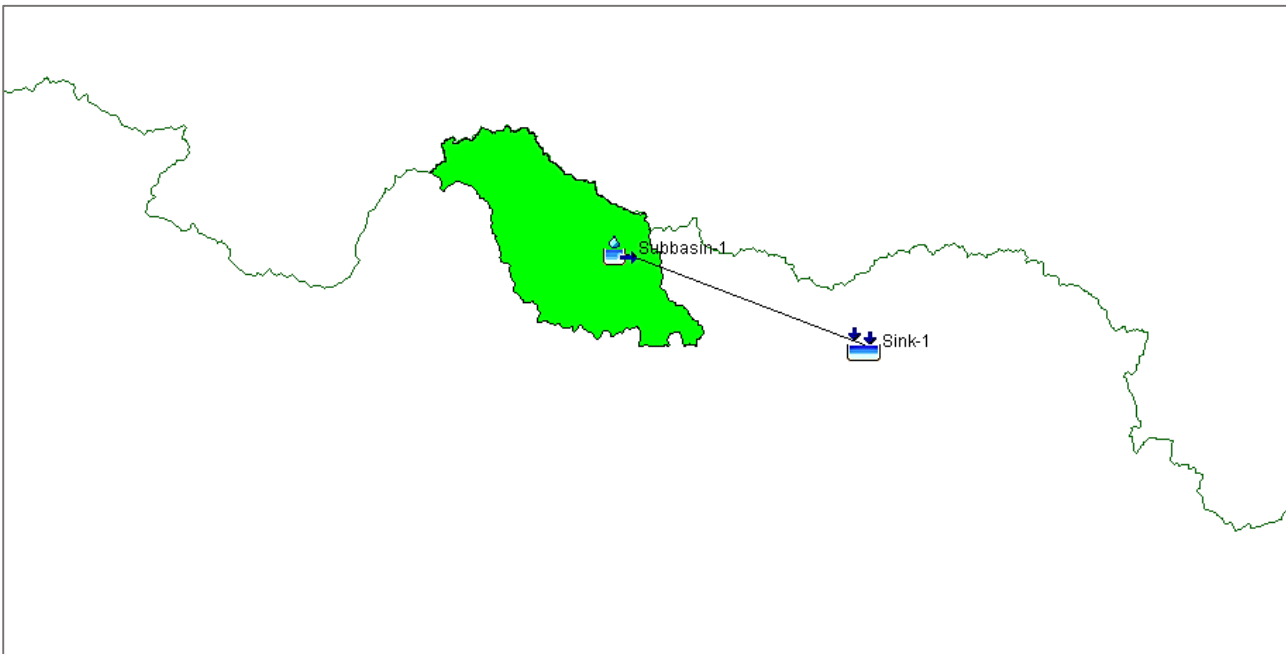


Figure 71 Sub-basin representation in HEC-HMS

and rainfall-runoff transformation methods. In this case, the sub-basin is represented by the "sub-basin creation tool" and the outlet is represented by the element "sink"; the two are simply connected, without reaches (Figure 71); the stream has not been inserted since the short distance of 4 km between the outlet of the sub-basin and the area of interest. Moreover, a preliminary analysis with the presence of the reach, as connection of the two elements, has been performed obtaining the same outflow result with respect to the one without.

The infiltration model used is the SCS-CN method with a CN of 86, determined above, and the rainfall-runoff transformation method is the SCS Unit Hydrograph.

The "Meteorologic Model" data set contains the set of information required for the definition of the precipitations, which must be used together with the basin model. The component includes multiple precipitation, snowmelt and evapotranspiration method. For the case studied only precipitation data are required and the specified hyetograph has been selected.

The "Control Specifications" component sets the simulation time of the hydrological model, and allows to specify the time interval to be used in the calculations.

Finally, the "Time-series data" requires the input data specified in the "Meteorologic Model"; for the present computation, these data are represented by the hyetograph of *Figure 69*.

After the definition of the input parameter the results are available in graphical (*Figure 73*) and tabular format for each basin element. In detail, *Figures 72-74-75* present, respectively, the hydrological losses, the

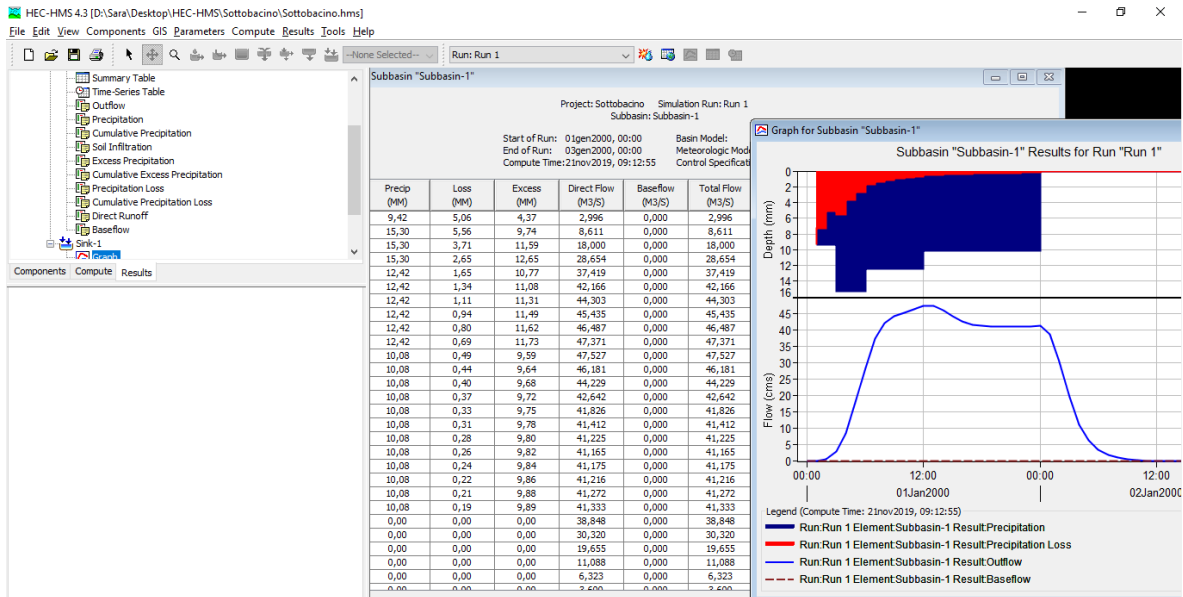


Figure 73 Screen of HEC-HMS results

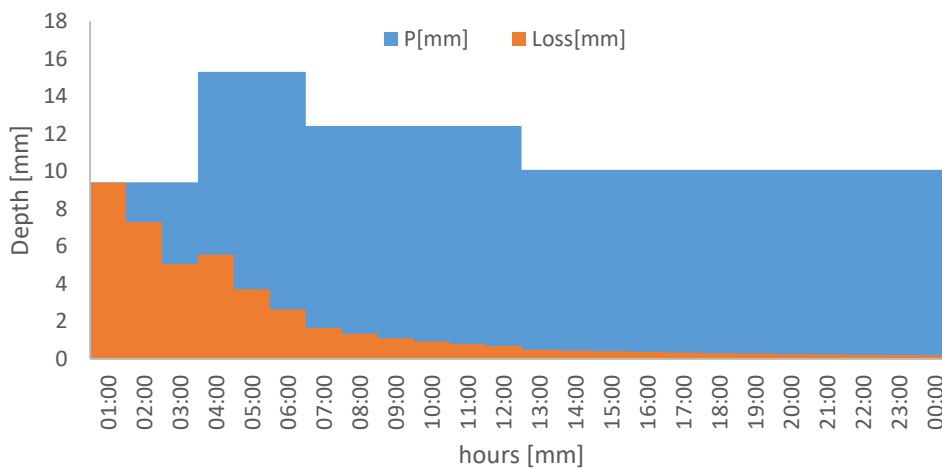


Figure 72 Precipitation and hydrological losses graph

conversion from rainfall into runoff depth, and the discharge hydrograph at the downstream section of the modelled basin. The latter presents a peak discharge equal to 47,5 m<sup>3</sup>/s after thirteen hours from the beginning of the rainfall. Moreover, the hydrograph, after the peak value, presents a plateau which extends until the end of the rainfall.

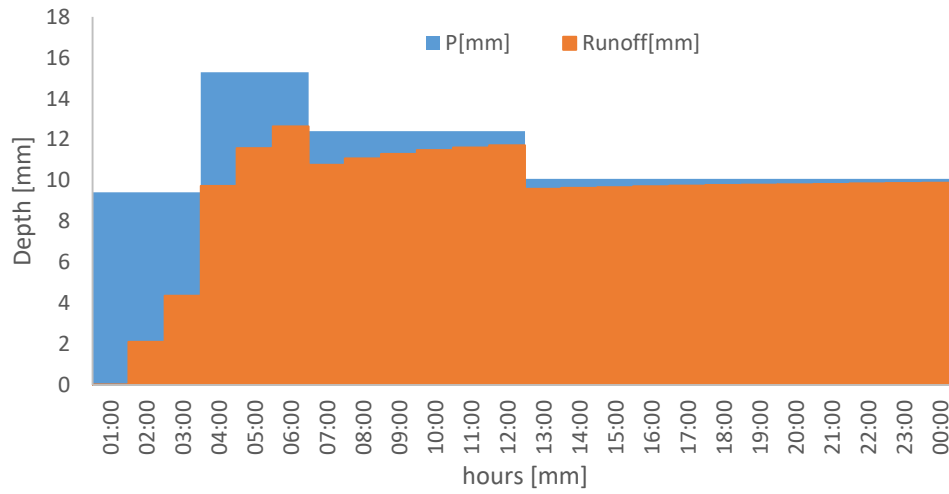


Figure 75 Rainfall-Runoff graph

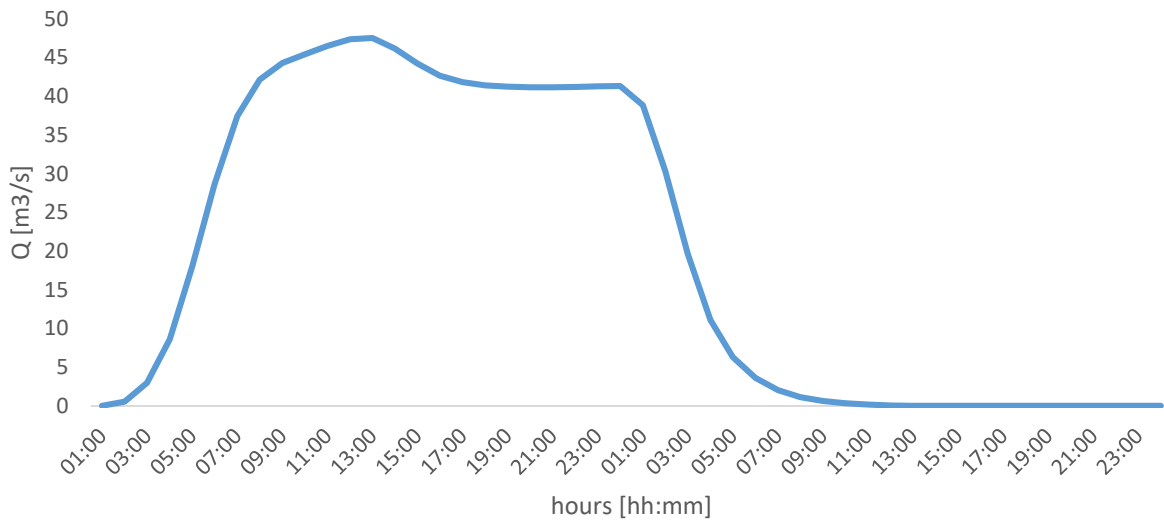
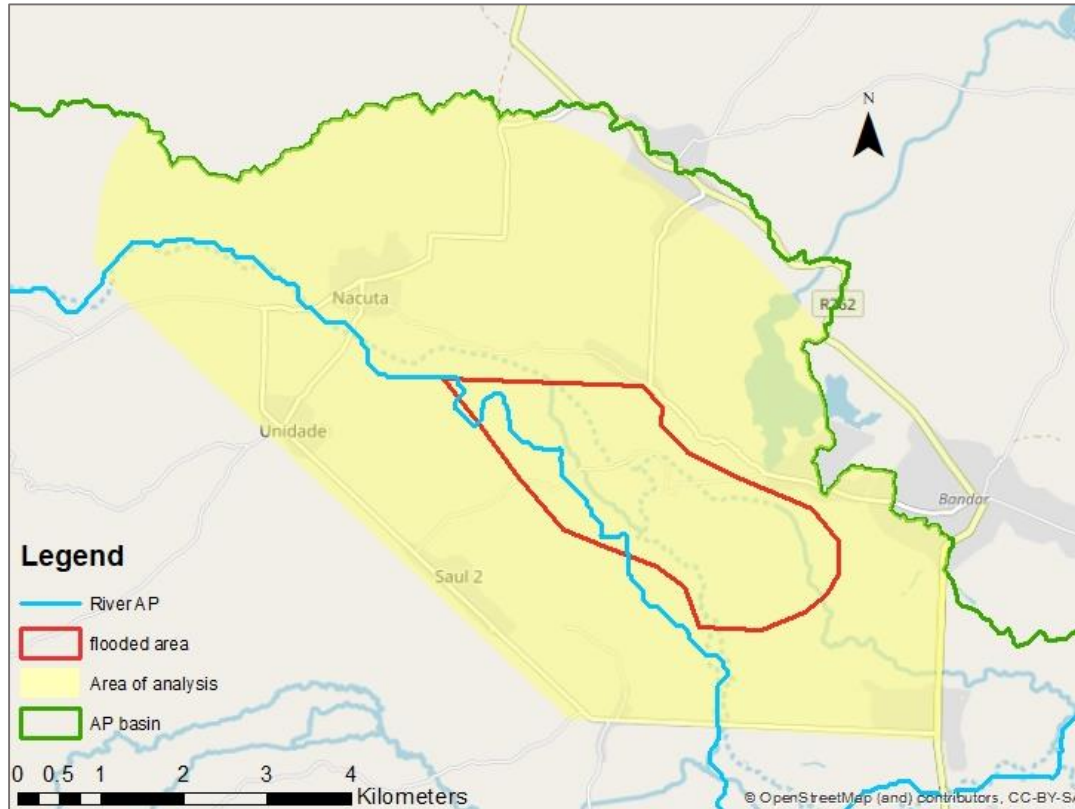


Figure 74 Runoff Hydrograph

## 3.2 FLOOD MODELING

### 3.2.1 COMPUTATIONAL DOMAIN

Starting from the design flood determined above, two-dimensional models of the flood have been created. The territorial context is depicted in *Figure 76*. The area contoured in red is the one which has been indicated



*Figure 76 Extension of the area of flood modelling*

as prone to flood during the rainy season and, in order to perform the simulation, a greater area has been chosen as a computational domain. The area of analysis is bounded by two secondary roads, visible in *Figure 76*, and by the watershed perimeter of the Rio Maguide, indicated in green. Finally, the computational domain has been extended upstream to ensure a certain river distance between an upstream boundary condition and the town of Nacuta, in order to perform a flood simulation which includes the village with a limited sensitivity to the upstream boundary condition. The computational domain, hatched in yellow in *Figure 76*, has an area of about 50 km<sup>2</sup>. The maps in *Figures 77-78* depict the morphologic characteristics of the domain in terms of contour maps of elevation and slope. As can be noticed by the figures, the area of interest is quite flat and the mainstream path is not evident from the DEM.

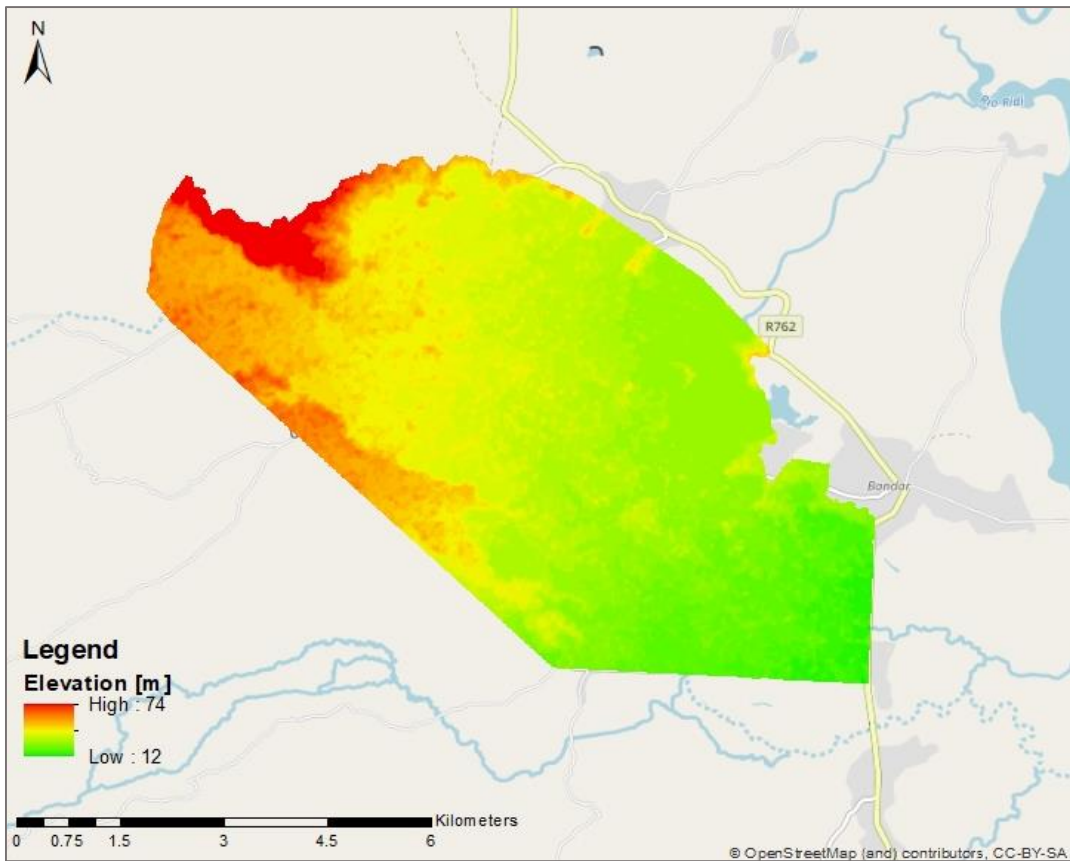


Figure 77 DEM elevation map of the domain

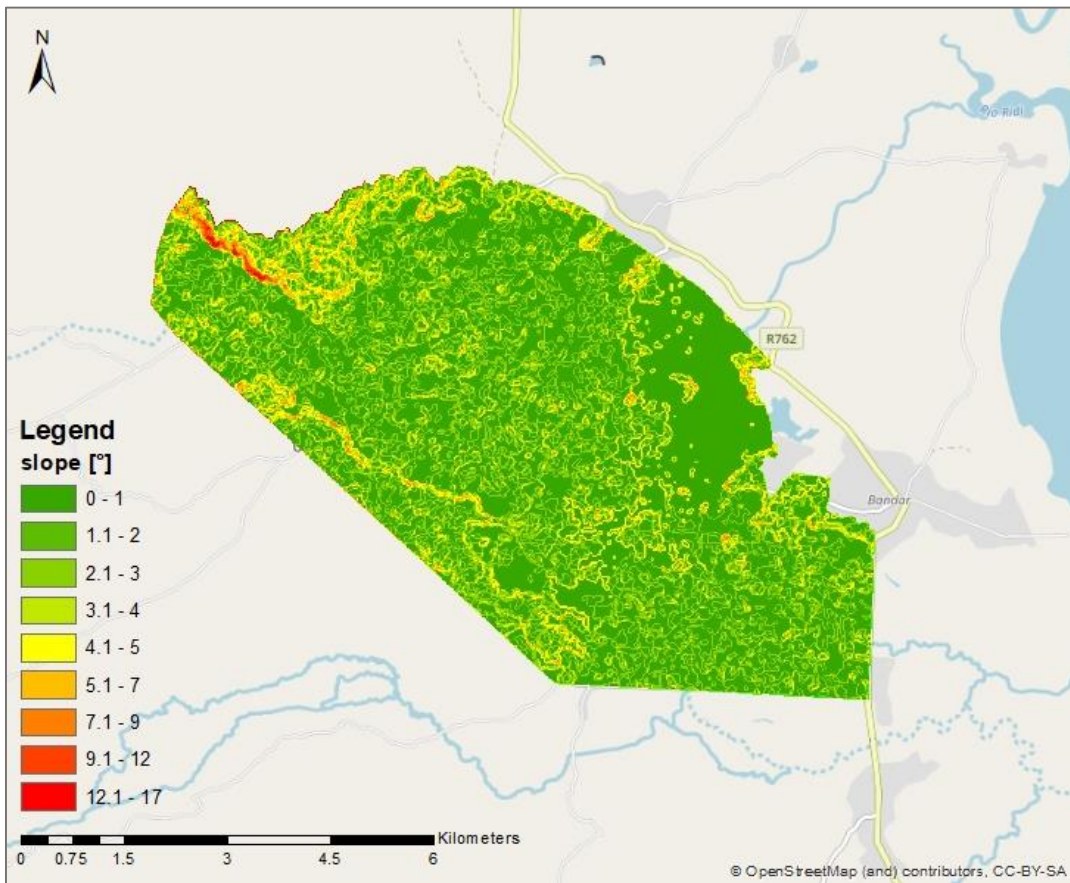


Figure 78 Slope map of the domain

### 3.2.2 MATHEMATICAL MODEL AND BOUNDARY CONDITIONS

Two-dimensional river modelling is based on the *Shallow Water Equations*: the basic mass conservation equation and two (horizontal) components of momentum conservation. Accordingly, it requires boundary condition at the upstream and at the downstream (in case of subcritical flow) ends.

The inflow area (*Figure 79*) is represented by intersection between the domain boundary and the path of the Rio Maguide as determined above. As Inflow discharge, we assigned the maximum runoff discharge of the hydrograph obtained using HEC-HMS.

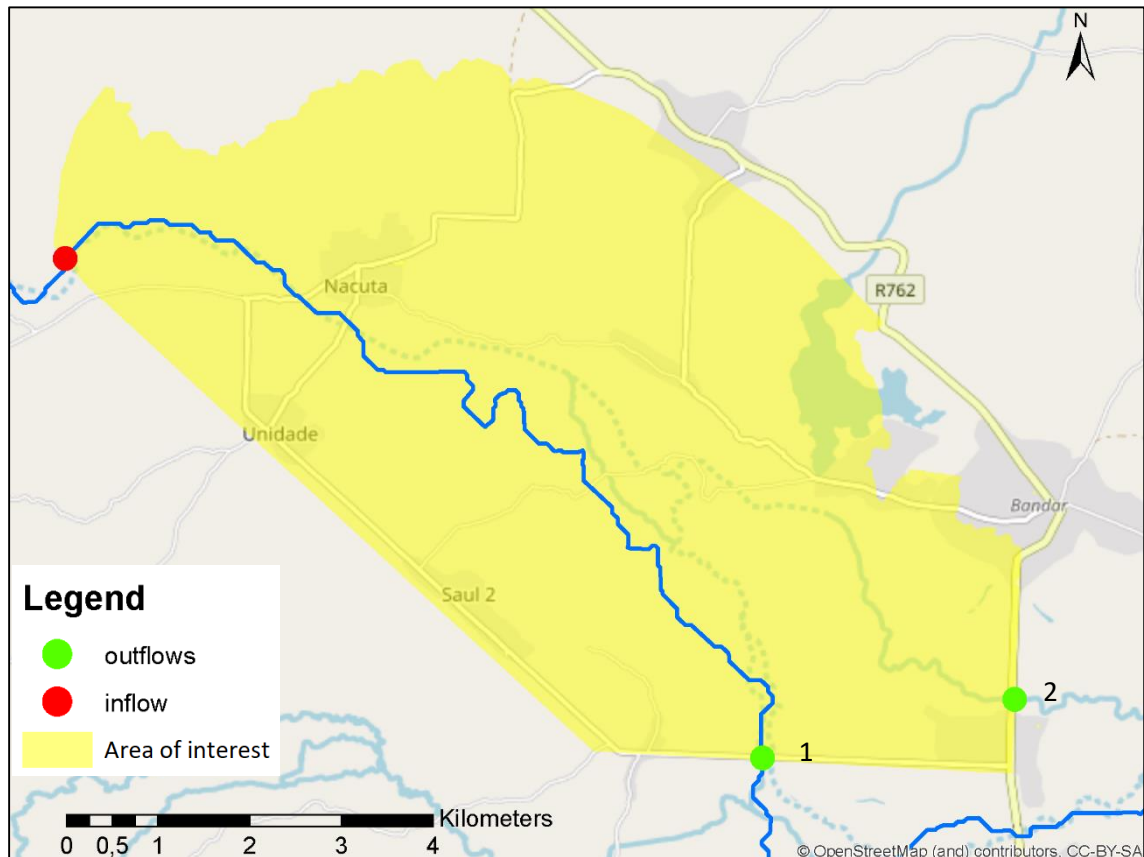


Figure 79 Position of the boundary conditions

Two outflows are placed at the points where the river flows below the roads bounding the computational domain (green points in *Figure 79*), as it passes through openings in the road embankments. The water elevation values to be input at the two points have been computed by an energy balance between the opening cross section (with a flow assumed at critical depth) and its immediately upstream section (see the sketch in *Figure 80*).



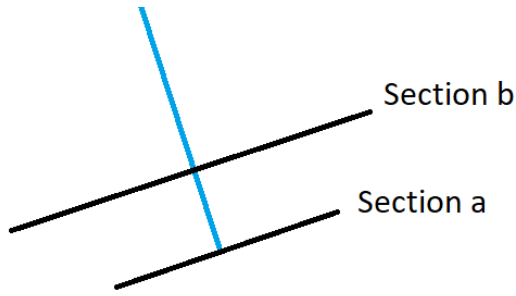


Figure 80 Detail of the section

$$E_a = E_b$$

$$E_a = dc + \frac{Q^2}{2gA_a} \quad \text{with}$$

$$A_a = B_a * dc ; \quad dc = \sqrt[3]{\frac{Q^2}{g * B_a^2}}$$

$$E_b = h_b + \frac{Q^2}{2gA_b} \quad \text{with } A_b = B_b * h_b$$

Equation 21 Energy balance equations

These computations were run before the mission and the detailed surveys of the openings reported in chapter 1. Therefore, for a preliminary estimation,  $B_a$  was measured from Google Earth with the Ruler instrument,  $B_b$  was supposed to be equal to twice  $B_a$  and the discharges  $Q$  passing through the two openings at the peak of the event were assumed as follows:

- $Q_1 = 60\% Q_{peak}$  was the discharge supposed to pass through point 1 of Figure 78
- $Q_2 = 40\% Q_{peak}$  was the discharge supposed to pass through point 2

Following the procedure just mentioned the relative elevations found are:

$$h_1 = 17.1 \text{ m a.s.l.}$$

$$h_2 = 13.6 \text{ m a.s.l.}$$

### 3.2.3 COMPUTATIONAL TOOLS USED

Two software products were used to perform the analysis, namely *River2D* and *STORM*.

*River2D* is a two-dimensional, depth-averaged finite element model developed and distributed by the university of Alberta (Canada). The software is suitable for use on natural streams and rivers and is freely available (<http://www.river2d.ualberta.ca/>). As it solves the basic mass conservation equation and two components of momentum conservation, the outputs from the model are two velocity components (in x and y directions) and a depth at each computational node. The vertical velocity is discarded and the pressure distribution is assumed to be hydrostatic. The *River2D* model suite includes four programs: *R2D\_Bed*, *R2D\_Ice*, *R2D\_Mesh* and *River2D*. *R2D\_Bed* was designed for editing the bed topography, *R2D\_Mesh* program is used for the creation of the computational meshes that will be the input file for *River2D*. *R2D\_Ice* is used in the modelling of ice-covered domains for developing ice topographies, therefore it was not relevant for the present application. These programs are typically used in succession in order to determine the geometry, the mesh and then perform the analysis.

## R2D\_BED

The first step was the creation of a bed file from the Digital Elevation Model. The zone under study covers a large area and the large file created, maintaining cell size of 12,5 m, caused the crash of the program. Therefore, the DEM has been divided into a zone with finer topography made of 12,5 m cell size and a rough one made by cell size of 50 m (*Figure 81*).



*Figure 81 Different spatial resolution zones*

## R2D\_MESH

This second program of the suite is used to define the inflow and outflow areas (*Figure 79*), to input the appropriate boundary conditions and the computational mesh. To define the latter, the user is asked to enter the spacing between the boundary nodes and a uniform node spacing. In this model, the value of 50 m has been initially input for both regions of *Figure 80*. Then, a region refinement, corresponding to the refined region showed in *Figure 81*, can be introduced in order to give a more detailed representation of the topography related to the mainstream path. The mesh provided in *R2D\_Mesh* is triangular one.

## R2D

The last component of the suite is the numerical solver. It permits to perform steady and unsteady analyses; in the present case only the first one has been run.

Steady flow can be defined as the type of flow in which the fluid properties remain constant with time, while the unsteady flow can be defined as the type of flow in which the fluid properties change with time. In general, an unsteady model is considered a better representation of reality than a steady one, as it gives the possibility to know the dynamics of an event, the wave celerity and the wave volume that in a steady flow model is instead infinite. However, in the present case the geometry of the system was quite challenging for the solver and thus the steady model was preferred to arrive at a result.

As mentioned, a second software used is *STORM*, that is part of a suite called *iRIC* (<https://i-ric.org/en/>). *The latter* is a free software platform for numerical simulation of flow and morphodynamics in rivers. Its name stands for International River Interface Cooperative which was started in 2007 by Professor Yasuyuki Shimizu (Hokkaido University) and Dr. Jonathan Nelson (USGS) with the purpose of the software development. The platform supports a wide variety of computational solvers, ranging from one-dimensional to three-dimensional models, shown in *Table 18*<sup>32</sup> with some key properties.

*Table 18 Descriptions of 13 public domain flow and morphodynamics models available in the iRIC interface*

Mode	Dimension	Time variation	Hydrostatic	Coordinate system	Inflow/outflow	Sediment transport/bed evolution/bank erosion	Local grid refinement
FaSTMECH	2D/Quasi-3D	Quasi-steady	Y	Curvilinear orthogonal	One/one	Y/Y/N	N
Morpho2DH	2D	Unsteady	Y	Curvilinear nonorthogonal	One/one	Y/Y/N**	N
Nays2DH	2D	Unsteady	Y	Curvilinear nonorthogonal	Two/one	Y/Y/Y	N
Nays2DFlood	2D	Unsteady	Y	Curvilinear nonorthogonal	Many/one	N/N/N	N
NaysCUBE	3D	Unsteady	N	Curvilinear nonorthogonal	One/one	Y/Y/N	N
Delft3D	2D/3D*	Unsteady	Y	Curvilinear nonorthogonal	Many/many	Y/N/N	N
SToRM	2D	Unsteady	Y	Unstructured-triangles	Many/many	N/N/N	Y
River2D	2D	Unsteady	Y	Unstructured-triangles	Many/many	N/N/N	Y
CERI1D	1D	Unsteady	Y	NA	One/one	N	
Mflow_02	2D	Unsteady	Y	Unstructured-triangles	Many/many	Y/Y/N	Y
SRM	NA	Unsteady	NA	NA	Spatial/one	N/N/N	N
NaysEddy	3D	Unsteady	N	Orthogonal structured	One/one	Y/Y/N	Y
ELIMO	2D	Unsteady	Y	Curvilinear orthogonal	NA	N/N/N	N

\* Hydrostatic with morphodynamics, nonhydrostatic without morphodynamics.

\*\* Mud and debris flow capability.

Y: yes

N: no

For the project purpose, it was important to select a solver permitting a local grid refinement, the presence of multiple outflows and the capability to provide flood inundation in a large spatial domain. The software *STORM* was used.

## STORM

*“SToRM (System for Transport and River Modeling) is a two-dimensional surface-water flow code based on the shallow water equations [...] and provides steady and unsteady versions in the same package.”*<sup>33</sup>

The model was developed by Francisco Simões of the U.S. Geological Survey National Research Program and it is suitable to obtain flow solutions in complex domains thanks to an unstructured grid. As *River2D* it permits to define multiple boundary conditions of inflow and outflow and to add a refined grid in critical zones of the domain with a faster computation.

<sup>32</sup> “The international river interface cooperative: Public domain flow and morphodynamics software for education and applications.” *J.M. Nelson et al. 3 October 2015.*

<sup>33</sup> <https://www.brr.cr.usgs.gov/gstl/project-SToRM.html>

All the solvers incorporated in *iRIC* presents a common user interface to define the topographic information, the grid creation, the boundary condition setting and finally the calculation parameters.

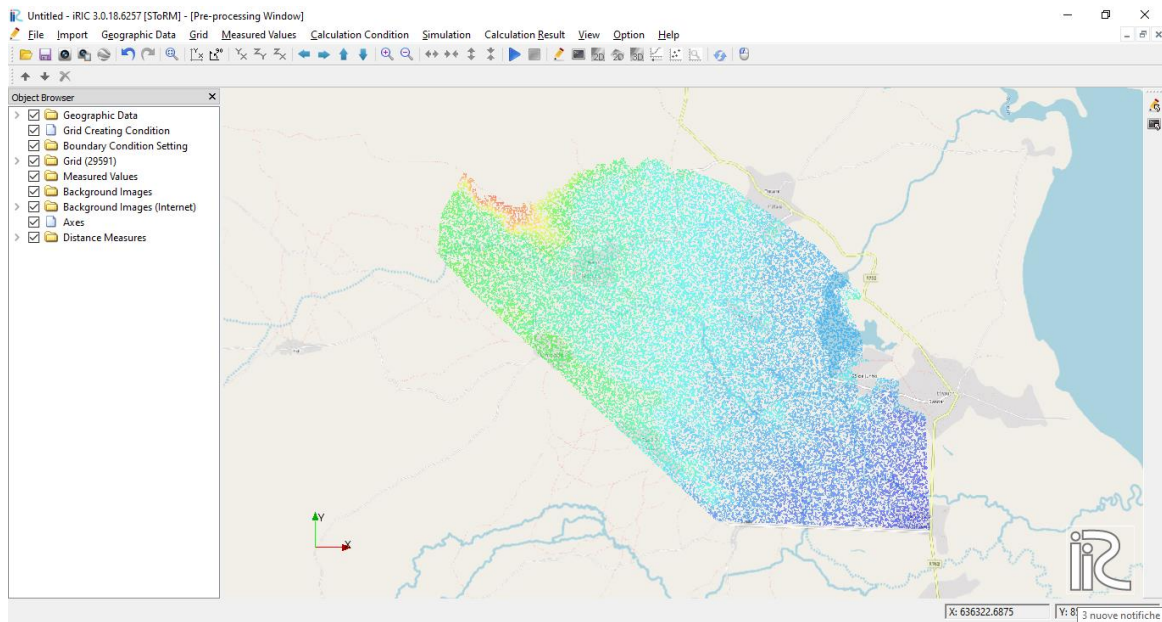


Figure 82 *iRIC* interface and elevation representation of the area of interest

In particular, for the geometry construction it is possible to insert as input file a text file, like for *River2D*, and to specify the coordinate system in order to add a background image, which helps the user in grid and boundary condition drawing.

Like the Alberta's software, *STORM* permits the grid creation with triangular elements, inserting the maximum area of the elements, which defines the level of refinement of the mesh, and its minimum vertices angle in order to avoid thin elements. The following data has been inserted:

- Minimum angle for cell vertices: 30°
- Maximum area for cells: 1250 m<sup>2</sup>

The maximum area inserted corresponds to half the area of the DEM cell of 50 m side. Then, the refinement region has been drawn as described above. The maximum area inserted corresponds to the half area of the DEM cell of 12,5 m side.

The procedure to define the boundary condition is the same as for *R2D\_Mesh*.

Then, *iRIC* permits to define the roughness drawing polygons around the interested area. For the sake of simplicity and also for data scarcity a unique polygon and a unique Manning's coefficient of 0,035 sm<sup>-1/3</sup> has been set.

The calculation condition setting offers four different entry screens:

1. *Initial Conditions*: it is used to specify the initial state of the dependent variables through three different ways: using multiple coverage polygons defined by the user; using a uniform flow field for the entire computational domain; and using a flow solution computed in a previous model run. In the project the uniform initial condition option has been chosen, setting the values of the flow velocity equal to 0 m/s and stage at start of a numerical simulation equal to 41 m a.s.l.
2. *Cell Wetting and Drying*: in this entry screen, it is determined how the wet-dry cell boundaries are treated in *STORM*. In particular, the user is asked to define the threshold depth below which a cell

can be considered dry. A higher threshold value improves stability and computational efficiency, but decreases the accuracy of the results. The threshold for drying cells is set to 0,003 m.

3. *Solution Parameters*: this screen contain parameter related to the numerical methods, time interval, duration of the simulation.
  - There are three *numerical methods* that can be chosen and they are Order 1, Order 2, and Order 3. Order 1 is the least accurate but the fastest while the Order 3 is the most accurate but its computational requirements make it less useful for use in practical applications. The first one has been chosen.
  - The *time step size* must be small enough to ensure numerical stability at all times during the calculations.
  - The *number of time steps* entry dialog require the total number N of time steps to determine the length of the run which is equal to  $N \cdot \Delta t$ .
  - The *maximum velocity* entry dialog is useful to ensure to the user that an obtained solution is accurate and that it does not contain the results of unstable calculations. In fact, imposing a value of velocity higher than any flow velocity can have, like 30 m/s which is the one used in the project, the user can check that the velocity of the model does not present absurd values.
4. *General Options*: in this screen can be defined the type of resistance coefficient choosing between Manning, Chezy or Drag coefficient.

The results of the model are saved in a text file that contains the current time step, the inflow discharge and the outflow discharge of the first boundary condition.

### 3.2.4 MODELLING RESULTS

Steady analysis was performed with a flow rate equal to the peak of the hydrograph, thus 47,5 m<sup>3</sup>/s. The results obtained using the two software tools are reported below considering the flood area and the water depth (*Figures 85-88*). The results obtained from the two solvers are quite similar to each other.

A distinct river reach is not well identified, as one sees several scattered areas, partially disconnected. This is due to the resolution of the DEM, that is not fine enough to get a sounder result. However, the sub-reach of the river flowing towards outlet 1 is visualized by a track of higher water depths (*Figures 87-88*). Comparatively, the amount of water flowing towards the lake and then towards outlet 2 is less, which is somehow contradicting the evidences of the areas flooded during Kenneth (*Figure 9*) and the state of this reach, that was somehow better than that of the other during the mission (*Figure 16*). This could be due to morphologic change occurred after the collection of the images based on which the DEM was built (possibly by Kenneth itself), or again to the poor resolution that does not enable incised river beds to be seen. This behaviour is shown comparing the flooded area extracted by SNAP and the two modelled with River 2D and iRIC (*Figure 83-84*).



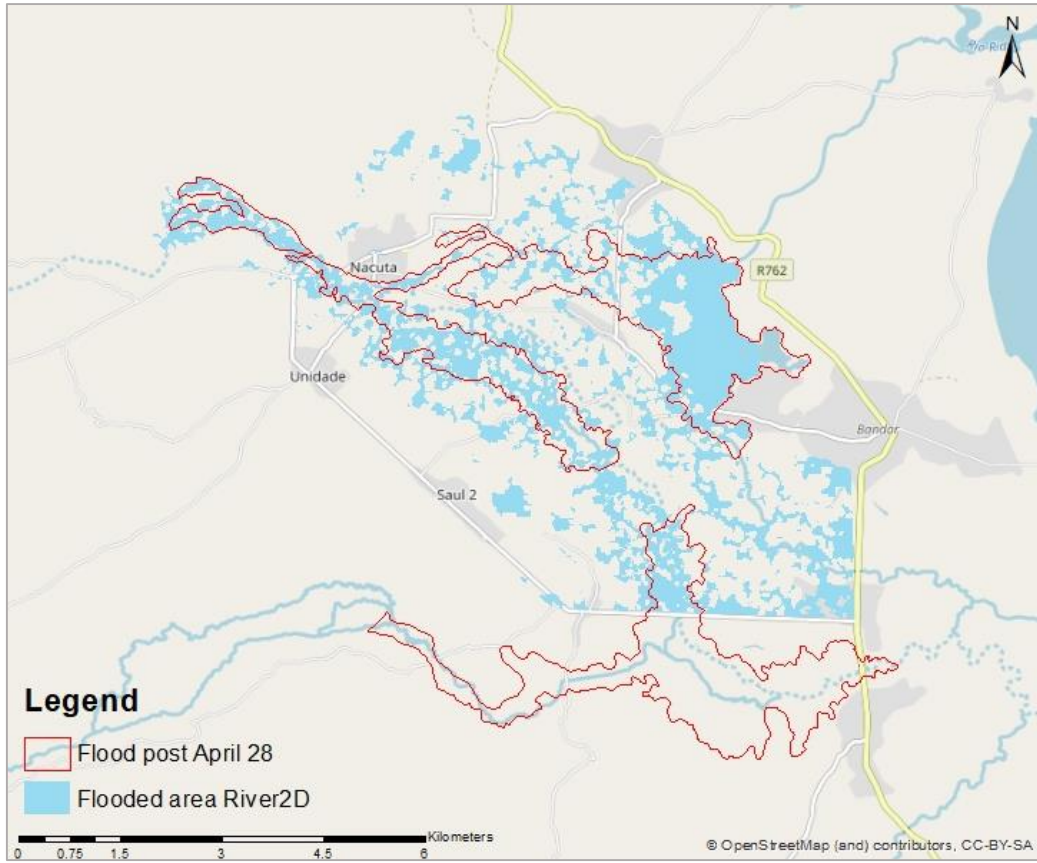


Figure 83 Flooded area with R2D compared with the flooded area extracted by SNAP

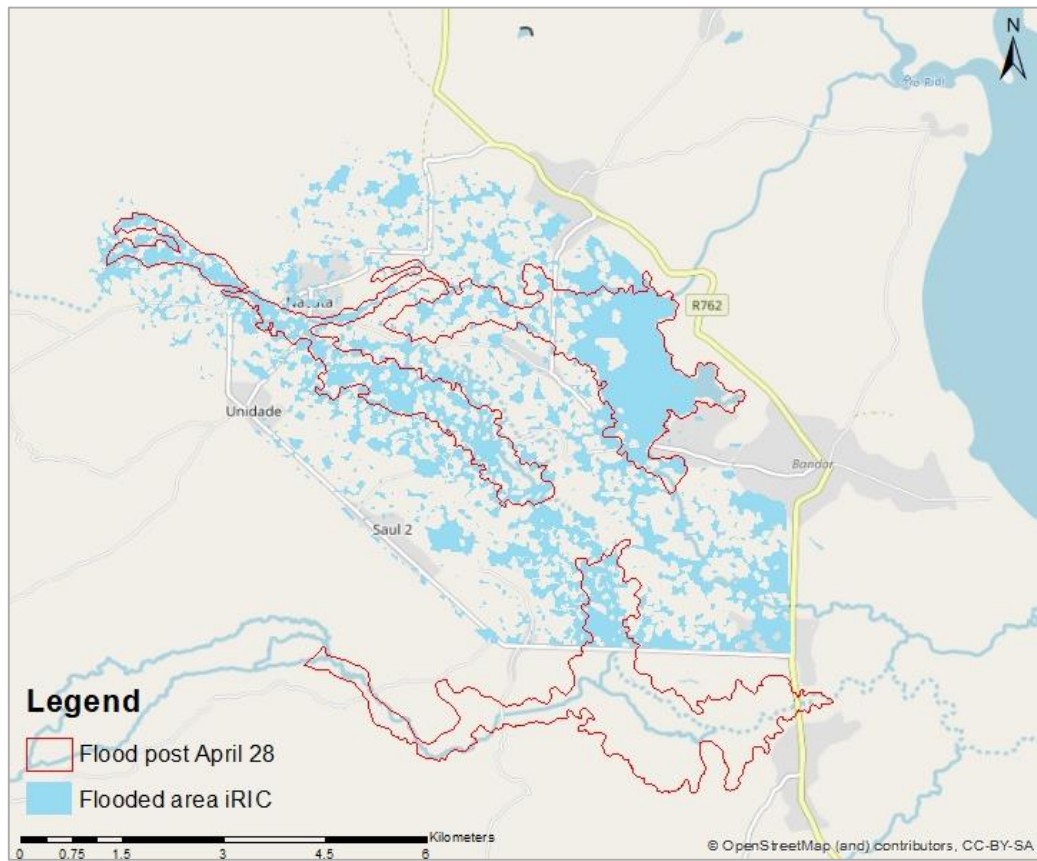


Figure 84 Flooded area with iRIC compared with the flooded area extracted by SNAP



The *iRIC* flooded area presents more scattered area disconnected from the main flood body. This can be due to the fact that in *STORM* there is no possibility to account for the infiltration capacity of the soil, while in *River2D*, the Storativity and Transmissivity parameters represent the groundwater behaviour. In particular, the Storativity is defined as “the volume of water the ground will release from storage per unit surface area of the ground per unit decline in the water table”<sup>34</sup> and the Transmissivity as the rate at which groundwater flows horizontally through an aquifer. The larger these values are, the more the soil is permeable. It is true that these parameters may affect significantly the solution only in transient conditions, but it is also true that convergence was not fully reached as discussed below.

---

<sup>34</sup> *River2D - User Manual – September 30, 2002*

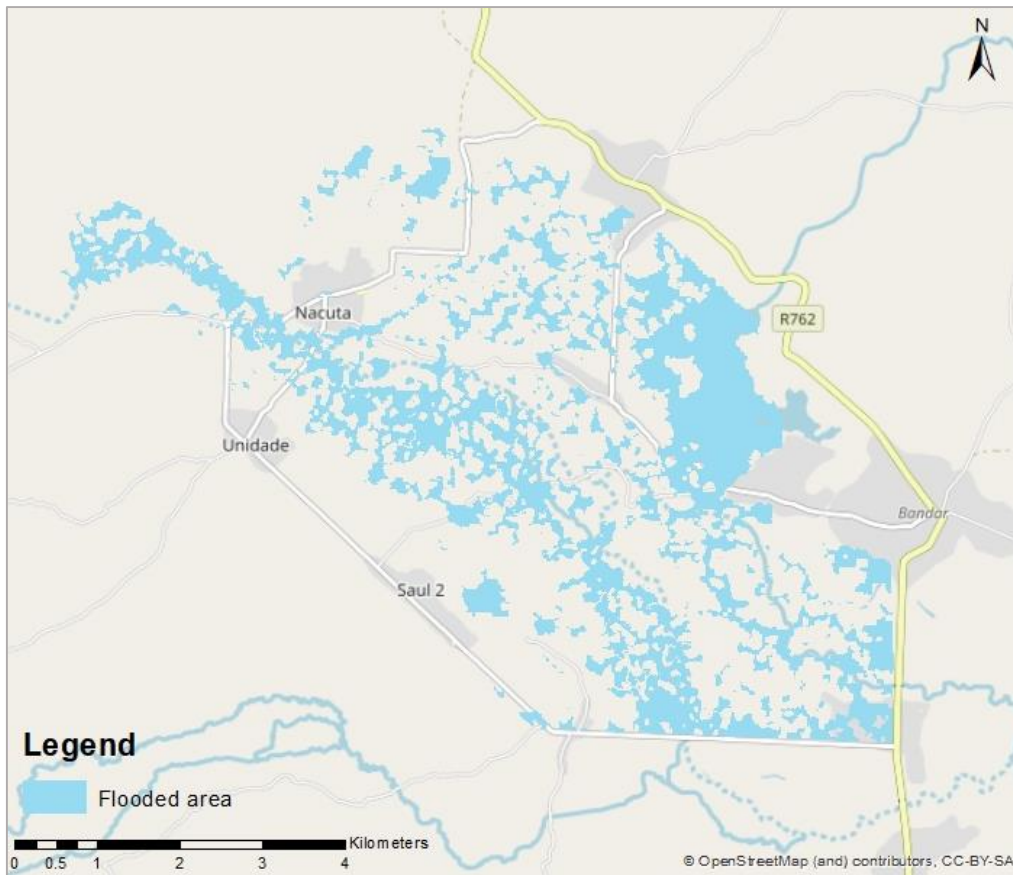


Figure 86 R2D flood extension

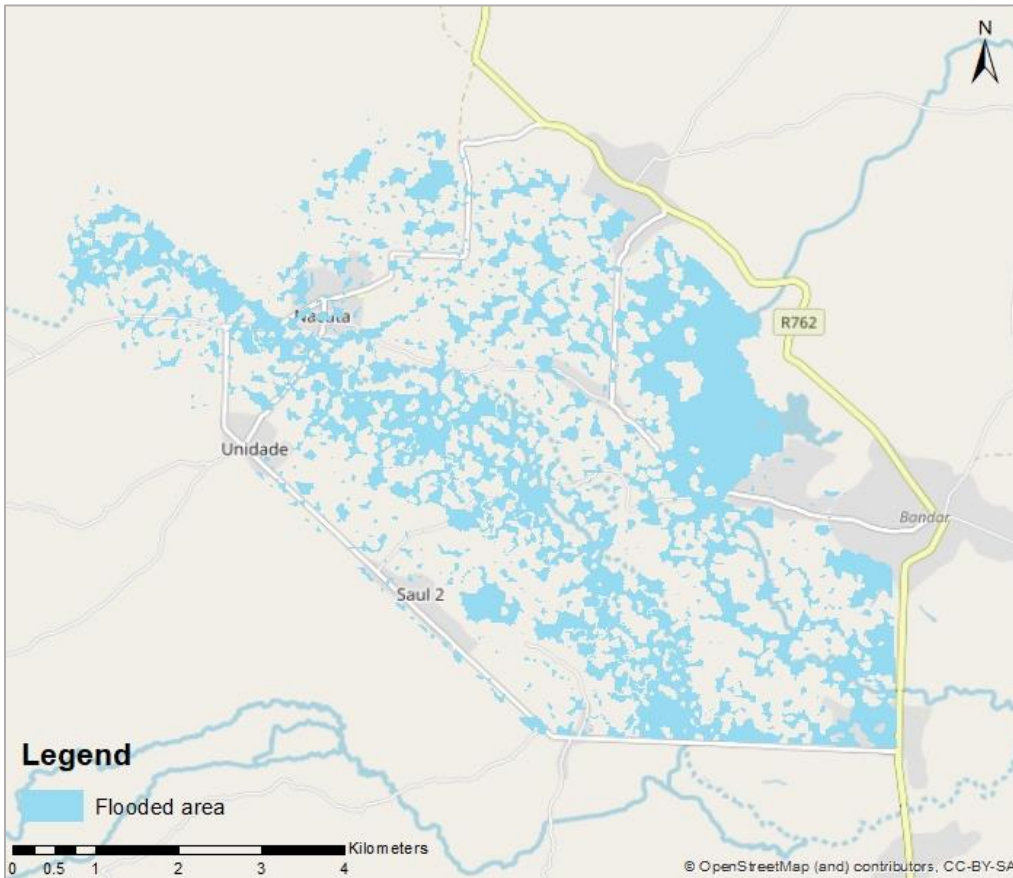


Figure 85 iRIC flood extension

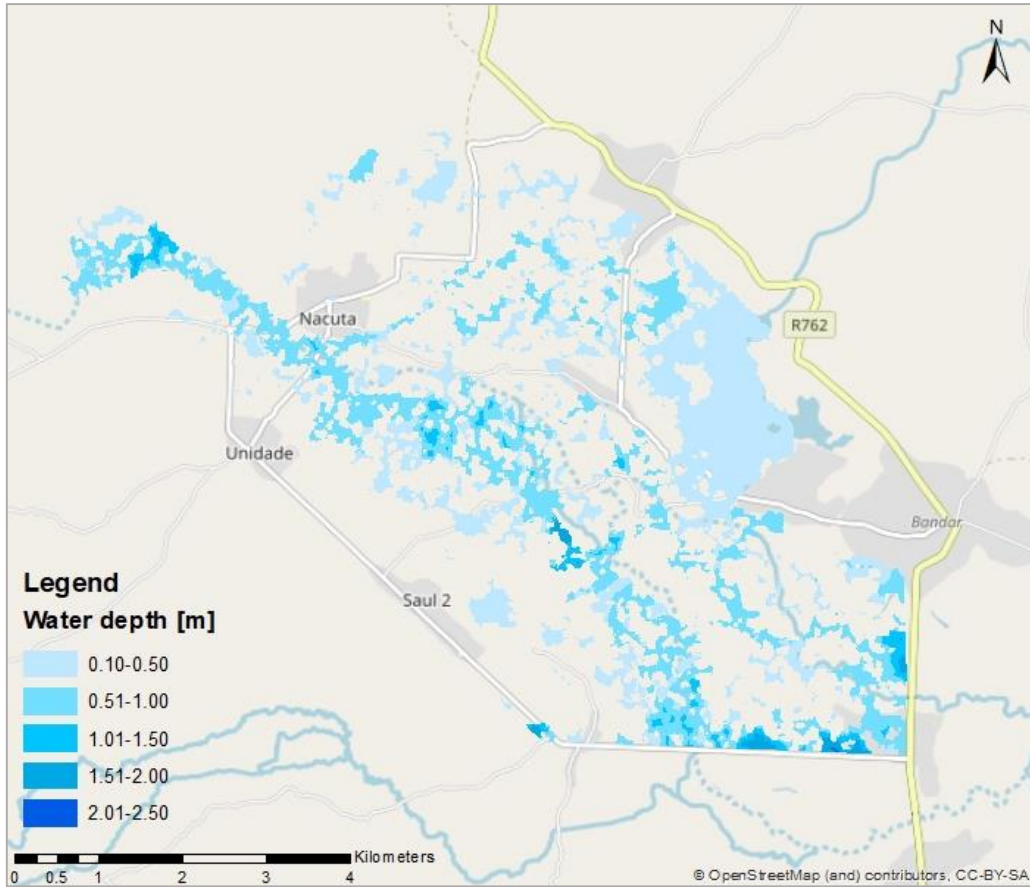


Figure 88 R2D water depth

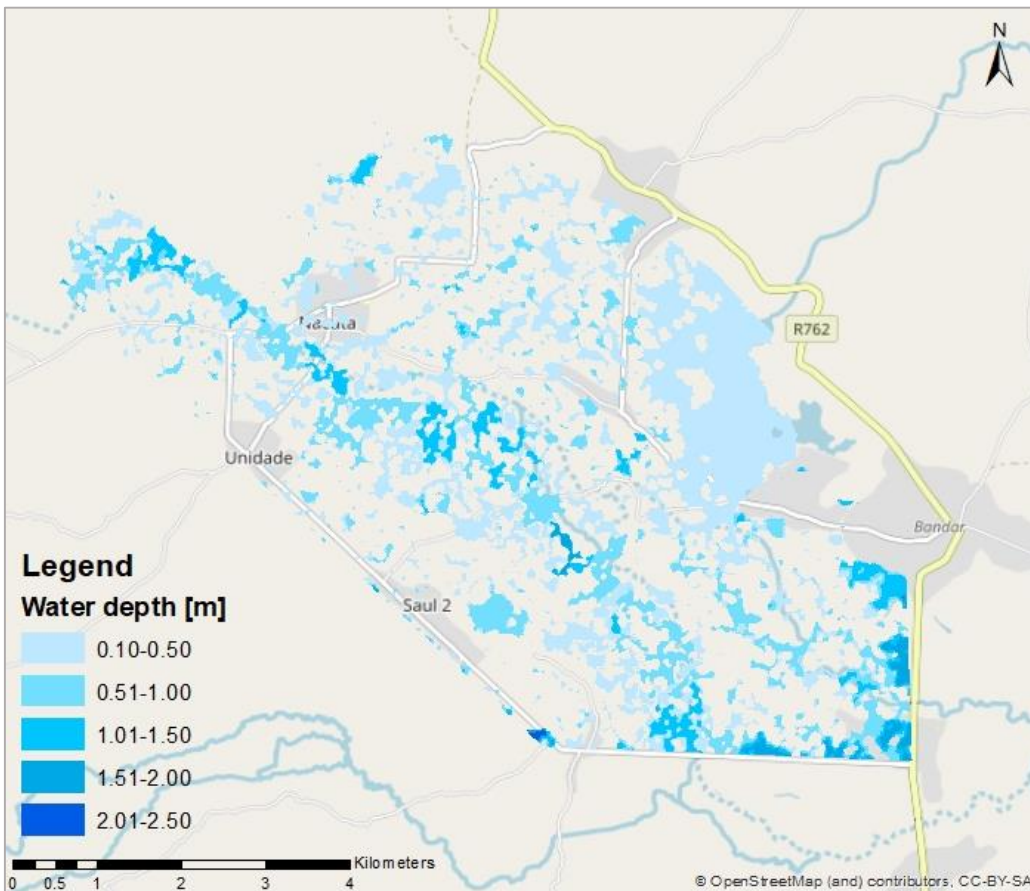


Figure 87 iRIC water depth

While in an unsteady model the final time of the simulation is the real final time of the hydrograph, in a steady case one must set a final time large enough for the solver to reach convergence. The latter is achieved, for example, when the outflow discharge is equal to the inflow discharge. However, after fourteen days of run with *River2D*, the outflow value was still oscillating around 30,5 m<sup>3</sup>/s. Therefore, the convergence was not reached and it could be concluded that *River2D* was not able to manage effectively the case under investigation. The results are considered, however, useful to get a view of the pattern of the flood, even though not fully quantitative.

*iRIC*, and in particular the solver *STORM* that was used here, presents several advantages compared to the *River2D* software. First of all, the time computation is much smaller: 3 days of computation against 14 days. Moreover, as already mentioned, the background base map permits to the user to easily define the grid and the boundary condition position. *iRIC* allows the user to extract a shapefile representing the contour of depth, velocity or water surface elevation in order to produce, in a very quickly way, hazard maps. On the contrary, after modelling with *River2D*, the points have to be extrapolated and then interpolated using appropriate GIS functions; therefore, the map production requires more time. By contrast, in *iRIC*, it is not possible to visualize the evolution of the flood extension during the simulation; it can be depicted only after the end of the computation (*River2D* offers instead the possibility to see the flood evolution, at any time of the computation). Another limitation of *STORM* is that the software does not give information related to the discharge of the second outflow; so its convergence cannot be established with certainty. The model reaches the final result after 815 minutes with an outflow discharge of 37 m<sup>3</sup>/s (with only the first outflow considered); however, there is no way to know the value of the discharge outflowing through the second boundary condition.

### 3.3 RISK MAPS

As already explained at the end of the second chapter, the production of risk maps supports the development of emergency operations. These maps are created overlapping the layer of facilities, offices, crucial points, roads, etc. and the map of the flooded area, with its relative water depth (*Figures 89-90*).



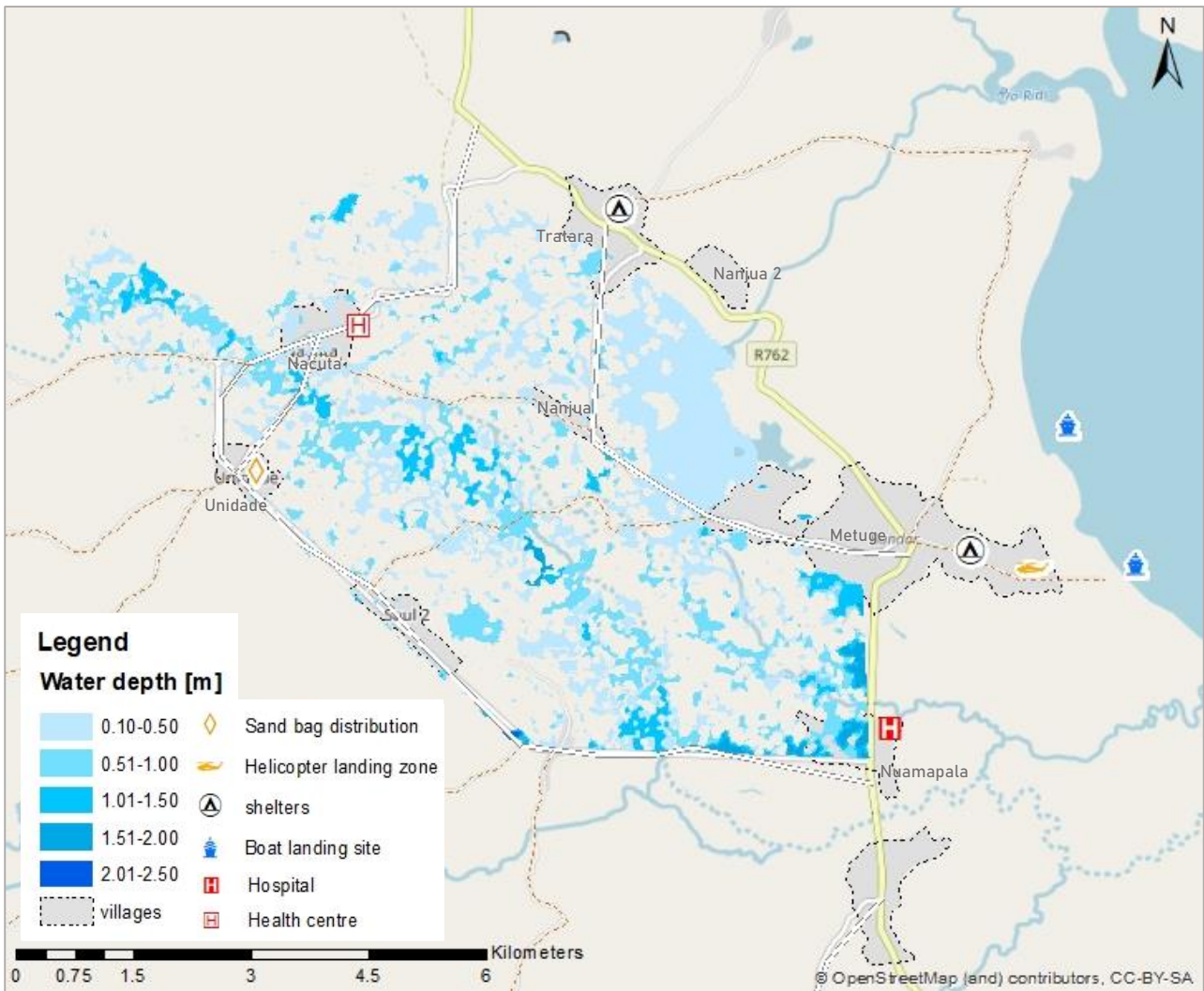


Figure 89 Risk map of the studied area

First of all, it is worth noting that the villages most prone to the flood are Nuamapala and Nacuta, that present a lower elevation compared to the others. Interviewed people of those villages confirmed the modelling result; in particular, people of Nuamapala noticed that only one part of the village (the northernmost) was severely flooded, while the southern and the eastern sides (where a hospital is present) are more elevated and hardly flooded. Second, the village of Nanjua is right in the middle of the flooded area. This village was indeed heavily hit by the recent floods induced by Kenneth, as already explained. In the model, however, water depths at Nanjua are not very high. The villages of Saul 2 and Unidade, as reported by locals, are on the safe side of the floodplain where a lot of fields are present and floods are hardly possible (as a matter of

fact, one can consider that they would like to bring more water in that area to increase the productivity of their fields during the dry periods).

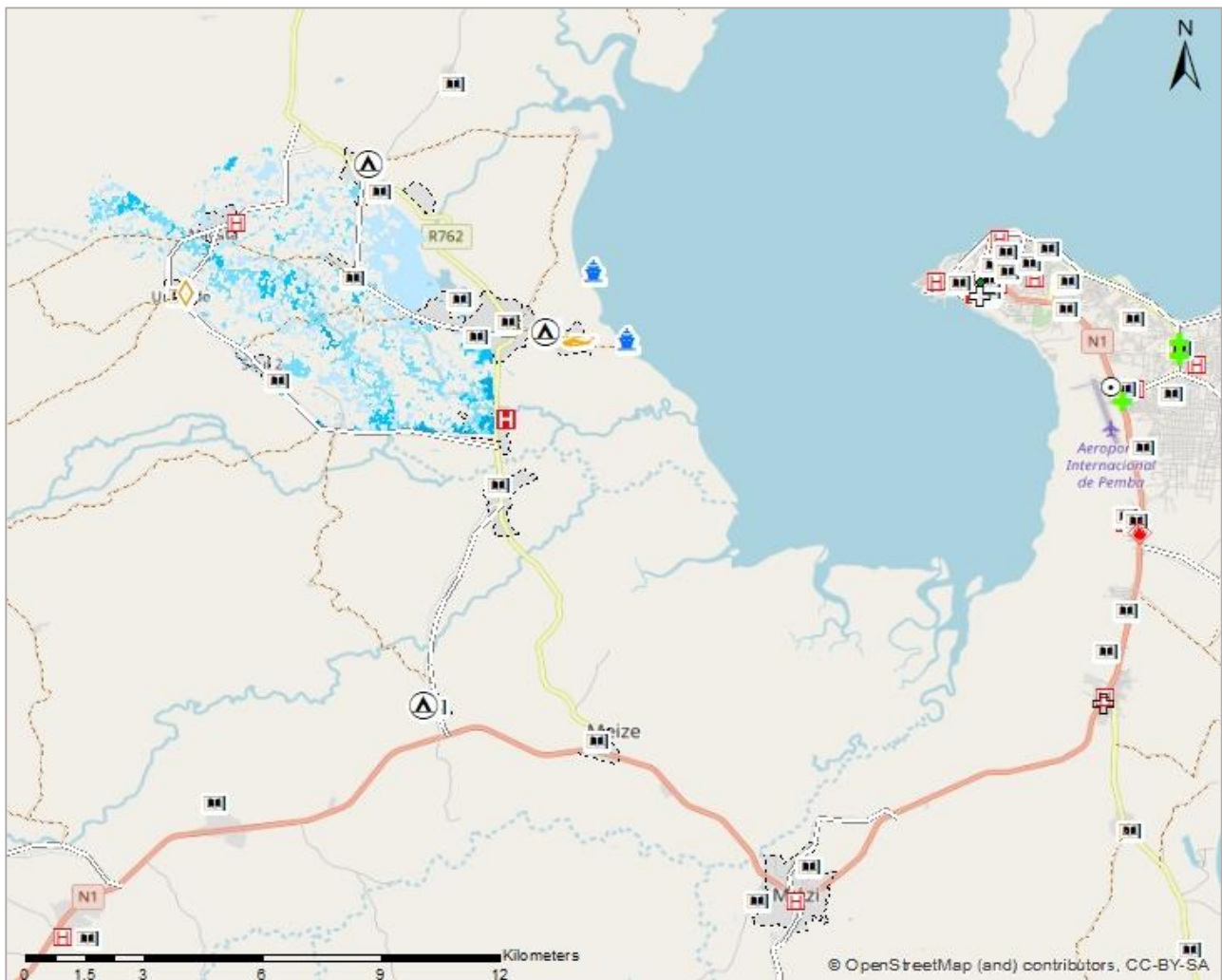


Figure 90 Risk map

Finally, given its position and importance, it is possible to assume that the capital of the district, Metuge, could be a good location for an Operative Emergency Centre or for reception centres, where people impacted by any event could find help and basic support. The town of Metuge is near to the sea and located at the centre of the road network that ensures a connection to Pemba.



## 4. MITIGATION MEASURES

After collecting the needed data for the area under consideration (chapter 2), and after modelling a design flood in the present condition (chapter 3), the main aim of this study is to propose suitable mitigation measures that could avoid the flooding of the rural area. The design of mitigation measures is treated in this chapter.

### 4.1. CONCEPT

The above descriptions and analyses have shown that the Rio Maguide flows in a rural area that is generally flat; moreover, the deposition of sediment, supplied from the upstream portion of the basin, has completely buried the river bed in some parts; the absence of a well-defined bed lets the river braid forming several channels; finally, a wide flood area is returned by hydraulic modelling and processing satellite images taken during events. Based on this, mitigation measures can be thought following a general principle of restoring a good shape of the river bed, in this way increasing the conveyance. This kind of intervention is also stimulated by its relative simplicity compared to other solutions.

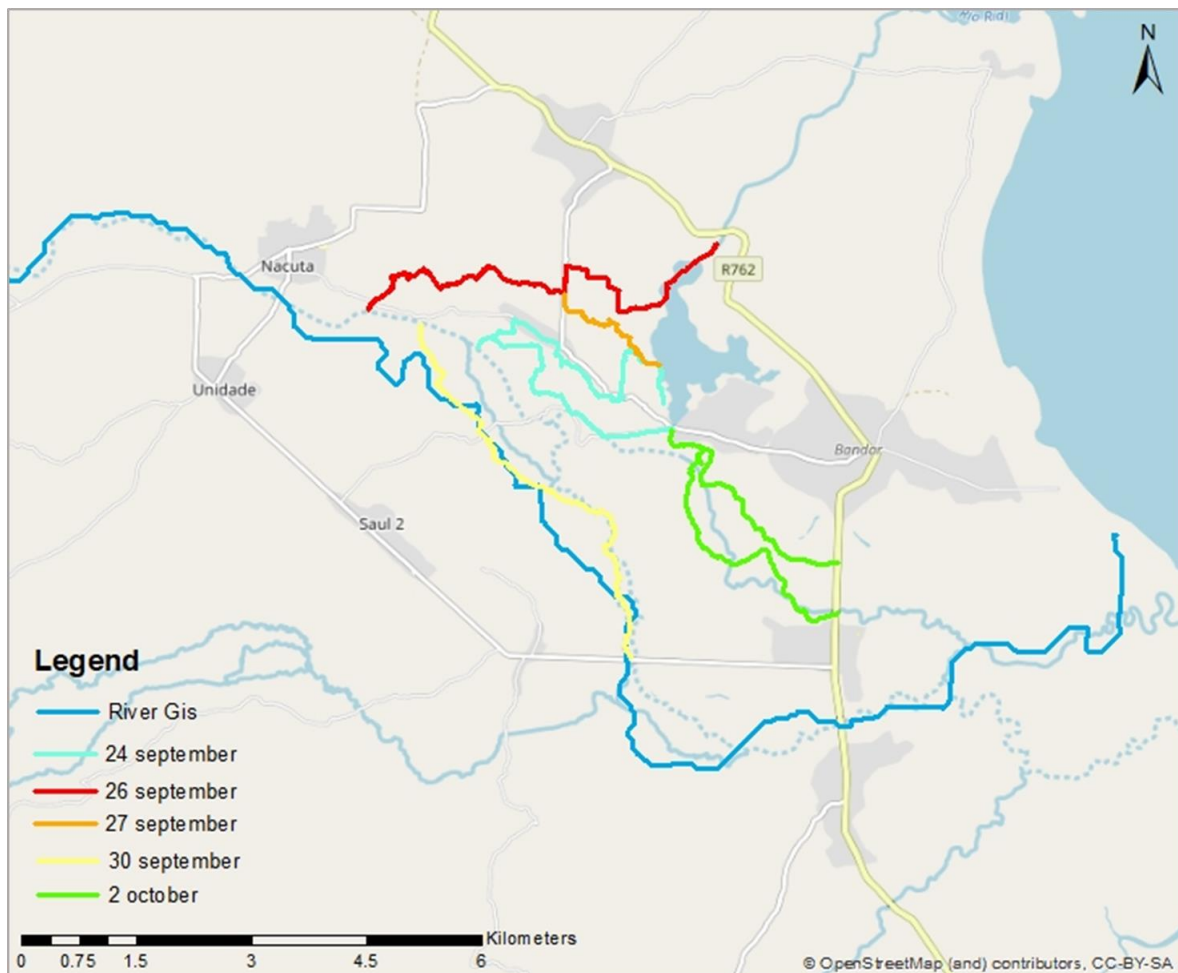


Figure 91 Sub-reaches of the Rio Maguide after the field survey

During the field survey (chapter 1), different reaches have been walked along as shown in *Figure 91*. In addition, a key part of the river system is the presence of the lake near the village of 25 de Junho (*Figure 92*). This basin is used as a natural storage area for the water carried by one of the sub-reaches investigated during the field survey. By interviewing the local population this seemed to be a good solution also to store water to be used by farmers during dry periods.



Figure 92 The lake near 25 de Junho (September 2019)

Based on the map of *Figure 91*, three possible solutions are taken into consideration, as shown in figures *Figures 93 to 95*. Basically, the three solutions differ in terms of the reaches discharging water into the lake: *solution A* uses only the red/orange reach of *Figure 91*, *solution B* uses a cyan one and *solution C* uses both. In the following of the chapter, the solution A will be further exploited because, as already shown in the analysis of the sub-reaches (*Figure 16*) done in the first chapter, after cyclone Kenneth, the upper branch is now a preferential way of flowing water thanks to its very good state with the water confined within deep banks (this is also evident looking at the map of the flooded area post Kenneth produced with SNAP and depicted in *Figure 9*). The solution A was then preferred to the second one. *Solution C* would likely require a greater computational effort due to the introduction of multiple junctions, therefore, as a first attempt, Solution A seemed to be the best option. The modelling of the third solution could be considered as a further step of the modelling, that has not been implemented yet but could be beneficial since it would obviously increase the discharge capacity of the network.

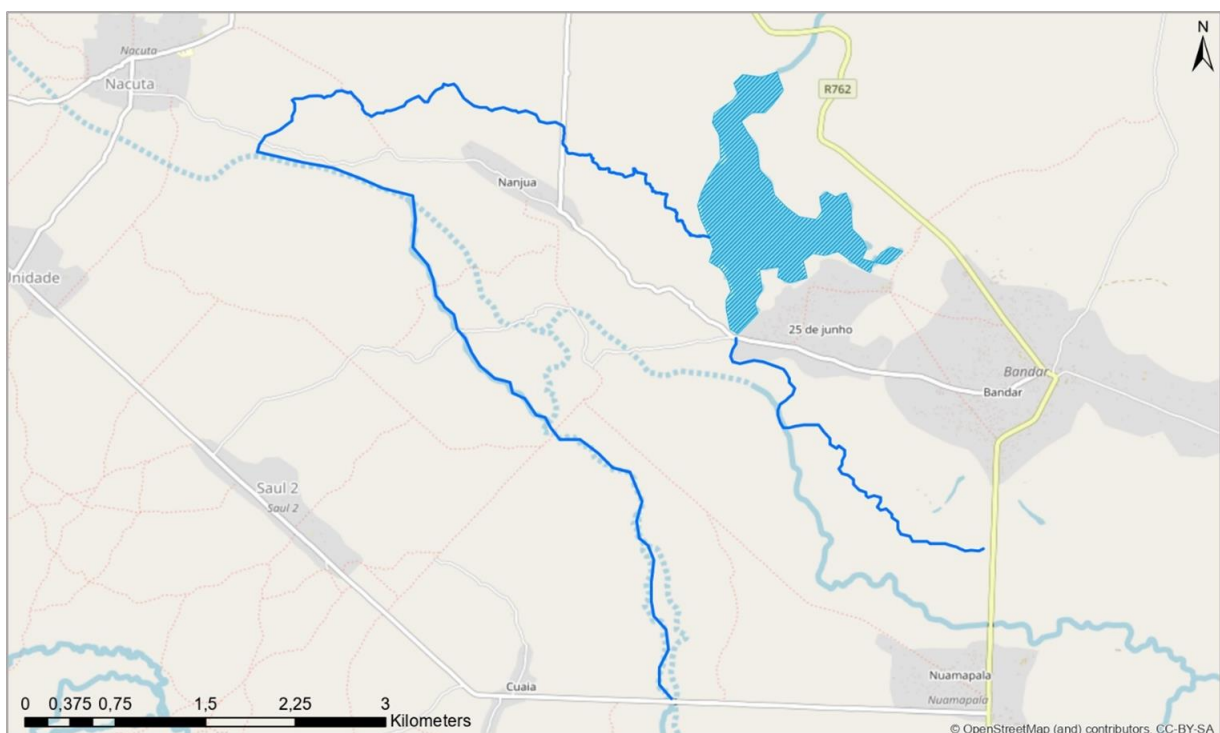


Figure 93 Solution A

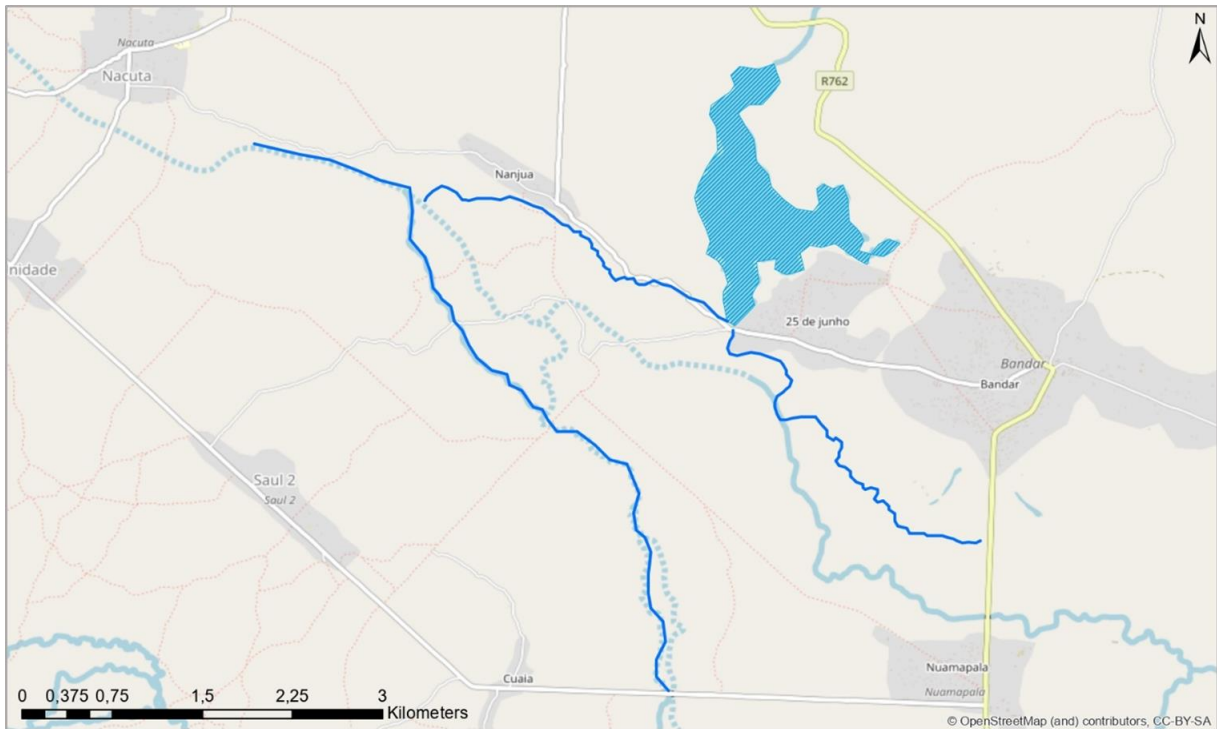


Figure 94 Solution B

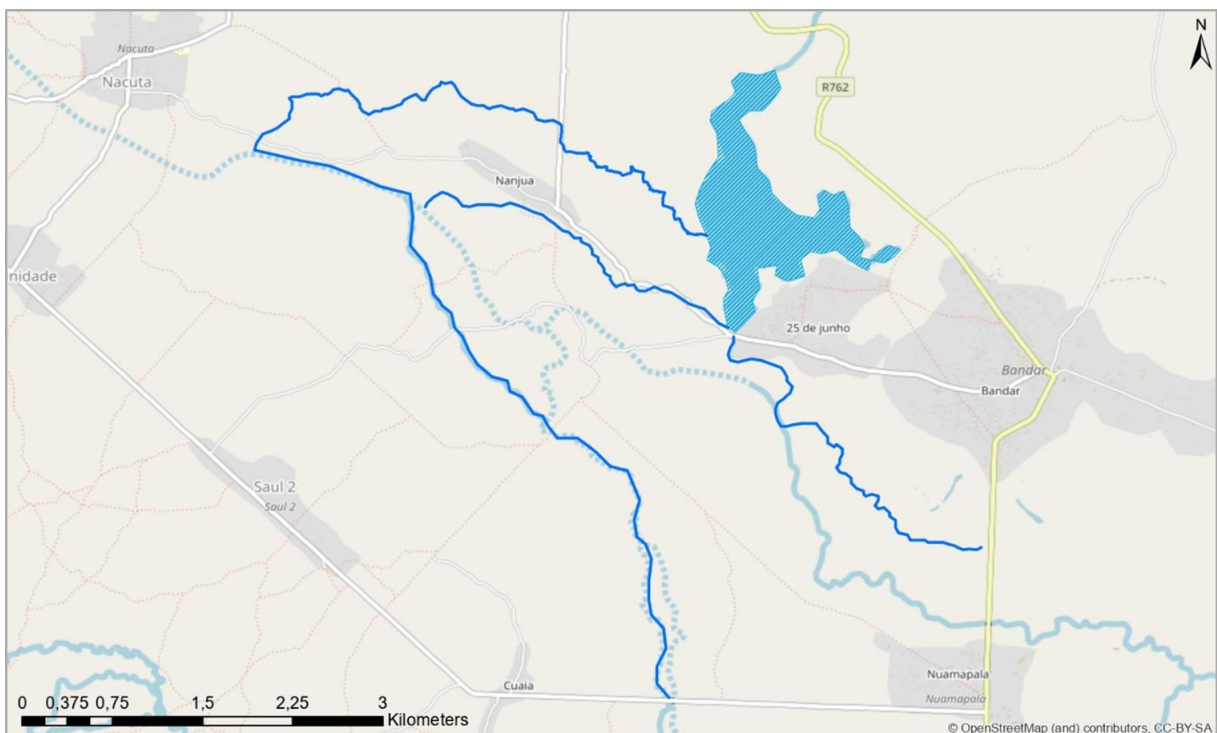


Figure 95 Solution C

For any solution, however, the main countermeasures foreseen are the excavation of the river bed and the construction of earthen levees, possibly combined with each other. These are relatively simple interventions, feasible in the area of interest. Starting from a first attempt of deep excavation without levees, the solution may be optimized step by step by progressively reducing the depth of the dig and by using that same soil to build levees.

However, in any configuration the design condition would correspond to a network of channels. Therefore, a one-dimensional hydraulic analysis has been used to explore how any design solution would contribute to mitigating the floods of the Rio Maguide (some preliminary, and somehow unsuccessful, attempts to model design conditions with a two-dimensional approach are reported in *Appendix 2*). The one-dimensional analysis has been performed using the software *HEC-RAS*, the *Hydrologic Engineering Center's (HEC) River Analysis System (RAS)* that allows the user to perform one-dimensional steady flow, one and two-dimensional unsteady flow calculations, sediment transport/mobile bed computations, and water temperature/water quality modelling (<https://www.hec.usace.army.mil/software/hecras/>). The geometry of the river under study is the starting point of the computation: sections at different length spans are detailed into the proper tool of the software; if needed also lateral weirs, inline structures or storage areas could be linked to the different reaches. Figure 92 depicts the plan of all the models run for the various design conditions: reach **a** is a short initial reach before the junction; reach **b** is the reach flowing to the lake and then to the outlet of the system through the North-South road (section 0); reach **c** is the one flowing to the outlet through the E-W road (section 1<sup>3</sup>).

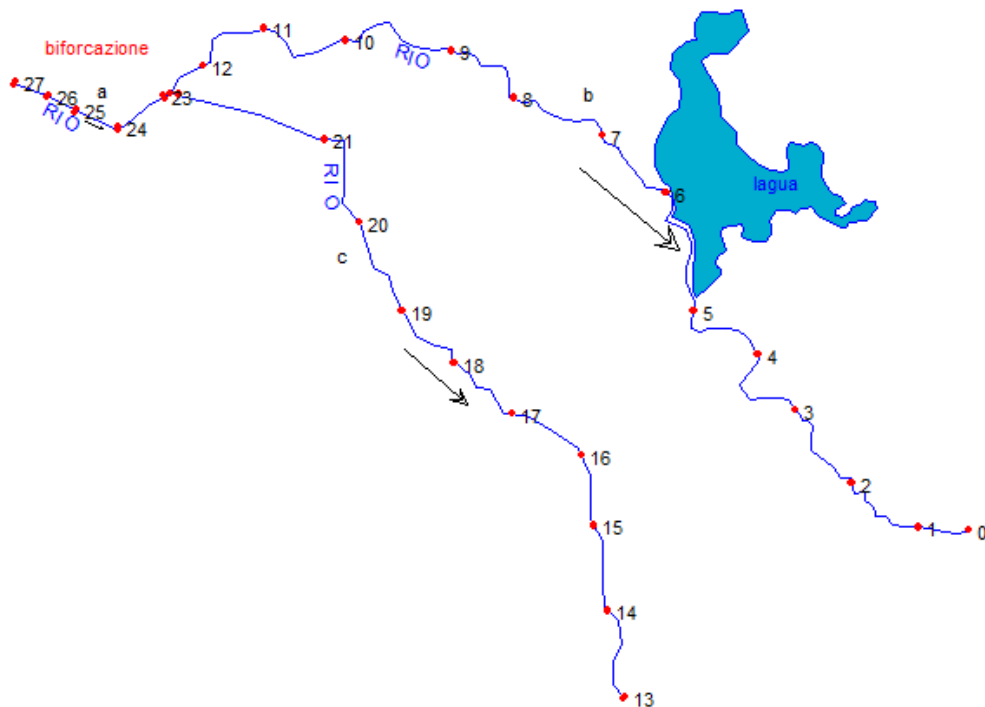


Figure 96 Plan for the one-dimensional models of design conditions

Different scenarios have been considered for excavation depth on **a**, **b** and **c** as shown in *Figures 97-98-99*, where the black dashed line is the present elevation of the ground as retrieved from the DEM of the area, and the orange line is a sample uniform excavation which corresponds to a preliminary uniform digging of  $h=1,5\text{ m}$ , starting point for all the scenario developed in the following. Then, scenarios are as follows:

- deep excavation only (*Scenario 1*);
- deep excavation with levees built (*Scenario 2*);
- superficial excavation with levees (to minimize the ground excavated and then used for the construction of the levee) (*Scenario 3*);
- intermediate excavation with levees (*Scenario 4*).

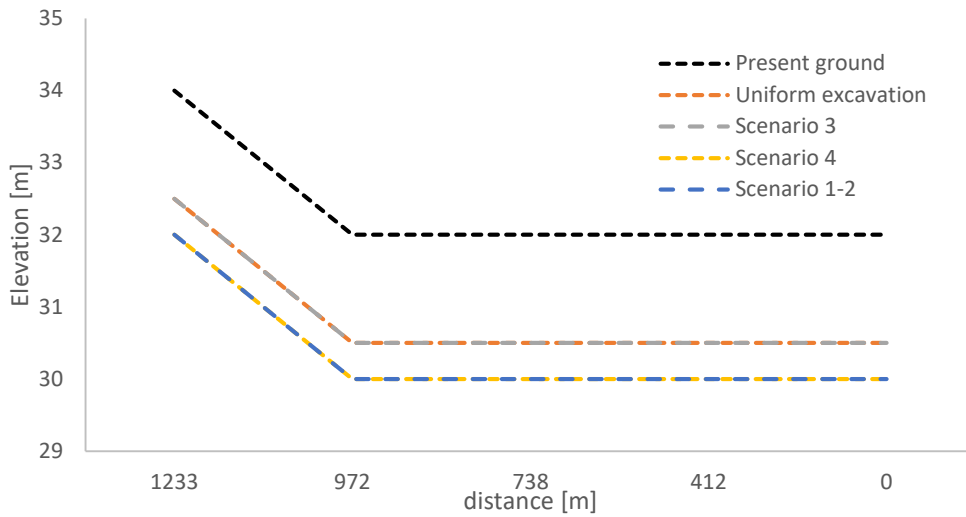


Figure 99 Section of sub-reach a with excavation depth for each scenario

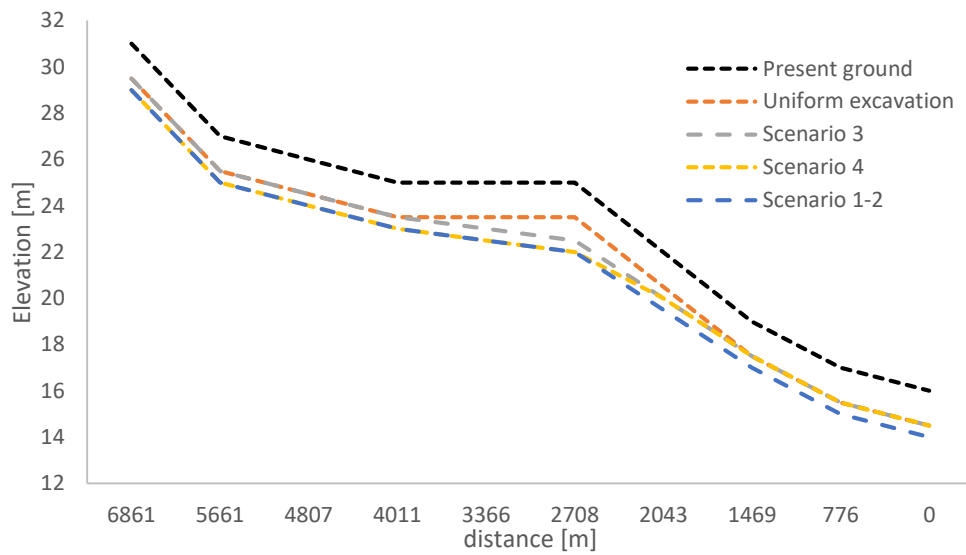


Figure 98 Section of sub-reach b with excavation depth for each scenario

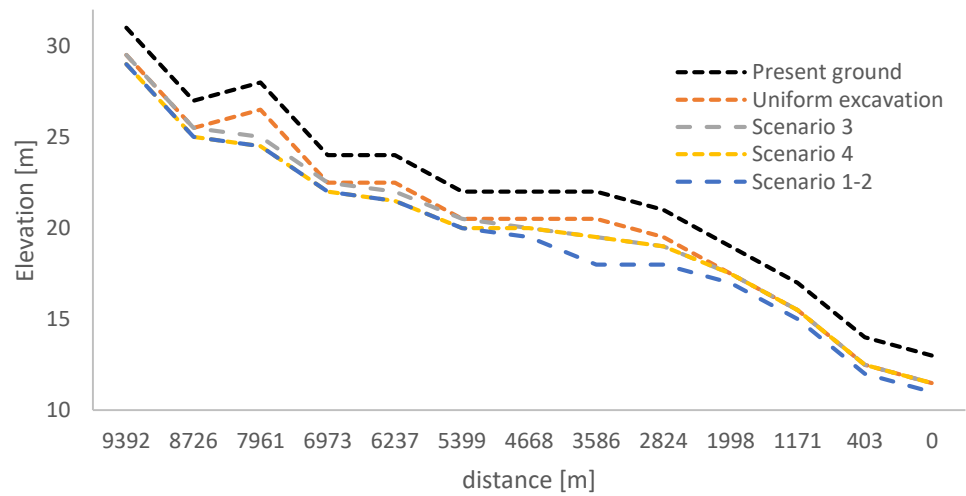


Figure 97 Section of sub-reach c with excavation depth for each scenario

Table 19 Section width of each section for the different scenarios

Reach	River Station	Section Width [m]		
		Scenario 1-2	Scenario 3	Scenario 4
<b>a</b>	27	30	20	<sup>3</sup> 0
	26	30	20	<sup>3</sup> 0
	25	30	20	<sup>3</sup> 0
	24	30	20	<sup>3</sup> 0
	2 <sup>3</sup>	30	20	<sup>3</sup> 0
<b>b</b>	12	15	10	10
	11	15	10	10
	10	15	10	10
	9	15	10	10
	8	15	10	10
	7	15	10	10
	6	15	10	10
	5	10	10	10
	4	10	10	10
	3	10	10	10
	2	10	10	10
	1	10	10	10
0	10	10	10	
<b>c</b>	22	15	10	10
	21	15	10	10
	20	15	10	10
	19	15	10	10
	18	15	10	10
	17	10	10	10
	16	10	10	10
	15	10	10	10
	14	10	10	10
	13	10	10	10

A particular attention has been put on the methods used for building the levees. Two main approaches are developed: one considering a levee with a uniform height from the present elevation of the ground; the other with local heights obtained adding a proper freeboard to the water stage computed in each section, so that the levee height varies section by section.



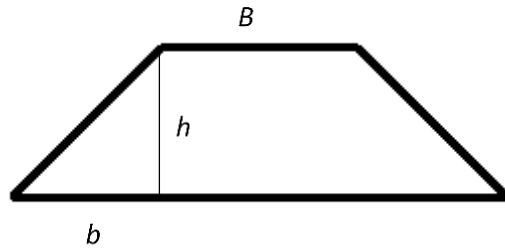


Figure 100 Sketch of the section of a levee

**Homogeneous levee:** for each section of  $a$ ,  $b$  and  $c$  the difference between the water stage elevation (wse) and the ground has been calculated and the maximum value for each sub-reach has been taken as reference for the computation of the dimensions of the levee (shown in *Figure 100*); then the max height has been increased by 0.10 m in favour of safety. Considering *Figure 100*:

$$B=2 \text{ m (fixed);}$$

$$h=\max (\text{wse-ground}) +0.10 \text{ m;}$$

$$b=3/2*h.$$

**Levee considering the freeboard:** for each section of  $a$ ,  $b$  and  $c$  the height of the levee has been calculated as the sum of wse and the freeboard (fixed at 1 m); consequently, to compute the height of the levee, the elevation of the ground has been subtracted to the height of the levee. Considering *Figure 100*:

$$B=2 \text{ m (fixed);}$$

$$h= ((\text{wse}+1 \text{ m}) - \text{ground});$$

$$b=3/2*h.$$

As a consequence of this differentiation, the volume of soil used for the levees varied with respect to the different approach used.

The construction of levees also requires a more accurate reasoning about the type of material to be used. As seen during field survey, the different reaches present different types of soil in the river bed.

For the yellow lines in *Figure 101*, digging is very easy because the soil is mainly made of sand; however, the

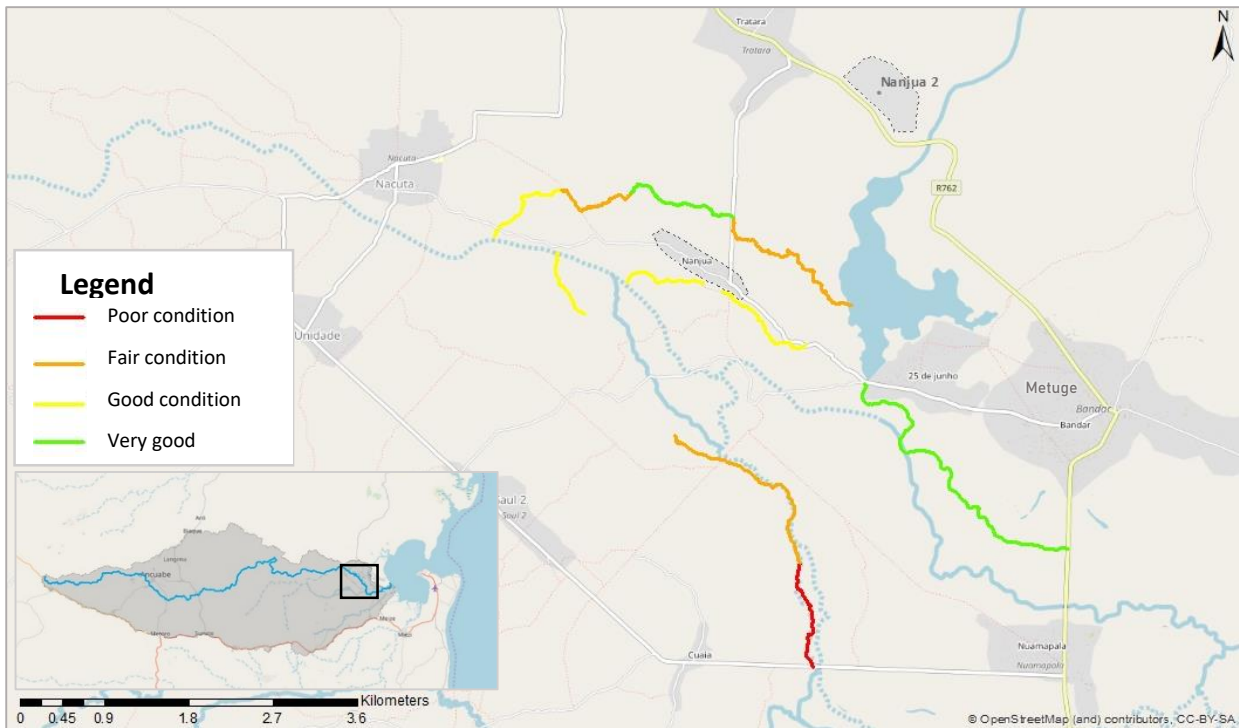


*Figure 101 River bed condition (same of Figure 8)*

latter does not present a good performance when used for building levees: it has a high permeability and this can cause problems of erosion at the base of the embankment. On the contrary, the green and orange lines present both river banks and flow ridges made of clay; the difference consists in the fact that in the green paths the banks are high and visible while in the orange ones are very low or absent. However, this type of soil is very good for the construction of levees due to the fact that its main property is low permeability. A good recommendation for the construction of the embankment could be mixing sand with clay in order to increase its resistance: it would be sufficient to move the requested material were needed. Otherwise, a fine-soil core may be put in the middle of the levees built with more permeable soil.

Different reasoning has been done about red path: as already mentioned, these latter are characterized by very dense vegetation. Walking through them it was nearly impossible to distinguish the river bed and the fields; a first intervention in this area should be a complete cleaning and deforestation of the path of the river, followed by excavation/enlarging of the bed and, consequently, by the construction of levees.

## 4.2. MODELLING APPROACH

The design scenarios have been modelled using two different discharge hydrographs. The first one is the hydrograph presented in *Chapter 3*, with a peak discharge  $Q=47,5 \text{ m}^3/\text{s}$  of, that was also used in the two-dimensional analysis of the present conditions. The second hydrograph has a peak flow rate  $Q=100 \text{ m}^3/\text{s}$ . For the sub-basin considered for the hydrologic analysis of chapter <sup>3</sup> this would correspond to an event with a return period of 300 years; alternatively, it could be considered an event with the same return period of 10 years but with a precipitation over an area that is roughly twice the area considered in chapter 3.

The models (*Figure 96*) include a river junction and the lake as a storage area connected with reach **b** through a lateral structure. In principle, this would allow the computation of a discharge partition and of the volume

storage in the lake by a single model, run in unsteady-flow mode. Indeed, obviously, the unsteady model gives the possibility to account for water volumes, whilst in the steady analysis it is not possible to account for the volume stored in the natural lake. However, unfortunately, the relative complexity of the model made it crash when run with the complete geometry in unsteady mode. Therefore, a mixed approach was used, as described below.

Steady analyses have been performed for a variety of incoming flow rates to compute the separation of the discharge in the reaches **b** and **c** (Figure 102). This separation is computed by ensuring that the flow energy is balanced at the river junction. The analysis showed that, in general, 54% of the total discharge is carried by sub-reach **b** and the remaining 46 %by sub-reach **c**. Then, in the unsteady analyses for the two hydrographs mentioned above, the two streams were considered separately and reach-specific hydrographs were used as upstream boundary conditions, based on the partition determined in the steady analysis (Figures 103-104).

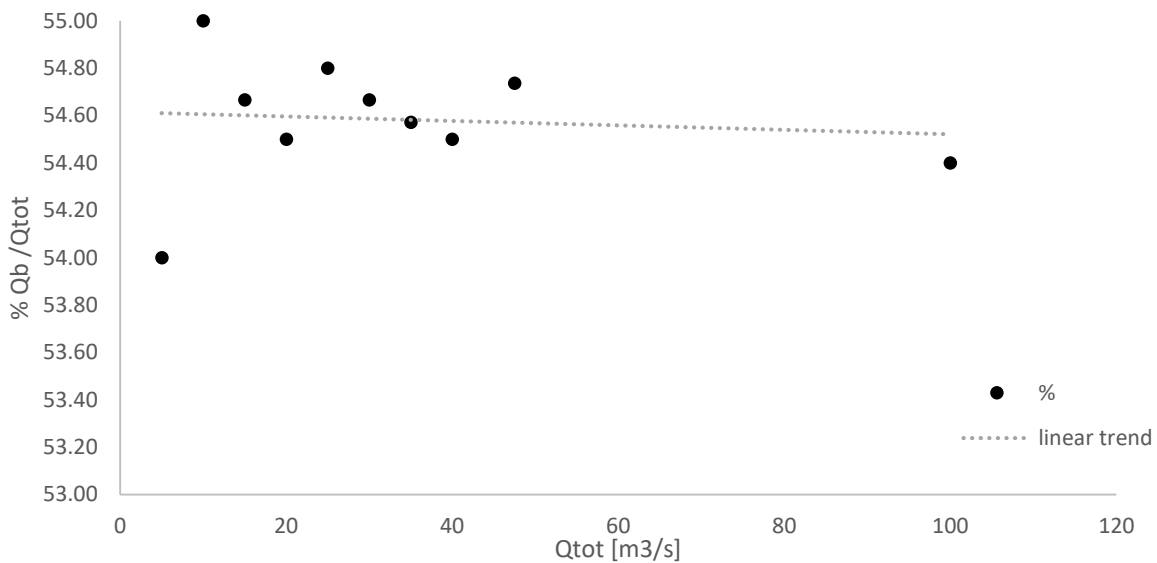


Figure 102 Percentage distribution of discharges in reach b

As downstream boundary conditions, uniform flow has been input for both reaches because the field survey (Figure 101) showed that multiple openings are present below the roads bounding the computational domain, the total area of opening being larger than the areas of the excavated cross section.

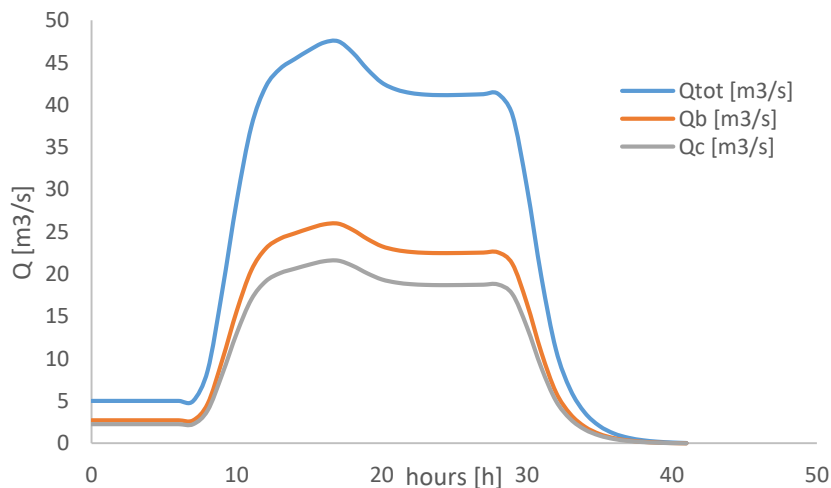


Figure 103 Hydrograph, case of peak discharge  $Q=47,5 \text{ m}^3/\text{s}$

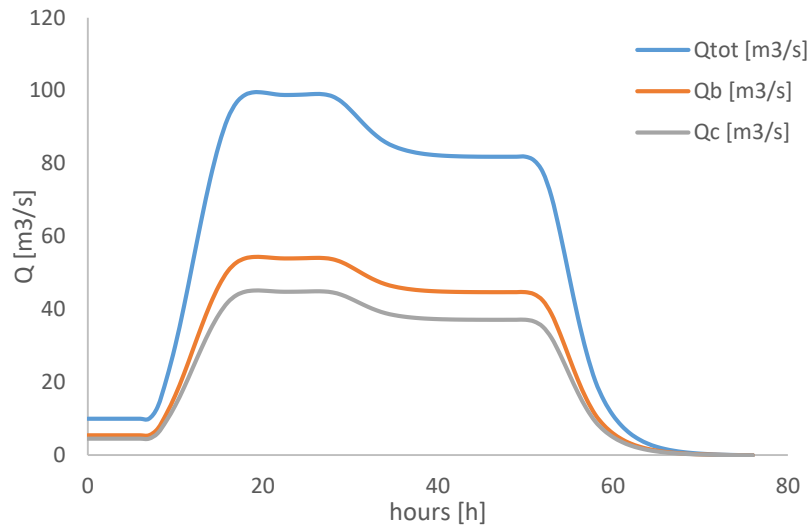


Figure 104 Hydrograph, case of peak discharge  $Q=100 \text{ m}^3/\text{s}$

## 4.3. MODELLING APPROACH

### 4.3.1. SCENARIO 1: DEEP EXCAVATION ONLY

The first solution is a scenario in which the excavation of the river bed permits the flowing of the design discharge of  $47,5 \text{ m}^3/\text{s}$  without overflow. Moreover, the geometry presented is achieved digging the minimum volume of soil. The profile of the excavated river bed has been obtained by trials; starting from a uniform excavation, the depth of the latter was modified as necessary to achieve the objective. *Figures 105-106-107* show the water profile for each sub-reach, as obtained from a steady model of the complete system. In general, for any design configuration a steady model will be used to check the freeboard at peak, while an unsteady model will reveal the interaction between the river reaches and the lake.

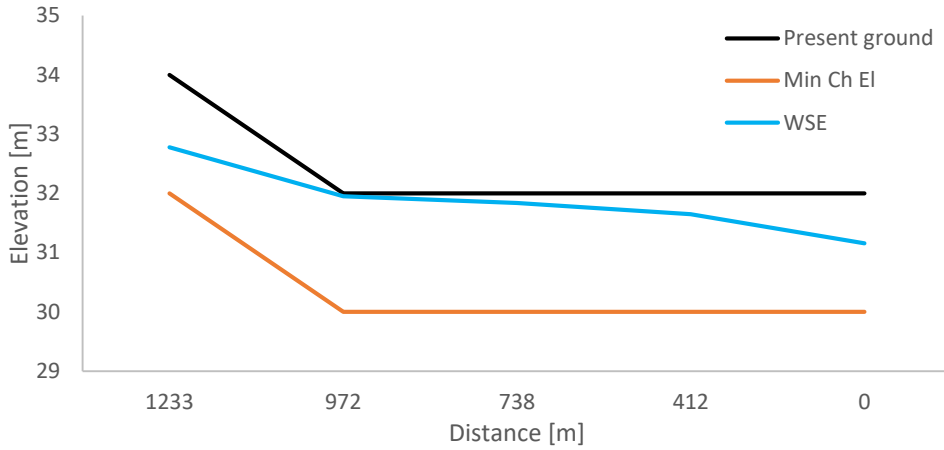


Figure 107 Profile of steady case of reach a, Scenario 1,  $Q=47,5 \text{ m}^3/\text{s}$

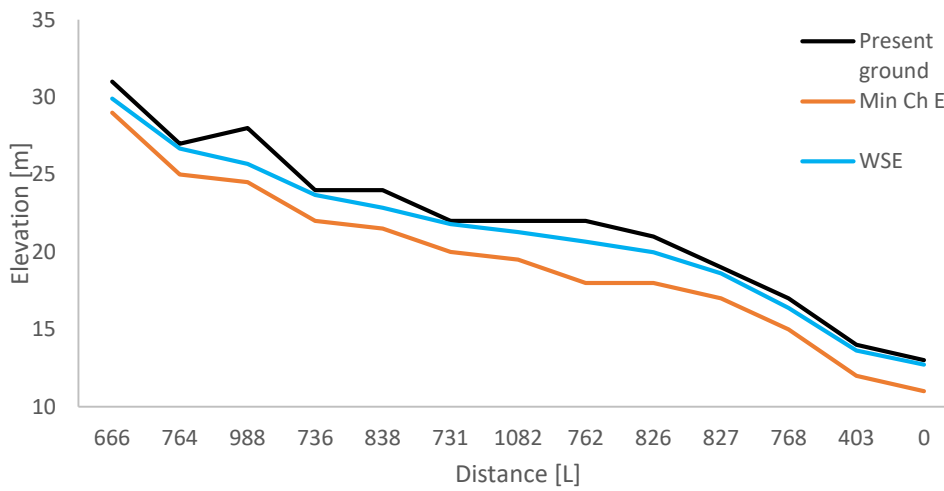


Figure 106 Profile of steady case of reach b, Scenario 1,  $Q=47,5 \text{ m}^3/\text{s}$

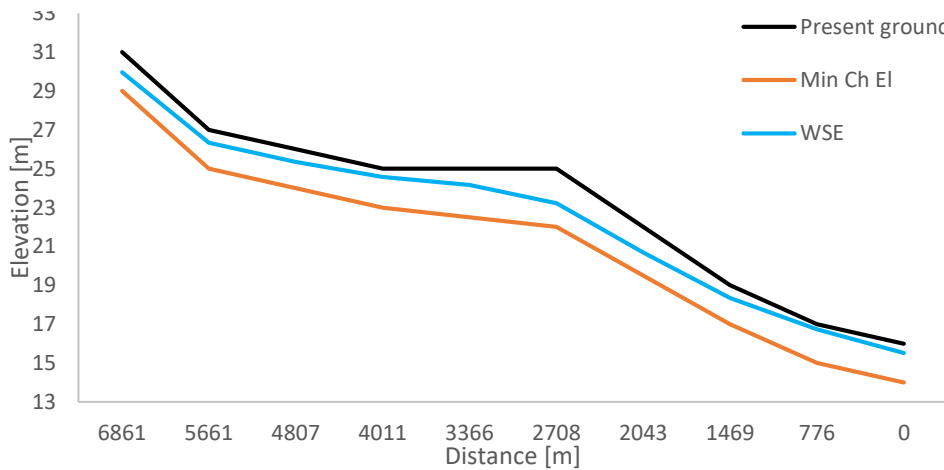


Figure 105 Profile of steady case of reach c, Scenario 1,  $Q=47,5 \text{ m}^3/\text{s}$

For the design discharge, a levee is theoretically not needed. However, the difference between the water elevation and the river banks is not satisfactory in all the three sub-reaches: for the reach **a**, the minimum freeboard is 5 cm, 20 cm for reach **b** and 27 cm for **c**.

A second computation was run with the increased flow rate of 100 m<sup>3</sup>/s. Obviously, in this case the water elevation exceeds the banks (corresponding, as mentioned, to the present ground elevation), as depicted in Figures 108-109-110.

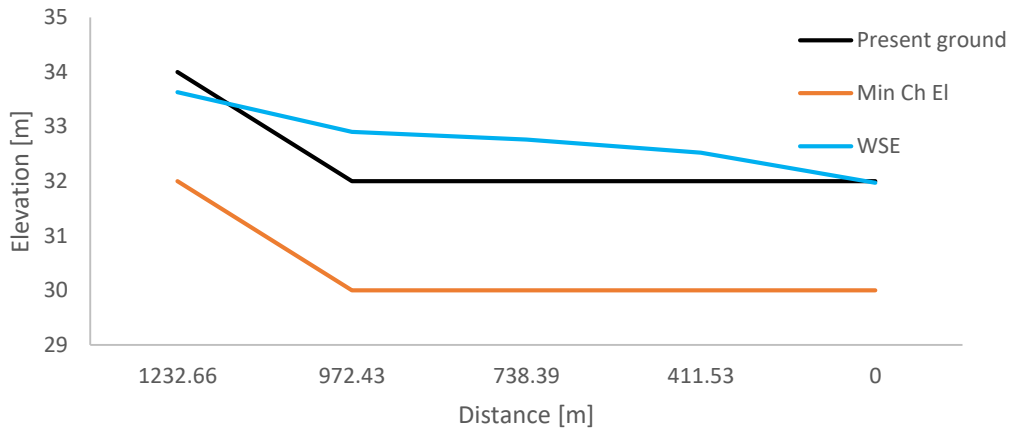


Figure 110 Profile of steady case of reach a, Scenario 1, Q=100 m<sup>3</sup>/s

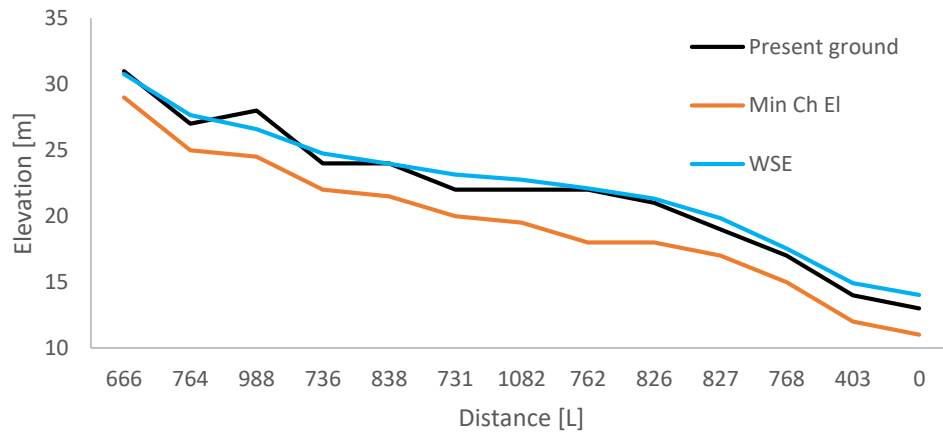


Figure 109 Profile of steady case of reach b, Scenario 1, Q=100 m<sup>3</sup>/s

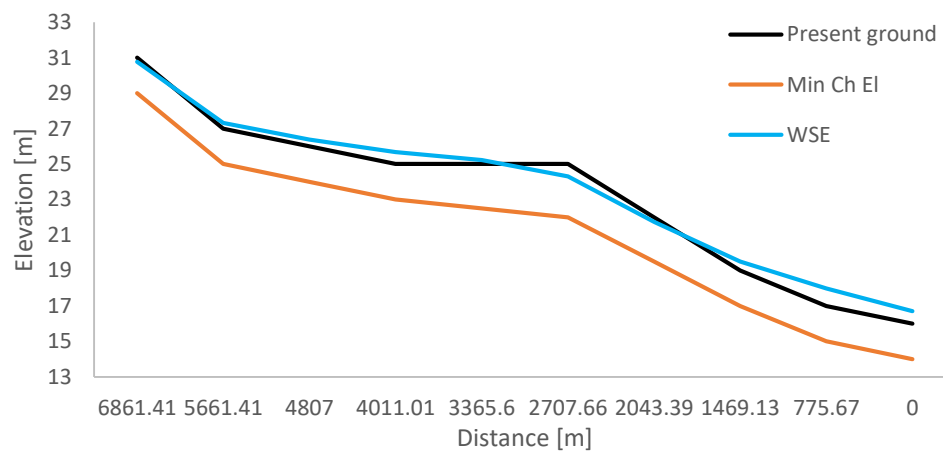


Figure 108 Profile of steady case of reach c, Scenario 1, Q=100 m<sup>3</sup>/s



The unsteady analysis was applied, as mentioned above, to individual reaches with their hydrographs (Figures 103-104). The profiles of the maximum free surface are similar to those obtained from the steady models, as expected considering the limited length of the reaches and revealing a negligible storage in the lake (Figures 111-112-113-114).

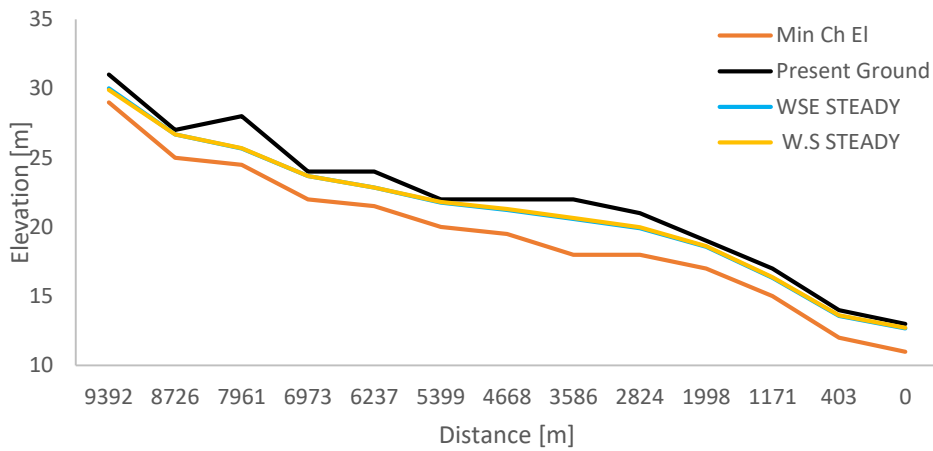


Figure 112 Comparison between steady and unsteady case of reach b, Scenario 1,  $Q=47,5 \text{ m}^3/\text{s}$

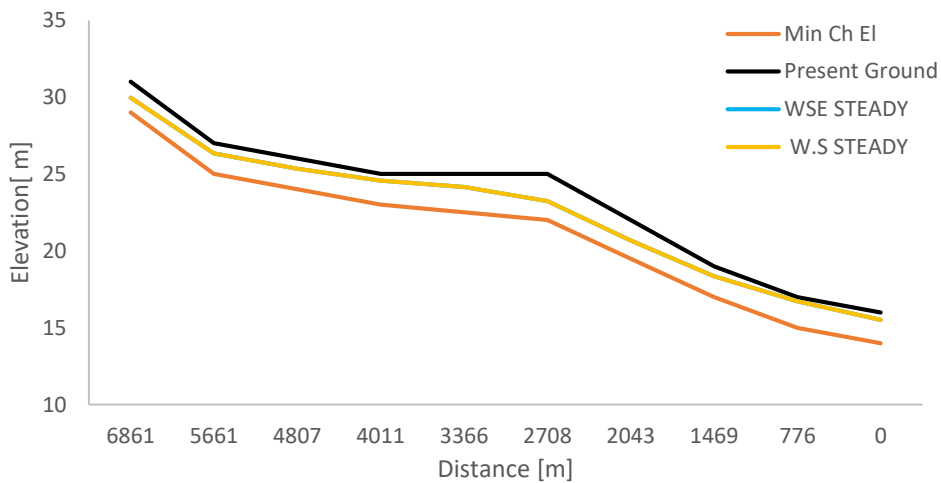


Figure 111 Comparison between steady and unsteady case of reach c, Scenario 1,  $Q=47,5 \text{ m}^3/\text{s}$

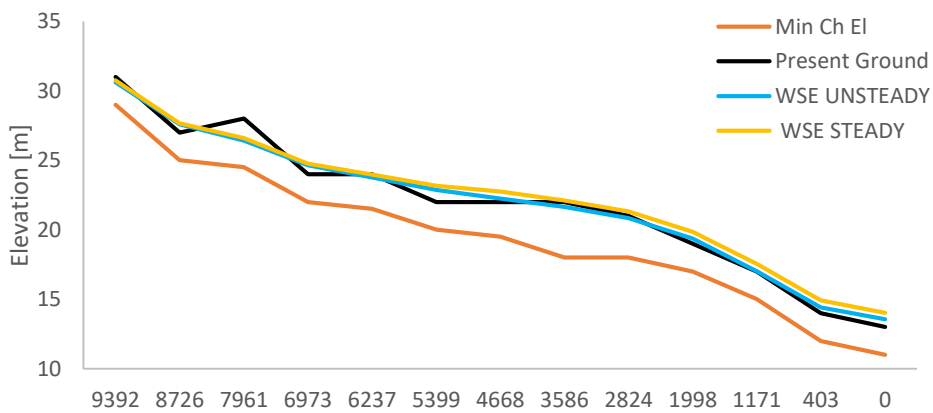


Figure 113 Comparison between steady and unsteady case of reach b, Scenario 1,  $Q=100 \text{ m}^3/\text{s}$

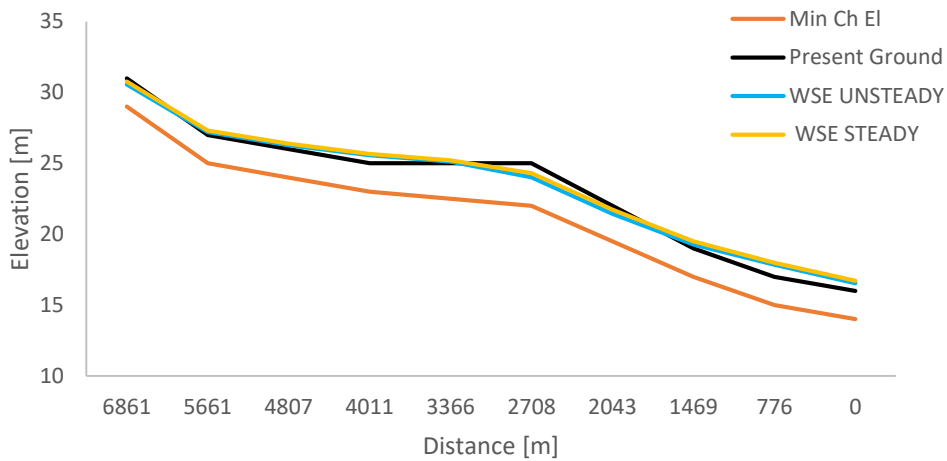


Figure 114 Comparison between steady and unsteady case of reach c, Scenario 1,  $Q=100 \text{ m}^3/\text{s}$

Indeed, *Figure 115* shows the discharge hydrograph just upstream and just downstream of the lake. The two curves are quite similar to each other, indicating that the volume of water entered into the storage area can be considered negligible with respect to the total flow arriving at the section of the lateral weir. This can be due to the fact that the geometry corresponds to a deep excavation which involves a low wave on the lateral structure and, consequently, less water volume inflows in the storage area. In other words, excavating the river increases the relative elevation of the storage, reducing its capacity. The storage is more effective with the higher flow rate of  $100 \text{ m}^3/\text{s}$  (*Figure 116*).

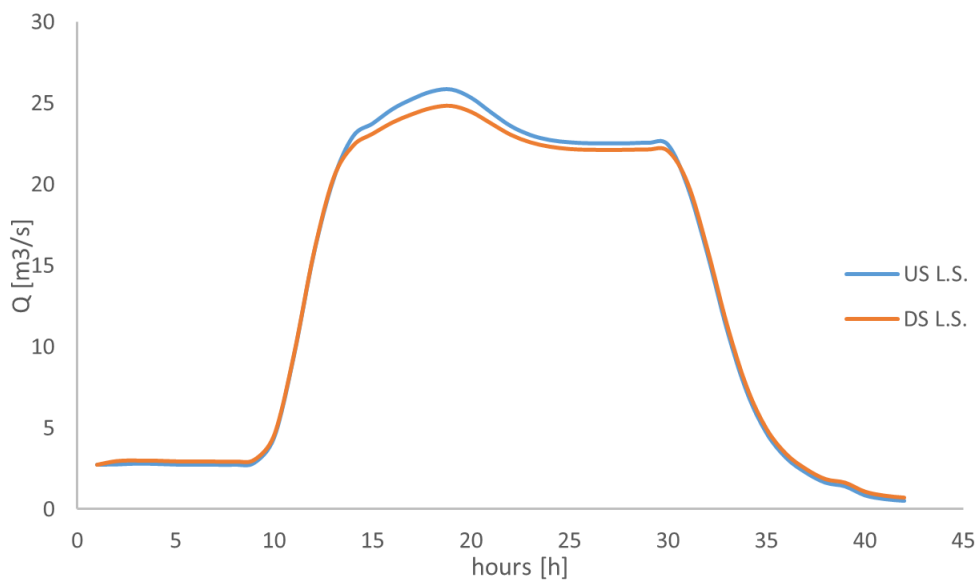


Figure 115 Hydrographs of the upstream and downstream section of the lateral weir, Scenario1,  $Q = 47,5 \text{ m}^3/\text{s}$

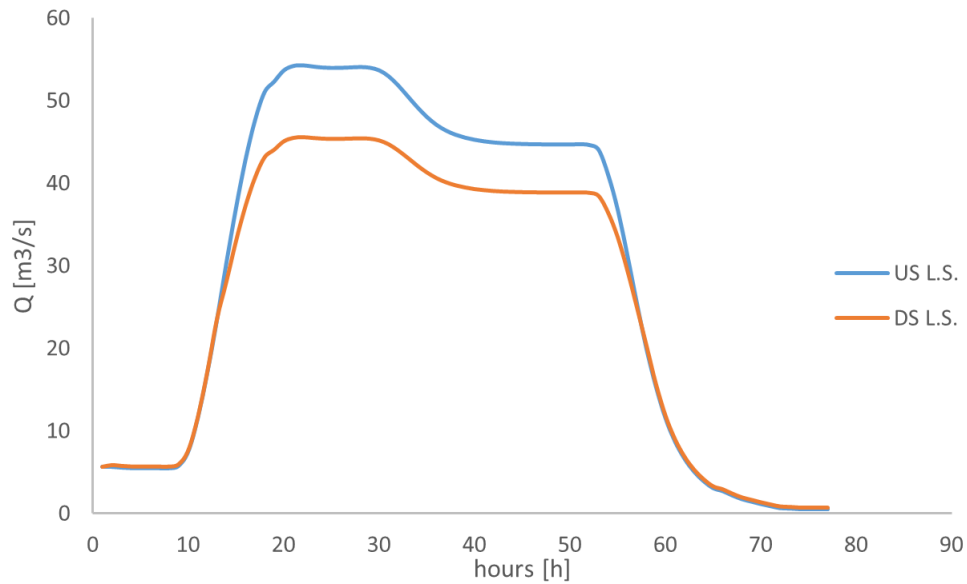


Figure 116 Hydrographs of the upstream and downstream section of the lateral weir, Scenario1,  $Q = 100 \text{ m}^3/\text{s}$

The volume stored in the lagoon has been computed as the difference of these two volumes, calculated with the trapezoidal method. For the lower discharge:

$$\text{VOL US L.S} = 1957896 \text{ m}^3$$

$$\text{VOL DS L.S.} = 1938708 \text{ m}^3$$

$$\text{VOL STORED} = 19188 \text{ m}^3$$

For the higher discharge:

$$\text{VOL US} = 8089938 \text{ m}^3$$

$$\text{VOL DS} = 7085394 \text{ m}^3$$

$$\text{VOL STORED} = 1004544 \text{ m}^3$$

As expected, with same geometry condition, a greater discharge produces a considerable increase of the wave volume. In this case, the volume stored in the natural basin is comparable in term of order of magnitude with the upstream hydrograph volume and the lagoon is exploited better.

#### 4.3.2. SCENARIO 2: DEEP EXCAVATION WITH LEVEE

*Scenario 1*, just presented, involves a large volume of excavated soil, equal to  $563302 \text{ m}^3$  with respect to the following. In *scenario 2*, this soil is used to build levees, without using additional material. Since the flood with  $47,5 \text{ m}^3/\text{s}$  was already contained in the sections in the previous scenario (even though with negligible freeboard), we now consider the discharge of  $Q=100 \text{ m}^3/\text{s}$ .

For the levees design, two different criteria have been followed. The first one consists in building levees with a uniform height in each reach, ensuring a minimum freeboard of 10-20 cm for each reach. The details of the levees are reported in the table below (*Table 20*). With this first procedure, the volume necessary to build

the levees is equal to 168877 m<sup>3</sup>. The resultant profiles are presented in the following graphs (Figure 117-118-119)

Table 20 Table of uniform levee design

Reach	hmax [m]	h [m]	b [m]	B [m]	Length [m]	Area [m2]	Vol [m <sup>3</sup> ]	Vol*2 [m <sup>3</sup> ]	Vtot [m <sup>3</sup> ]
a	0.900	1	1.5	2	12 <sup>3</sup> 2.66	<sup>3</sup> .5	4 <sup>3</sup> 14.31	8628.62	168877.01
b	1.16	1. <sup>3</sup>	2	2	9 <sup>3</sup> 91.57	5.2	488 <sup>3</sup> 6.16	97672. <sup>33</sup>	
c	0.98	1.2	1.8	2	6861.41	4.56	<sup>3</sup> 1288.0 <sup>3</sup>	62576.06	

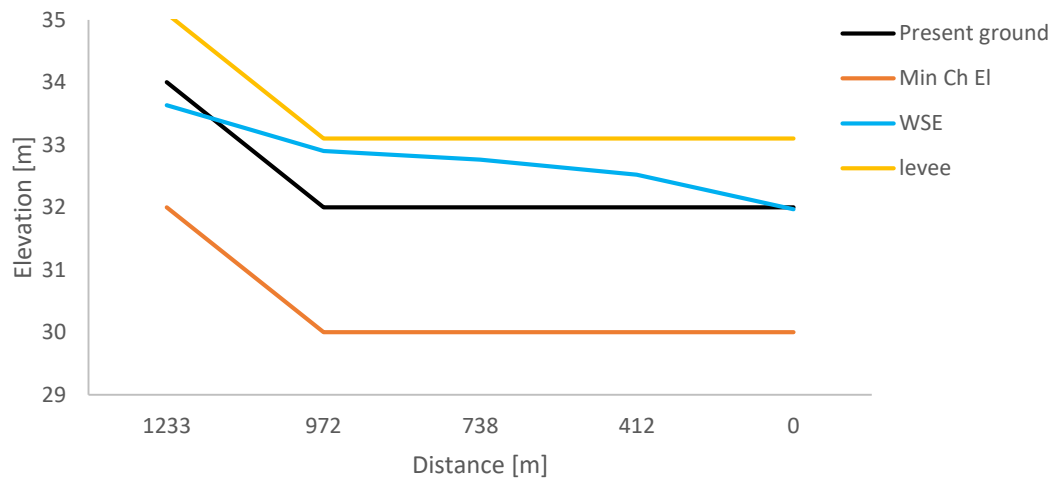


Figure 117 Profile of water depth and uniform levees in reach a for the Scenario 2 of table 20, Q=47,5 m<sup>3</sup>/s

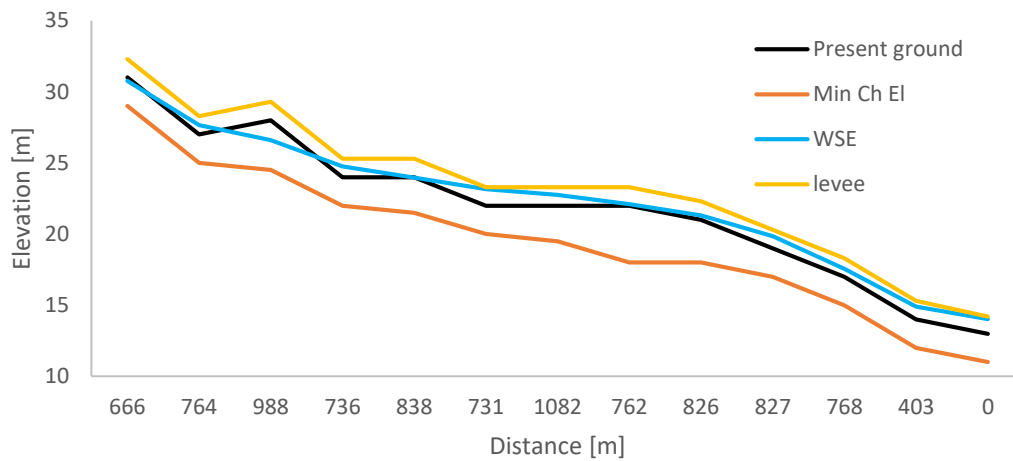


Figure 119 Profile of water depth and uniform levees in reach b for the scenario 2 of table 20,  $Q=47,5 \text{ m}^3/\text{s}$

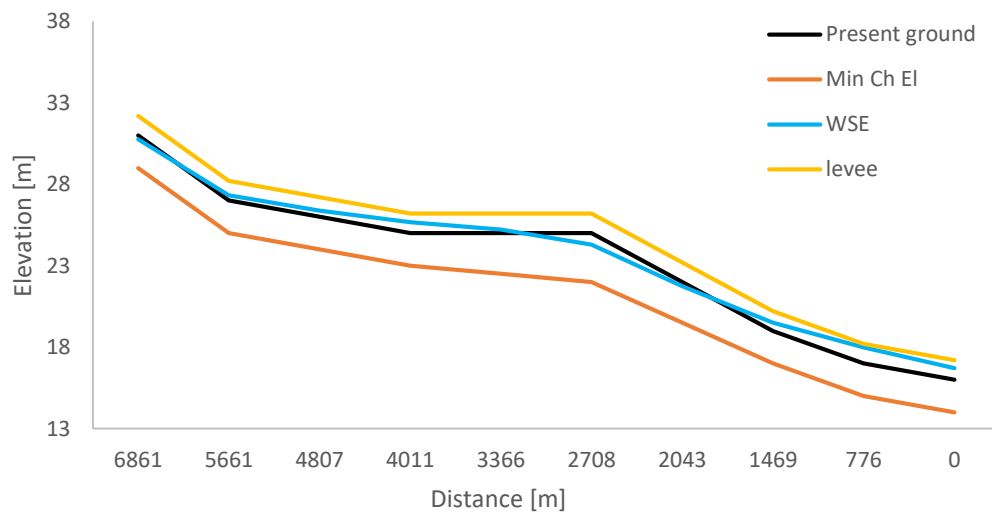


Figure 118 Profile of water depth and uniform levees in reach c for the Scenario 2 of table 20,  $Q=47,5 \text{ m}^3/\text{s}$

The profiles of Figures 117-119 are not optimal, since the freeboard is generally low but unnecessarily high in some places (as occurs in the third section of reach **b**, Figure 115). Therefore, a second procedure was implemented providing a hydraulic freeboard of 1 m in each section, and avoiding the waste of material where the ground was already high, Geometric computations are listed in Table 21. The total volume of material necessary to build the levees has been obtained summing up the values of the last column of the table and multiplying the result by two, since each levee has to be built on the right and the left of the river course. From the procedure, the volume of soil used is  $160314,7 \text{ m}^3$ , value comparable to the one of the first approach. However, the volume necessary for the levees construction is much lower than the excavated one, causing a great amount of material wasted. On the other hand, the surplus material can be used in order to increase the width of the levee (the minor with of the trapeze indicated with B in Figure 100) ensuring greater stability of the embankment. The resulting profiles are presented in Figures 121-123.

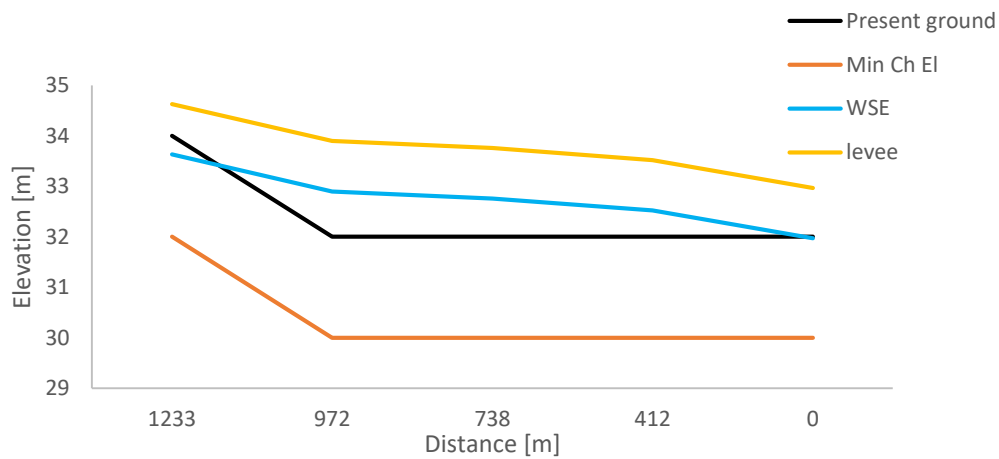


Figure 120 Profile of water depth and levees in reach a for the Scenario 2 of table 21,  $Q=47,5 \text{ m}^3/\text{s}$

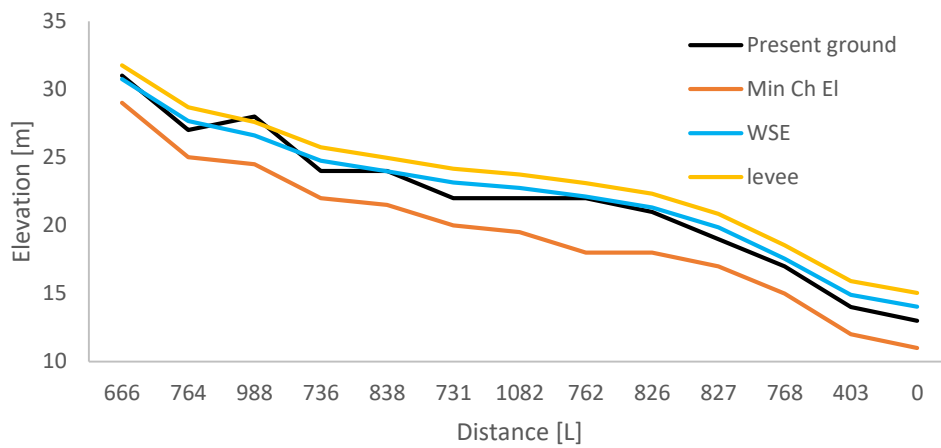


Figure 121 Profile of water depth and levees in reach c for the Scenario 2 of table 21,  $Q=47,5 \text{ m}^3/\text{s}$

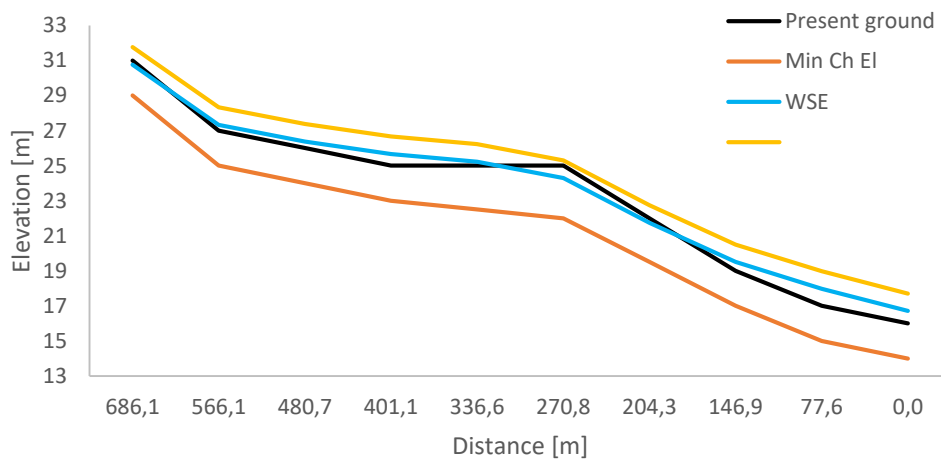


Figure 122 Profile of water depth and levees in reach c for the Scenario 2 of table 21,  $Q=47,5 \text{ m}^3/\text{s}$



Table 21 Table of design levee with freeboard of 1m, Scenario 2, Q=47,5 m3/s

Reach	River Sta	Min Ch El (m)	Top Width (m)	WSE (m)	Present ground (m)	Distance (m)	Vol. dug (m3)	freeboard (m)	Levee El. (m)	h levee (m)	b (m)	B (m)	Area (m2)	Vol (m3)
a	27	32	30	33.63	34	260.23	7806.9	1	35	0.6	0.9	1	1.2222	159.0266
a	26	30	30	32.9	32	234.04	14828.1	1	34	1.9	2.9	1	7.315	1807.793
a	25	30	30	32.76	32	326.86	16827	1	34	1.8	2.6	1	6.4064	1796.675
a	24	30	30	32.52	32	411.53	22151.7	1	34	1.5	2.3	1	4.9856	1840.659
a	23	30	30	31.97	32	0	12345.9	1	33	1.0	1.4	1	2.3424	481.9839
b	12	29	15	30.76	31	665.83	9987.45	1	32	0.8	1.1	1	1.6264	541.453
b	11	25	15	27.67	27	764.44	21454.05	1	29	1.7	2.5	1	5.845	4179.964
b	10	24.5	15	26.6	28	988.27	46008.64	1	28	0.0	0.0	0.0	0.0	0
b	9	22	15	24.75	24	735.6	25858.05	1	26	1.8	2.6	1	6.335	5460.358
b	8	21.5	15	23.97	24	838.05	29505.94	1	25	1.0	1.4	1	2.3424	1843.059
b	7	20	15	23.16	22	731.36	23541.15	1	24	2.2	3.2	1	9.1584	7186.642
b	6	19.5	15	22.75	22	1081.77	33996.19	1	24	1.8	2.6	1	6.335	5743.089
b	5	18	10	22.11	22	761.81	36871.6	1	23	1.1	1.7	1	2.9526	2721.677
b	4	18	10	21.32	21	826.48	23824.35	1	22	1.3	2.0	1	3.9336	3123.849
b	3	17	10	19.85	19	827.25	16537.3	1	21	1.9	2.8	1	6.9745	5766.97
b	2	15	10	17.55	17	767.92	15951.7	1	19	1.6	2.3	1	5.146	4104.372
b	1	12	10	14.91	14	402.79	11707.1	1	16	1.9	2.9	1	7.3726	4315.588
b	0	11	10	14.03	13	0	4027.9	1	15	2.0	3.0	1	8.2012	1651.681
c	22	29	15	30.76	31	1200	18000	1	32	0.8	1.1	1	1.6264	975.84
c	21	25	15	27.32	27	854.41	30816.15	1	28	1.3	2.0	1	3.9336	4040.614
c	20	24	15	26.38	26	795.99	24756	1	27	1.4	2.1	1	4.2366	3496.042
c	19	23	15	25.67	25	645.41	21621	1	27	1.7	2.5	1	5.845	4212.492
c	18	22.5	15	25.22	25	657.94	24437.81	1	26	1.2	1.8	1	3.4526	2249.973
c	17	22	10	24.3	25	664.27	19833.15	1	25	0.3	0.5	1	0.435	287.5807
c	16	19.5	10	21.74	22	574.26	15481.63	1	23	0.7	1.1	1	1.5257	944.8126
c	15	17	10	19.5	19	693.46	12677.2	1	21	1.5	2.3	1	4.875	3090.068
c	14	15	10	17.98	17	775.67	14691.3	1	19	2.0	3.0	1	7.8606	5774.122
c	13	14	10	16.71	16	0	7756.7	1	18	1.7	2.6	1	6.0876	2360.984

### 4.3.3. SCENARIO 3: SHALLOW EXCAVATION WITH LEVEE

In *Scenario 2*, the excavated volume was much larger than the volume used to build the levees. Therefore, in order to get a more balanced solution (in term of use of material excavated), a scenario with less digging is presented. *Figures 123-125* and *Figures 126-128* present, respectively, the profiles obtained for the two flow rates of 47,5 and 100 m<sup>3</sup>/s. for reach a we present the result of the steady mode, that was the only one performed for this reach. For reaches **b** and **c**, instead, we present a comparison between the profiles obtained in steady and unsteady conditions.

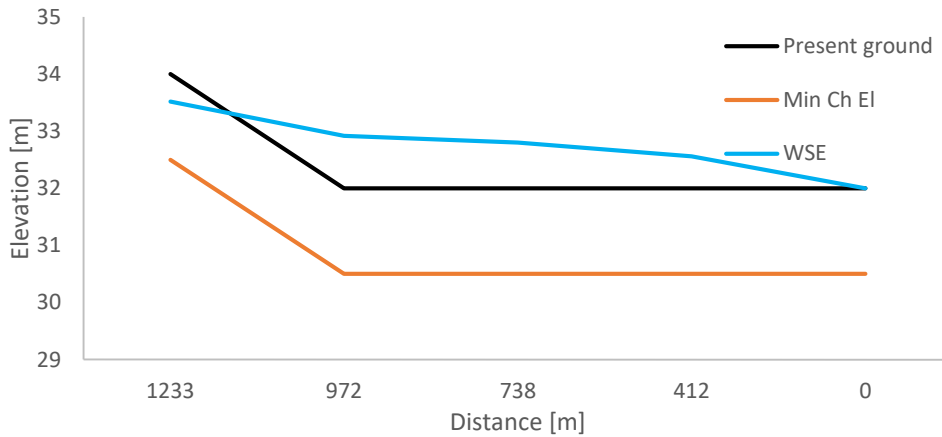


Figure 123 profile of water depth for  $Q = 47,5 \text{ m}^3/\text{s}$  in reach a, Scenario 3

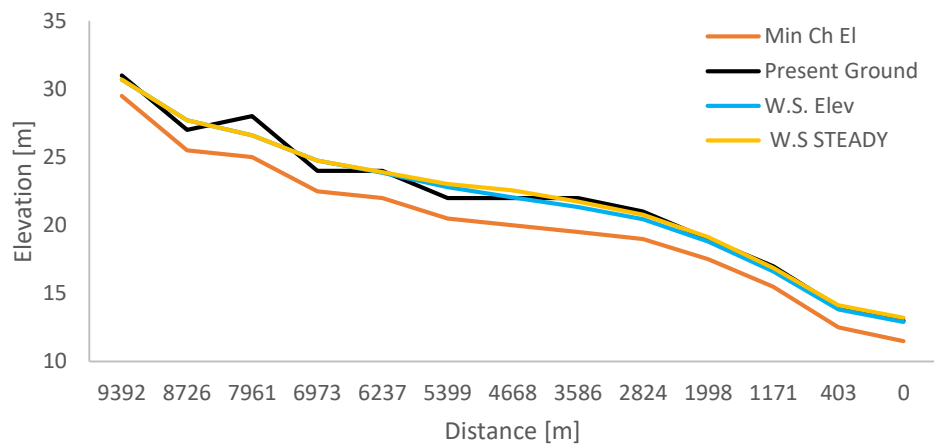


Figure 125 profile of water depth for  $Q = 47,5 \text{ m}^3/\text{s}$  in reach b, Scenario 3

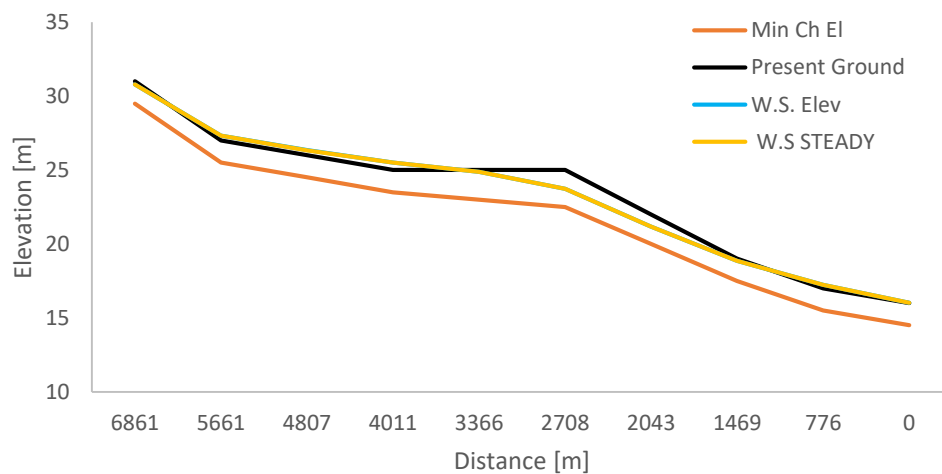


Figure 124 profile of water depth for  $Q = 47,5 \text{ m}^3/\text{s}$  in reach c, Scenario 3

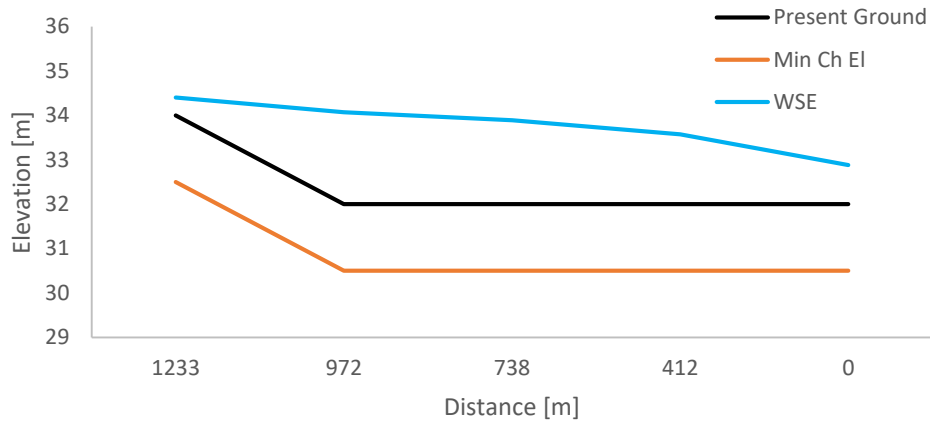


Figure 128 profile of water depth for  $Q = 100 \text{ m}^3/\text{s}$  in reach a, Scenario 3

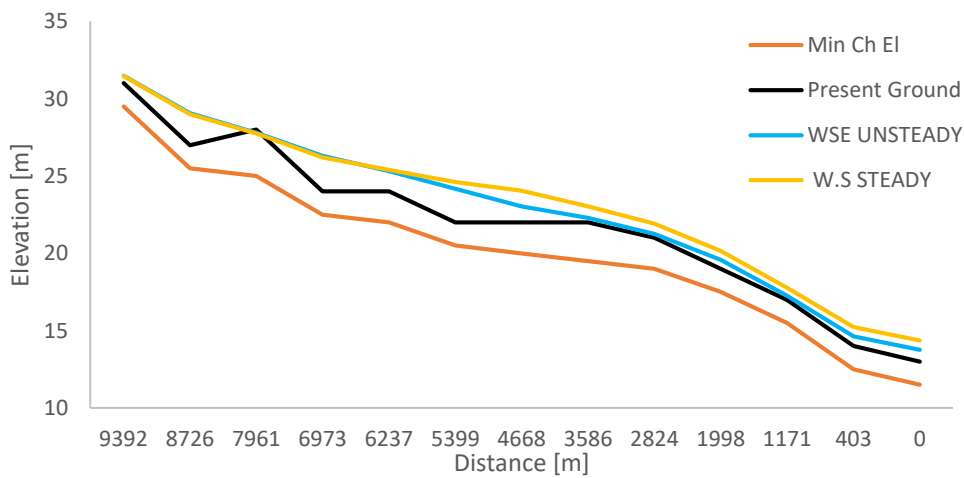


Figure 127 profile of water depth for  $Q = 100 \text{ m}^3/\text{s}$  in reach b, Scenario 3

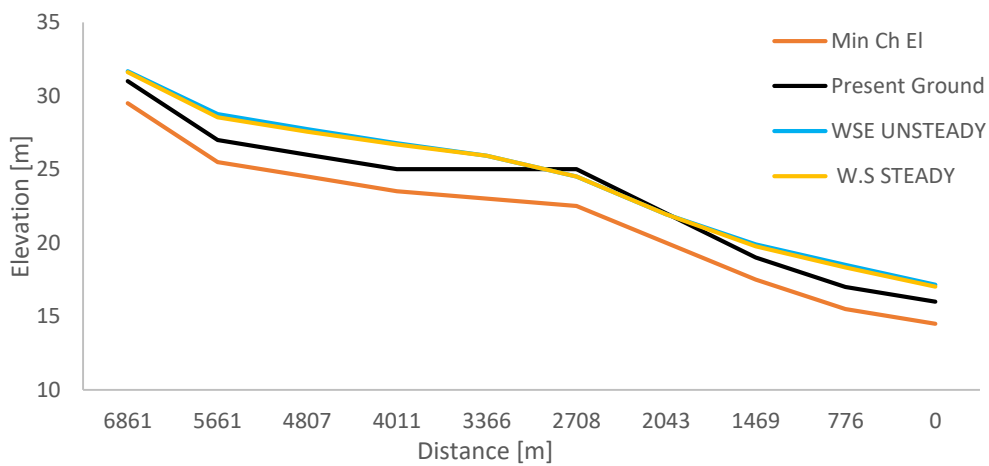


Figure 126 profile of water depth for  $Q = 100 \text{ m}^3/\text{s}$  in reach c, Scenario 3

Comparing Figures 129 and 130 with the analogous ones for Scenario 1 (115 and 116, respectively), it is evident that the volume of the flow laminated in the lake is much higher in this second case, even if the flow hydrographs of the upstream section are obviously the same. In fact, the second scenario presents a river bed with shallower excavation, generating a higher wave on the lateral weir respect the first scenario.

Hydrographs upstream and downstream of the weir are presented in *Figures 129 and 130* for the two flow rates.

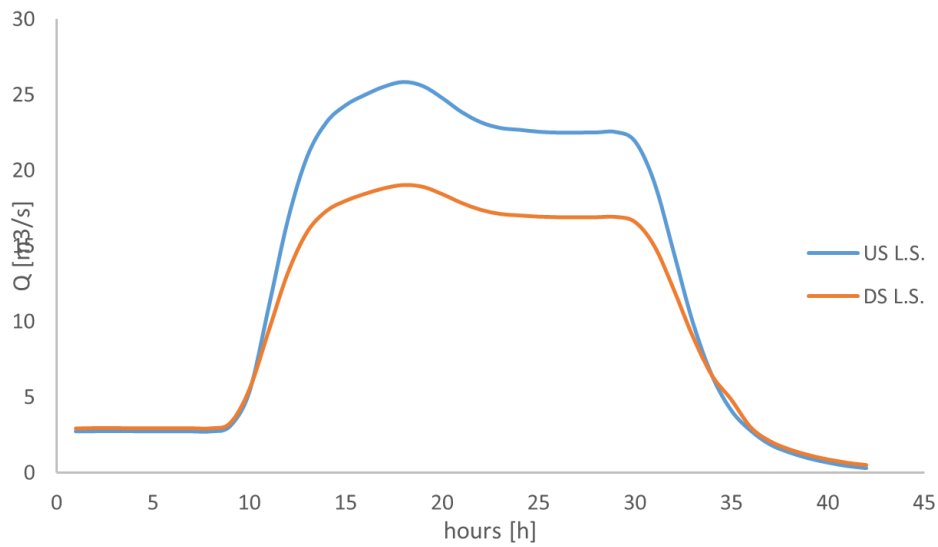


Figure 129 hydrographs in the upstream and downstream sections of the weir for  $Q = 47.5 \text{ m}^3/\text{s}$ , Scenario 3

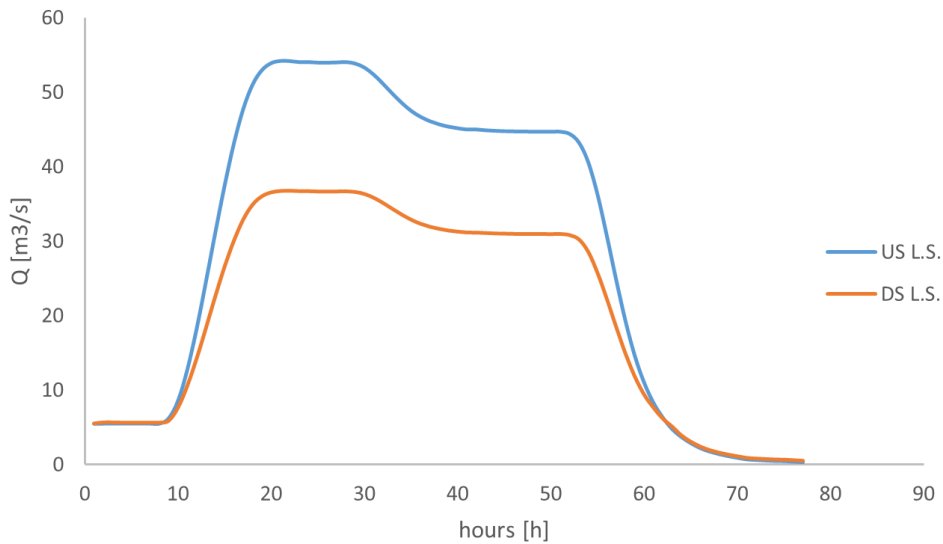


Figure 130 hydrographs in the upstream and downstream sections of the weir for  $Q = 100 \text{ m}^3/\text{s}$ , Scenario 3

For  $Q = 47,5 \text{ m}^3/\text{s}$ :

VOL US L.S. =  $1923894 \text{ m}^3$

VOL DS L.S. =  $1502136 \text{ m}^3$

VOL STORED =  $421758 \text{ m}^3$

For  $Q = 100 \text{ m}^3/\text{s}$

VOL US L.S. =  $8061318 \text{ m}^3$

VOL DS L.S. =  $5702292 \text{ m}^3$

VOL STORED L.S. =  $2359026 \text{ m}^3$

Since the excavation is less than for the previous scenarios, construction of levees is in this case needed also for the flow rate of 47,5 m<sup>3</sup>/s. Two procedures are considered also in this case, with the first sufficient to ensure a minimum freeboard and the second able to ensure a freeboard of 1 m. The total volume of digging in this scenario equals 328541,2 m<sup>3</sup>. The first procedure requires a total volume which is about one half of the one excavated (*Table 22*). The resulting levees are presented as follows (*Figures 131-133*).

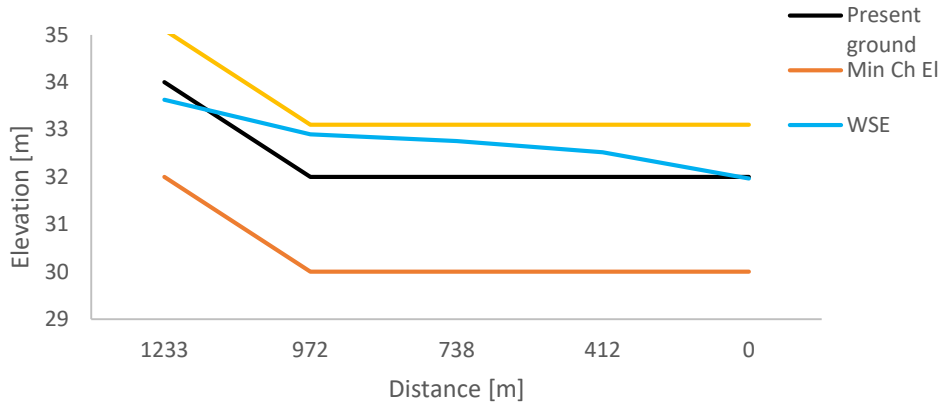


Figure 132 Profile of water depth and uniform levees in reach a for the Scenario 3 of table 22,  $Q=47,5 \text{ m}^3/\text{s}$

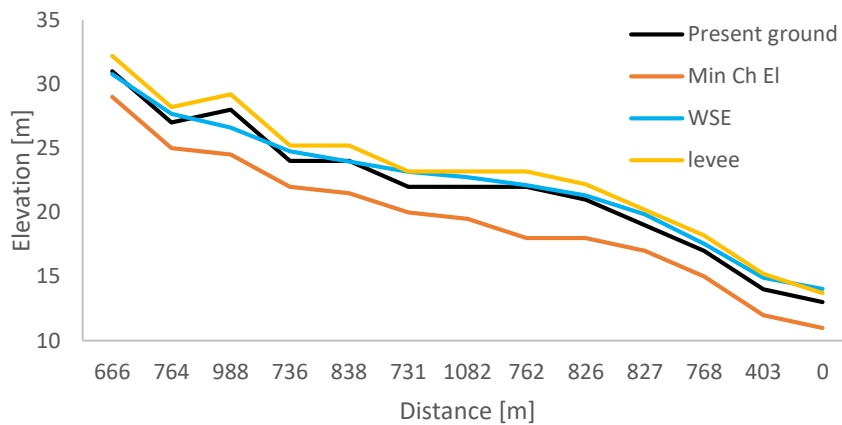


Figure 131 Profile of water depth and uniform levees in reach b for the Scenario 3 of table 22,  $Q=47,5 \text{ m}^3/\text{s}$

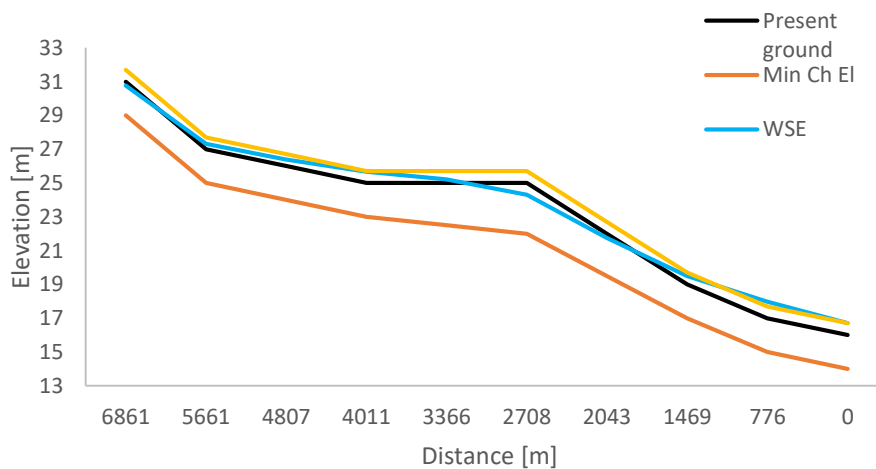


Figure 133 Profile of water depth and uniform levees in reach c for the Scenario 3 of table 22,  $Q=47,5 \text{ m}^3/\text{s}$

Table 22 Table of uniform levee design for  $Q=47,5 \text{ m}^3/\text{s}$ , Scenario 3

Reaches	hmax [m]	h [m]	b [m]	B [m]	Lenght [m]	Area [m <sup>2</sup> ]	Vol [m <sup>3</sup> ]	Vol*2 [m <sup>3</sup> ]	Vtot [m <sup>3</sup> ]
a	0.92	1.10	1.65	2.00	1232.66	4.02	4949.13	9898.26	129356
b	1.02	1.20	2.00	2.00	9391.57	4.80	45079.54	90159.07	
c	0.50	0.70	1.05	2.00	6861.41	2.14	14649.11	29298.22	

The profiles obtained with the second procedure are depicted in Figures 134-136

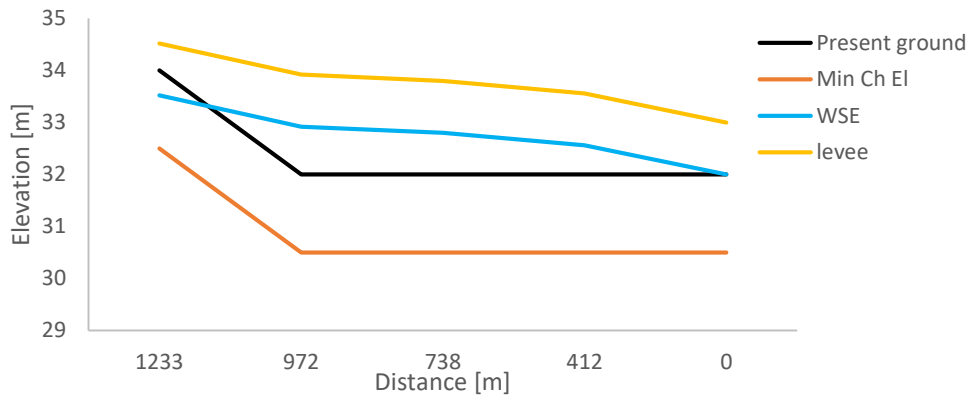


Figure 135 Profile of water depth and levees in reach a for the Scenario 3 of table 23,  $Q=47,5 \text{ m}^3/\text{s}$

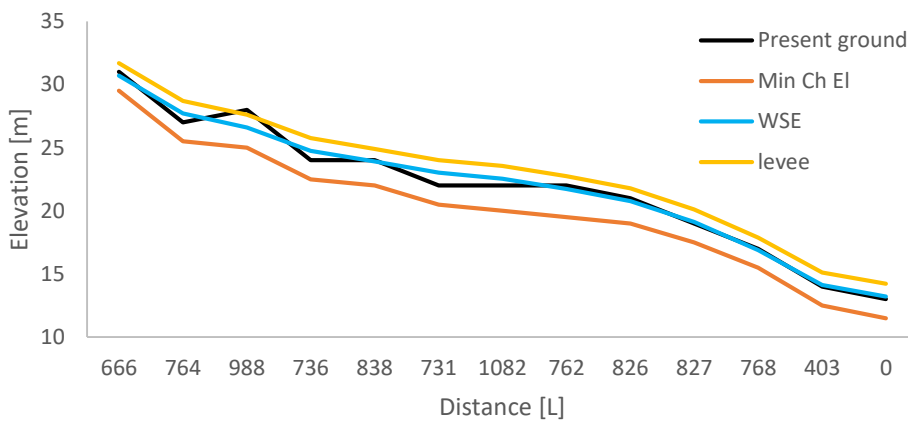


Figure 134 Profile of water depth and levees in reach b for the Scenario 3 of table 23,  $Q=47,5 \text{ m}^3/\text{s}$

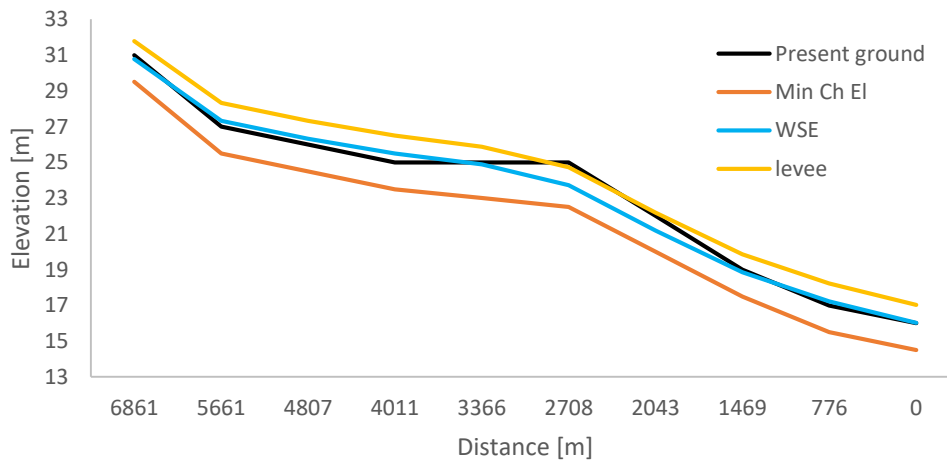


Figure 136 Profile of water depth and levees in reach c for the Scenario 3 of table 23,  $Q=47,5 \text{ m}^3/\text{s}$



The resultant volume obtained is equal to 150662,01 m<sup>3</sup>. It can be noticed that the volume required for the levee building can be assumed comparable with the one necessary to stem the discharge of 100 m<sup>3</sup>/s in the previous scenario. However, the amount of material wasted is less than half of the one computed before.

Table 23 Table of levee design with freeboard of 1m, Q=47,5 m3/s, Scenario 3

Reach	River Sta	Min Ch El (m)	Top Width (m)	WSE (m)	Present ground (m)	Distance (m)	Vol. dug (m3)	Freeboard (m)	Levee el. (m)	h levee (m)	b (m)	B (m)	Area (m2)	Vol (m3)
a	27	32.50	20	33.52	34	260.23	3903.45	1	34.5	0.5	0.8	2	1.45	188.09
a	26	30.50	20	32.92	32	234.04	7414.05	1	33.9	1.9	2.9	2	9.37	2315.56
a	25	30.50	20	32.80	32	326.86	8413.5	1	33.8	1.8	2.7	2	8.46	2372.61
a	24	30.50	20	32.56	32	411.53	11075.85	1	33.6	1.6	2.3	2	6.77	2499.60
a	23	30.50	20	32.00	32	0	6172.95	1	33.0	1.0	1.5	2	3.50	720.18
b	12	29.50	10	30.70	31	665.83	4993.725	1	31.7	0.7	1.0	2	2.09	696.03
b	11	25.50	10	27.71	27	764.44	10727.03	1	28.7	1.7	2.6	2	7.80	5576.34
b	10	25.00	10	26.60	28	988.27	26290.65	1	27.6	0.0	0.0	2	0.00	0.00
b	9	22.50	10	24.75	24	735.6	12929.03	1	25.8	1.8	2.6	2	8.09	6968.74
b	8	22.00	10	23.90	24	838.05	15736.5	1	24.9	0.9	1.3	2	2.96	2331.91
b	7	20.50	10	23.02	22	731.36	11770.58	1	24.0	2.0	3.0	2	10.16	7973.07
b	6	20.00	10	22.55	22	1081.77	18131.3	1	23.6	1.6	2.3	2	6.70	6070.36
b	5	19.50	10	21.74	22	761.81	23044.75	1	22.7	0.7	1.1	2	2.26	2079.28
b	4	19.00	10	20.77	21	826.48	15882.9	1	21.8	0.8	1.2	2	2.43	1926.20
b	3	17.50	10	19.12	19	827.25	12402.98	1	20.1	1.1	1.7	2	4.12	3408.01
b	2	15.50	10	16.88	17	767.92	11963.78	1	17.9	0.9	1.3	2	2.87	2289.87
b	1	12.50	10	14.12	14	402.79	8780.325	1	15.1	1.1	1.7	2	4.12	2412.60
b	0	11.50	10	13.22	13	0	3020.925	1	14.2	1.2	1.8	2	4.67	941.04
c	22	29.50	10	30.78	31	1200	9000	1	31.8	0.8	1.2	2	2.47	1483.56
c	21	25.50	10	27.32	27	854.41	15408.08	1	28.3	1.3	2.0	2	5.25	5396.52
c	20	24.50	10	26.32	26	795.99	12378	1	27.3	1.3	2.0	2	5.25	4335.27
c	19	23.50	10	25.50	25	645.41	10810.5	1	26.5	1.5	2.3	2	6.38	4594.46
c	18	23.00	10	24.88	25	657.94	13033.5	1	25.9	0.9	1.3	2	2.87	1870.96
c	17	22.50	10	23.73	25	664.27	16527.63	1	24.7	0.0	0.0	0.0	0.00	0.00
c	16	20.00	10	21.18	22	574.26	12385.3	1	22.2	0.2	0.3	2	0.41	253.03
c	15	17.50	10	18.85	19	693.46	9507.9	1	19.9	0.9	1.3	2	2.78	1761.81
c	14	15.50	10	17.23	17	775.67	11018.48	1	18.2	1.2	1.8	2	4.72	3469.50
c	13	14.50	10	16.02	16	0	5817.525	1	17.0	1.0	1.5	2	3.60	1396.44

One must have borne in mind that the construction of the levees, in this scenario, had to be designed with reference to 47,5 m<sup>3</sup>/s of peak flow rate. With Q=100 m<sup>3</sup>/s, the volume of soil necessary for the construction of the levees is not sufficient. With the first procedure, the volume of the levee is 335666,36 m<sup>3</sup> as shown in Table 24.

Table 24 Table of uniform levee design for Q=100 m<sup>3</sup>/s, Scenario 3

Reach	hmax [m]	h [m]	b [m]	B [m]	Lenght [m]	Area [m <sup>2</sup> ]	Vol [m <sup>3</sup> ]	Vol*2 [m <sup>3</sup> ]	Vtot [m <sup>3</sup> ]
a	2.07	2.10	3.15	2.00	1232.66	10.82	13331.22	26662.44	335666.36
b	2.60	2.70	2.00	2.00	9391.57	10.80	101428.96	202857.91	
c	1.68	1.70	2.55	2.00	6861.41	7.74	53073.01	106146.01	

Table 25 Table of levee design with freeboard of 1m for Q=100 m<sup>3</sup>/s, Scenario3

Reach	River Sta	Min Ch El (m)	Top Width (m)	WSE (m)	Present Ground (m)	Distance (m)	Vol dug (m <sup>3</sup> )	freeboard (m)	Levee el. (m)	h levee (m)	b (m)	B (m)	Area (m <sup>2</sup> )	Vol (m <sup>3</sup> )
a	27.00	32.50	20.00	34.40	34.00	260.23	3903.45	1.00	35.40	1.40	2.10	2.00	5.74	746.86
a	26.00	30.50	20.00	34.07	32.00	234.04	7414.05	1.00	35.07	3.07	4.60	2.00	20.26	5007.45
a	25.00	30.50	20.00	33.89	32.00	326.86	8413.50	1.00	34.89	2.89	4.33	2.00	18.29	5130.47
a	24.00	30.50	20.00	33.57	32.00	411.53	11075.85	1.00	34.57	2.57	3.85	2.00	15.03	5550.66
a	23.00	30.50	20.00	32.88	32.00	0.00	6172.95	1.00	33.88	1.88	2.82	2.00	9.06	1864.56
b	12.00	29.50	10.00	31.47	31.00	665.83	4993.73	1.00	32.47	1.47	2.20	2.00	6.17	2055.42
b	11.00	25.50	10.00	28.99	27.00	764.44	10727.03	1.00	29.99	2.99	4.48	2.00	19.38	13855.88
b	10.00	25.00	10.00	27.76	28.00	988.27	26290.65	1.00	28.76	0.76	1.14	2.00	2.39	2091.33
b	9.00	22.50	10.00	26.21	24.00	735.60	12929.03	1.00	27.21	3.21	4.81	2.00	21.86	18841.99
b	8.00	22.00	10.00	25.40	24.00	838.05	15736.50	1.00	26.40	2.40	3.60	2.00	13.44	10574.93
b	7.00	20.50	10.00	24.60	22.00	731.36	11770.58	1.00	25.60	3.60	5.40	2.00	26.64	20904.54
b	6.00	20.00	10.00	24.04	22.00	1081.77	18131.30	1.00	25.04	3.04	4.56	2.00	19.94	18079.08
b	5.00	19.50	10.00	23.04	22.00	761.81	23044.75	1.00	24.04	2.04	3.06	2.00	10.32	9515.09
b	4.00	19.00	10.00	21.92	21.00	826.48	15882.90	1.00	22.92	1.92	2.88	2.00	9.37	7440.82
b	3.00	17.50	10.00	20.16	19.00	827.25	12402.98	1.00	21.16	2.16	3.24	2.00	11.32	9358.79
b	2.00	15.50	10.00	17.78	17.00	767.92	11963.78	1.00	18.78	1.78	2.67	2.00	8.31	6630.01
b	1.00	12.50	10.00	15.23	14.00	402.79	8780.33	1.00	16.23	2.23	3.34	2.00	11.91	6970.52
b	0.00	11.50	10.00	14.37	13.00	0.00	3020.93	1.00	15.37	2.37	3.55	2.00	13.15	2649.05
c	22.00	29.50	10.00	31.61	31.00	1200.00	9000.00	1.00	32.61	1.61	2.41	2.00	7.10	4260.06
c	21.00	25.50	10.00	28.54	27.00	854.41	15408.08	1.00	29.54	2.54	3.81	2.00	14.76	15158.88
c	20.00	24.50	10.00	27.55	26.00	795.99	12378.00	1.00	28.55	2.55	3.82	2.00	14.84	12246.79
c	19.00	23.50	10.00	26.68	25.00	645.41	10810.50	1.00	27.68	2.68	4.02	2.00	16.13	11627.49
c	18.00	23.00	10.00	25.92	25.00	657.94	13033.50	1.00	26.92	1.92	2.88	2.00	9.37	6105.93
c	17.00	22.50	10.00	24.52	25.00	664.27	16527.63	1.00	25.52	0.52	0.78	2.00	1.45	955.69
c	16.00	20.00	10.00	21.93	22.00	574.26	12385.30	1.00	22.93	0.93	1.39	2.00	3.15	1952.36
c	15.00	17.50	10.00	19.77	19.00	693.46	9507.90	1.00	20.77	1.77	2.65	2.00	8.23	5216.98
c	14.00	15.50	10.00	18.32	17.00	775.67	11018.48	1.00	19.32	2.32	3.48	2.00	12.71	9338.97
c	13.00	14.50	10.00	17.02	16.00	0.00	5817.53	1.00	18.02	2.02	3.03	2.00	10.16	3940.64

#### 4.3.4. SCENARIO 4: INTERMEDIATE EXCAVATION WITH LEVEE

Since the volume of soil excavated is not enough for the construction of levees for the larger discharge, a further scenario has been analysed. It presents larger cross sections than the previous one and consequently, higher volume of soil excavated. *Figures 137-139* and *Figures 140-142* depict, respectively, the profiles obtained for the two flow rates of 47,5 and 100 m<sup>3</sup>/s. As in the previous scenario, for reach *a* the results are presented in a steady mode while for reaches *b* and *c*, a comparison between the profiles obtained in steady and unsteady conditions is presented.

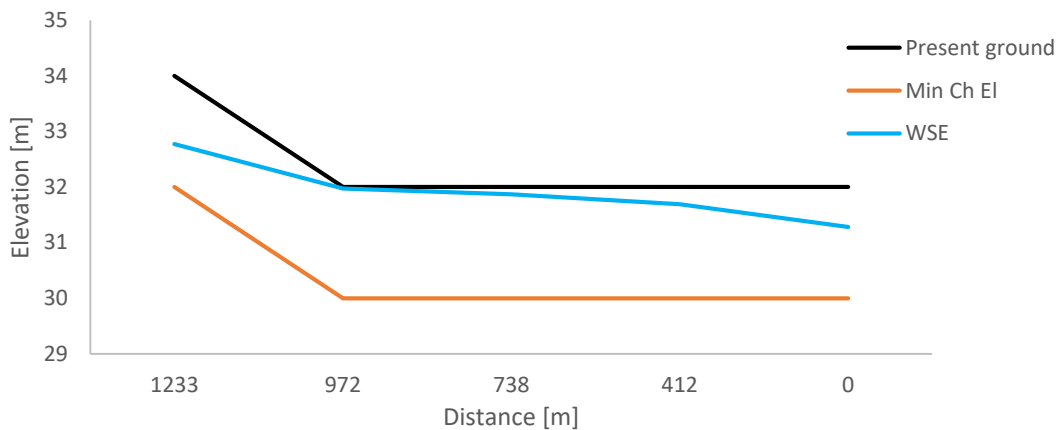


Figure 137 profile of water depth for  $Q = 47,5 \text{ m}^3/\text{s}$  in reach *a*, Scenario 4

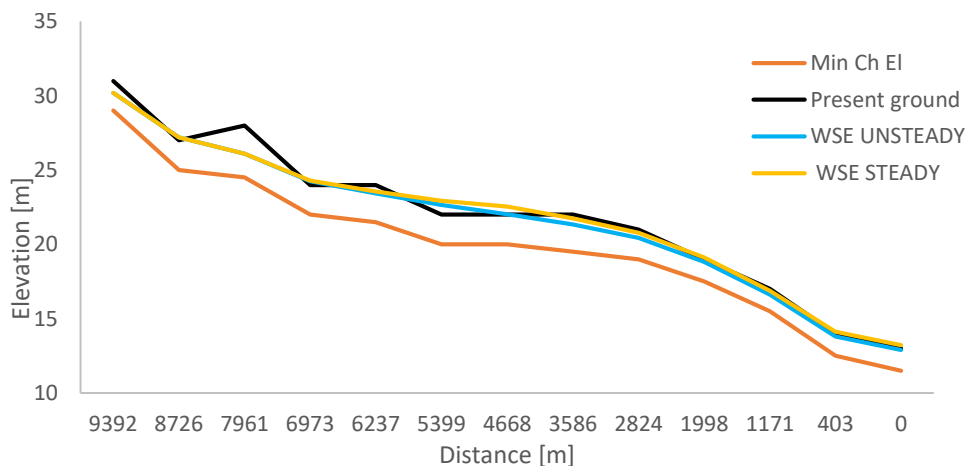


Figure 138 profile of water depth for  $Q = 47,5 \text{ m}^3/\text{s}$  in reach *b*, Scenario 4

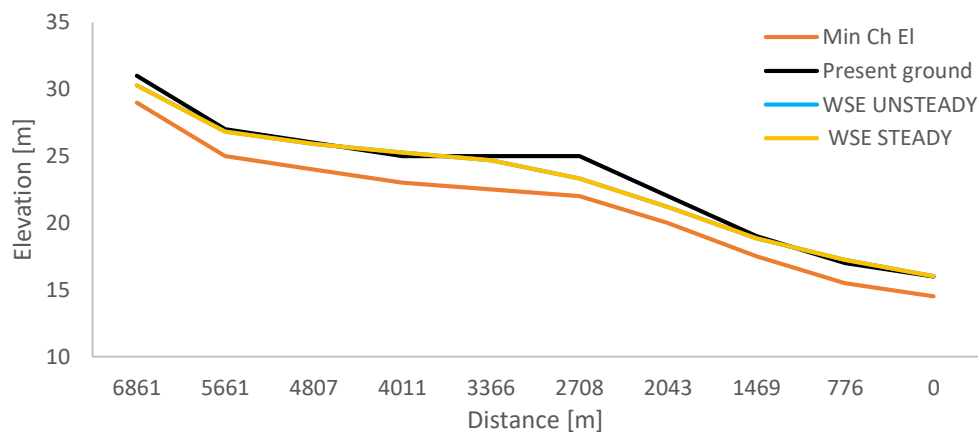


Figure 139 profile of water depth for  $Q = 47,5 \text{ m}^3/\text{s}$  in reach *c*, Scenario 4

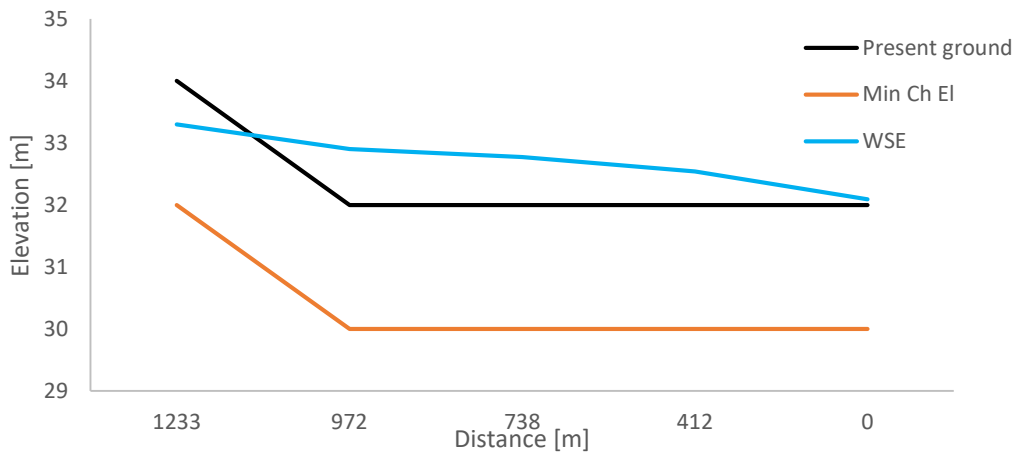


Figure 141 profile of water depth for  $Q = 100 \text{ m}^3/\text{s}$  in reach a, Scenario 4

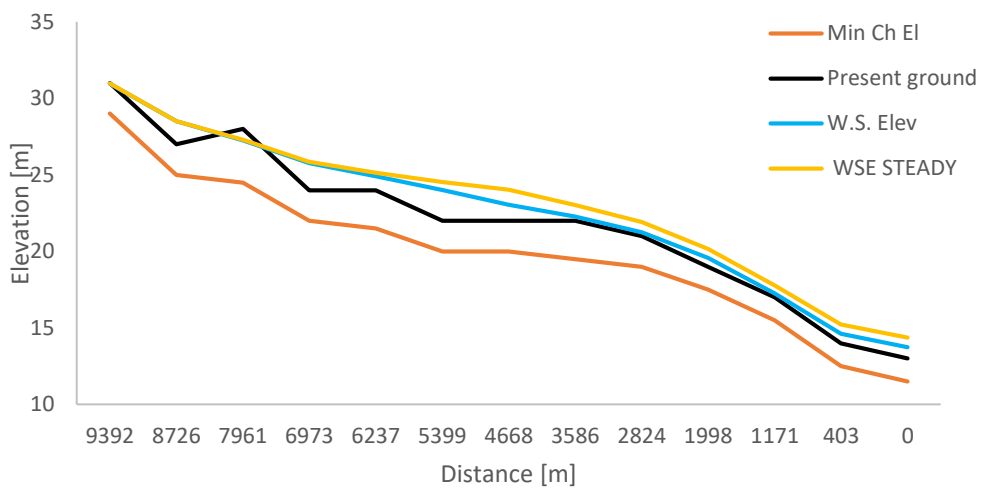


Figure 142 profile of water depth for  $Q = 100 \text{ m}^3/\text{s}$  in reach b, Scenario 4

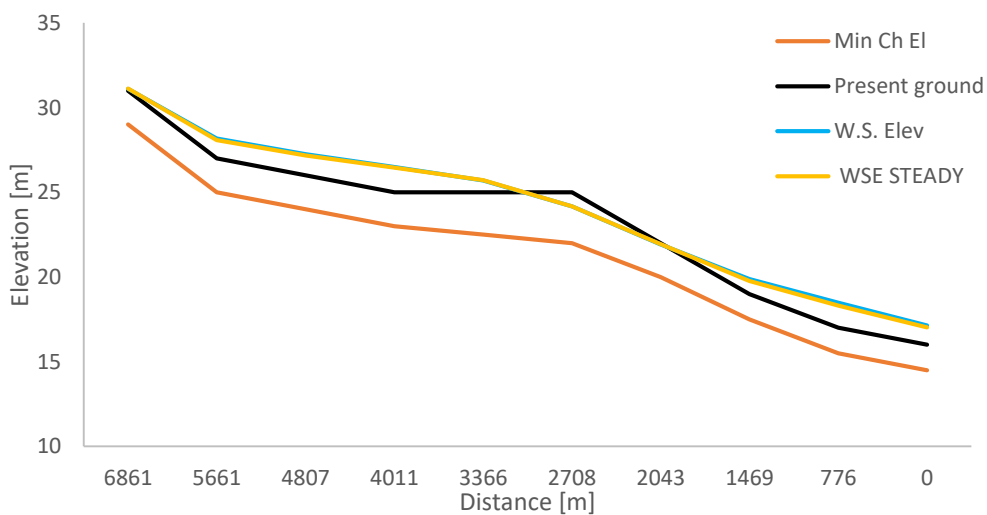


Figure 140 profile of water depth for  $Q = 100 \text{ m}^3/\text{s}$  in reach c, Scenario 4

It can be noticed that, for the lower discharge, since reach a is enlarged of 10m with respect to the previous scenario, no overflowing occurs. Moreover, the discrepancy of the results in reach **b**, between the steady and the unsteady case, is similar to the previous scenario, especially in the downstream section of the lateral

structure, since, there, the geometry is the same; while, in the reach *c* the two profiles are approximately the same.

The last scenario geometry presents an intermediate excavation, and it is expected a value of stored volume intermediate between the two cases presented above. The results are in agreement with this assumption even though it can be noticed that the volumes presented in the *Scenario 3*, for same discharge value, are very close to the one of *Scenario 4*; because, in this geometry, with respect to the previous one, the excavation of the river bed interests especially the reach *a* and the upstream sections of the reaches *b* and *c*. In particular, the elevation of the river bed in the weir section is the same in the two cases, this suggests that the wave height on the lateral structure is the same.

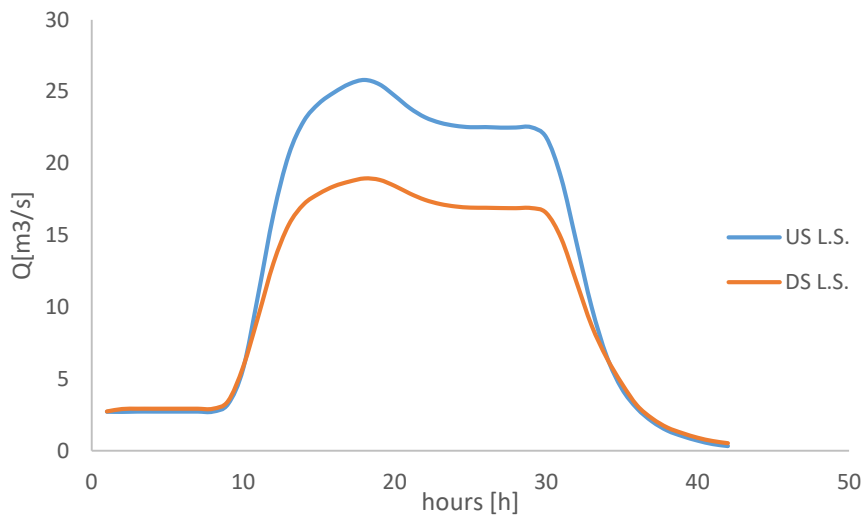


Figure 144 Hydrographs in the upstream and downstream sections of the weir for  $Q = 47,5 \text{ m}^3/\text{s}$ , Scenario 4

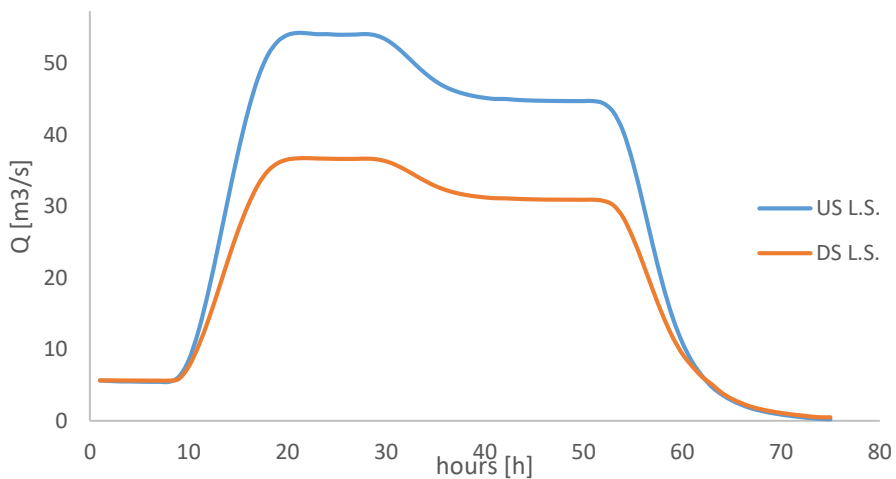


Figure 143 Hydrographs in the upstream and downstream sections of the weir for  $Q = 100 \text{ m}^3/\text{s}$ , Scenario 4

For  $Q=47,5 \text{ m}^3/\text{s}$

VOL US L.S =  $1947906 \text{ m}^3$

VOL DS L.S.=  $1529370 \text{ m}^3$

VOL STORED=  $418536 \text{ m}^3$

For  $Q=100 \text{ m}^3/\text{s}$

VOL US L.S=  $8059518 \text{ m}^3$

VOL DS L.S= 5698764 m<sup>3</sup>

VOL STORED L.S= 2360754 m<sup>3</sup>

Since no overflow occurs in reach *a* for the lower discharge, considering the first procedure of construction, the levees are not necessary and, consequently, the volume of soil necessary to build uniform levee is 89686 m<sup>3</sup> (Table 26); much lower value respect the volume of soil excavated, which is 409739,7 m<sup>3</sup>. The resulting levees are presented as follows (Figures 145-146).

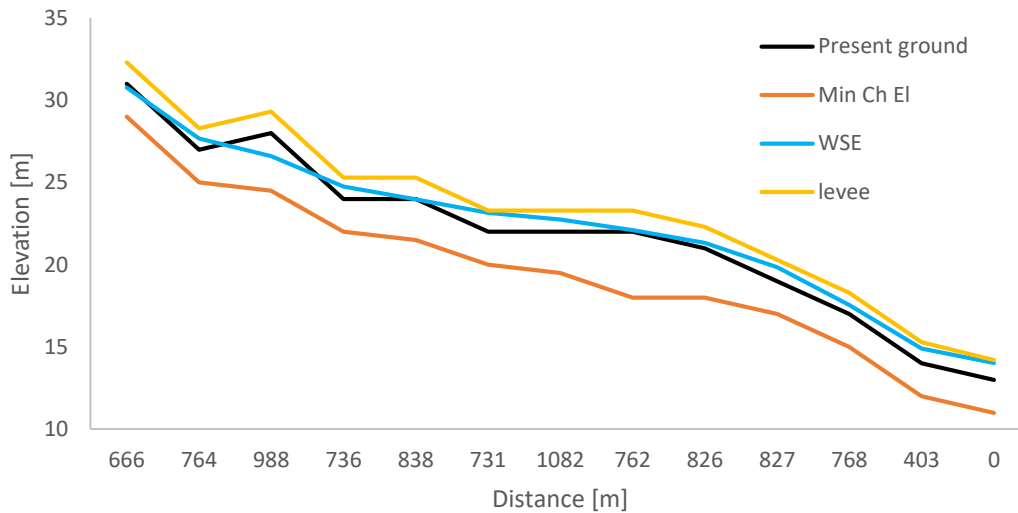


Figure 146 Profile of water depth and levees in reach *b* for the Scenario 4 of table 26, Q=47,5 m<sup>3</sup>/s

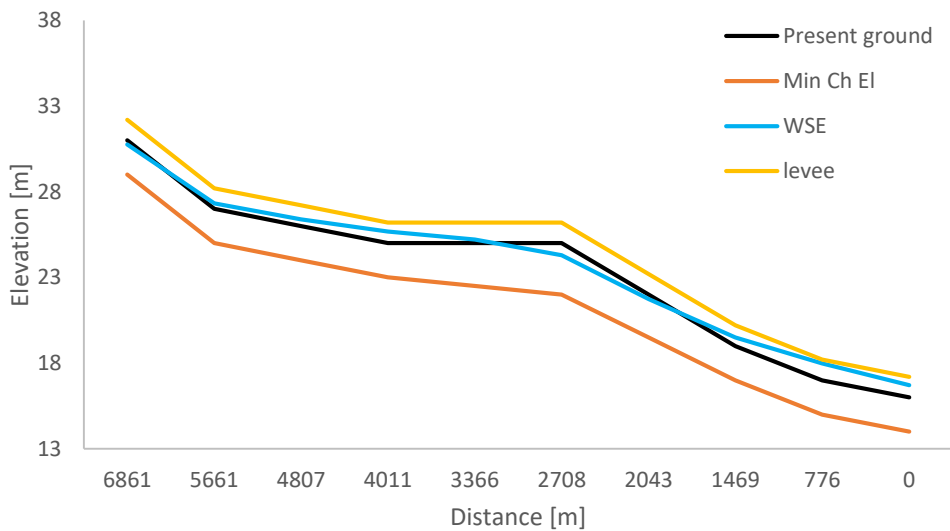


Figure 145 Profile of water depth and levees in reach *c* for the Scenario 4 of table 26, Q=47,5 m<sup>3</sup>/s

Table 26 Table of uniform levee design for Q=47,5 m<sup>3</sup>/s, Scenario 4

Reach	hmax [m]	h [m]	b [m]	B [m]	Lenght [m]	Area [m <sup>2</sup> ]	Vol [m <sup>3</sup> ]	Vol*2 [m <sup>3</sup> ]
<b>a</b>	-	-	-	-	-	-	-	-
<b>b</b>	0.94	1.10	1.65	2.00	9391.57	4.02	37707.15	75414.31
<b>c</b>	0.27	0.40	0.60	2.00	6861.41	1.04	7135.87	14271.73



With the alternative procedure, a higher volume is necessary since the original river bank of reach *a* does not ensure 1m of a safety freeboard. The volume of material required is equal to 110249,1 m<sup>3</sup> (Table 27). The alternative result is depicted in the Figures 147-148-149.

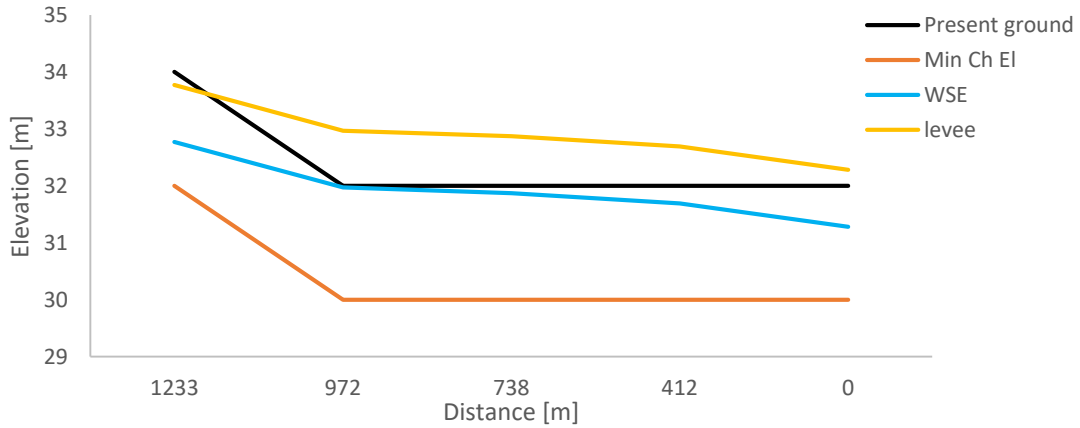


Figure 149 Profile of water depth and levees in reach *a* for the Scenario 4 of table 27,  $Q=47,5 \text{ m}^3/\text{s}$

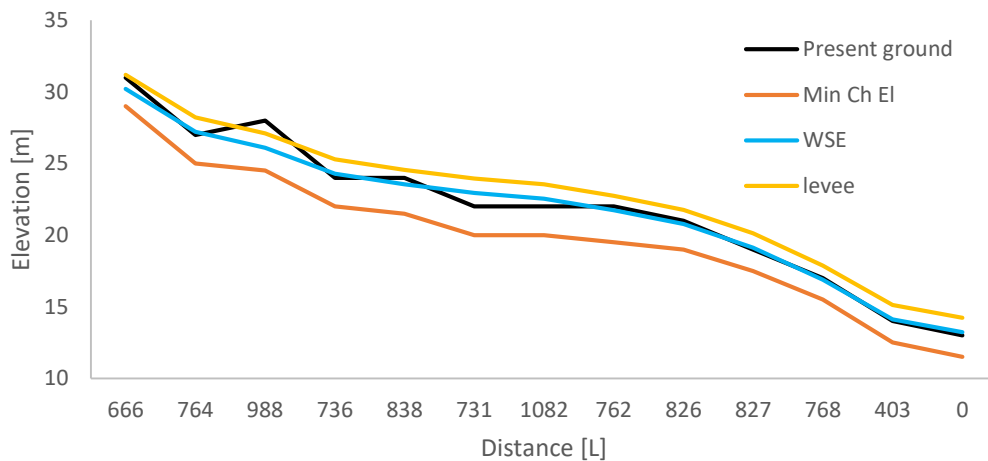


Figure 148 Profile of water depth and levees in reach *b* for the Scenario 4 of table 27,  $Q=47,5 \text{ m}^3/\text{s}$

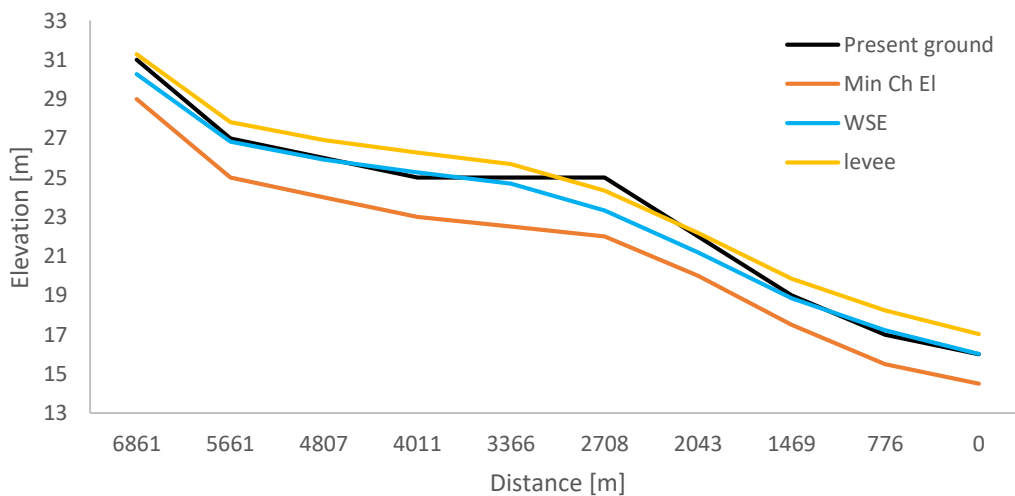


Figure 147 Profile of water depth and levees in reach *c* for the Scenario 4 of table 27,  $Q=47,5 \text{ m}^3/\text{s}$

Table 27 Table of the levee design with freeboard of 1m, Q=47,5 m3/s, Scenario 4

Reach	River Sta	Min Ch El (m)	Top Width (m)	WSE (m)	'resent ground (m)	Distance (m)	Vol dug (m3)	freeboard (m)	Levee el. (m)	h levee (m)	b (m)	B (m)	Area (m2)	Vol (m3)
a	27	32.00	30.00	32.77	34.00	260.23	7806.90	1.00	33.77	0.00	0.00	0.00	0.00	0.00
a	26	30.00	30.00	31.97	32.00	234.04	14828.10	1.00	32.97	0.96	1.44	2.00	3.30	816.14
a	25	30.00	30.00	31.87	32.00	326.86	16827.00	1.00	32.87	0.87	1.30	2.00	2.87	805.17
a	24	30.00	30.00	31.69	32.00	411.53	22151.70	1.00	32.69	0.68	1.02	2.00	2.05	758.18
a	23	30.00	30.00	31.28	32.00	0.00	12345.90	1.00	32.28	0.28	0.42	2.00	0.68	139.43
b	12	29.00	10.00	30.20	31.00	665.83	6658.30	1.00	31.20	0.19	0.28	2.00	0.43	144.22
b	11	25.00	10.00	27.21	27.00	764.44	14302.70	1.00	28.21	1.21	1.81	2.00	4.61	3296.84
b	10	24.50	10.00	26.10	28.00	988.27	30672.43	1.00	27.10	0.00	0.00	0.00	0.00	0.00
b	9	22.00	10.00	24.29	24.00	735.60	17238.70	1.00	25.29	1.29	1.93	2.00	5.07	4369.75
b	8	21.50	10.00	23.55	24.00	838.05	19670.63	1.00	24.55	0.55	0.82	2.00	1.55	1220.37
b	7	20.00	10.00	22.94	22.00	731.36	15694.10	1.00	23.94	1.94	2.91	2.00	9.53	7474.63
b	6	20.00	10.00	22.55	22.00	1081.77	18131.30	1.00	23.55	1.55	2.32	2.00	6.70	6070.36
b	5	19.50	10.00	21.74	22.00	761.81	23044.75	1.00	22.74	0.73	1.09	2.00	2.26	2079.28
b	4	19.00	10.00	20.77	21.00	826.48	15882.90	1.00	21.77	0.77	1.15	2.00	2.43	1926.20
b	3	17.50	10.00	19.12	19.00	827.25	12402.98	1.00	20.12	1.12	1.68	2.00	4.12	3408.01
b	2	15.50	10.00	16.88	17.00	767.92	11963.78	1.00	17.88	0.87	1.30	2.00	2.87	2289.87
b	1	12.50	10.00	14.12	14.00	402.79	8780.33	1.00	15.12	1.12	1.68	2.00	4.12	2412.60
b	0	11.50	10.00	13.22	13.00	0.00	3020.93	1.00	14.22	1.22	1.83	2.00	4.67	941.04
c	22	29.00	10.00	30.28	31.00	1200.00	12000.00	1.00	31.28	0.28	0.42	2.00	0.68	406.56
c	21	25.00	10.00	26.83	27.00	854.41	20544.10	1.00	27.83	0.82	1.23	2.00	2.65	2720.66
c	20	24.00	10.00	25.91	26.00	795.99	16504.00	1.00	26.91	0.91	1.36	2.00	3.06	2523.13
c	19	23.00	10.00	25.27	25.00	645.41	14414.00	1.00	26.27	1.27	1.90	2.00	4.95	3569.63
c	18	22.50	10.00	24.69	25.00	657.94	16291.88	1.00	25.69	0.69	1.03	2.00	2.09	1362.46
c	17	22.00	10.00	23.33	25.00	664.27	19833.15	1.00	24.33	0.00	0.00	0.00	0.00	0.00
c	16	20.00	10.00	21.18	22.00	574.26	12385.30	1.00	22.18	0.18	0.27	2.00	0.41	253.03
c	15	17.50	10.00	18.85	19.00	693.46	9507.90	1.00	19.85	0.85	1.27	2.00	2.78	1761.81
c	14	15.50	10.00	17.23	17.00	775.67	11018.48	1.00	18.23	1.23	1.84	2.00	4.72	3469.50
c	13	14.50	10.00	16.02	16.00	0.00	5817.53	1.00	17.02	1.02	1.53	2.00	3.60	1396.44

With  $Q=100 \text{ m}^3/\text{s}$  the first procedure provides a volume of material required for the levees construction, which is slightly higher than the excavated one and is equal to  $412060 \text{ m}^3$ . Therefore,  $2320 \text{ m}^3$  of additional material is necessary. (Table 28). The alternative solution requires a total volume of soil of  $366534.9 \text{ m}^3$  (Table 29), without additional material. In Figures 150-151-152 and in Figures 153-154-155 the results of the first and the second procedure are reported, respectively.

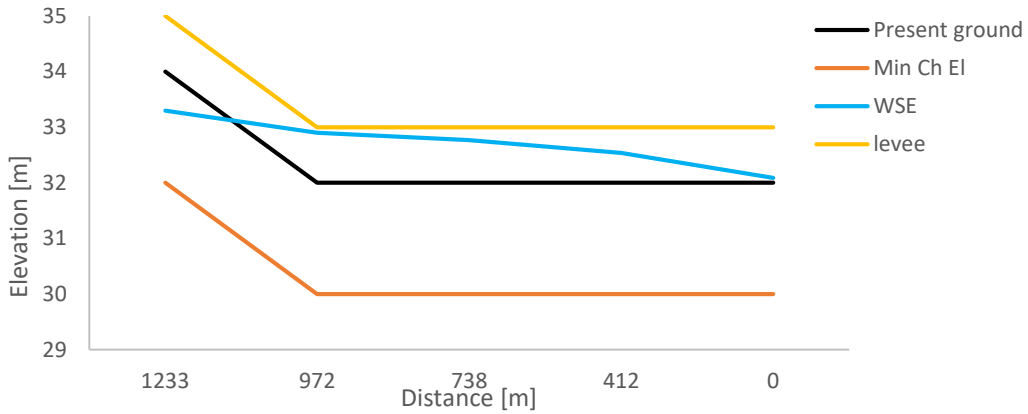


Figure 152 Profile of water depth and levees in reach a for the Scenario 4 of table 28,  $Q=100 \text{ m}^3/\text{s}$

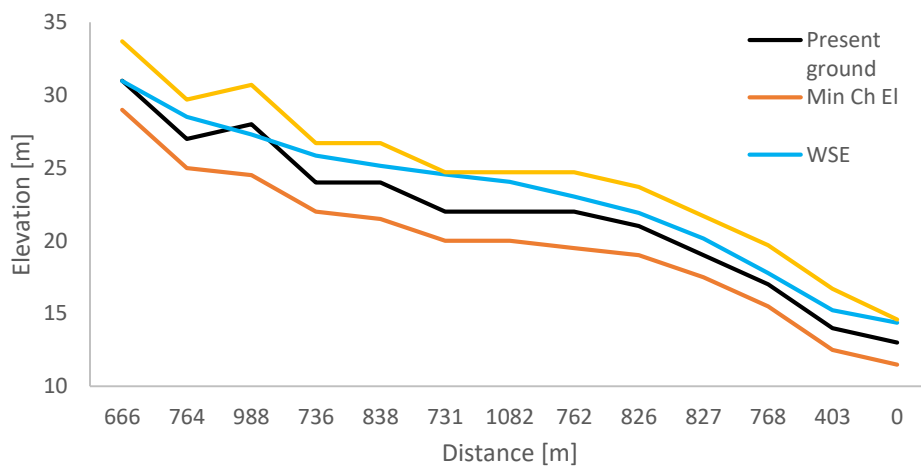


Figure 151 Profile of water depth and levees in reach b for the Scenario 4 of table 28,  $Q=100 \text{ m}^3/\text{s}$

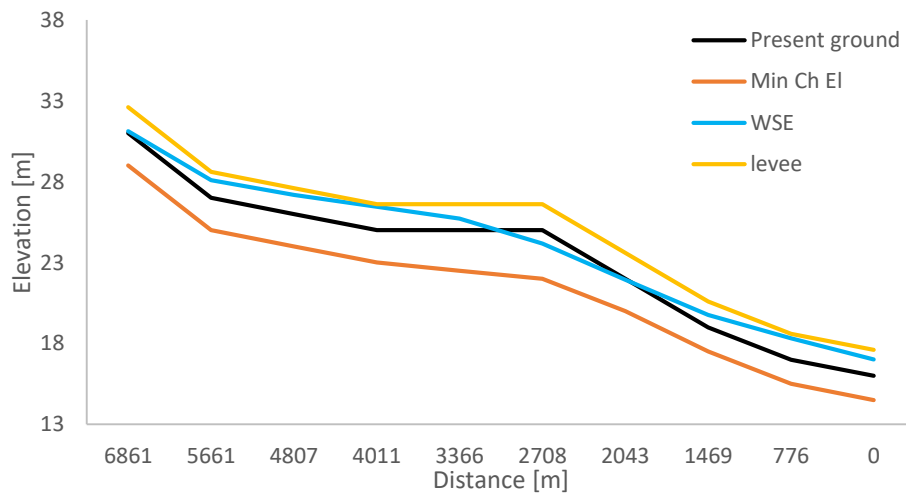


Figure 150 Profile of water depth and levees in reach c for the Scenario 4 of table 28,  $Q=100 \text{ m}^3/\text{s}$

Table 28 Table of uniform levee design for  $Q=100 \text{ m}^3/\text{s}$ , Scenario 4

Reach	$h_{\text{max}}$ [m]	$h$ [m]	$b$ [m]	$B$ [m]	Lenght [m]	Area [m <sup>2</sup> ]	Vol [m <sup>3</sup> ]	Vol*2 [m <sup>3</sup> ]
a	0.90	1.00	1.50	2.00	1232.66	3.50	4314.31	8628.62
b	2.54	2.70	4.05	2.00	9391.57	16.34	153411.30	306822.59
c	1.45	1.60	2.40	2.00	6861.41	7.04	48304.33	96608.65

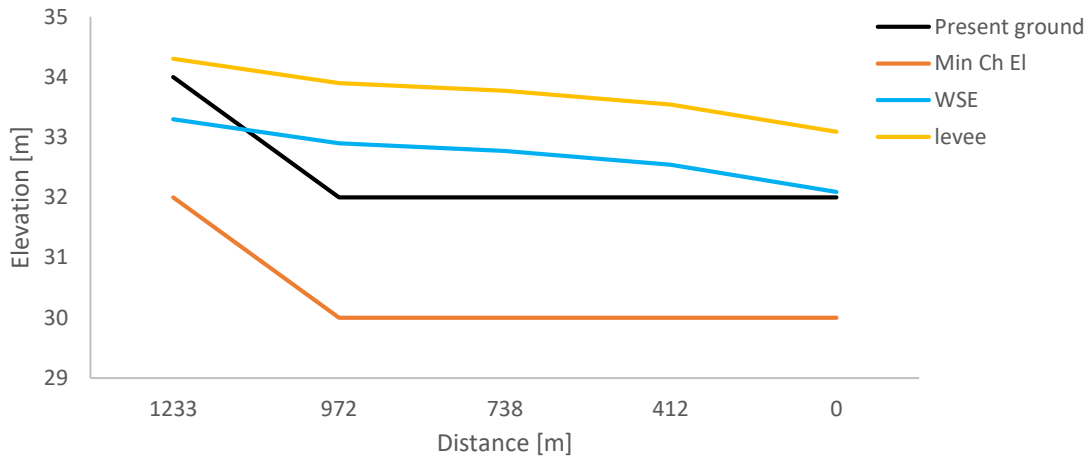


Figure 153 Profile of water depth and levees in reach a for the Scenario 4 of table 29,  $Q=100 \text{ m}^3/\text{s}$

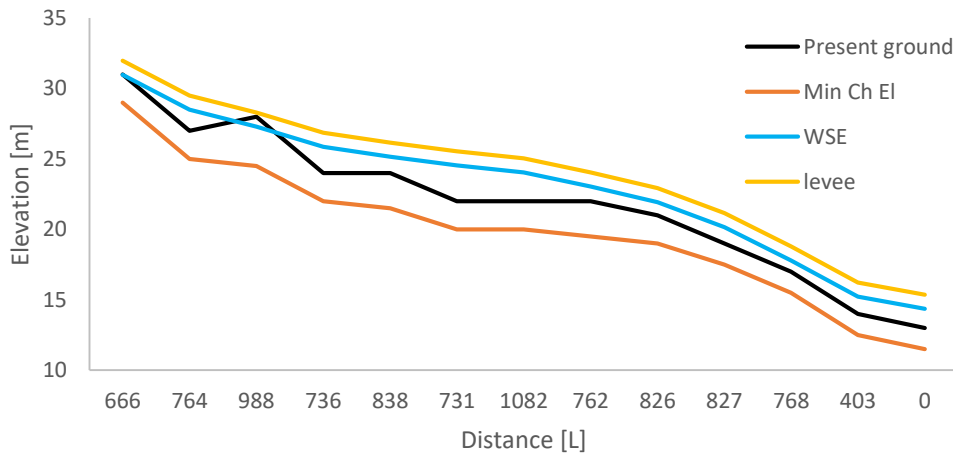


Figure 154 Profile of water depth and levees in reach b for the Scenario 4 of table 29,  $Q=100 \text{ m}^3/\text{s}$

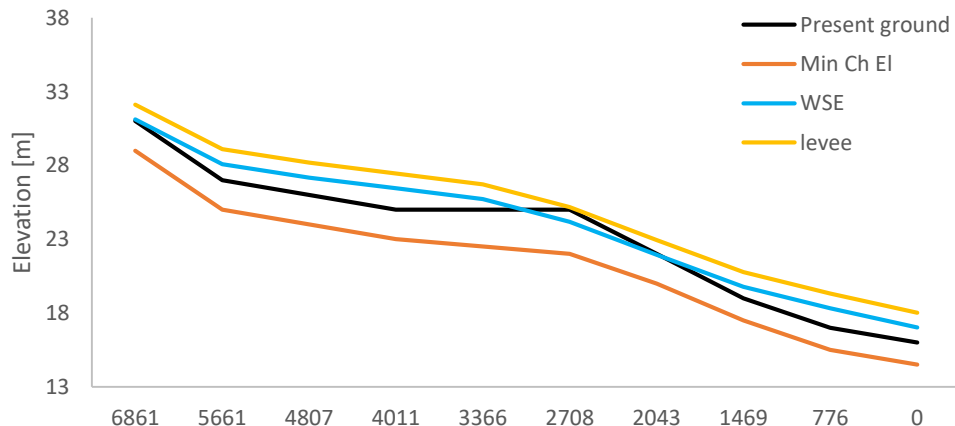


Figure 155 Profile of water depth and levees in reach c for the Scenario 4 of table 29,  $Q=100 \text{ m}^3/\text{s}$

Table 29 Table of levee design with a freeboard of 1m, Q=100 m3/s, Scenario 4

Reach	River Sta	Min Ch El (m)	Top Width (m)	WSE (m)	Present ground (m)	Distance (m)	Vol dug (m3)	freeboard (m)	Levee el. (m)	h levee (m)	b (m)	B (m)	A arg (m2)	Vol (m3)
a	27	32.00	30.00	33.30	34.00	260.23	7806.90	1.00	34.30	0.29	0.43	2.00	0.70	91.69
a	26	30.00	30.00	32.90	32.00	234.04	14828.10	1.00	33.90	1.90	2.85	2.00	9.22	2277.35
a	25	30.00	30.00	32.77	32.00	326.86	16827.00	1.00	33.77	1.77	2.65	2.00	8.23	2308.24
a	24	30.00	30.00	32.54	32.00	411.53	22151.70	1.00	33.54	1.54	2.31	2.00	6.64	2450.49
a	23	30.00	30.00	32.09	32.00	0.00	12345.90	1.00	33.09	1.09	1.63	2.00	3.96	814.15
b	12	29.00	10.00	30.97	31.00	665.83	6658.30	1.00	31.97	0.96	1.44	2.00	3.30	1099.42
b	11	25.00	10.00	28.50	27.00	764.44	14302.70	1.00	29.50	2.50	3.75	2.00	14.38	10280.07
b	10	24.50	10.00	27.29	28.00	988.27	30672.43	1.00	28.29	0.00	0.00	2.00	0.00	0.00
b	9	22.00	10.00	25.85	24.00	735.60	17238.70	1.00	26.85	2.85	4.27	2.00	17.87	15402.35
b	8	21.50	10.00	25.15	24.00	838.05	19670.63	1.00	26.15	2.15	3.22	2.00	11.22	8830.54
b	7	20.00	10.00	24.54	22.00	731.36	15694.10	1.00	25.54	3.54	5.31	2.00	25.88	20306.13
b	6	20.00	10.00	24.04	22.00	1081.77	18131.30	1.00	25.04	3.04	4.56	2.00	19.94	18079.08
b	5	19.50	10.00	23.03	22.00	761.81	23044.75	1.00	24.03	2.03	3.04	2.00	10.23	9431.02
b	4	19.00	10.00	21.92	21.00	826.48	15882.90	1.00	22.92	1.92	2.88	2.00	9.37	7440.82
b	3	17.50	10.00	20.16	19.00	827.25	12402.98	1.00	21.16	2.16	3.24	2.00	11.32	9358.79
b	2	15.50	10.00	17.78	17.00	767.92	11963.78	1.00	18.78	1.78	2.67	2.00	8.31	6630.01
b	1	12.50	10.00	15.23	14.00	402.79	8780.33	1.00	16.23	2.23	3.34	2.00	11.91	6970.52
b	0	11.50	10.00	14.36	13.00	0.00	3020.93	1.00	15.36	2.36	3.54	2.00	13.07	2633.12
c	22	29.00	10.00	31.12	31.00	1200.00	12000.00	1.00	32.12	1.12	1.68	2.00	4.12	2472.96
c	21	25.00	10.00	28.09	27.00	854.41	20544.10	1.00	29.09	2.09	3.13	2.00	10.72	11013.38
c	20	24.00	10.00	27.18	26.00	795.99	16504.00	1.00	28.18	2.18	3.27	2.00	11.49	9480.39
c	19	23.00	10.00	26.45	25.00	645.41	14414.00	1.00	27.45	2.45	3.67	2.00	13.89	10011.60
c	18	22.50	10.00	25.72	25.00	657.94	16291.88	1.00	26.72	1.72	2.58	2.00	7.88	5133.63
c	17	22.00	10.00	24.18	25.00	664.27	19833.15	1.00	25.18	0.18	0.27	2.00	0.41	270.13
c	16	20.00	10.00	21.94	22.00	574.26	12385.30	1.00	22.94	0.94	1.41	2.00	3.21	1984.99
c	15	17.50	10.00	19.77	19.00	693.46	9507.90	1.00	20.77	1.77	2.65	2.00	8.23	5216.98
c	14	15.50	10.00	18.32	17.00	775.67	11018.48	1.00	19.32	2.32	3.48	2.00	12.71	9338.97
c	13	14.50	10.00	17.02	16.00	0.00	5817.53	1.00	18.02	2.02	3.03	2.00	10.16	3940.64

#### 4.4.SYNTHESIS AND RECOMMENDATIONS

A summary of the scenarios presented in the previous sections is given in *Table 30*. The latter contains the total volume of excavated soil  $W_{exc}$  as representative of the effort of digging, the water volumes stored in the lake ( $W_{lake}$ , with a further specification of the flood flow rate) as representative of the exploitation of the storage, and the volumes of material needed to build the levees  $W_{lev}$  considering the different discharges and design. It is noticed that, even if in the previous sections *Scenarios 1* and *2* have been presented in a sequence, they are actually the two parts of a single scenario of largest excavation. Instead, *Scenario 3* and *4* merged excavation and construction of the levees for the sake of brevity.

*Table 30 Summary of the design scenario. In bold, the cases with excavated volumes largely insufficient to build the levees.*

Scenario	$W_{exc}$ [m <sup>3</sup> ]	$W_{lake47}$ [m <sup>3</sup> ]	$W_{lake100}$ [m <sup>3</sup> ]	$W_{lev-47-1}$ [m <sup>3</sup> ]	$W_{lev-47-2}$ [m <sup>3</sup> ]	$W_{lev-100-1}$ [m <sup>3</sup> ]	$W_{lev-100-2}$ [m <sup>3</sup> ]
1	563302	19188	1004544	-	-	-	-
2	563302	19188	1004544	-	-	168877	160315
3	328541	421758	2359026	129356	150662	<b>335666</b>	<b>436143</b>
4	409738	418536	2360754	89686	110249	412060	366535

The clues to read the values in the table are (1) the comparison between excavated and reused soil volumes and (2) the water volumes stored in the lake.

In relation to the former, the last solution is the best one in terms of material use. In particular, it presents the lowest ratio between the excavated volumes and the volumes used to build the levees. Compared to the first two scenarios, it implies less excavation operations ensuring lower expenditure and time to achieve the prescribed geometry. Moreover, if compared with the third scenario, which is the most advantageous in terms of cost of excavation, also a more severe event can be mitigated while for *Scenario 3* the balance between soil excavation and reuse is positive only for the lower flow rate (see the numbers in bold in the table).

The best exploitation of the lake is achieved by *Scenario 3* and *Scenario 4*, with similar volumes of water stored in the lake. The mitigation measures presented has to take into account the presence of water in the storage area which is determinant for the agriculture community, since the zone suffers of water scarcity during dry seasons. After the field survey this topic seemed indeed to be crucial for the population: having the possibility of storing water that could be used during dry periods for agricultural purpose, main source of livelihood. A mitigation measure that can fulfil this scope has surely an added value.

Moreover, the already mentioned analysis of how much climate change is threatening this area has shown how quickly are growing intensity and frequency of events such as cyclones and storms; simultaneously the poverty and unpreparedness characterizing these regions is the greater obstacle in developing mitigation measure that need continuous maintenance, such as, for example, little periodic digging interventions. Also for these reason it seems worthy to recommend a deeper and more important intervention, such as that depicted in *Scenario 4*, able to face more intense events. If built according to the proposals mentioned above about the levees, it is also expected to last more in terms of time.

A more effective mitigation system may be achieved increasing the number of storage areas. Moreover, it was mentioned above that the southern part of the study area (close to the villages of Unidade and Saul 2) has a larger elevation than the rest and thus is less affected by floods, while locals would benefit from the possibility of water storage. A system like that shall be within the scope of future investigation, would be a combination between a flood protection and spate irrigation system.



Future analyses shall also assess the (possibly negative) impacts of the proposed mitigation measures on the surroundings, as it is frequent that a protection at some location may worsen the safety conditions elsewhere.

The flood risk in the area significantly derives from the sediment aggradation that reduces the conveyance. After the realization of the mitigation measures, the process of bed filling with sediment will proceed. There is a value in evaluating a time after which major excavation shall be repeated to restore the conveyance of the river reaches. Such a computation would require an estimation of likely sediment volumes supplied to the area of interest by the upstream portion of the basin. Some methods are available to perform such analyses starting from precipitation and soil cover data, like for example the methods based on the USLE and following equations.

There is, finally, a need to assess a residual risk deriving from discharge conditions worse than those considered in design. These analyses may be performed with a suitable combination between one- and two-dimensional modelling, the former for the river reaches and the latter for the floodplain areas close to points where overflow is expected to occur.

## 5. CONCLUSIONS

According to recent studies, catastrophes due to climate change are increasing every year in terms of intensity and frequency. The most vulnerable countries are the poorest ones, where means and awareness are lower than in developed regions. The sub-Saharan context is where most of these countries are located and where an increasing number of floods and drought are hitting the population. The scope of this thesis consisted in the assessment and mitigation of the flood hazard and risk in the rural area of Metuge, a district of Cabo Delgado situated in the north of Mozambique. The area is crossed by the Rio Maguide that finally flows into the canal of Mozambique.

It is well known that performing detailed studies in developing countries is hindered by the scarcity of good-quality data. Therefore, if one wants to export the methods of analysis that are typically used in developed regions, a great deal of effort must be put in the search of suitable data. All the evaluations performed in this thesis are based on hydrologic and hydraulic numerical modelling. The data collected to meet the modelling goals were related to the morphology of the site and the precipitation. The data-seeking phase was significantly corroborated by a mission on site, during which the area under study has been visited in detail; even though this did not provide quantitative data, it was crucial to increase the knowledge of the place.

No detailed surveys are available for the study area. Some free Digital Elevation Models have been found on the Internet and are those provided by space agencies as a result of shuttle missions. The spatial resolution of these data is much coarser than resolutions typically used in hydraulic modelling; it ranged between 90 and 12,5 m, that are large values compared to the width of the Rio Maguide in the study area. According to the literature, the vertical accuracy of these data may be within some metres, thus generally unacceptable. However, the general pattern of the topography seemed reasonable. Between the sources that yielded similar elevation ranges, the DEM with the best resolution of 12 m (ALOS PALSAR) was chosen.

Rainfall data are available from different services, and may be based on rain gauges or interpolation of radar observations from satellites. The comparison among all the data sources revealed a certain agreement in the average monthly precipitation, with variation coefficients of less than 20% in the rainy season. The chosen data (the only ones that were not free) were those with a temporal resolution of 1 hour, while all the others were at least daily.

Soil cover data were retrieved from three sources. They were quite different from each other. However, the uncertainty in the soil coverage limitedly impacted the following developments, since the soil cover was only used to estimate a bulk curve number for the quantitative assessment of the hydrologic losses due to infiltration.

The above data were used to determine depth-duration-frequency curves for rainfall, the hydrographic network with the times of concentration of the sub-basins and a synthetic flood hydrograph to be used in the following analysis. A small sub-basin, close to the study area, was chosen as a support for the modelling. The analysis was done with reference to a relatively low return period, considering the area of interest and the precipitation pattern that involves a dry and a rainy season.

Using two different software products, *River 2D* and *iRIC*, hazard maps were obtained, depicting the current situation of floods in the area of interest. The second software had some advantages compared to the first one, related in particular to the computational time needed to run any simulation, and is thus recommended. The hazard maps provide a view of a flooded area with values of the expected water depth. The results were compared to the real situation of the inundated area coming from satellite images taken after cyclone Kenneth, the last most devastating event hitting the area. From this comparison it was observed that the

model, though run with sub-optimal data, can simulate the considered event with a good approximation. In particular, it was quite satisfactory to find evidence of a main gateway of the water: an upper sub-reach excavated by previous intense events.

The comparison between the flooded area in the hazard maps and the area flooded during Kenneth provides the only possible (though weak) validation of the entire modelling package. It is unfortunately impossible to validate any ingredient (geometric/hydrologic data, numerical model, ...) independently on the others. However, the result obtained with the first part of the analysis was considered enough satisfactory to proceed with the second. It must be borne in mind that, in the end, nothing better than this is available in the considered region.

The results of the models for the present condition and the direct observation performed on site were the basis for a second step, the was the design of possible mitigation measures. The approach taken in this phase was the classic one of hypothesizing a solution and undertaking a hydraulic verification of its performance. The mitigation measures were in terms of restoring the previous conveyance of some reaches along which the river braids. These reaches have been, in time, completely filled with sediment supplied from the upstream portions of the basin. Therefore, the mitigation measures referred to sediment excavation, that is a feasible intervention with limited possibilities. The excavation was possibly coupled with the construction of earthen levees. Finally, it was also decided to take advantage of the presence of a lake that was seen as a natural storage area. Given the nature of the measures under design, this part was approached by one-dimensional modelling.

The mono-dimensional analysis was performed using the software *HEC-RAS*. After the field survey, three possible solutions were taken into consideration to perform this analysis. After choosing a solution to proceed with, its geometry was built and a critical discussion about the type of intervention has been undertaken. Four scenarios were developed:

- *Scenario 1*: deep excavation only;
- *Scenario 2*: deep excavation with levees (actually, scenarios 1 and 2 are two parts of a single one);
- *Scenario 3*: superficial excavation with levees;
- *Scenario 4*: intermediate excavation with levees.

For each of them, steady and unsteady models were performed. The steady models were used to compute a division of discharges into the different reaches and for an analysis of the freeboard at peak flow. The unsteady models were instead useful to assess the storage capacity of the lake. According to a comparative analysis of the introduced scenarios, the best one is the last (that was indeed reached after a series of trials), because it yields a good balance between the sediment excavated and reused to build the levees, a good exploitation of the storage capacity of the lake and the ability to protect the place up to a flood discharge of  $100 \text{ m}^3/\text{s}$ .

The study performed in this work met an ambitious objective to perform a first analysis of the flood risk in the study area and propose suitable and feasible mitigation measures. Of course, several future developments of this study are possible:

- the use of a more refined DEM with higher resolution (for example 1 X 1 meter) which can lead to higher accuracy both in hydraulic modelling and in *ArcGis* operation phases;
- two-dimensional modelling with *iRIC* based on this more refined DEM;
- the use of a faster software that can help in facing the computational effort required by the unsteady 2D modelling;
- mono-dimensional analysis with *HEC-RAS* of the other two solution developed after field survey;

for what concern the refinement of the operations employed can be useful to:

- increase the number of reservoirs to enlarge the volume of the storage area available for the district; in parallel it helps also in mitigating the flooding;
- analyse all the possible scenarios taking in consideration the real applicability of them in the context (considering costs, equipment, etc.) and how, such modification of the water network, can affect the downstream area;
- evaluate the residual hazard and risk for events with flow rates higher than those considered in this work;
- evaluate the time needed by the river, through the implementation of erosion prediction models such as, for example, the Universal Soil Loss Equation (USLE), Modified Universal Soil Loss Equation (MUSLE) and Revised Universal Soil Loss Equation (RUSLE), to redeposit material into the river bed and to completely fill again its path with sediment.

## BIBLIOGRAPHY

Guevara, M. E. & Rojas, J. C., (2019) *Flood Modeling using Conventional Land Surveys, Digital Mapping, and Drone Survey*, 2289 -2295.

Karlsson, J. M. & Arnberg, W., (2011) *Quality analysis of SRTM and HYDRO1K: a case study of flood inundation in Mozambique*, *International Journal of Remote Sensing*, 32:1, 267-285, DOI: 10.1080/01431160903464112.

Khaddor, I., Achab, M., Ben jbara, A. & Alaoui, A. H. (2019) *Estimation of Peak Discharge in a Poorly Gauged Catchment Based on a Specified Hyetograph Model and Geomorphological Parameters: Case Study for the 23–24 October 2008 Flood, KALAYA Basin, Tangier, Morocco*, DOI:10.3390/hydrology6010010.

Tadesse , A., Shimeles, S. & Alemu, E., (2019), *Ground-Based Surveying Versus the Need for a Shift to Unmanned Aerial Vehicles (UAVs): Current Challenges and Future Direction*.

Lumbroso, D., Ramsbottom, D., & Spaliveiro, M., (2008) , *Sustainable flood risk management strategies to reduce rural communities' vulnerability to flooding in Mozambique*, 34-42.

Christie, F., & Hanlon, J., (2001), *Mozambique and the Great Flood of 2000*.

Shimizu, Y., Nelson, J., Ferrel, K. A., Asahi, K., Giri, S., Inoue, T., Iwasaki, T., Jang, C., Kang, T., Kimura, I., Kyuka, T., Mishra, J., Nabi, M., Patsinghasanee, S. & Yamaguchi, S. (2019), *Advances in computational morphodynamics using the International River Interface Cooperative (iRIC) software*.

Nelson, J. M., Shimizu, Y., Abe, T., Asahi, K., Gamou , M., Inoue, T., Iwasaki, T., Kakinuma , T., Kawamura, S., Kimura, I., Kyuka, T., McDonald , R. R. , Nabi , M., Nakatsugawa g , M., Simões, F. R. , Takebayashi , H. & Watanabe , Y., (2015), *The international river interface cooperative: Public domain flow and morphodynamics software for education and applications*.

Simões, F.J.M., (2011), *Finite volume model for two-dimensional shallow environmental flow*, 173-182.

Nones, M., (2019), *Dealing with sediment transport in flood risk management*, 677–685.

Scharffenber, W.A., Fleming, M.J., (2010), *Hydrological Modeling System HEC-HMS User's Manual*, United States Army Corps of Engineers: Davis, CA, USA.

United States Army Corp of Engineering (USACE). *Hydrologic Modeling System HEC-HMS*, USACE: Washington, DC, USA, 2000.

Steffler, P. & Blackburn, J., 2002. *River2D. Two-Dimensional Depth Averaged Model of River Hydrodynamics and Fish Habitat. Introduction to Depth Averaged Modeling and User's Manual*. Software manual. University of Alberta, Canada.

Crotti, G. (2017). *HEC-RAS quick guide*.

Radice, A., & Crotti, G. (2017). *River2D quick guide*.

Radice, A., & Crotti, G. (2017). *Two-dimensional river modelling*.

Simões, F.J.M., (2013), *Using STORM—A Short Primer*.

Tonolo, F.G., (2018), *Flood Mapping with Sentinel-1 data in SNAP*.

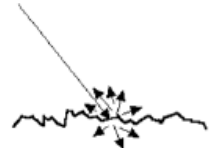
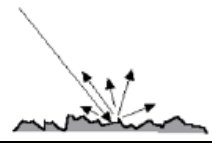

## APPENDIX 1: SATELLITE IMAGES PROCESSING

Considering the devastating impact that cyclone Kenneth had on Cabo Delgado and the resulting flooding of the large part of the main rivers in the region, a specific study on Rio Maguide has been performed. The aim of this study is to extract the extent of the flood occurred as a consequence of the cyclone and the following intense rainfalls by comparing two specific satellite images and by processing them using an advanced software called SNAP 6.0<sup>35</sup>.

### SNAP 6.0

The key idea behind the use of this software is that of comparing two different satellite images, the first one taken before the event (on a date belonging to the dry season, in order to be sure that no water is visible). The other satellite image has to be taken some days after the starting of the event, when the peak of the rainfall records is reached. The images used by the software are Synthetic Aperture Radar (SAR) satellite imagery. SAR provides high-resolution, day-and-night and weather-independent images. Their systems have a side-looking imaging geometry and are based on a pulsed radar installed on a platform with a forward movement. The radar system transmits electromagnetic pulses with high power and receives the echoes of the backscattered signal in a sequential way. The different response of the signal gives an indication of the surface on which it is reflecting (*Table A1*).

*Table A1 Reflectance on wet or dry soil and water surfaces*

	Dry soil: some of the incident radar energy is able to penetrate into the soil surface, resulting in less backscattered intensity
	Wet soil: the large difference in electrical properties between water and air results in higher backscattered radar intensity
	Flooded soil: radar is specularly reflected off the water surface resulting in low backscattered intensity. The flooded area appears dark in the SAR images

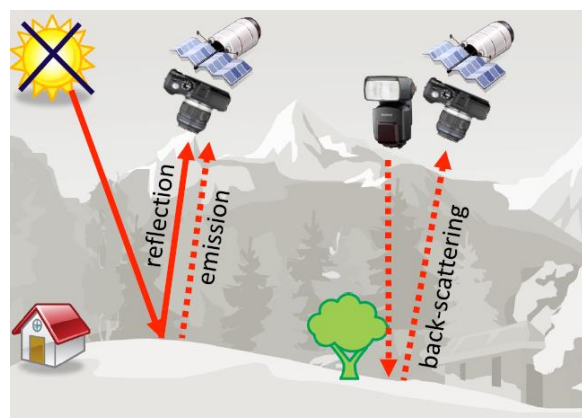


*Figure A1 Illustration of SAR imaging process*

<sup>35</sup> SNAP 6.0 is a free software developed by ESA (European Space Agency) and SEOM (Scientific Exploitation of Operational Missions) ideal for Earth Observation processing and analysis.



SAR data from Sentinel-1, a SAR mission from ESA, is available free of charge on two different portals:

Copernicus Open Access Hub developed by a Serco and GAEL Systems consortium under a contract with the European Space Agency (ESA);

EO Browser powered by Sinergise with contributions from the European Space Agency (ESA).

For both sources, a search option becomes available which can be used to specify the data need such as region of interest, product type, sensor mode, sensing period, among others. For sensing period, the image of the 30<sup>th</sup> of August 2018 has been chosen as suitable as pre-event and, for the post-event one, an image taken on the 28<sup>th</sup> of April 2018 was selected, even if the peak of rainfall had not been reached yet on that day. In the sensor mode the Level-1 Ground Range Detected (GRD) Sentinel-1 data has been chosen, which incorporates already some basic pre-processing. The workflow that has been implemented with SNAP 6.0 is summarized in the flow diagram of *Figure A2*.

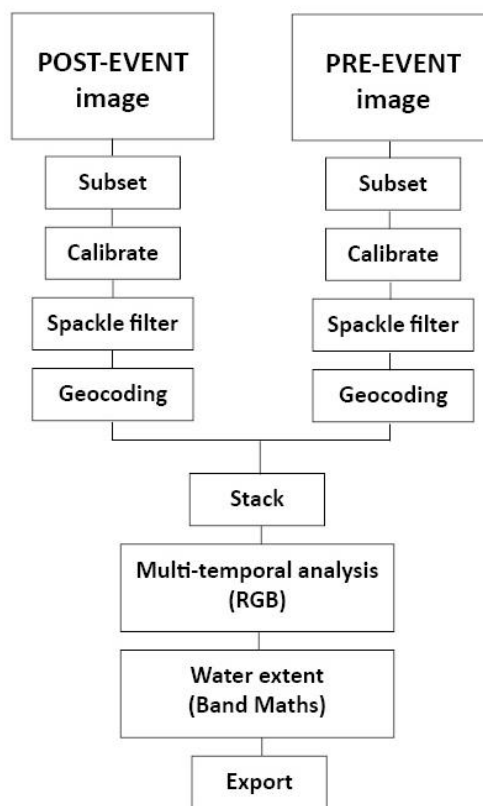


*Figure A2 SNAP workflow*

The acronym RGB stands for Red, Green and Blue that are the primary additive colours. A digital image in true-colour (RGB) is the overlap of three digital greyscale images acquired in the three spectrum bands corresponding to red, green and blue light. It is possible to visualize colour images starting from three images in greyscale, corresponding to different bands of the electromagnetic spectrum. One simply needs to “add” the light intensity of the three images to show on the monitor a single colour image. The light intensity is given by the Digital Number (DN) associated to each pixel that determines the tone of grey of that specific pixel. When the DN is near to 0 the light intensity is almost null, associated to black coloured pixel. On the contrary, when the number is high the pixel is nearer to white. With the software SNAP it is possible to associate the different electromagnetic spectrum bands to the pre or to the post-event satellite image.

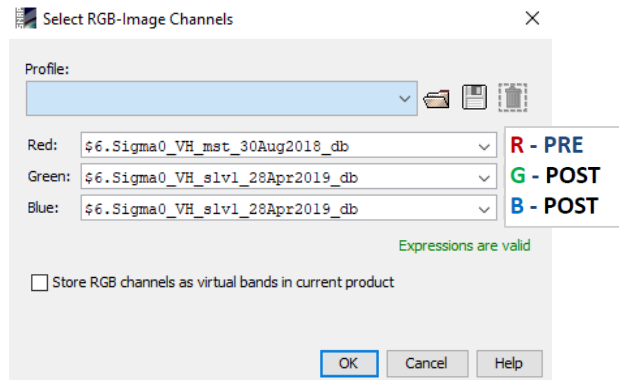


Figure A3 RGB image window from SNAP

This is a key passage in the recognition of the flooded areas. In this case, it has been chosen to attribute the red band to the pre-event image and the other two bands to the post-event so that the pixels in red are those for which the pre-event has higher values of DN's with respect to the post highlighting the water bodies present on the image.

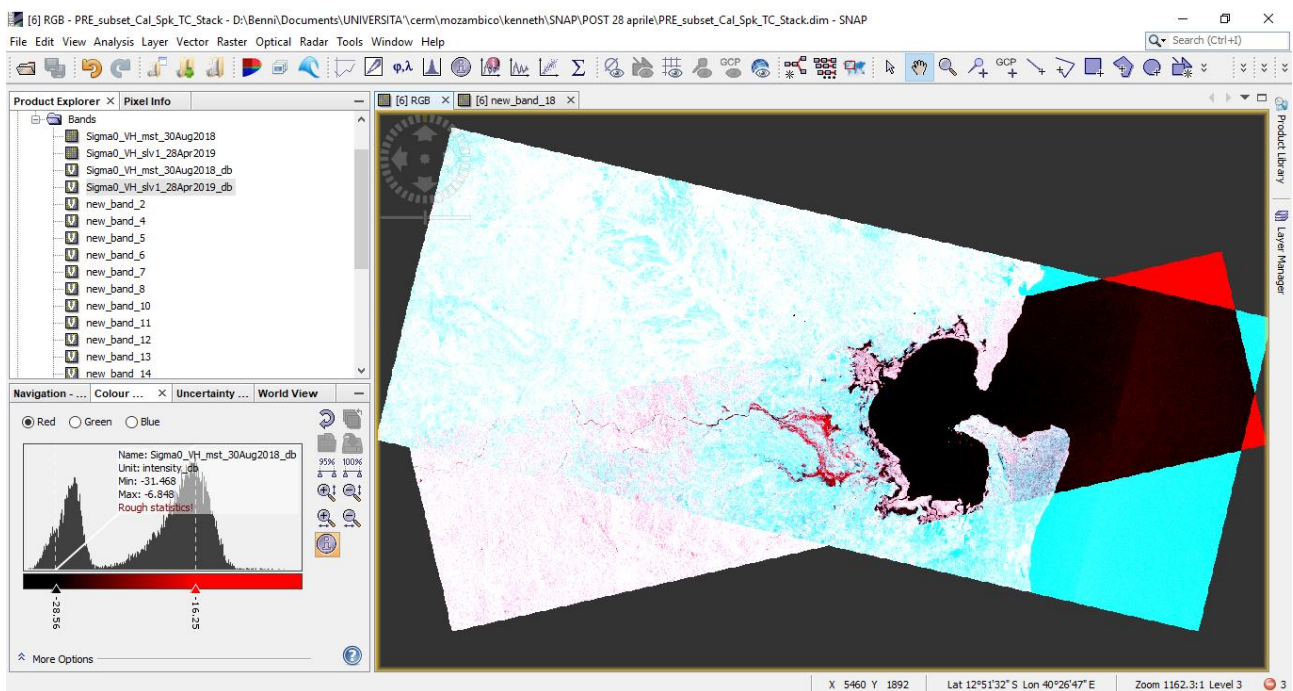
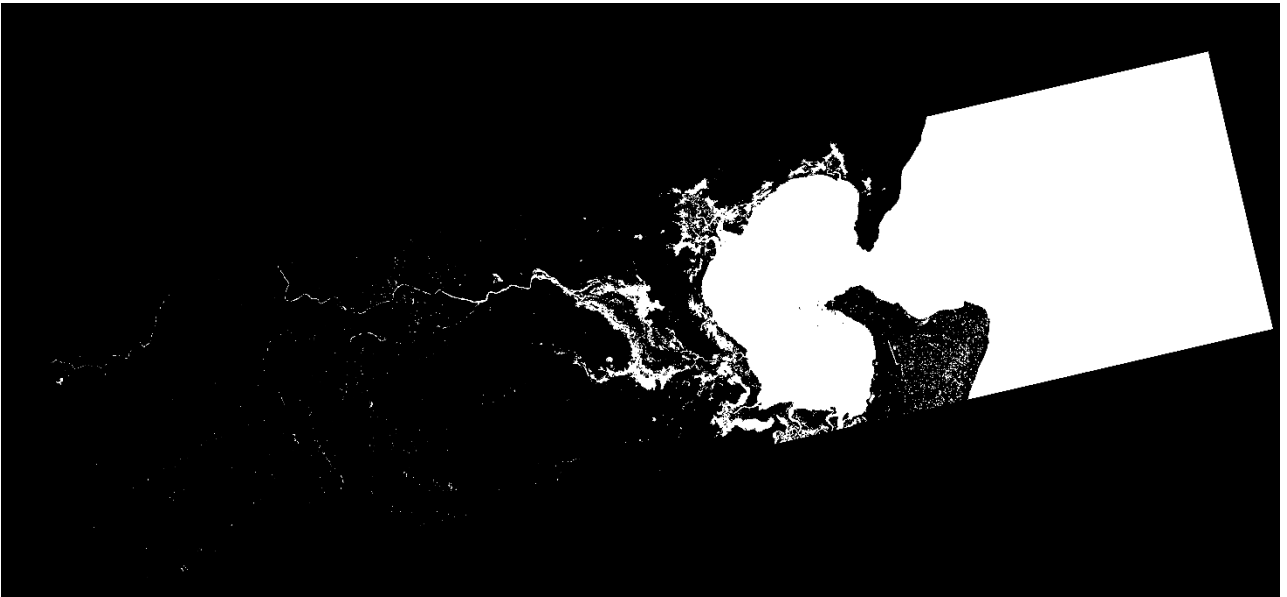


Figure A4 Processed image (the red pixels are those flooded in the post-event image and dry in the pre-event one)

After some other simple steps in which the Band Maths calculator has been used to solve a query that asks to select only the pixels that had a specific range of value to highlight the threshold between flooded and non- flooded areas, it has been possible to extract a binary image where the white pixels are those related to the inundated area (Figure A5). It is also possible to directly upload the result on Google Earth and simply visualize it on the area of relevance and rapidly have an idea of the correctness of the procedure. The following passage will just be the uploading of this image on ArcGIS and the production of flood maps.



*Figure A5 Resulting image of the flooded area (that is Figure 22 of chapter 1)*

## APPENDIX 2: TWO-DIMENSIONAL MODELLING OF DESIGN CONDITION

A two-dimensional analysis seemed a coherent continuation of the models for the current state of the area done with *iRIC*: some modifications of the geometry of the area would have mimicked different mitigation measures devised to avoid the flooding of the area. A single main path of the river was considered, that was the one resulting from the GIS calculations for the AlosPalsar DEM described in chapter 2.

Three possible mitigation measures have been produced:

- excavation of the path of the main river;
- levee of a limited length of the river, relatively far from its path;
- excavation + levee along the whole length of the studied area following its path.

### EXCAVATION

The geometry of the river was changed performing a digging of its path with height  $h=0,7\text{ m}$  and width  $B=25\text{ m}$  (size of two neighbouring pixels of the DEM chosen) along the whole length of the studied area. The considered inflow discharge was  $Q=47,5\text{ m}^3/\text{s}$ . The depth of the excavation was found using the *Chézy-Strickler* formula.

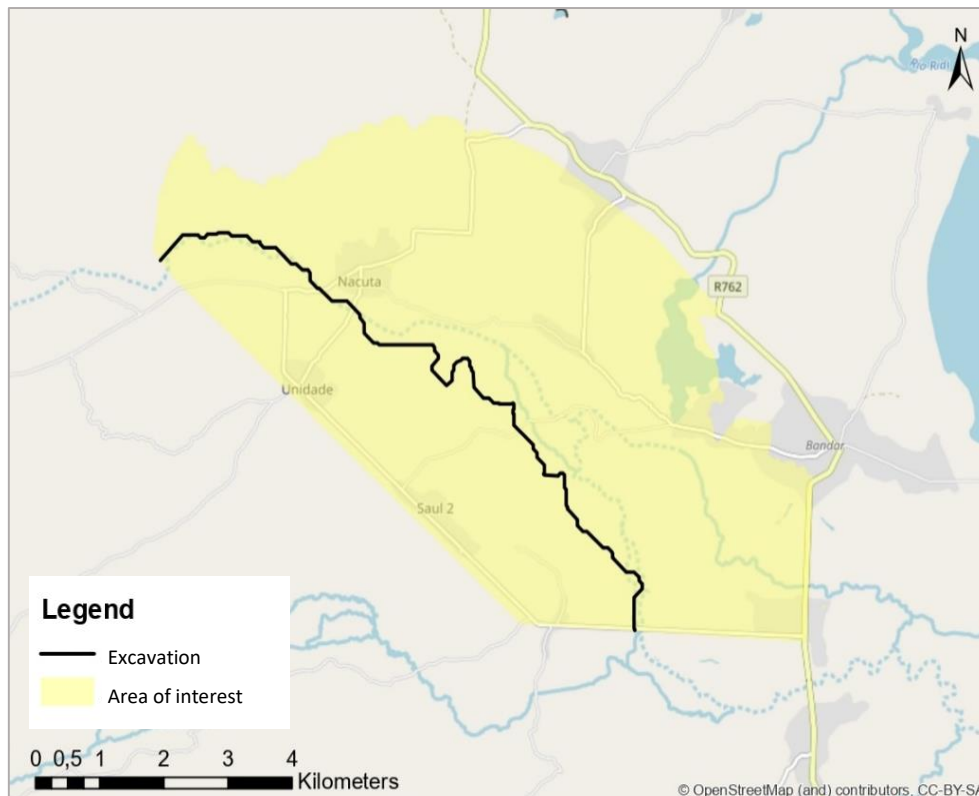


Figure B 1 Excavation

The outflow discharge at the end of the computation was  $Q=49.9 \text{ m}^3/\text{s}$ , demonstrating a satisfactory convergence of the model. The following figures (Figure B2-B3) represent the resultant flood extension and its water depth.

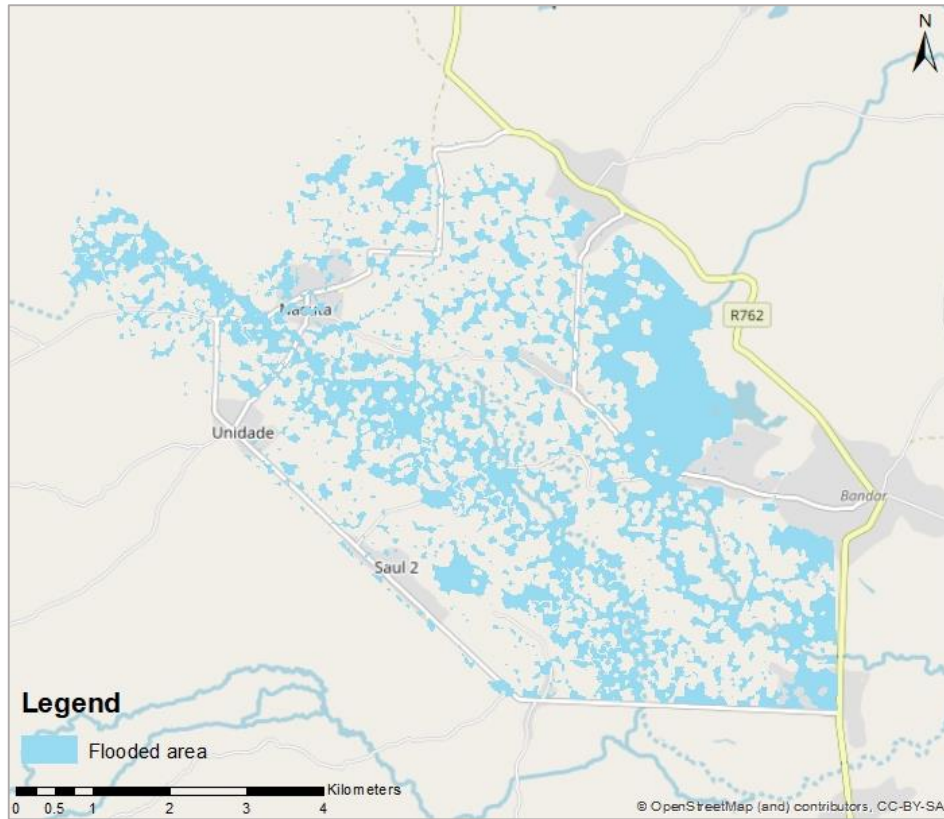


Figure B 2 Flooded area extension for the excavated solution

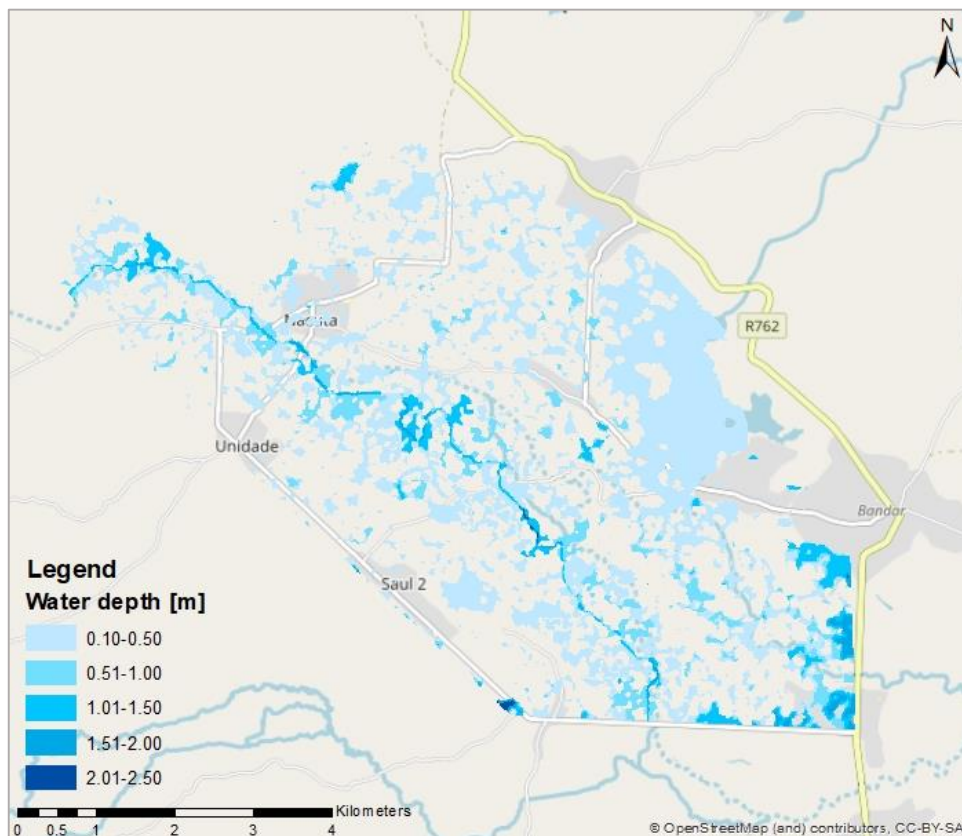
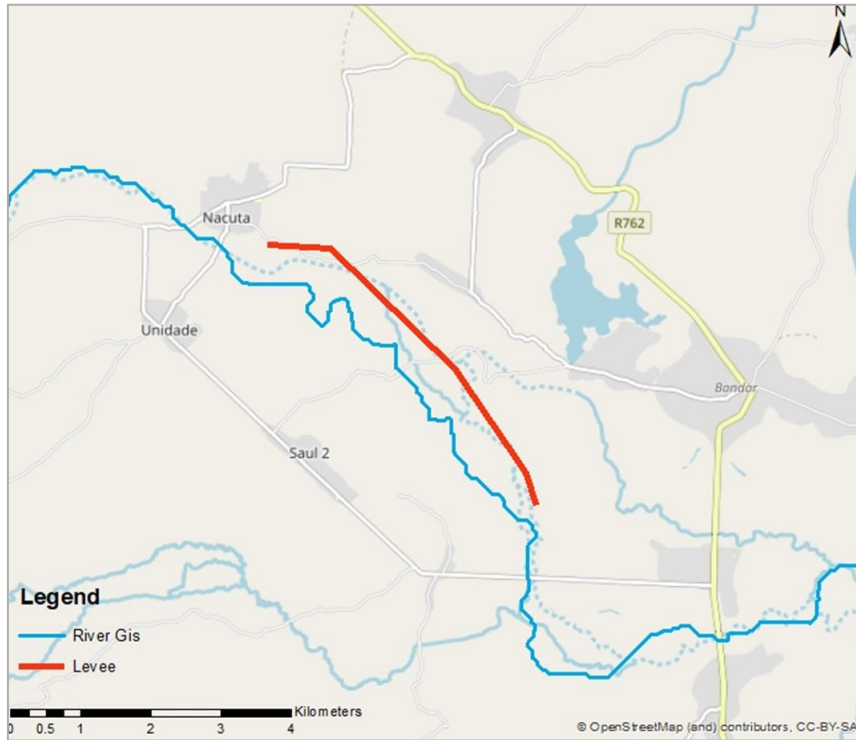


Figure B 3 Water depth of the excavated solution

## LEVEE

The second solution was the construction of a levee, with a height of 1m, along a limited length of the river. As shown in *Figure B4* this levee was built keeping a certain distance from the river path to allow a partial inundation of the fields neighbouring the river. This choice was done in order to simplify its construction and to reduce its overall length (it should have been greater if it had to follow the path of the river), that was about 6 km.



*Figure B 4 Levee*

The outflow discharge at the end of the computation is  $Q=34,1 \text{ m}^3/\text{s}$ . The following figures (*Figure B5-B6*) represent the resultant flood extension and its water depth.



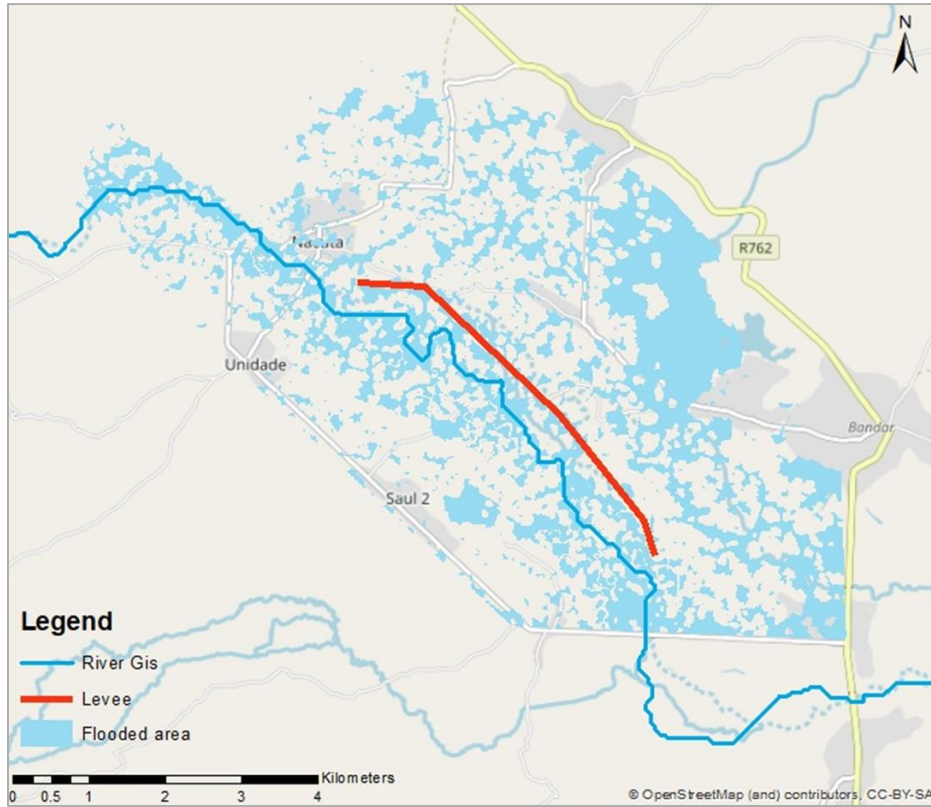


Figure B 5 Flooded area extension for the solution with levee

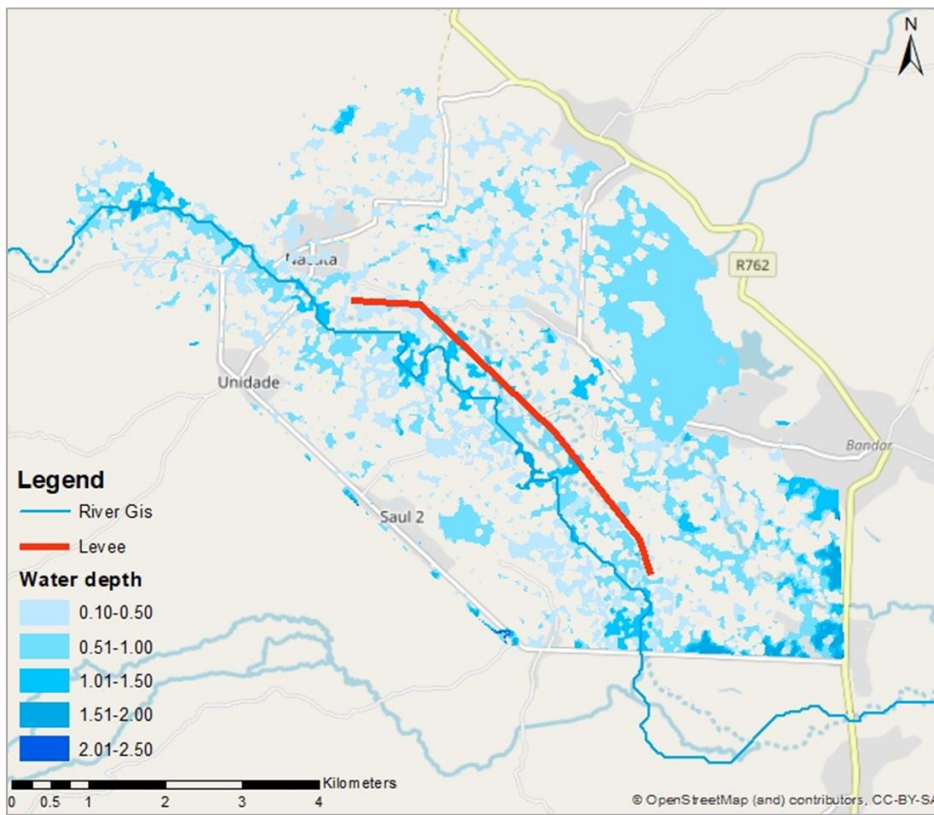
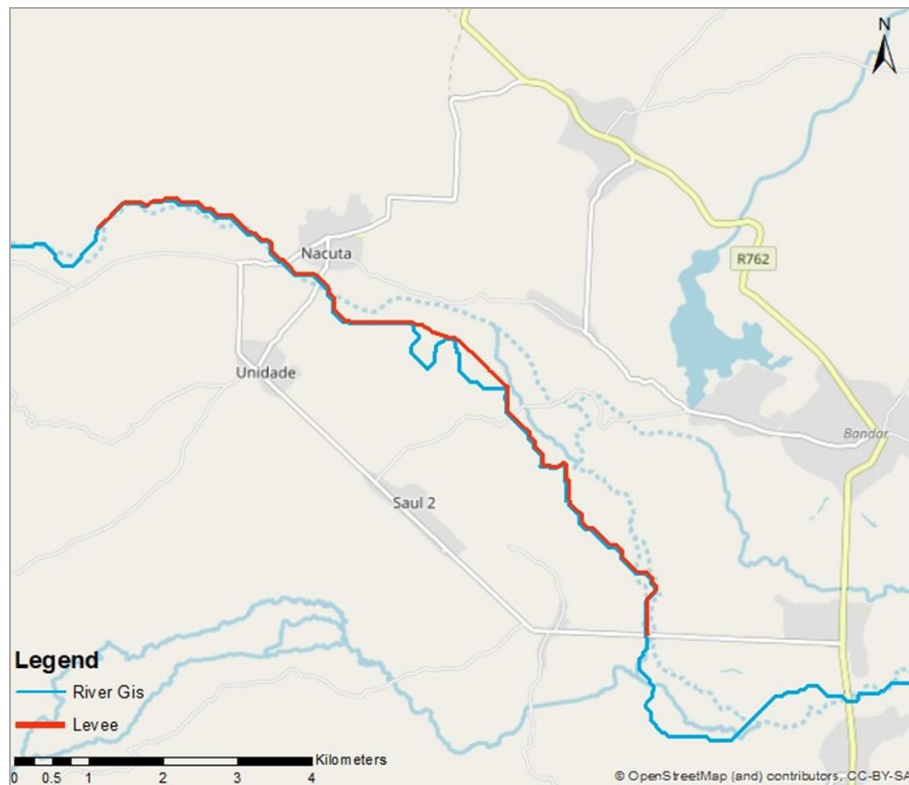


Figure B 6 Water depth of the solution with levee



## EXCAVATION + LEVEE

The third solution was a mix of the previous two. The difference consisted in the construction of a levee along the river path. In this case the ground that was excavated would be directly used for the construction of the bank, so the solution would have been convenient to reduce the costs for the transport. Consequently, the length of the embankment was approximately equal to the total length of the river belonging to the area of interest. Approximately, because in the zone where the bends of the river are too deep, a linearization of the levee was assumed as shown in *Figure B7*. The depth of the excavation and the height of the levee were assumed equal to 1,5 m



*Figure B 7 Excavation and Levee*

The outflow discharge at the end of the computation is  $Q=40,6m^3/s$ . The following figures (*Figure B8-B9*) represent the resultant flood extension and its water depth.

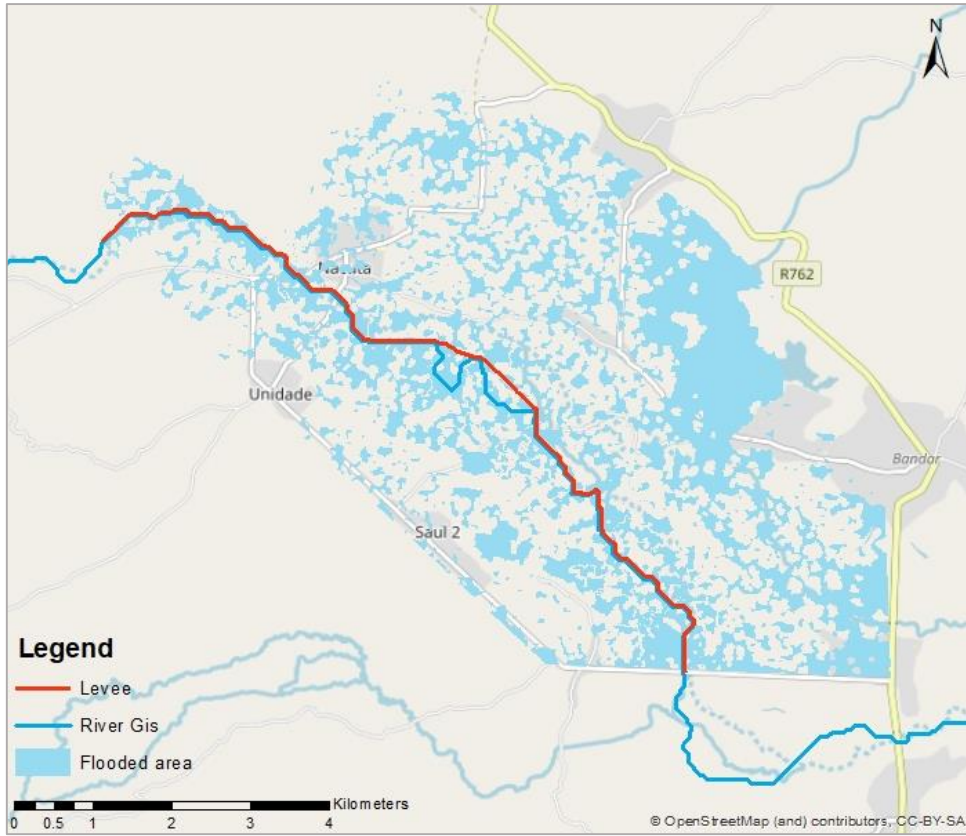


Figure B 9 Flooded area extension for the excavated solution with levee

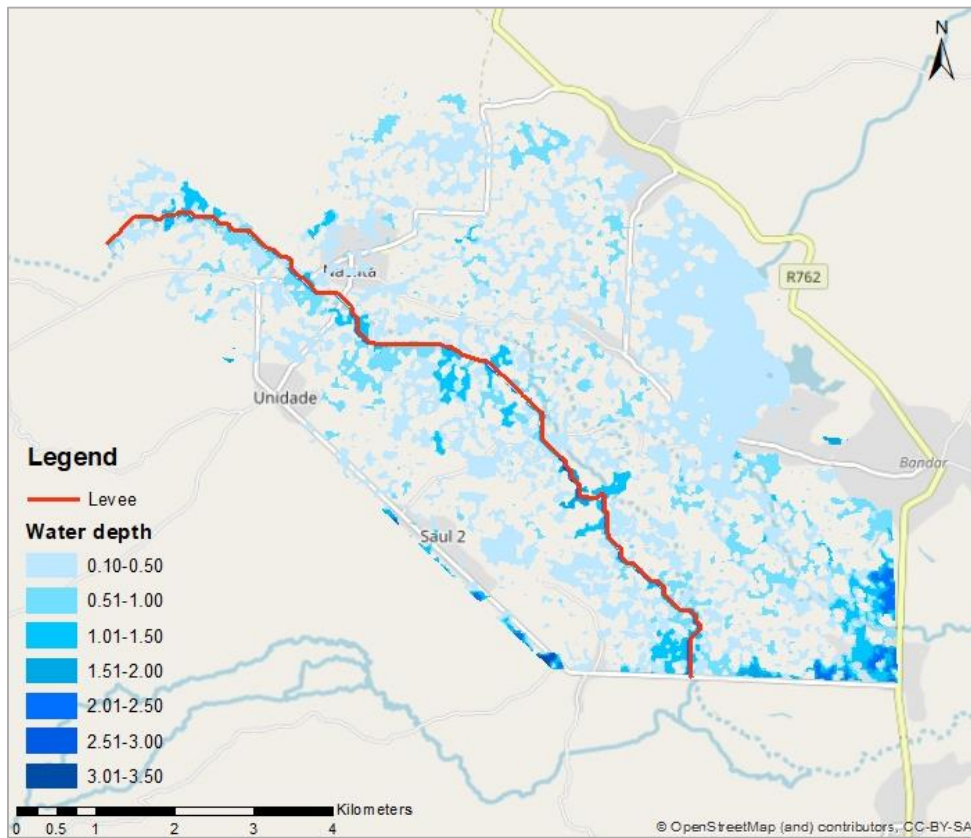


Figure B 8 Water depth of the excavated solution with levee

## CONSIDERATIONS

As shown in the previous figures, the results are not satisfactory. None of the solutions is able to keep the water within a prescribed region. The only visible differences are in the water elevations, but these differences are not large enough to consider any of those solutions adequate.

The inadequacy of the design solutions may in turn spot an inappropriateness of the modelling approach. In fact, on the one hand the output of *iRIC* for the present conditions has been validated thanks to the comparison with the real flood extrapolated by *SNAP*, thus can be considered reliable. On the other hand, the used DEM has a pixel dimension that may be incompatible with modelling of design conditions. The section of the river is, in some zones, much lower than the minimum pixel dimension (12,5 m × 12,5 m); digging two neighbouring cells, even if results in a relatively wide bed, may create a patchy bed, without a consistency between elevations of adjacent cells. Moreover, the area of interest presents a topography which can be defined essentially as flat. It can be thus noticed that the zone at the left of the river presents a lower elevation distribution compared to the one on the right and the shallow excavation performed does not work with a 2-dimensional software which takes into account the whole elevation of the area received as input.